The Modelling, Testing and Design, of a Surface Piercing Propeller Drive

by

PETER KEVIN DYSON

A thesis submitted to the University of Plymouth
in partial fulfilment for the degree of

DOCTOR OF PHILOSOPHY

Department of Mechanical and Marine Engineering
Faculty of Technology

In collaboration with
Marinetech South Ltd
Defence, Evaluation and Research Agency, Haslar
Teignbridge Propellers Ltd

October 2000

The Modelling, Testing and Design, of a Surface Piercing Propeller Drive

Peter Dyson

Abstract

Surface Piercing Propellers (SPPs) are used for high speed vessels in order to avoid the high appendage drag and cavitation problems associated with conventional propellers. The set of forces to which they are subjected is far more complex and demanding than conventional propellers. Not only are the forces much increased, but each goes through large transients as successive blades pass through the water. This project has endeavoured to improve the techniques and data available to the designer, giving more confidence in the design of the shaft and bearing system.

Performance data has been measured on model propellers including both mean values and transients. Torque and thrust figures from these tests correlate well with results for similar propellers tested by previous workers. Mean side and vertical forces have been measured across a range of operating conditions and for different propellers. Each is typically between 20% and 40 % of thrust, and they have a considerable impact on the design of the propeller shaft.

The transients are analysed using frequency spectra to establish the nature and magnitude of the propeller excitation. The first two harmonics of blade rate are found to be dominant and peak to peak fluctuations may typically be 50% of mean values, frequently more. Comparisons are drawn between different blade skews and also different numbers of blades across a range of operating conditions.

The experimental data may be used to determine the input to a dynamic finite element model of the propeller, shaft and bearing system which has been developed. This permits designers to apply not only the steady set of forces to the system, but also the transient excitations. Thus a clearer picture can be gained of the fatigue loading imposed.
A transient loading model for a SPP has been developed and compared with the experimental results. This enables evaluation of the effect of changes to propeller geometry on excitation loads.

Taken together, the experimental data, finite element model and transient load model significantly extend the understanding of the behaviour of SPP systems and provide the designer with a useful tool for determining the complex transient stresses under which these systems operate

Contents

List of Figures

List of Tables

Acknowledgements

I am very grateful for the help and encouragement of the following people during the preparation of this thesis:

- My wife, Maggie, and the boys, Ben and Jonathan for their constant support.
- Dr David Grieve of the University of Plymouth, for acting as Director of Studies, for his sustained encouragement and advice, and for his ready availability whenever I needed to talk things over.
- Dr John Chudley for acting as supervisor, and for his unwavering optimism in the face of my unwavering realism.
- Mr David Short for offering valuable advice from his wealth of experience.
- The technical staff in the Department for their skill and willingness to help, particularly Rob Crocker, Neil Fewings, Terry Richards, Colin Stansbury and Mike Stringer.
- Mr John Wiltshire of DERA for his continuous practical help and encouragement.
- Rob Madle and Bill Thompson of Teignbridge Propellers Ltd for their advice.

Declaration

At no time during the registration for the degree of Doctor of Philosophy has the author been registered for any other University award.

This work was funded by EPSRC Research Grant GR/L11571 and was part of the UK Fast Craft Programme managed by Marinetech South Limited.

Principal sponsors were Teignbridge Propellers Ltd and DERA Haslar.

Publications by the author, in connection with this research, are included at the end of the thesis.

Signed 

Date 12 October 2000

1. INTRODUCTION

1.1. Background to Surface Piercing Propellers

High speed craft, that is craft designed for sustained speeds above 30 knots, were at one time a luxury in the domain of the leisure and racing boat fraternities. Increasingly, they are now routinely used in many commercial and military applications. Propulsion systems for these craft are a key issue, with the usual design demands of low initial and through life costs, low weight, low volume and high efficiency imposing conflicting requirements.

As conventional propellers are used at progressively higher speeds two factors begin to dominate their operation and lead to a degradation in performance. Firstly, cavitation becomes excessive and destructive; since cavitation cannot be avoided at high speed, blades must be designed to accommodate it, with a supercavitating wedge section which encourages the formation of a large vapour bubble across the entire suction surface. This avoids the damaging collapse of small vapour bubbles, but reduces the effectiveness of the propeller since the pressure on the back of the blade becomes limited to vapour cavity pressure, rather than the classical pressure distribution expected for a foil. Thus the dominant component of lift from the blade comes from the pressure face. Secondly, the hydrodynamic drag on the support structure for the propeller and shaft becomes excessive at speed and propulsive efficiency therefore deteriorates significantly.

In order to avoid the second of these problems, racing power boat designers have become accustomed to mounting propellers so that the shaft line is approximately on the waterline when the vessel is planing. This also has the advantage that the propeller diameter is not limited by the clearance available under the vessel or the need to avoid excessive shaft inclination, and may be sized with more emphasis on efficiency. Thus surface piercing

propellers (SPPs) were born as a result of the need for lightweight, high speed propulsors in racing craft and have evolved in that fraternity for number of years.

In commercial high speed applications, the most popular propulsion system is undoubtedly the waterjet, which has gained almost universal acceptance in a wide range of applications from jet-skis to high speed ferries. Continued development has led to higher efficiencies, and many other advantages are claimed including improved manoeuvrability and reduced vibration. However there remain some drawbacks, principally the installation weight, inlet duct configuration and possible air ingestion in a seaway or on very high speed craft. Amongst the alternatives to waterjet propulsion, the surface piercing propeller is attractive because of its relative simplicity and low weight.

However, designers wishing to specify SPPs find that, although some good applied research has been carried out on the subject, available performance data is scarce compared with that for alternative high speed propulsors. The result is that, where SPPs are used, confidence in their performance predictions is low, and drive systems tend to be over-engineered in order to allow for the large number of unknowns. Consequently, all-up weight tends to be higher than it needs to be, adversely affecting performance and costs are increased; alternatively if higher risk designs are used then reliability may be low.

1.2. Project Aims

The SPP system under consideration for this work comprises the propeller, shaft, bearings and bearing housings. This constitutes a dynamic system, excited principally by the time varying hydrodynamic loads exerted on the propeller, together with some input from the engine, and subject to support stiffnesses at the bearing housings and shaft coupling.

The propeller excitation is the aggregate of the lift forces generated by the blade sections, and may be analysed as a six component force (3 forces, 3 moments) acting at the hub. This complex transient load system induces stresses in the shaft and propeller blades, and transmits forces to the hull structure, which depend on the system dynamics and are difficult to predict.

Previous design methods have used mean loads to determine mean stresses and have then made allowance for unknowns by the use of large factors of safety, or uncertainty factors.

The aim of this project is to develop a methodology which will allow the system to be designed accounting for the dynamic loads imposed and thus introduce more certainty into the design process.

1.3. Project Overview

The project addresses the need for specific experimental data to supplement that already available from other workers. While some mean load data and performance charts currently exist, and are available to designers, there is very little information on time varying loads. An experimental programme has been devised which provides both mean and transient loads. These measurements have been used to determine the nature of the hydrodynamic excitation applied to the propeller system, and form the basis of the input to a finite element model. Computer models of transient loading conditions have also been developed to advance understanding of the excitation forces and together, these models and experimental data have been formulated into a design method. Validation against real data has been carried out at component level (with individual propellers and shafts) and at physical model level (using the experimental test rig).

1.4. Organisation of Thesis

Subsequent chapters of the thesis are organised as follows.

- **Chapter 2:** Surface Piercing Propellers - Current State of Development.

  An overview of work undertaken on SPPs is given. Work carried out on the theoretical front has advanced understanding of the factors influencing SPP performance and extends to a 3D propeller model. However the conditions modelled are limited and experimental results remain the key source for the designer. Experimental work is reviewed and this shows that, while there are data for some methodical tests measuring mean performance, there is a lack of knowledge of the time varying loads imposed by SPPs over the range of operating conditions.

- **Chapter 3:** Finite Element Modelling of the Propeller Drive System.

  A finite element model of a propeller, together with its associated added mass when submerged and partially submerged, was constructed and validated against laboratory tests. Following this a model of a propeller-shaft system was created and subjected to a transient load regime of a type expected from the experimental test programme. In determining these predicted transient loads, a computational model was developed which may be used to show the effects of changes in blade shape and immersion on the excitation amplitudes.

- **Chapter 4:** Design and Commissioning of Test Rig , and Experimental Procedure.

  A test programme was undertaken to determine the mean and time varying loads imposed on a SPP system. For this, a purpose made test rig was designed and manufactured. This was installed into a circulating water channel with a low pressure facility. The range of tests covered comparisons between four propellers of different blade profile, but having the same pitch, diameter and area ratio and the operating conditions variables were advance coefficient, immersion and angle of yaw.

- **Chapter 5:** Presentation and Discussion of Experimental Results

  Mean results are presented and are found to compare well with results of previous workers. Of particular interest are the side and vertical forces which impose a significant load on the shaft. Also commented upon are the effects of shaft yaw which may be used, with care, to augment the propulsive thrust. The transient results are presented in both the time and frequency domains, and are also summarised across the operating range by presenting the RMS values of the vibration amplitudes. The differences between the propellers tested and the influence of operating conditions are discussed.

- **Chapter 6:** Design Methodology.

  By scaling and applying the mean and time varying loads to the finite element model developed in Chapter 3, the peak stresses in the shaft may be determined. A typical example is taken of a craft in service and stresses are examined using both a mean load approach and the finite element transient model. The former gives stress levels well within yield limits, while the latter shows that peak stresses closely approach the infinite life fatigue limit for the material. Thus a revised design giving lower stress levels would be recommended.

- **Chapter 7:** Conclusions and Recommendations.

  Conclusions are drawn and recommendations are made in the light of this project for further work.

- **Appendix A:** Mean Propeller Performance Data.

  Mean experimental performance data is presented in graphical form. Plots of the key performance coefficients are given, comparing the effect of different propellers, immersions and angles of yaw across the operating range tested.

- **Appendix B:** Transient Propeller Performance Data.

  Transient experimental results are presented in graphical form. For each of the three components of force, and three of moment, results are presented in both the time and frequency domains. These are given for each propeller at 50% immersion, zero yaw, and also for the 4 bladed straight trailing edge propeller for different immersions and yaw angle. To facilitate comparisons, and identify behaviour across the operating range, the RMS values of fluctuations are plotted against advance coefficient for each case.

- **Appendix C:** Illustrations of the Test Rig.

  Photographs of the test rig and presented.

- **Appendix D:** Typical PAFEC Data File.

  A typical data file is presented, showing the modular structure of the code and particular features of PAFEC which were implemented for this particular application.

- **Appendix E:** Publications.

  Papers presented by the author in connection with this work and the final EPSRC report are reproduced.

2. SURFACE PIERCING PROPELLERS - CURRENT STATE OF DEVELOPMENT

2.1. General Principles

A comparison of propulsive efficiencies for different types of system is given by Allison (1978) (Figure 1). Although this data is now somewhat old, and waterjet efficiencies have developed to significantly higher levels, it does show clearly the tail-off of conventional

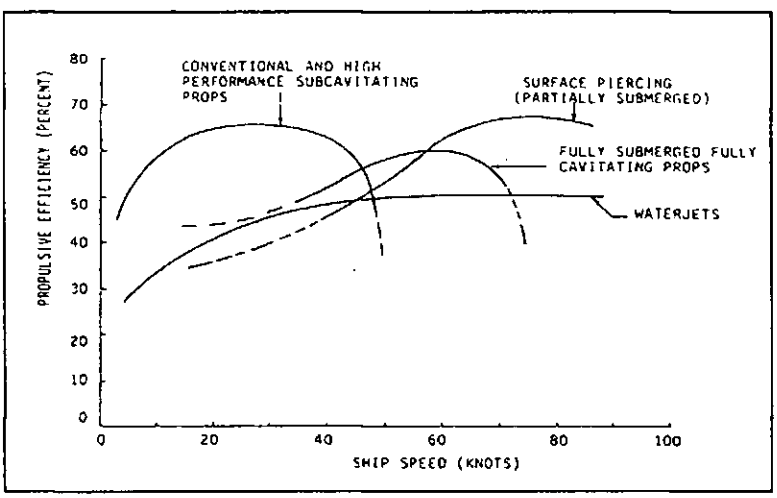

Figure 1. Comparative Propulsive Efficiencies (from Allison(1978)).

propeller efficiency and the advantage of the SPP above 60 knots. Rarely is a decision to use a particular configuration made on grounds purely of propulsive efficiency, and if other factors such as installation simplicity and weight are taken into account, then the range of applicability for SPPs stretches to much lower speeds.

As far as hydrodynamics are concerned, the principles are similar to those for a supercavitating blade, for which a vapour cavity covers the back and lift is produced principally by pressure on the face. However the blade now ventilates rather than cavitates, with what was a vapour filled cavity becoming an air filled one. Also, what was a pseudo-steady process (with relatively small variations due to shaft inclination and vessel wake) becomes a transient one, with lift forces becoming intermittent as each blade enters

and leaves the water. The existence of the cavity leads to a significant change in the design of the blade section. Rather than being a conventional foil shape whose principal purpose is to accept a wide range of angles of attack without separation, the section is wedge shaped (Figure 2). The sharp leading edge promotes separation in order to establish a stable cavity, while thicker sections near the trailing edge provide structural rigidity; in this region, provided the metal lies within the bubble, then its shape and thickness do not influence the hydrodynamics. A sharp corner near the trailing edge provides a stable reattachment point for the cavity, and a pronounced cup on the face near the trailing edge improves lift to drag ratio.

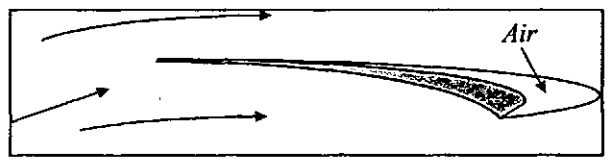

Figure 2. Typical SPP Blade Section.

In studying the performance of SPPs it is useful to refer to an operating regime chart (Figure 3) first produced by Brandt (1972) and since quoted by others (Olofsson (1996),

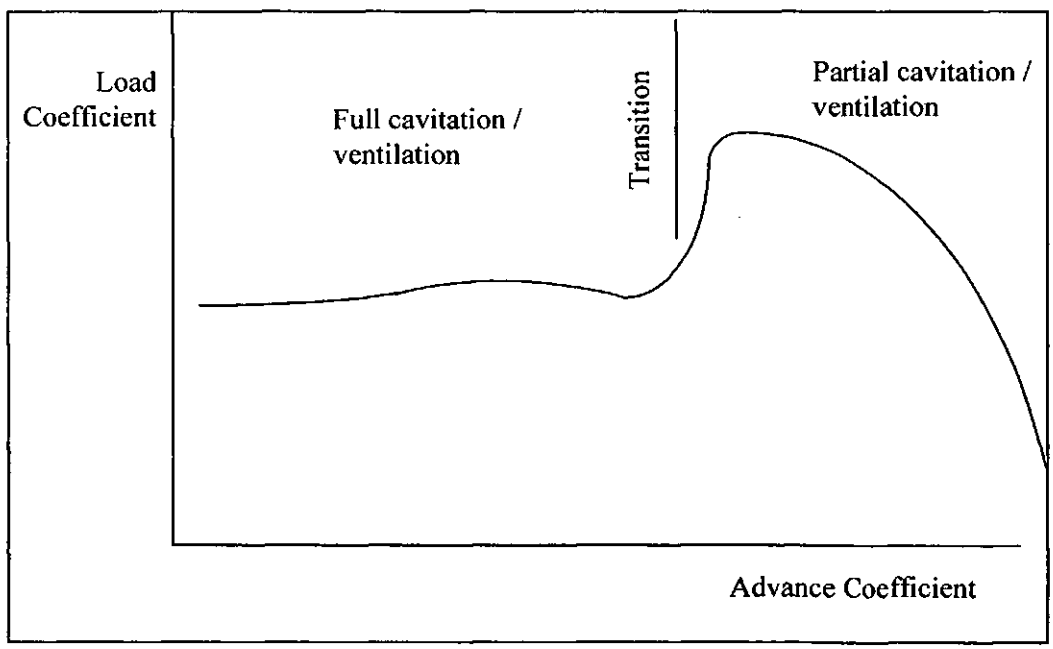

Figure 3. Operating Regimes.

Kruppa (1972)). The key point arising from this is the clear distinction between partial ventilation or cavitation and full ventilation or cavitation. In the "partial" regime, cavities cover only part of the back of the blade which allows some hydrodynamic lift from this surface. In the "full" regime a cavity covers the entire back and lift is dominated by forces on the blade face; thus the thrust and torque coefficients fall and become less dependant on advance coefficient, since without the suction surface contribution, lift becomes less dependent on angle of attack on the foil. The fall in output in the fully ventilated regime is graphically illustrated by results from Ferrando and Scarmadella (1996) who tested a conventional propeller over a range from fully immersed to low immersion ratio. As can be seen from Figure 4 the pattern of rising thrust coefficient with decreasing advance coefficient is maintained for the surface piercing cases, though at a lower level than the fully submerged cases, up to the point where full ventilation occurs; there is then a marked fall in K_t compared with the fully submerged propeller which is able to benefit from the increased angle of attack at high load.

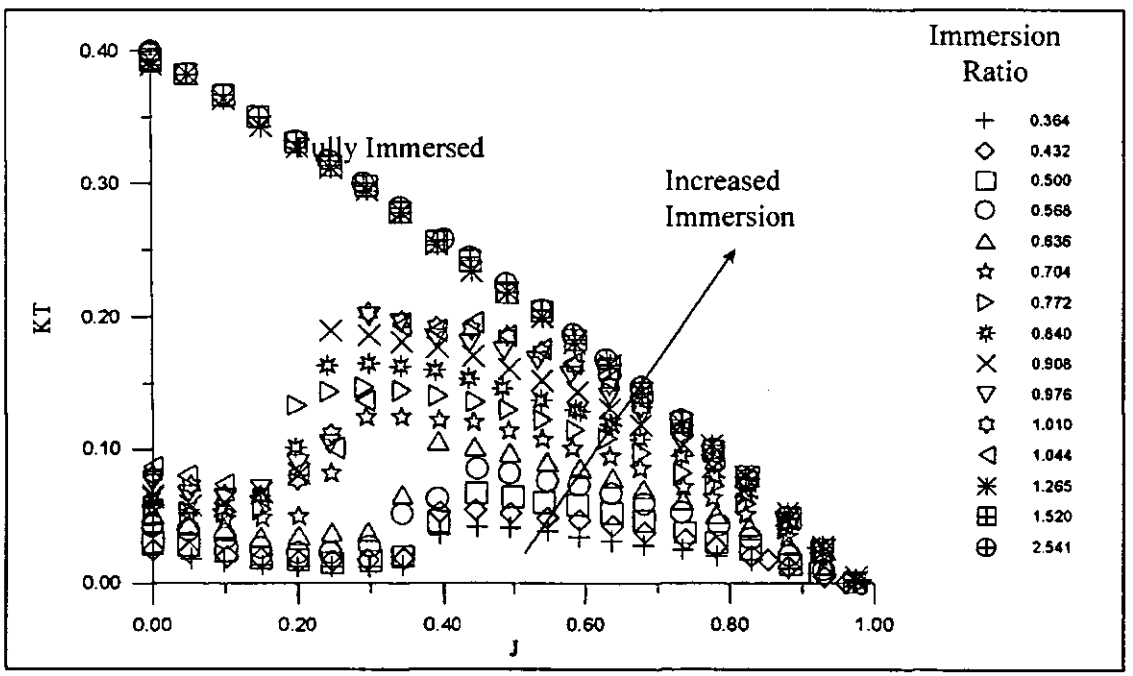

Figure 4. SPP Performance (from Ferrando and Scarmadella (1996)).

It should be said that, in the interests of brevity, the term "ventilation" is used here where strictly speaking, ventilation and cavitation may be taking place, with a mixture of air and cavity bubbles forming. The relative influence of these two types of cavity has been investigated by Brandt (1972) and further expanded upon by Olofsson (1996).

The position of the transition region is clearly an important factor to the designer, since performance changes abruptly in this region, instabilities exist, vibrations levels have been observed to rise and efficiency peaks on the partially ventilated side of transition where lift/drag ratios are highest. The nature of the water surface and spray pattern also changes markedly, with the surface being substantially elevated in the fully ventilated region.

2.2. Review of Theoretical Work

Substantial modifications to conventional foil theory need to be implemented in order to analyse SPPs. Firstly, the flow field is modified by the presence of the gas bubble attached to the back of the blade and trailing into the wake. Work in this area has already been carried out for the case of supercavitating sections, and in this respect, SPPs behave similarly. However the presence of the free surface, and the consequent transient nature of the flow field, together with the constantly changing wetted span of the blades requires further modifications to the theory.

DP Wang has developed the linearised theory for a 2-dimensional ventilated foil entering vertically into an infinitely deep ocean (1977). He then considered the case of a foil entering and exiting the water obliquely (Wang (1979). Examination of the initial and boundary conditions which Wang used for this transient process gives an insight into the physical situation. Referring to Figure 5, it is assumed that the cavity is formed as soon as the leading edge penetrates the water; the trailing edge, similarly gives rise to the other cavity wall. Initially the water is motionless, which implies an initial condition for the

velocity potential (ϕ) of zero in the entire flow field. The free surface and free cavity walls

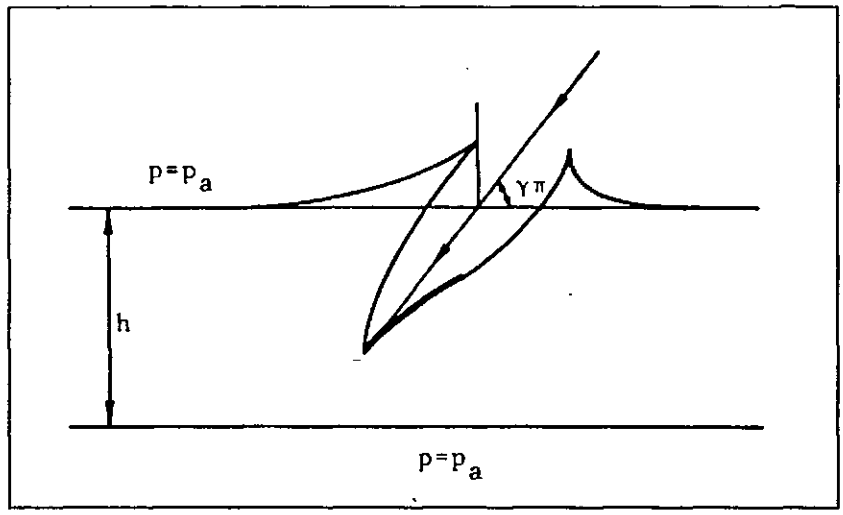

Figure 5. Oblique Entry of Fully Ventilated Foil into a Layer of Thickness h (from Wang DP (1979)).

are subject to constant (atmospheric) pressure throughout the process, from which it may be deduced that ϕ is constant with time on these surfaces during the transient (for a steady flow situation, the velocity along these surfaces would be constant). Finally the foil itself is impermeable and fluid velocity normal to its surface equals that of the foil.

The long and complex procedure is carried out for a circular arc foil section and yields pressure distributions, which by integration over the wetted surface give force and moment coefficients for various states of immersion. Since this is a 2-dimensional analysis, the length of arc swept by a blade is simulated by the thickness, h, of a layer of water through which the blade passes. Examination of the force coefficient transients shown in Figure 6 reveal that loading increases with h, demonstrating that the proximity of the water surface has a significant effect on the flow and pressure fields; for comparison, the load at $t = \infty$, $h = \infty$, which is equivalent to the supercavitating case remote from the surface in deep water, forms an upper bound to the surface piercing cases. The advance coefficient, λ, also has an effect, with load rising as λ rises, but it must be born in mind that for each λ the angle of attack is reset to give smooth entry, so each is an "on design" case.

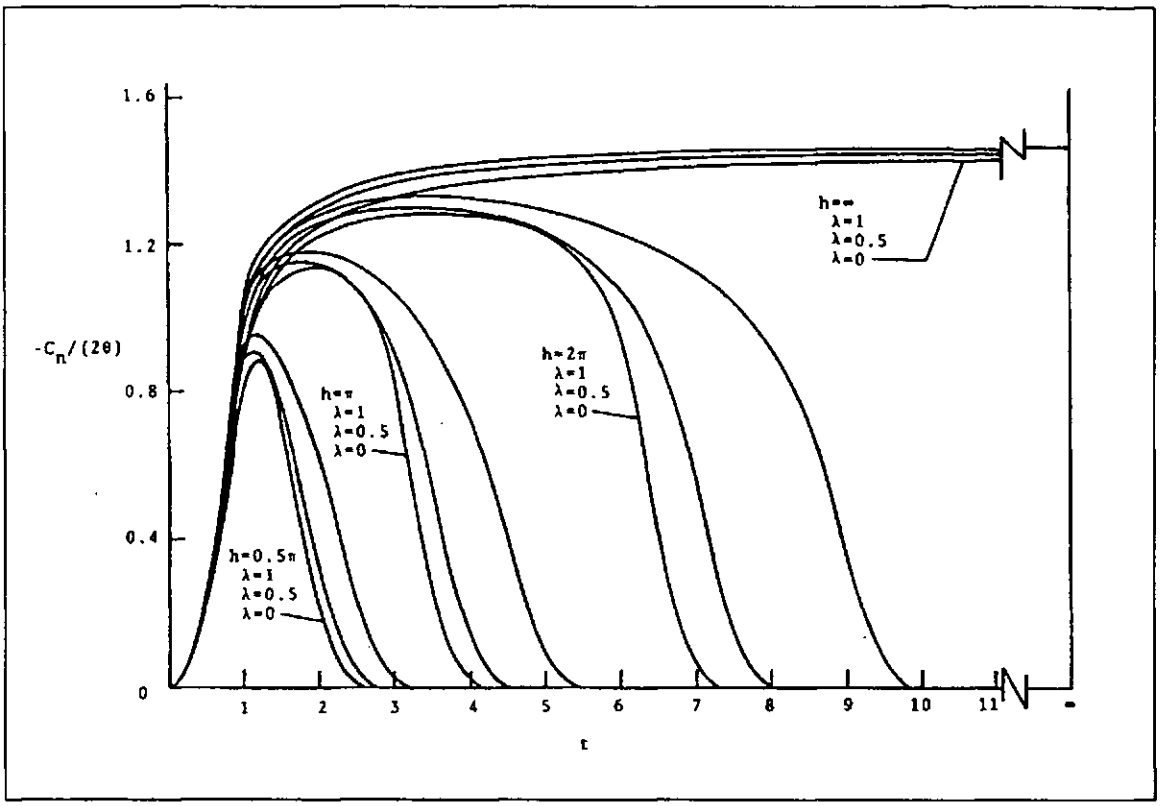

Figure 6. Force Coefficient versus Time and Advance Ratio (λ) for a Circular Arc Foil Entering a Layer (from Wang DP (1979)).

At this point, it is worth considering the effect of angle of attack on the foil. Classical foil theory gives the lift coefficient - angle of attack relation as $C_L = 2\pi\alpha$. However, it can be shown that for the simple case of a flat plate with a long cavity attached, $C_L = \frac{\pi}{2}\alpha$; the presence of the cavity, with its effect on pressure on the back of the blade reduces lift to one quarter of it non-cavitating value. One implication of this is that the lift force is less sensitive to changes in angle of attack, and thus vibration forces which would be induced by these changes are reduced.

Work by Furuya (1985) extended Wang's analysis to that of 3-dimensional flow through a ventilated, partially submerged propeller. Representing the blades as a series of lifting lines, Furuya first used Wang's theory to determine the lift force on a 2-dimensional foil, assuming that incidence angle is determined by the blade geometry and global flow directions. This lift force then modifies the pressure and flow fields, which produces

induced flow velocities, and changes the incidence angle. Wang's theory is again employed using these new conditions, and the iterations continued until convergence. In a further extension to existing theory, Furuya applied his code to a two-term camber foil section, a type often used for ventilating propellers. Integrating over all blades, allowing for the varying wetted span, and averaging over time, he produced torque and thrust coefficients for comparison with experimental results by Hadler & Hecker (1968). In the fully ventilated region, results for thrust coefficients compared favourably, but there were significant discrepancies with torque coefficients, attributed to the effects of non-linearity, thickness of blade and cavity, and relatively large induced velocities at low J. Nonetheless the paper provides a valuable understanding of the way in which the flow is established during the transient, and the variation of lift force with rotation.

On this latter point, Furuya's work detects a lift force reversal on the leading edge of the blade as it strikes the water surface, since the flow first impinges on the back of the blade

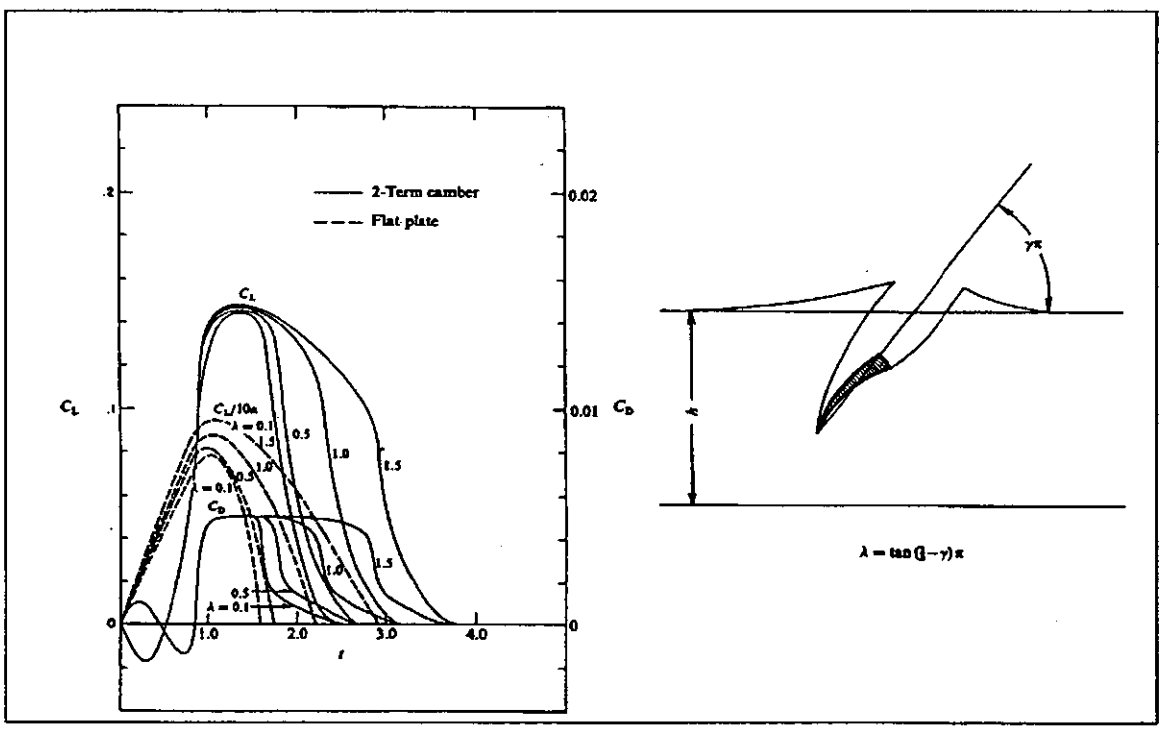

Figure 7. Two Dimensional Lift and Drag Coefficients for Tulin-Bukart Two Term Camber and Flat Plate Calculated with Wang's Theory (from Furuya (1985)).

before conventional flow is established (Figure 7). This reversal, he suggests, may explain fatigue failures experienced with such blade shapes and points to a move away from two-term camber type profiles, with their negative slope region at the leading edge, to ones with a smoother straight line front section.

GQ Wang (1992) investigated the cases of fully submerged propellers near the surface and fully ventilated propellers. He employed a similar approach to DP Wang, using a lattice of sources to represent blade and cavity thickness, vortices to give lift, and an image of the blades to impose free surface conditions. For the ventilated case, blade thickness was ignored. For the submerged propeller, the proximity of the free surface was found to significantly modify the flow and reduce loading, and his results were well supported by experimental data. In the ventilated case, he determined both potential and viscous forces and thus found thrust and torque coefficients. Comparison was made with both experimental results by Hadler & Hecker (1968), and others, and with Furuya's (1985) theoretical results; satisfactory agreement over a limited range was claimed.

Work discussed so far has addressed thrust and torque, derived from a knowledge of lift and drag on the blade sections. Vorus (1991) has considered the nature of side and vertical forces, which, for SPPs, have a significant impact on shaft and bearing design, and of moments about transverse axes which can produce a small vessel trimming torque and a significant steering torque. By applying conventional propeller theory, treating the hub as an integrator of individual blade forces, he considers the cyclical loading on the propeller. Approximating the blade loading to a step function and expressing this as a Fourier series, he utilises the fact that the first harmonic of the lift force on the blades provides a steady side/vertical force. His analysis also accounts for variation in lift force away from the simple step due to propeller inclination and yaw, since lift increments may be estimated from a knowledge of changes in incidence angle by using the lift equation previously

discussed, $\Delta C_L = \frac{\pi}{4}\Delta\alpha$. Thus, starting with a blade lift calculated from the total thrust requirement and a known blade lift distribution, he is able to estimate the influence of inclination, yaw, rake and skew on side/vertical loads, and also on moments. As far as propeller geometry is concerned, he concludes that blade rake has a significant impact on vertical force and the moment about a horizontal axis, both of which can affect vessel trim. However blade skew is of only secondary importance in terms of these forces, although it may be utilised to reduce vibration forces and reduce blade stresses by spreading the leading edge impact time. Inclination and yaw angle have a significant impact, with transverse forces produced which may be in the order 50% of thrust, and steering torque in the same order as the shaft torque.

While this review of theoretical aspects is by no means fully comprehensive, references have been chosen to illustrate the particular challenges which SPPs present, and the advances which have been made in the understanding of their behaviour. There are significant gaps, not least in the analysis of the transition and partially ventilated regions, in the determination of the effect on water surface level, particularly at low J and in the knowledge of time varying loads. In these areas, and others where agreement between theory and practice is far from good, the contribution of experimental workers is vital, and it is to this we now turn.

2.3. Review of Practical Testing

Hydrodynamic performance data is derived almost universally from model scale tests and little data has been found in the open literature relating to full scale testing. Broadly there are two categories of experimentation; that taking an overview, carrying out conventional testing of the propeller as a whole, and that which examines the detail, looking at the performance of a single blade. While the former usually relates only to the steady state, the latter provides information on the dynamic behaviour of individual blades.

2.3.1. Propeller Performance Testing

A summary of four significant contributions to the experimental database is shown in Table 1.

Table 1. Experimental Test Details.

	Hadler & Hecker (1968)	Rose & Kruppa (1991) Rose et al (1993)	Ferrando & Scamardella (1996)	Olofsson (1996)
Propeller	NSRDC super-cavitating No 4002 12" dia P/D 1.319 2 bladed No 3820 15.5" dia P/D 1.628 3 bladed No 3767 16" dia P/D 1.18 3 bladed No 3768 10"dia P/D 1.18 3 bladed	Rolla 250 mm dia P/D 0.9, 1.1, 1.2,1.4, 1.6 4 bladed A_e/A_o=0.8	SPP No E9401 250 mm dia P/D 1.2 A_e/A_o=0.8 Wageningen B No E042 180 mm dia P/D 1.4 A_e/A_o=0.95 Large dia model No E1184 294 mm dia P/D 0.85 A_e/A_o=0.525	KaMeWa 841-B 250 mm dia P/D 1.24 4 bladed A_e/A_o=0.58
Advance coeff't & max velocity	0 - 1.3 6.4 m/s	0.7 - 1.6 8 m/s	0 - 1.45 approx. 4.7 m/s	0.4 - 1.3 12 m/s
Cav No.	Atm	0.2	Atm	0.15
Inclin'n		$4^0, 8^0, 12^0$	$4^0, 6^0, 8^0$	$0 - 5^0$
Yaw				$0\text{-}30^0$
Imm'n Ratio	33% - 60%	30%, 47.4%, 58% (tied to inclination)	40% - 80% (and fully submerged)	33%
Test Environ-ment	Towing tank	Cavitation tunnel	Towing tank & cavitation tunnel	Cavitation tunnel

Early work by Hadler & Hecker (1968) provided a good foundation and has frequently been referred to in the literature, particularly when validation of theoretical work has been required. They provide in their paper an excellent historical perspective, tracing the earliest SPPs back over one hundred years, and then report an extensive series of tests. They note the two distinct operating regimes - base (or partially) ventilated with the bubble forming on the blunt trailing edge of the blade, and fully ventilated with the bubble extending from the leading edge across the suction surface. Efficiency is higher in base vented, as a result of a higher lift/drag ratio, and can approach that of conventional propellers. However, efficiency reduces significantly as operation moves into the fully ventilated region and the range of operation at high efficiency is significantly reduced compared with conventional propeller experience.

In the fully ventilated condition, at low advance coefficients, a rise in surface level upstream of the propeller is observed, indicative of significant blockage of flow through the inter-blade spaces and the associated pressure field. This is supported by another worker in the discussion section of the paper, with the comment that the blockage can lead to low mass flow being accelerated through the disc, and thus low thrust and torque.

On the subject of foil section, the importance of using the supercavitating type wedge with concave pressure face is discussed, and compared with a conventional aerofoil which shows a marked fall in performance under fully ventilated conditions, since the bubble formation adversely changes the effective camber. This last point is supported by Shaozong & Hengshun (1988) who tested both wedge and crescent shaped sections. They found their performance similar in the partially ventilated region, but observed a more marked fall in K_t and K_q as operation moved into the fully ventilated regime. Finally from Hadler & Hecker (1968), observations in the transition region reveal considerable vibrations as a result of flow instabilities. Although a low number of blades was used for

propellers in this work, which would in any case increase vibration levels, this observation is characteristic of the transition region in general.

Since the practical consideration of machinery arrangement makes shaft inclination almost inevitable, Hecker (1973) went on to perform further tests, this time on 8 bladed propellers, specifically to determine the effects of blade rake and shaft inclination. His results indicate that shaft angle should not exceed rake angle and that excessive (above 20^0) shaft and rake angles should be avoided. Regarding the vertical force, he found that the dominant factor was submergence, with this force increasing by as much as a factor of five between 30% and 50% submergence, even though thrust only doubled.

Kruppa (1972) has made valuable contributions in the field of testing SPPs over many years. In this paper he discusses the scaling laws which are relevant. A key scaling parameter is the Froude number, $Fr = \frac{V}{\sqrt{gD}}$. As a descriptor of the fluid inertia effects (which form cavities) compared with gravity effects (which destroy them), it is important that Fr is modelled if similar flow conditions are to be recreated in the model as exist at full scale. It can be argued that the cavitation number, $\sigma = \frac{p_{static} - p_{vapour}}{\frac{1}{2}\rho V^2}$, amounts to the same condition; this would only be true, however, if the cavities were purely ventilated. In fact some cavitation (with vapour cavities rather than air) can also occur and indeed may trigger ventilation. Thus the cavitation number also needs to be modelled in scale tests. This necessitates the use of variable pressure test tanks. Other scaling considerations concern viscous effects (Reynolds number) and surface tension (Weber number); Kruppa comments on the test conditions required to avoid scaling problems with these. He also raises the problem of tunnel wall and blockage effects.

Later, in a further paper on testing, Kruppa (1992 Testing ...) comments on the need for a knowledge of wake conditions in a test channel; it is unlikely that real wake conditions can be modelled, since little data on this exists, but at least the test conditions need to be well defined. He also discusses shaft inclination, pointing out the need to measure forces perpendicular to the shaft line and include these in the horizontal force calculation. Referring to his own tests on a 7 bladed controllable pitch SPP, he comments on the lowering of efficiency near the design point as inclination is increased, and also quotes typical maximum loadings in the region of $K_t/J^2 = 0.2$, rising to perhaps 0.35 for higher immersions. Elsewhere (Kruppa 1992 Aspects ...) he quotes a value of 0.5 for low P/D and high immersion ratios, but nonetheless, the thrust required to overcome 'hump' conditions and to give adequate acceleration at low speed needs to be carefully considered.

Rose and Kruppa (1991) and Rose et al (1993) have carried out a methodical series of tests, measuring thrust and torque, together with vertical and horizontal forces and moments. By reducing pressure they were able to test at a cavitation number of 0.2, a value in the region of the full scale figure. Typically the ratio of vertical force to thrust is in the region of 0.6 in the working range at high immersion, and falls with immersion ratio; the ratio of side force to thrust is highest at low immersion, also in the region of 0.6. Using their results, they go on to comment on shaft design considerations and bearing forces. Radojcic (1997) correlates their results, fitting polynomial curves, in order to aid the design process.

Ferrando & Scamardella (1996) have also recently embarked on a testing programme. Their testing takes in various depths up to fully immersed, which clearly demonstrates the divergence between conventional and SPP operation, particularly at high load. They also attempt to correlate immersion by redefining the torque and thrust coefficients in terms of immersed disc area. A similar approach had been used by Hadler & Hecker (1968), using a

different form of coefficient, though Kruppa (1972 Testing ...) was uncertain about it for fully ventilated conditions in view of the difficulty in determining the position of the free surface. His scepticism appears to be confirmed by these results, which correlate reasonably for partial ventilation, but show scatter for fully ventilated conditions. This test programme continues.

Figure 8 gives a broad comparison of a selection of results from several of these workers. Although there are differences in propeller types used and test conditions, the curves do knit together as a family and an overall picture is clear, showing qualitatively the effect of pitch / diameter ratio on load and transition, and the effect of immersion ratio.

2.4. Single Blade Testing

It has been recognised that, in addition to the essential performance data described above, a

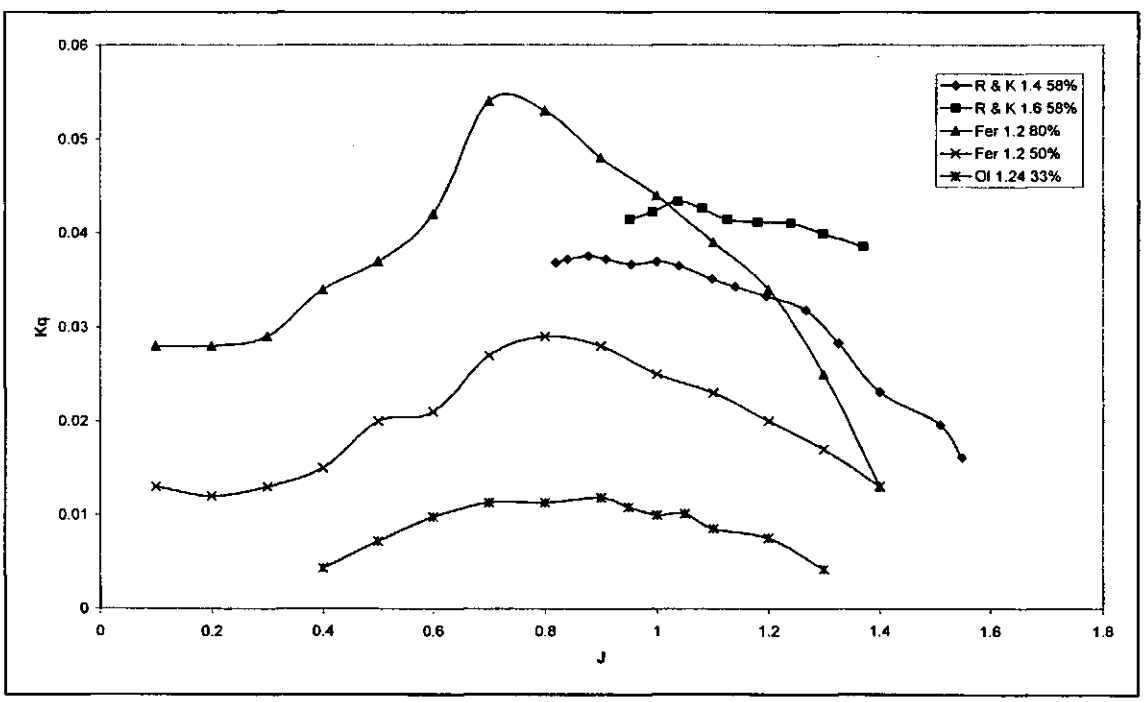

Figure 8. Comparison of Torque Coefficient versus Advance Coefficient from Various Workers. (Rose et al (1993), Ferrando (1996), Olofsson (1996)).

level of detail below that is required if a better understanding of the operation of SPPs is to be gained.

In a major piece of work, Olofsson (1993 & 1996) mounted a blade on a flexure housed in the hub, in order to investigate the transient forces acting during one revolution. An

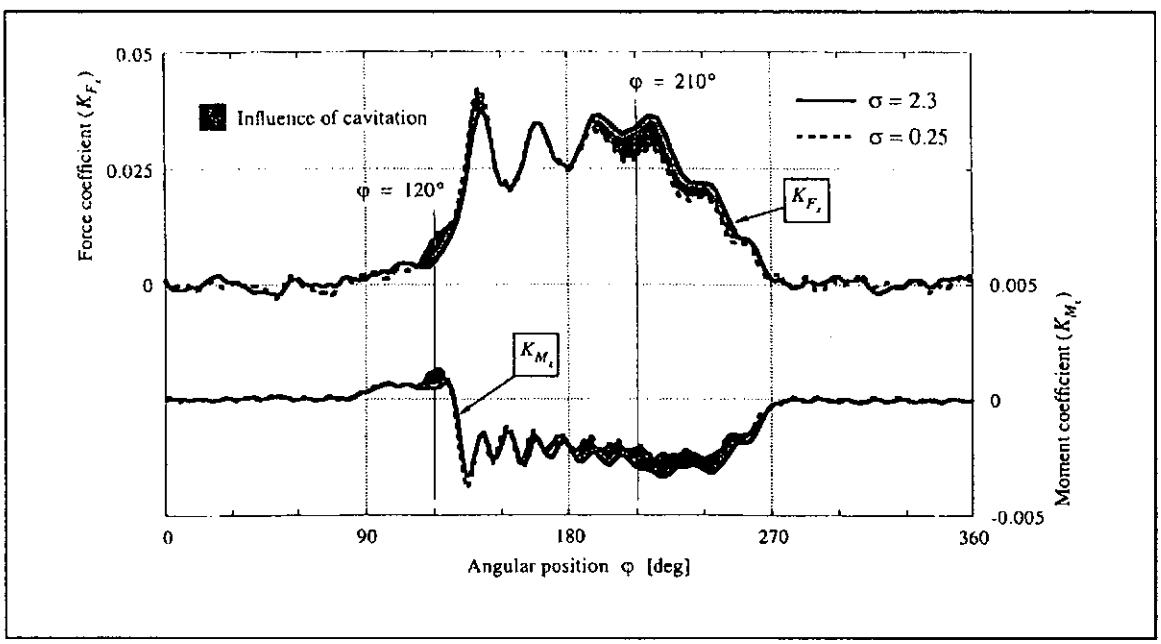

Figure 9. Influence of Cavitation on Dynamic Blade Load Coefficients (from Olofsson(1996)).

example of the loading pattern observed from his work is shown in Figure 9. Clearly visible are the initial impact and sudden rise in load as the blade strikes the water. This particular example also shows the effect of cavitation, two cases being compared with the same J and Froude number but different cavitation numbers. It is evident that a decrease in cavitation number causes two conflicting phenomena: during the entry part of the rotation, there is an increase in force, during the exit phase a reduction. The decrease in cavitation number encourages cavity growth, particularly in the tip region. This is supported by photographic evidence and, as Olofsson explains, leads to a cavity blockage effect, reducing axial velocity and increasing angle of attack leading to an increase in lift; alternatively, the rapid growth of cavities, encouraged further by the increased angle of attack, may degrade hydrodynamic performance and reduce lift. The former occurs in the

entry phase, the latter at exit. The overall effect is indeterminate, and both rises and falls in total lift have been reported. What is clear is that a cavitation number effect exists which should be accounted for when modelling.

He also investigated the effects of varying Froude number, the criterion which governs the depth to which a cavity is drawn down and its duration before collapse. Similar reasoning as for cavitation number applies; he concluded that above Fr = 4, effects are negligible while below this figure careful attention needs to be paid to scaling this quantity.

Vibration characteristics were also investigated by Olofsson. The fluctuations which are visible in Figure 9 are attributable to blade inertia effects, and when a Fourier analysis is carried out, the fundamental frequencies are those of the blade in air and in water. Interestingly, Froude number appears to affect vibration characteristics inasmuch as, at low Froude, when cavities are smaller, the damping effect of the water is more pronounced.

From among many other conclusions which Olofsson drew, one more is commented upon here. The effect of yaw angle had been little reported upon previously, but appears to be of some significance. Figure 10 illustrates the change of efficiency as yaw changes up to 30^0 and demonstrates a marked improvement. Effectively, under conditions of optimum yaw, the horizontal force produced by the propeller is providing useful thrust, with the resultant of the horizontal and axial shaft forces being directed forward.

An individual blade has also been investigated by Keller (1995), in work which was particularly interesting since it was carried out at full scale during sea trials. By instrumenting links, trunnions and the blade root of a controllable pitch SPP with strain gauges, he was able to assess the transient stress levels and frequency spectrum from which he was able to deduce information about fatigue loading on the system.

2.5. Applications

Application of SPPs is increasingly extending beyond the original rather narrow category

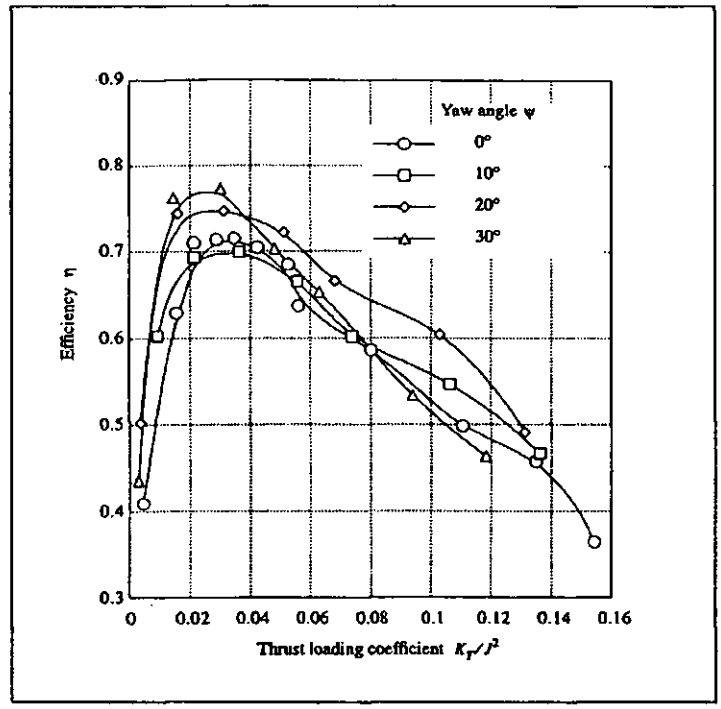

Figure 10. Propeller Efficiency versus Thrust Loading Coefficient at Various Yaw Angles (from Olofsson (1996)).

of racing power boats. One example of the latter is the SM Racer (Acompara 1995), an Endurance Racer designed for a cruise speed of 80 knots, which achieved a top speed of 104 knots. This was equipped with four Rolla designed stainless steel four bladed SPPs, having 15^0 rake and skewed such that the trailing edge was straight (the cleaver style of blade). Some other recently documented examples of typical applications are:

- Cary 21 m yacht, capable of 60 knots (Pike (1997)). This has a single Arneson Drive powered by a Lycoming TF40 gas turbine, supplemented by two Deutz diesel powered Amjet waterjets. The latter are used for manoeuvring and cruise conditions with the Arneson trimmed out of the water; this is then lowered and used with the waterjets for full power.

- Magnum 13.5 m fast patrol boat (Speed at Sea (1997)), capable of speeds in excess of 52 kts and powered by Arneson Drives / Rolla propellers.
- VSV 50 (Very Slender Vessel) (Motor Boat (1996)), top speed of 50 kts on diesel or gas turbine powered Mercuiser Drives / Rolla Propellers. Applications as camera platform for yachting events and in military patrol work.
- Super Dvora Israeli Navy patrol boat (The Naval Architect (1996)), 23 m with a top speed of 50 kts using MTU diesels, Arneson Drives with Rolla propellers.
- Corsair SES (Allison (1978) & MER (1993)), ferry or military platform, approximately 45 kts, propelled by dual mode (submerged/SPP) controllable pitch SPP.
- The examples quoted here demonstrate the increasing range of applications for which SPPs are being considered.

Perhaps the fullest description of a design procedure in the open literature is given by Allison (1978). In his comprehensive review of Propellers for High Performance Craft, he discusses the data required for the design process, referring for illustration to the design of a large Surface Effect Ship. He considers both engine and hull matching, emphasising the need to size the propeller with reference to both the 'hump' condition, when it may be fully submerged, and the full speed condition. He also reports on impact pressure measurements and predictions which are used to model the transient stresses arising in the blade, essential information if fatigue loading calculations are to be carried out reliably. He further discusses blade structural design, comparing practical static and dynamic results from strain gauge measurements with finite element stress models.

Kamen (1998), in a readable account of his own considerable experience with SPPs, describes their advantages and some common problems encountered. The latter include: vibration, which, he finds, often arises from shaft misalignment rather than being an inherent propeller problem; poor performance astern, resulting from either poor

hydrodynamic performance of the 'cleaver' type blades astern, or because of the installation configuration, either within a tunnel or with side curtains; finally, he comments on the problems of overcoming the 'hump' resistance with a SPP which is probably fully submerged and whose top half is operating in a highly disturbed wake. In a brief look to the future, he envisages the possibility of applications to larger, low speed vessels, the use of controllable pitch and counter-rotating configurations, and the use of composite materials for blades.

A practical account of a SPP installation is given by Van Tassel (1989). Describing the development of the Air Drive concept, a SPP in a tunnel, he discusses the steps which he took to ensure that the propeller was supplied with sufficient ventilation air. The problem experienced was that the tunnel filled with water, drawn in by the propeller, particularly when the craft operated in displacement mode. By modifying the tunnel, with either extra ventilation holes and valves, or with a liner forming a duct through which air could be drawn from the transom to the region immediately upstream of the propeller, a successful design was achieved.

In a follow up paper Van Tassel (1992) describes the development of a steering system for use with the Air Drive, using trim tabs to enhance steering capability. He also describes the use of engine exhaust discharged into the tunnel to supplement ventilation air, a technique used in racing powerboat installations. Initially it was feared that high peak pressures in the tunnel, occurring when the craft came off the plane rapidly, would be large enough to risk water being forced into the engine through the exhaust. This fear proved to be unfounded.

2.6. Summary

The key issues which have arisen in this review, as far as the practical implementation of SPPs is concerned are:

- the need for more extensive performance data;
- the need to pay close attention to scaling requirements when testing at model scale;
- the need for data over a range of immersions, in order to assess performance in critical regions of the operating envelope, particularly around the 'hump';
- the need to investigate shaft orientation more closely, particularly yaw, in view of Olofsson's conclusion that this can be used to significantly increase efficiency;
- the need to investigate hull/propeller interaction in various configurations more closely;
- the need for reliable system design from a stress and fatigue point of view. (Although Kamen (1998) writes about the remarkably smooth operation of SPPs at high speed, this is judged from the perspective of passenger comfort. From an engineering point of view, there are considerable vibration induced loads on the drive system, analysed by Olofsson (1996), Keller (1995) and Allison (1978). There is also both written (Furuya (1985)) and anecdotal evidence of failures occurring, either in blades or shafts which would appear to be the result of fatigue.).

Many of these points provide a springboard from which the current SPP project was launched.

3. FINITE ELEMENT MODELLING OF THE PROPELLER DRIVE SYSTEM

3.1. Overview of FE Modelling in this Project

The requirements of the design methodology which is being developed are that it should be capable of use by designers, with relative ease, to confidently design systems allowing for the peak stress conditions which will occur during operation. These peaks occur as a result of the dynamic behaviour of the system, excited by the hydrodynamic loads. The load data gathered during the experimental phase of this work, therefore, will need to be scaled and applied to a FE model of the system being designed, in order to carry out a parametric study.

Finite element codes are now well developed tools used by most medium to large engineering companies for routine stress and dynamic analysis. One such code, popular with many companies, is PAFEC (Program for Automatic Finite Element Computation) and this was used for the work because of its availability in both the University and in industry. However the design process developed is portable with relative ease to other codes.

The level of detail which the FE modeller needs to include is often a difficult matter of judgement; too little leads to unacceptable inaccuracy and too much is expensive in modelling and computational time. The propeller-shaft system of this project could be viewed at its most simple level as a beam and lumped mass. Added levels of complexity then bring in the effect of blade flexibility on the dynamics of the system and the effect of entrained water around the blades as an added mass. By modelling the entire propeller, and then by making an allowance for the added mass, the relative importance of these effects were examined.

3.2. The FE Method

3.2.1. Static Analysis

The finite element method for stress analysis is now a well established technique. Refinements to the basic method are constantly being implemented; different elements are being developed for specialised applications, solution times are being reduced, model sizes are increasing, grid generation is being simplified and graphical interfaces are continually improving. However the fundamental principle remains the same; the object to be modelled is represented by a set of node points and adjacent nodes are connected to form elements. Deflection of the object is assumed to follow some function, and the parameters which define this function, the degrees of freedom, (usually the nodal deflections) are sought. These are found, to a level of approximation, by minimising a functional. The term "Finite Element Method" is generic covering a range of methods which minimise a functional; in the most easily understood of these, the functional is energy, and the condition sought is the stable one when energy is a minimum.

The central equation relates the column vector of applied forces with the stiffness matrix and the freedoms:

$$\{F\} = [S]\{u\}$$

There may be as many as 6 freedoms per node (3 translations, 3 rotations).

The assembly of the stiffness matrix for the structure plays a key role in the FE method. This is a matrix of influence coefficients, relating forces at a node with deflections at any other node; it is symmetric since the force arising at node 'b' due a deflection at node 'a' is the same as the force at node 'a' arising from the same deflection at node 'b'. The stiffness matrix of the structure comprises a summation of matrices for individual elements which, broadly, are derived as follows:

- element geometry is transformed from curvilinear co-ordinates to rectilinear using a mapping technique; this amounts to an interpolation procedure, usually polynomial, for points within the element, defined in terms of nodal positions;
- a means of expressing the displacement of any point within the element, in terms of (unknown) nodal displacements is defined; frequently the interpolation function used for this is the same as the transformation function mentioned above; in this case the elements are described as isoparametric;
- strains over the element are related to unknown nodal displacements through the interpolation polynomial and its derivatives;
- stresses in the element are related to strains using the elasticity matrix;
- elemental strain energy is related to strain and stress expressions;
- the stiffness matrix is derived in terms of material elasticity and element geometry; this is done, in principle, by differentiating the elemental strain energy with respect to each nodal deflection for the element, and setting this equal to the appropriate nodal force.

Once the global stiffness matrix has been assembled, then constraints are imposed; these often take the form of zero displacement at restrained nodes, each of which has the effect of reducing the number of equations to be solved by one. Finally the set of simultaneous equations is solved using a method which may need some sophistication to overcome memory storage problems.

Considerable effort has been expended by programmers in developing new elements to carry out specific tasks, with the prime objective of making models more efficient in terms of computational time, while maintaining an acceptable level of accuracy. Thus elements for beams, or thin shells, for example have a significantly reduced number of degrees of freedom, but may be used in only a restricted range of applications. The degree of the

interpolating polynomial, which is tied to the number of defining nodes for the element, also has a significant impact on the accuracy and speed of solution, and needs careful consideration.

3.2.2. Dynamic Analysis

Dynamic analysis has a two-fold function in relation to this project: to determine resonant frequencies and mode shapes, and to provide information on the transient performance of a propeller-shaft system when excited by the hydrodynamic forces. The same stiffness matrix already described is employed, but additionally a mass matrix is required and, if damping is to be considered, a damping matrix. The governing equation now relates the column vector of applied forces to the deformation forces and inertia forces. Thus, omitting the sin ωt factor, the equation

$$\{F\} = [S]\{u\} - \omega^2[M]\{u\}$$

applies to the undamped motion for each element, and may then be assembled for all elements.

For calculation of the natural frequencies, this equation is set to zero (no applied force) and the values of ω which satisfy it for all deflections (the eigenvalues) are found. The ratios between deflections at any given ω (the eigenvectors) are the mode shapes.

For the calculation of the transient response to an arbitrary excitation the previous governing equation is replaced by the more general

$$\{F\} = [S]\{u\} - [M]\{\ddot{u}\}$$

which is solved by a time-step procedure.

3.2.3. PAFEC

PAFEC is a widely used finite element package which has been continuously developed over the 20 years or so of its life. The principal developments in recent years have been in

graphical presentation, with pre- and post- processors for developing models and analysing results respectively; these graphical interfaces in PAFEC are collectively known as PIGS (PAFEC Graphical Interface System).

In spite of the graphical interfaces, the fundamental input to the solver remains a text based one; the data input file is an ASCII text file comprising a series of modules which define geometry, elements, material properties, boundary conditions and solution controls. This may be written either directly or by using PIGS while building the model graphically. The existence of this data file may at first seem restrictive, requiring significant specialist knowledge, but it in fact becomes a very useful facility for checking input, making modifications and carrying out procedures which are not possible in PIGS.

The following paragraphs describe a number of considerations specific to the use of PAFEC in this particular modelling situation.

3.2.3.1. Element Geometry Limitations

Computational efficiency depends on selecting appropriate elements, particularly for transient analyses which require an iterative procedure and may thus have lengthy solution times. When designing a FE model the choice of element shape and grid density depends on a compromise between accuracy and speed. Frequently, to economise on the number of four sided elements used, a grid which is significantly distorted from rectangular is necessary or aspect ratios may be high. Because of the mapping procedure within PAFEC which transforms the grid to a rectangular one, these distortions introduce errors. Consequently warning and error messages are produced; for example values for 2D quadrilateral elements are as follows (where aspect ratio, R, is the ratio of the longest to the shortest elemental sides):

	Warning	Error
Max side aspect ratio, R	$5 \leq R < 15$	$R \geq 15$
Min corner angle, θ_{min}	$25^0 < \theta_{min} < 45^0$	$\theta_{min} \leq 25^0$
Max Corner angle, θ_{max}	$135^0 < \theta_{max} < 155^0$	$\theta_{max} \geq 155^0$

The restrictions imposed by this may mean adaptation of the grid as a model is built. Side aspect ratio dictates against very long thin elements, so that a larger number of elements may be needed, and corner angles may require the use of triangular elements at extremities of the model.

3.2.3.2. 2D Semi-Loof Elements

Two dimensional elements are the most economical way of modelling plate type structures, and a variety of these are available in PAFEC. The particular requirements for modelling a propeller blade are that the element should be capable of modelling bending loads, be generally curved and be able to accommodate variable thickness across the element. These conditions rule out many of the possibilities offered, such as plane stress, plane strain or faceted elements; however the semi-Loof element is suitable. This is a curved quadrilateral 8-noded element with three translatory degrees of freedom at each node. Bending is handled by 8 "dummy" nodes, placed approximately at the quarter points along the sides; to these are attributed the rotational freedoms, about mutually perpendicular in-plane axes at the midside nodes (Figure 11).

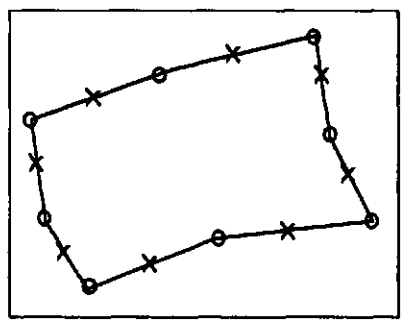

Figure 11. Semi-Loof Element.

Briefly, the theory uses shape functions based on 8 term polynomials (since there are 8 nodes defining each element) to transform the elements into curvilinear co-ordinates. Displacements of points within elements are expressed in terms of nodal displacements using the same polynomials, modified with an extra term, which adds an extra degree of freedom allowing the element surface to bulge at the centre. Rotations about two axes at any point in the element are also expressed in terms of modified polynomials. By making assumptions about the shear deflections, the number of degrees of freedom is reduced to 32, three translatory freedoms at each of the eight nodes, and two rotations at each midside node. The expression for strain follows, including that due to both direct stress and bending and this is developed to the strain energy equation from which the stiffness matrix is identified.

From this description it can be seen that the element is unusual in that it includes rotation at points along its edges as degrees of freedom attributed to mid-side nodes. This restricts the types of element to which it may be connected, and care must be exercised in the use of the "COUPLING" module to ensure that freedoms are passed correctly from an element of one type to an adjoining one of a different type.

The ability to specify variable thickness makes these elements particularly useful. However, in developing an FE model of the propeller blade, it was found that, although the element has the facility to model variable thickness, this could not be programmed using the PIGS graphical interface. This therefore dictated the use of text based input, requiring a more disciplined approach to the design, and having the inconvenience that the model had to be partially processed before it could be viewed and checked.

3.2.3.3. 3D Boss Elements

For modelling the propeller boss, the use of 3 D elements could not be avoided. However this constitutes a relatively small part of the full propeller, and the elements could be quickly defined because of their repetitive nature.

For the boss, 20 noded isoparametric brick elements were chosen, with corresponding 15 noded wedge elements for the shaft at the centre of the boss. It was later found that better results were achieved in comparison with experiment if 3-D elements were also used for the thicker portions of the blade. The development of these elements follows that described in the Static Analysis section above, with both interpolation and transformation functions being 3 dimensional quadratic expressions.

3.2.3.4. Use of Coupling

Two situations were encountered in which the "COUPLING" module had to be implemented to link one group of elements with another. Firstly, when linking elements for which freedoms do not correspond directly (2-D blade to 3-D boss elements; 2-D to 3-D elements on later models of the blade; beam elements used for the shaft to the 3-D elements of the boss), it was necessary to ensure that rotational degrees of freedom were passed between the types of elements; otherwise a hinge would be created at the interface. Secondly, in later models when 3-D elements were used for the blade root, the blade and boss were created as two distinct structures, with a small artificial gap between then; "COUPLING" provided a link between these structures, and provided a powerful method of modelling since it was not necessary for elements in each part of the structure to match geometrically, thus allowing considerable freedom.

3.2.3.5. Use of Cyclic Nodes

For structures with rotational symmetry, the use of "CYCLIC.NODES" appears to offer significant advantages. It permits a technique which models only one part of the structure,

(for example one blade and a segment of boss) and defines which elements are attached to adjacent segments, and the number of times a segment is repeated. This provided an economical way of modelling the propeller, giving results identical with the fully defined model much more quickly for a modal analysis. However, the asymmetric, transient load case described later could not be dealt with using this technique and this precluded its further use.

3.2.3.6. Master Degrees of Freedom

The determination of the eigenvalues and vectors is a computationally expensive process and several techniques for improving economy are used in PAFEC. One of these techniques divides the problem by recognising that comparatively few elements with large mass/stiffness ratios dominate the dynamic characteristics of most structures. These are designated as masters, with those which do not have a significant influence being slaves. The set of governing equations involving the slaves are simplified by omitting the mass terms and then used in the solution of the master equations. This two stage process is significantly quicker than solution of the full set of equations.

Although masters may be chosen manually, it is better to allow PAFEC to make the selection on the basis of which freedoms are important in terms of the kinetic energy content. Those with high mass and/or low stiffness are selected. The only manual choices then needed are those in a transient analysis calculation for which full back-substitution is required in order to determine displacement histories.

3.2.3.7. Rigid Body Modes

A modal analysis of an unsupported structure leads to vibration in which the body acts as a rigid body with no distortion. The frequency of these modes should be zero, although numerical inaccuracy will yield small non-zero values. These values provide a means of

checking numerical accuracy: if ω_r is the frequency of the highest rigid body mode and ω_i is a computed resonant frequency, then the true value of frequency probably lies between:

$$\omega_i \left((1 \pm \left(\omega_r / \omega_i \right)^2 \right)^{0.5}$$

3.2.3.8. *Transient Analysis*

For the time step approach used in transient analysis, the governing equation is solved to find the acceleration at the current time step from the current displacement and velocity. The new velocity and displacement may then be found using a modified Taylor Series approach. This (the Newmark β method) uses some proportion (β) of the acceleration at the next time step to determine a mean acceleration, thus making some allowance for the way in which acceleration varies during the time step. A recurrence relation is then used for the solution of the equation. The choice of β influences the stability of the solution. A value of ¼ was chosen, corresponding with constant acceleration over the time interval, as this is unconditionally stable.

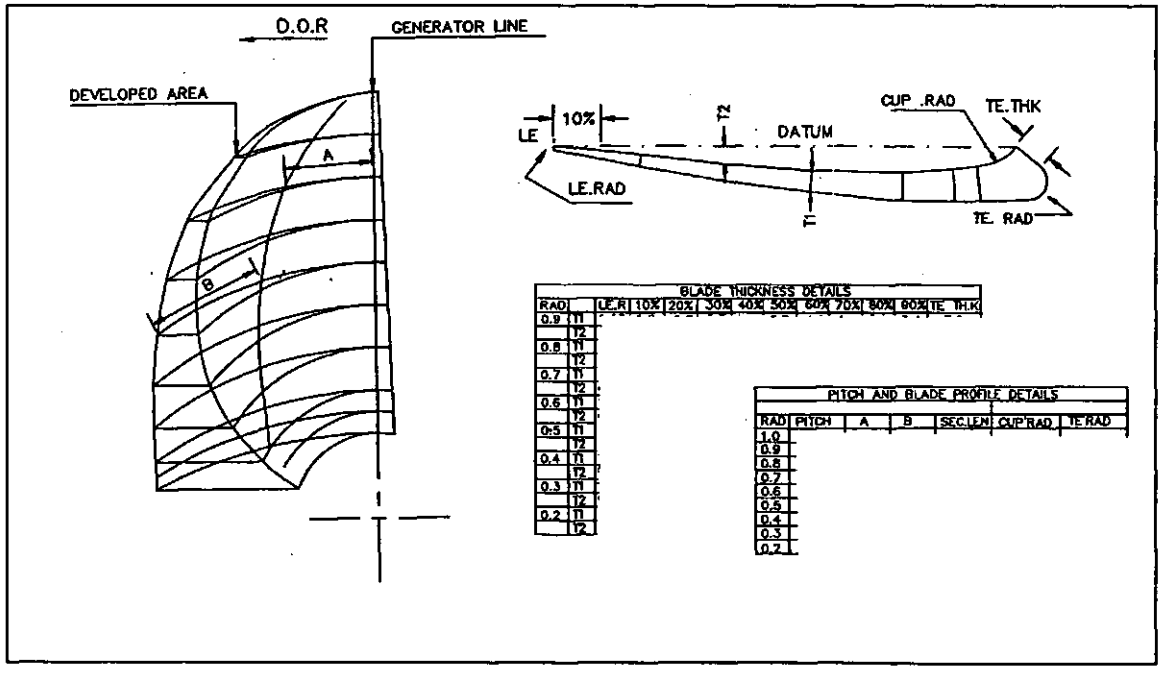

Figure 12. Typical Propeller Working Drawing.

3.3. Propeller Geometry

The FE modelling process requires the propeller geometry to be defined using a format which is suitable for input to the package. Thus co-ordinates of points on the blade faces and backs must be expressed in a suitable co-ordinate system.

Unfortunately from this point of view, working drawings of propellers (Figure 12) are produced with manufacture in mind, rather than computer modelling, and a significant amount of interpretation needs to be carried out.

A propeller blade is defined at a given radial section with reference to a helical line of a given pitch, formed about the shaft axis. This helix passes through a point on the generator line (point G on GO in Figure 13). This, in turn, is defined as being at the rake angle (usually aft) to a reference line, the directrix (DO), which is drawn perpendicular to, and passing through, the shaft axis. Points at radial stations on GO are then moved on the helix at their given radii, to give the blade skew; the locus of these points, R, becomes the blade reference line. It should be noted that this last rotation has effectively changed the rake of the blade section, giving rise to the term skew induced rake. It should be noted that, in the more complex propellers, pitch, rake and skew may all vary from one radial station to he next.

Once the blade reference has been defined, the distances to the leading and trailing edges on the blade surface at each radius are identified; chordwise stations between these are then determined. For each of these points the offsets perpendicular to the helical surface, which define points on the face and back of the blade, are taken from the working drawing where they are usually presented as a face offset and a metal thickness.

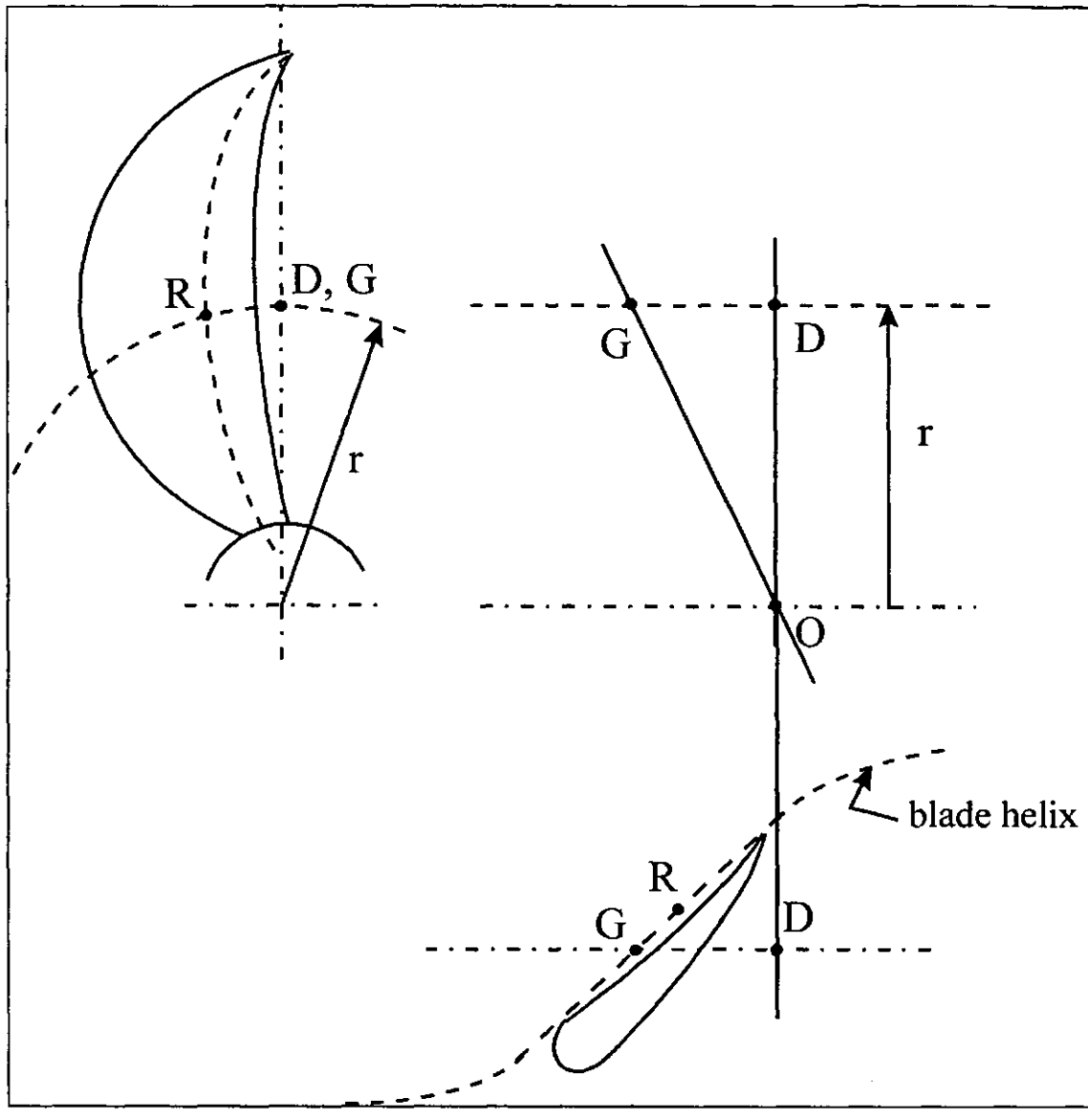

Figure 13. Propeller Geometry.

Generally, radial stations are spaced at intervals of 0.1 x radius, and the chord is divided into 10 equally space intervals. Approximately 80 points are thus defined which, with small modifications in some areas, forms the basis for the finite element grid.

The manipulations described above have been encoded into a "geometric" spreadsheet. This permits the input of data from working drawings (propeller diameter, pitch(es), rake(s), skews and offsets) and produces 3-dimensional polar co-ordinates for each point

on the face, back and camber surface. These may be quickly manipulated to a form suitable for input to the FE package as an ASCII file, defining nodal and elemental information.

3.4. Validation using Standard Propeller

Since one of the principal interests of this projects is the dynamic behaviour of the system, it was essential that the finite element model developed be validated against physical data, comparing resonant frequencies. The effectiveness of the model would be judged on the comparison of the lower mode resonance.

The propeller used for validation was dictated by availability; a conventional 3 bladed, 20 inch diameter, 13 inch pitch propeller, manufactured in high tensile brass (BS1400 HTB1) was obtained. Although this was somewhat different from a SPP in both blade section and profile, it would provide a valuable guide as to the modelling procedure.

3.4.1. Propeller Data

The propeller's dimensions were first checked against the drawings supplied by the manufacturer. Stations at intervals of 10% radius were marked, from 0.2R to 0.9R, which were then divided into 10% chord intervals from leading edge to trailing edge at each radius. Thus 88 measurement points were identified, at which the blade thickness was measured using callipers to an accuracy of $\pm$ 0.1 mm. Chord lengths at each radius, blade thickness in the tip region and boss details were measured. The root / boss fillet thickness was estimated at points across the blade. The manufacturer's drawings and inspection report were relied upon as far as pitch was concerned.

In order to establish physical properties, a cast sample of similar material was taken and machined into two flat strips approximately 4×20×100 mm. These were subjected to a 3 point bending test to find the elastic modulus and weighed to find density. A spectral

analysis was carried out to confirm that the sample and propeller were of similar material. The values established were:

$$\rho = 8152 \pm 70 \text{ kg/m}^3; \text{ E} = 88.2 \pm 4.7 \text{ Mpa}$$

The geometric spreadsheet was used to determine the volume of the propeller by integration, which gave a total mass of 9.6 kg. This compares with 9.78 kg by weighing the propeller, a discrepancy of 1.9%, giving confidence in the spreadsheet calculation.

3.4.2. Initial FE Model

3.4.2.1. Propeller Model

The propeller geometry was processed, using the spreadsheet, to produce polar co-ordinates for the blade surface. Since few points were defined in the tip region (when manufactured this area is generally faired by hand) a polynomial was fitted on the trailing and leading edges, relating semi-chord length to radius for r/R from 0.6 to 1.0. From this, chord lengths at r/R intervals of 0.02, between 0.9 and 1.0, were determined and used to establish the tip profile.

Since propeller geometries are generally defined at the radial and chordwise stations

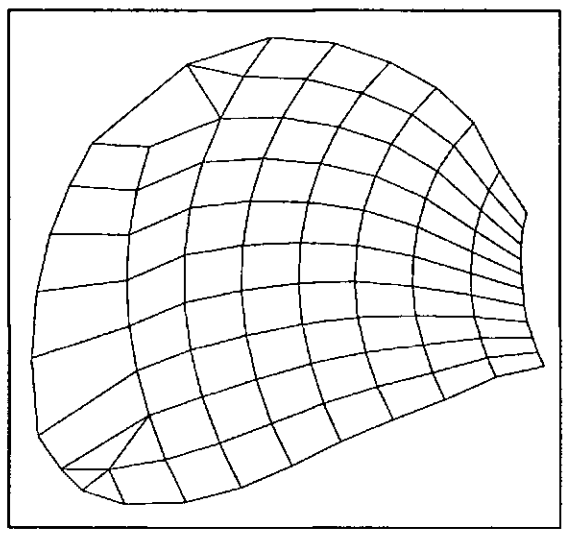

Figure 14. 2D Elements on Validation Propeller.

described above, these provided the obvious starting point for the creation of the FE model. The thin blade (in proportion to chord and radius) dictated against 3D elements in PAFEC, since in order to keep element proportions within the specified limits, the number of elements required would be very high leading to memory storage problems and long solution times. 2D 8-noded Semi-Loof elements were selected as the most suitable because of their variable thickness facility and ability to model in-plane bending. Corner nodes of these elements were defined by using the 10% radial and chordwise stations at points on a surface mid-way between face and back; PAFEC was allowed to interpolate linearly for midside nodes. Thus it was possible to model the blade using approximately 80 elements. A certain amount of tailoring was necessary in the blade tip region, and some use was made of 6 noded triangular Semi-Loof elements to ensure that element geometry remained within the appropriate aspect ratio and corner angle constraints (Figure 14).

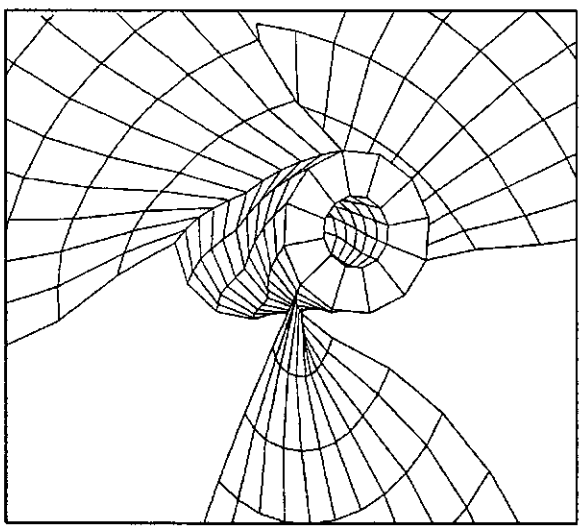

Figure 15. Boss and Blade Root Details.

The boss was modelled using 3D 20-noded isoparametric brick elements. The geometry of these was defined on the same helix as the blade in order to facilitate the coupling between blade root nodes and the boss, with 10 elements from front to back corresponding to the 10 elements across the blade (Figure 15).

Cyclic symmetry was exploited in the early stages of development, allowing only one blade and a segment of boss to be modelled; however, it was realised that this would be restrictive in more complex models for two reasons. Firstly, it would be necessary to model the effect of added mass due to water surrounding the blades. Since SPPs have only some blades submerged, then the model becomes asymmetric. Secondly the transient loading which would ultimately be applied to the blades would also be asymmetric. Consequently, the full propeller was modelled, replicating node points using the "SIMILAR.NODES" module and elements using "GROUPS.OF.SIMILAR.ELEMENTS".

Coupling was implemented between the 2D blade elements and the 3D boss elements to ensure that rotational degrees of freedom were transferred from one to the other.

A modal analysis was run to establish the eigenvalues, allowing PAFEC to select 30 master degrees of freedom automatically. The model was unsupported which meant that rigid body modes were produced, and since these should theoretically be at 0 Hz, it was possible to use them to indicate numerical accuracy.

3.4.2.2. Effect of Added Mass

Any object oscillating in water is subject to pressure forces proportional to the acceleration of its surface. These are most conveniently viewed as the effect of a virtual added mass. In order to simulate this, the initial simplistic approach was to artificially increase the metal density on the blade(s) immersed. Assuming the blade to be an infinitely long flat plate vibrating in a liquid, Harris (1996) gives the added mass per unit length as:

$$\Delta m = \pi \rho_w \left(\frac{c^2}{4} \right)$$

where c is the chord length and ρ_w is the water density. This is derived from a potential flow solution of the transient flow around a plate placed perpendicular to the flow to

determine the added pressure due to the transient. Using the geometric spreadsheet, this added mass was integrated across the blade, and the blade density raised to simulate this increase. The effect was to increase density from 8152 to 25,000 kg/m^3. In order to implement this, it was unfortunately not possible to replicate elements using "GROUPS.OF.SIMILAR .ELEMENTS" while at the same time specifying a different material property. Consequently, elements for the in-water blades had to be explicitly defined.

3.4.3. Experimental Validation Data

Experimental frequency spectrum testing was carried out on the propeller using a Bruel & Kjaer Dual Channel Signal Analyser Type 2034 (later tests were carried out using an ACE DP104 2 Channel analyser with similar results). The propeller was suspended on elastic of very low stiffness, with a B & K type 4374 accelerometer attached using double sided tape in the tip region of one of the blades. The accelerometer was of very low mass compared with the propeller. Excitation was applied with a small hammer at various points, with the best response occurring when this was on the same blade as the accelerometer. Since interest was only in resonant frequencies, and not transfer functions or mode shapes, the precise position of excitation was not relevant. Triggering of data collection was on a rising slope; frequency span was set to 1600 Hz, with a discretisation of 2 Hz (since there were 800 lines), giving a data collection time of 500 ms. A Hanning window was used on the output and a FFT was carried out by the signal processing software to give a frequency spectrum. Averages of at least 10 readings were taken, after which time most of the noise had been eliminated and there was very little change to the spectrum.

Testing was first carried out in air with the accelerometer attached to each blade in turn. Then one and two blades were fully immersed in water. In these cases the accelerometer was attached to an in-water blade, and that blade was the one which was excited. The 3

bladed propeller was particularly convenient for this test since there was no overlap between blades; hence one or two blades could be fully immersed without the in-air blade(s) touching the water.

A typical frequency spectrum for an in-air case is shown in Figure 16. Some of the modes occur in clusters of 3 frequencies (the first mode being at 360, 370, 388 Hz) which arise because of small manufacturing differences between blades. The dominant one is that on which the accelerometer was mounted, and it was therefore possible by observing the first mode, for which the effect is most marked, to distinguish between the blades. The principal frequencies are summarised in Table 2.

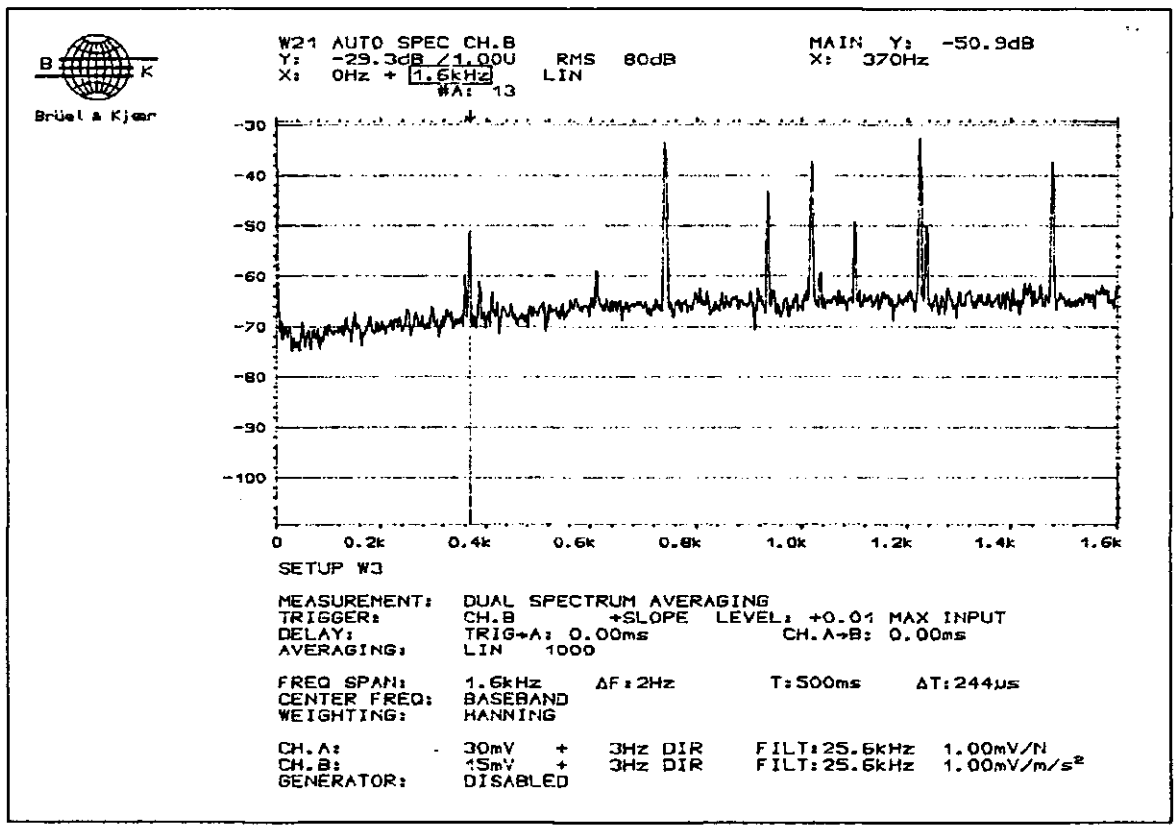

Figure 16. Frequency Spectrum (all blades in air).

Table 2. Resonant Frequencies for Validation Propeller

In air	One in water	Two in water
360/370/388	296/336/390	302/388
587/613/621	583/616/620	574/609/648
740	770	762
933	873/980	856/936
1016/1030	1042	1030
1101	1102	1124
1224/1234	1220/1320/1391	1277/1374/1409
1482	1462	1460

3.4.4. Comparison of Preliminary Results

The PAFEC analysis gave the first mode frequencies as:

Propeller in air: 256 Hz

One blade in water 188 Hz

Further runs were not carried out, and higher frequencies are not quoted since it may be seen immediately by comparison with Table 2 that this model is inaccurate both for the in-air case and in the proportion by which the frequency has been lowered by partial immersion.

3.5. Development of FE Model

Two problems were identified which, it was considered, were the major factors in producing the discrepancies. Firstly, some parts of the blade near the root and in the centre section had significant thickness which varied quite widely. This meant that some elements were far from uniform, an effect particularly marked near the root filet which was not accurately modelled; furthermore, the maximum blade thickness was in the region of 16% of blade span, which is approaching the point at which it is recommended that thick shell elements be considered. Secondly, the way in which added mass was modelled, using an

artificially increased blade density, was clearly too simplistic, since it attributed less mass to thinner parts of the blade and more to the thicker.

3.5.1. 3D Blade Elements

It is not possible in PAFEC to join thick and thin shell elements; consequently, the first modification was to replace all the thin semi-Loof elements with thick, generally curved ones. The effect of this was to move resonant frequencies significantly away from experimental values. This was attributed to the fact that thick elements were now being used for very thin sections, and as before, there were large variations in thickness across some elements. In view of this, an alternative strategy was sought which would lend itself to the modelling of SPP blades at a later stage. Full 3-D modelling was out of the question because of complexity and solution times, but it was possible to model thicker sections using 3-D isoparametric elements, and link these to semi-Loof elements for the rest of the thinner sections.

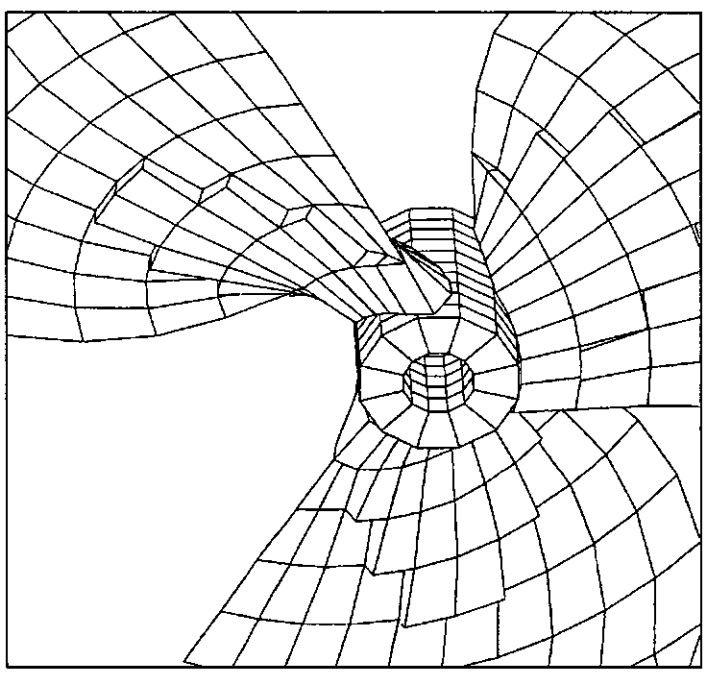

Figure 17. Modified Boss and Blade Root with 3D Elements.

In order to implement this it was necessary first to modify the geometry spreadsheet to produce co-ordinates of three blade layers - the back, face and camber surface. Nodes corresponding to these layers were then defined in PAFEC, which allowed 3-D elements to be substituted for 2-D ones where required.

Because of the constraints imposed by the coupling module, the entire strip of elements at the root had to be modelled in 3-D, using wedges at the ends and bricks in the centre. The use of these elements made it difficult to couple to the boss using the previous technique of continuing the blade helix into the boss. This prompted an investigation into alternatives, with the solution being to use a simply defined boss as a separate structure (Figure 17). The "COUPLING" module was then used to tie this in with the boss. Care had to be exercised in doing this to ensure that there was no overlap between boss and blade nodes, and a modification to the diameter of the boss was made to ensure that a small gap existed. This was then effectively filled by the "COUPLING" module during processing.

An area of 3-D elements was placed at the centre of the blade out to 0.6R, with the number of elements in each radial strip reducing at successive radii. The coupling module was again used, this time for its alternative purpose of transmitting rotational degrees of freedom wherever 2-D and 3-D elements were adjacent.

3.5.2. Added Mass

The simple model for added mass is clearly inadequate for several reasons. Firstly, raising the blade material density imposes the artificial condition that added mass depends upon the blade thickness at a given point. Secondly, end effects are not considered; near the edges the effect of added mass will be much reduced due to flow induced around the blade. Thirdly, no estimate is made of the added mass effect in torsional modes; this would require some chordwise distribution of added mass, again allowing for edge effects.

Fourthly, at any given point on the blade, flows induced by adjacent areas will affect the transient pressure exerted on the blade and therefore the added mass effect. A full solution to this problem would need to account for the fluid /solid interaction over the full range of frequencies, and would yield different added mass values for each mode.

A better estimate could be obtained by analysing potential flow on the blade. Newman (1992) carries out a derivation which develops the integral of pressure forces on a moving body:

$$\underline{F} = \iint_S p\underline{n}\,dS$$

For an unbounded fluid, this becomes:

$$\underline{F} = -\rho\frac{d}{dt}\iint_S \phi\underline{n}\,dS$$

The time dependant term is then isolated by a linear decomposition, considering the velocity potential as the sum of potentials due to unit body velocity in each of the six component directions (i) (3 translations, 3 rotations) multiplied by the respective velocities in those directions:

$$\phi = U_i\phi_i$$

giving:

$$\underline{F} = -\rho\frac{d}{dt}U_i(t)\iint_S \phi_i\,\underline{n}\,dS$$

where ϕ_i is the velocity potential relative to a frame of reference moving with the body. If a non-rotating body is now considered, then the time dependence of $\underline{n}$ vanishes and the differential is simplified. The force in each of the 3 component directions (j) becomes:

$$F_j = -\rho\dot{U}_i\iint_S \phi_i n_j\,dS$$

The boundary condition on the body must satisfy non-permeability, that is the normal component of fluid velocity equals the normal component of body velocity, or

$$\frac{\partial \phi}{\partial n} = \underline{U} \cdot \underline{n}$$

This amounts to the condition that each component of unit velocity satisfies the same condition, or

$$\frac{\partial \phi_j}{\partial n} = n_j \qquad (j=1,2,3)$$

so that

$$F_j = -\rho \dot{U}_i \iint_S \phi_i \frac{\partial \phi_j}{\partial n} dS$$

and an added mass tensor may be defined.

$$m_{ji} = \rho \iint_S \phi_i \frac{\partial \phi_j}{\partial n} dS$$

where m_{ji} is the equivalent added mass which yields an inertia force in the j th direction as a result of acceleration in the i th direction (i, j = 1,2,3 for a body which translates without rotation). It can be seen that this is calculated purely in terms of velocity potentials on the surface due to unit body velocity in each direction (ϕ_i) and normal components of surface velocity due to unit body velocity in each direction $\left(\frac{\partial \phi_j}{\partial n}\right)$. Rotational terms complicate this but the principle remains the same.

In order to include this concept into a PAFEC analysis, considerable simplification would be required, since masses may only be included as point masses at nodes, with no allowance for different equivalent effects in different directions. Thus full mass tensors cannot be accommodated. An iterative procedure is postulated in which, for a given vibration mode, a dominant direction of movement of the blade is identified. For unit velocity in that direction, surface potentials at nodes would then be calculated, using a

panel method for complex shapes, together with normal velocity components. This would lead to nodal values of added mass, which would allow calculation of inertial forces in the dominant direction due to movement in that direction. These could be added to the FE model as point masses.

While this process is possible, it is not considered prudent in this particular work for several reasons. Firstly the focus of this project is on the shaft and bearing system. As will be shown later, inertial effects of blades have a relatively low impact on this, and the added mass contribution an even smaller impact. Secondly, even if the analysis were carried out, it would still constitute an incomplete model since, for the surface piercing propeller, an unknown proportion of the blade surface is covered by a cavity. Finally, the analysis would need to carried out separately for each vibration mode which would be a very time consuming process.

Instead of this full analysis, an estimate of the added mass distribution is made for an approximation to the first bending mode, in which a plate is viewed as moving in a direction perpendicular to its plane. For this case, consider a flat plate of width 2a placed in an infinite field. Classical techniques (Milne-Thomson (1960)) yield:

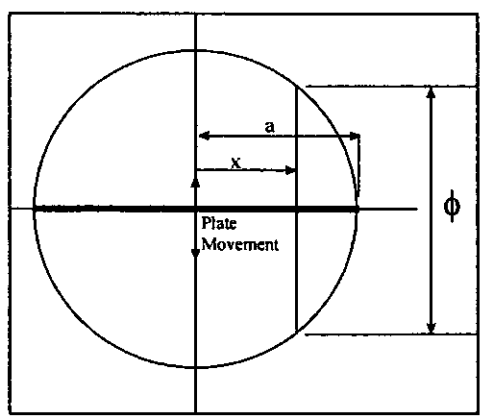

Figure 18. Schematic of Added Mass Distribution.

$$w = -iU\sqrt{(z^2 - a^2)}$$

where $w = \phi + i\psi$ and $z = x + iy$

Adapting this to determine the potential on the plate, by setting $y = 0$ and $x<a$ produces

$$\phi = U\sqrt{a^2 - x^2}$$

Thus ϕ at a point on the plate due to unit stream velocity equals the half chord of a circle based on the plate. Inserting this in the added mass equation produces a full circular distribution (Figure 18) and, when the integral is carried out, the expression used previously for the simple model is produced. Thus the effective added mass is the mass of fluid occupying the cylinder for which the plate forms a diameter.

Extending this principal to three dimensions, Newman (1992) gives the added mass for flow around a disc as $0.63 \cdot \frac{4}{3}\pi r^3$. The factor, 0.63, arises since flow may now take place around the disc over the entire circumference, rather than simply the edges in the 2-D case. A simple application of this was implemented for the propeller blade. Firstly the total added mass for a disc of equivalent area to the blade was calculated. This mass was then distributed over the blade by finding the proportion of it acting at each of 20 nodes, assuming the distribution was similar to that for a disc. The dimensions used for this calculation were the distances from the node to the centre of area of the blade (a), and to the nearest edge (b). Thus the added mass attributed to a given node was:

$$\Delta m_a = \frac{\Delta V}{\Sigma \Delta V} \cdot m_a$$

where $\Delta V = \Delta A\sqrt{(b^2 + 2ba)}$, in which ΔA is the elemental area associated with the node.

3.5.3. Results from Modified Model

The model using 3D elements for the thicker region of the blade and the added mass distribution approach described above was run using PAFEC to determine resonant frequencies in the free condition. Results were:

Propeller in air: 346 (1st bending), 550 (1st twisting) Hz

One blade in water: 269 (1st bending, in-water blade), 299 (1st twisting, in-water blade) Hz

Referring to the practical results in Table 2, these correspond to the 360/370/388 and 587/613/621 Hz clusters for the in-air case and frequencies of 296 and 336 Hz for the case of one blade in water. Thus, for the first two modes, PAFEC predicts values which have a discrepancy, at worst (for the in-water case, 2nd mode), of 11%.

3.5.4. Damping

The level of damping within a structure influences peak amplitudes, particularly in the region of resonant frequencies. A realistic value of the damping ratio was required for use in the FE model. Information on this subject is scarce; however Hylarides (1978) investigated a propeller excited in water. By measuring phase angles and comparing them with theoretical values for a single degree of freedom system, a value of 0.05 was found.

This is supported by experiments carried out by the author on a University work boat (Aquatay). Accelerometers were place on the aft bearing housing of the propeller shaft, and frequency response functions were measured. By analysing the half power points of the lowest frequency resonant peaks, a damping ratio of approximately 0.05 was found.

It is emphasised that both the work of Hylarides and the author were approximate, and a more detailed study would be a useful area for future research. However, the figure of 0.05

was considered satisfactory for this work, as later sensitivity studies showed that moderate variation in this value did not significantly influence the final peak stresses predicted, provided operation was away from resonance.

3.5.5. Summary of FE Modelling Strategy

A FE model of a conventional propeller comprising 2D semi-Loof and 3-D elements has been developed which predicts resonant frequencies in air with acceptable accuracy. A simple method which allows for the effect of added mass due to surrounding water by distributing point masses across a blade surface has also been proposed. This has been checked against experimental results for lower modes in the case of a partially immersed propeller. However the case of a blade with a cavity attached to one face has not been attempted.

The level of sophistication of these models is considered acceptable for the purposes of this work, since the propeller forms part of an overall system which is dominated by shaft and bearing stiffnesses.

3.6. Modelling of Propeller System and Excitation Loads

The SPP propeller and shaft constitute a dynamic system excited by time varying hydrodynamic forces. Thus in addition to the mean loads imposed on the blades, shaft and bearings, transients will arise resulting from inertial effects. To investigate these, a system model was created in PAFEC and transient analyses were run in which loads representing the hydrodynamic effects were sequentially applied to the blades. By examining the outputs from these analyses, maximum values of stress at critical points in the system could be determined and compared with fatigue strength for the material; also the nature of the forces transmitted to the hull structure through the bearings could be investigated.

3.6.1. Finite Element System Model

The propeller system which was initially modelled comprised a 23 inch diameter, 35 inch

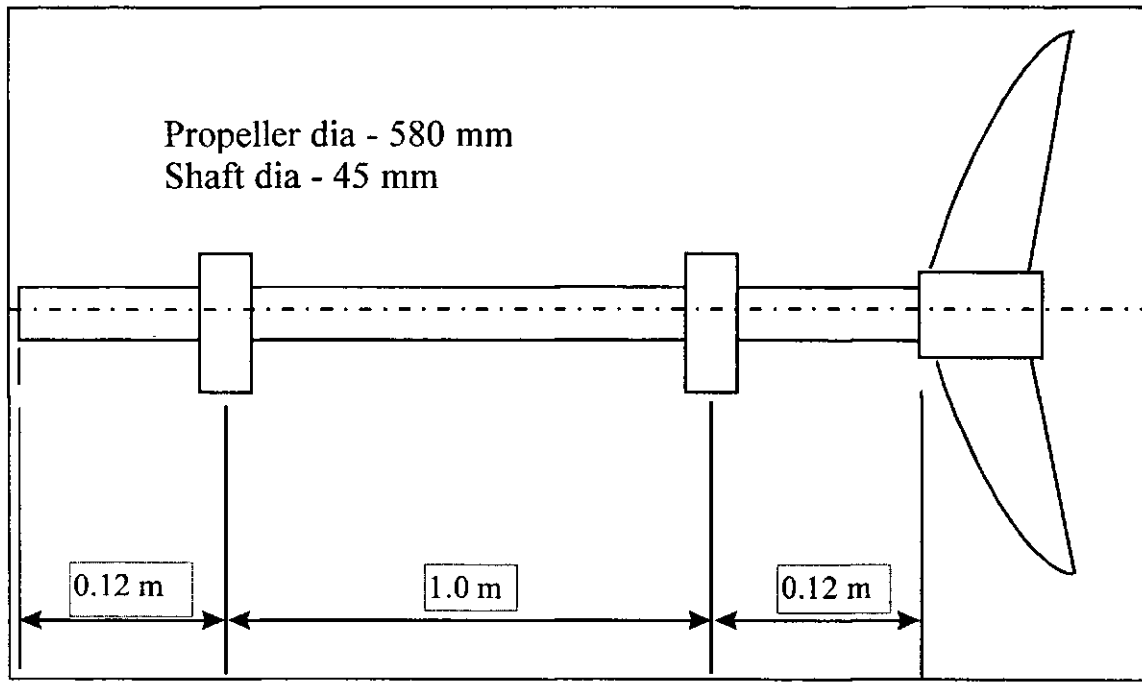

Figure 19. Shaft Layout.

pitch, 5 bladed SPP coupled to a duplex steel shaft whose layout was typical of this type of system (Figure 19). Aluminium was chosen for the propeller material for the development stages, since this would be used for the physical models against which validation would take place. However a change to AB2 aluminium bronze, from which the full scale propellers are made, was a simple procedure at a later stage.

This work was developed in parallel with the propeller validation, and consequently, the propeller model used comprised 2D semi-Loof elements for the blades and 3D isoparametric elements for the boss. To this, 3D wedge elements were added to fill the hub. Finally beam elements were used for the remainder of the shaft, with a "COUPLING" module transmitting the freedoms from this to elements in the hub.

Restraints were placed on the shaft at three points: aft and forward bearings (restrained vertically and horizontally in a plane perpendicular to the shaft) and at the forward end of the shaft where it connects to the gearbox (restrained in torsion and in the axial direction). Initially these were modelled as rigid supports but when it was found that reaction forces could not be extracted easily from the results file they were replaced with very stiff springs, allowing deflections to be extracted and converted to forces. In practice, shafts are generally supported in cutlass bearings and subsequently typical stiffness data, taken from previous experiments, was obtained. These values were used for the stiffness of the springs which were used to model the bearing supports. The propeller-shaft-support model is shown in Figure 20; this particular case is a 4 bladed propeller with zero rake used for the physical model testing, and shows the modifications made to include 3-D elements in the thickest regions of the blade.

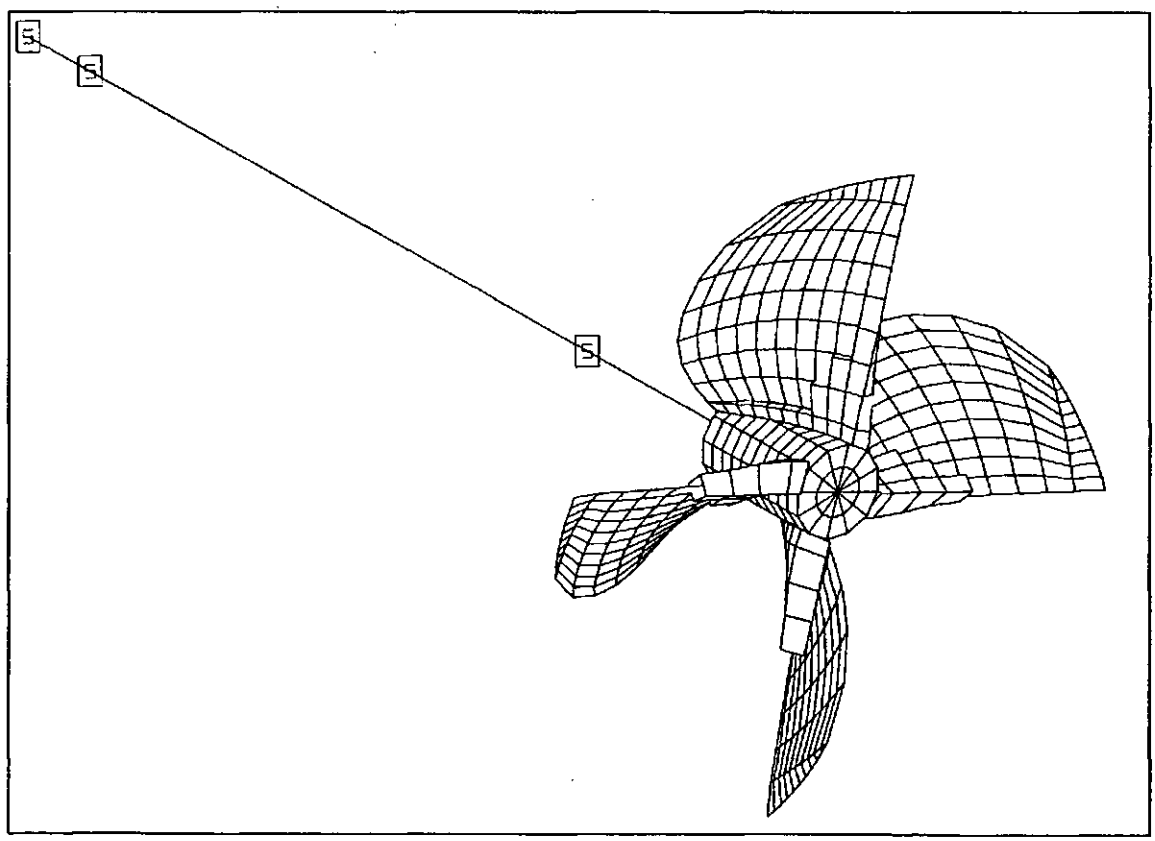

Figure 20. FEA of Model Propeller on Shaft.

3.6.2. Transient Loading - Initial Model (No.1 - "Plateau" Load at a Point)

In PAFEC, transient loads may be applied at nodes which are defined as master degrees of freedom. A series of time-load data lines form the "FORCING" module; the force data in these comprise the magnitude and direction of the force at each node subjected to a load at that time. Values are linearly interpolated by PAFEC between successive times. However, the application of transient loads is cumbersome if many points have to be loaded, since for every time-step, the force at all loaded nodes has to be defined, not simply those for which the linear slope changes. This restricted the number of nodes at which the load was defined.

The transient excitation was initially idealised as follows. Each blade was assumed to strike the water cleanly, and the load applied to that blade was assumed to act at a single node point, positioned close to the centre of area of the blade. Load rose linearly from zero, as the leading edge crossed the waterline to a maximum as the trailing edge crossed. It then remained on this plateau until the leading edge started to leave the water, falling to zero when the blade was fully clear.

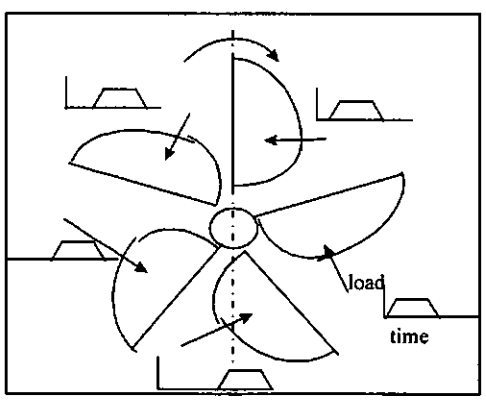

Figure 21. Simple Transient Load Application.

The load was taken to act in a direction perpendicular to the blade face at the node where it was applied. It was therefore necessary to determine this line of action for each blade. This was done by finding the direction cosines for the plane which passed through 3 adjacent nodes. These were then applied to resolve the applied forces into components in the axial, vertical and transverse directions.

The value of the load on the plateau was calculated such that the average axial component of force for all blades was equal to the thrust expected for his type of propeller at 50% immersion, using experimental results from Rose et al (1993).

The load profile described was applied to each of the five blades in turn at time intervals calculated to reproduce a 1500 rpm rotation rate. Thus, in effect, the blades were fixed in space and the waterline swept across them (Figure 21).

Because of the difficulties described above with formulating the "FORCING" module, a spreadsheet (referred to as the *load* spreadsheet) was found necessary for its creation. This

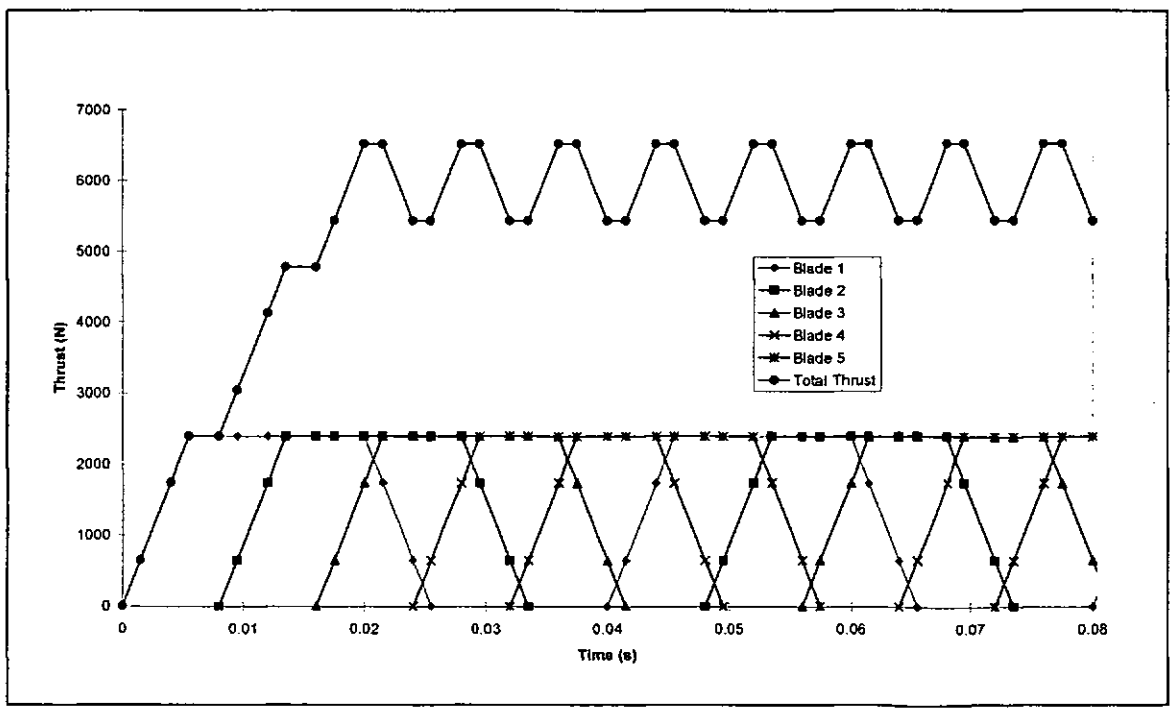

Figure 22. Aggregate Thrust using Plateau Load Profile.

both processed propeller geometry so that forces could be resolved and ensured that all forces were defined every time there was a change in slope of any of the nodal load lines. Figure 22 shows the way in which total thrust builds from zero to a fully developed state using this pattern. This profile was applied to the model in PAFEC running the transient analysis so that at least one revolution in the fully developed state had occurred. This meant running for 70 ms; time steps of 0.5 ms were used to achieve an output resolution fine enough to capture frequencies up to 1000Hz. Running times for the model were typically 16 hours, and the base size (storage) needed for the matrix had to be increased, typically, from the default to 7 Mb for the model to run.

3.6.2.1. *Output Processing - The Output Spreadsheet*

The post-processing capability of PAFEC is limited for the visualisation of time varying reaction forces. Consequently a method was developed which filtered the appropriate bearing displacement results from the text output file and transferred them to a spreadsheet

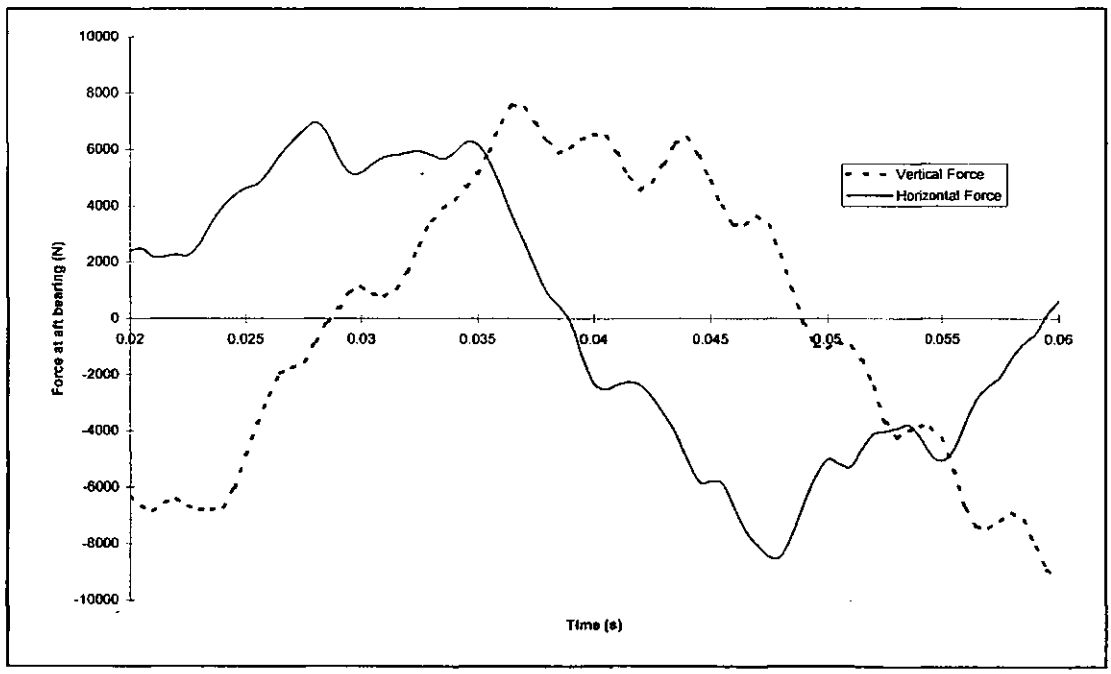

Figure 23. Force Variation at Aft Bearing (frame of reference fixed to propeller).

(the *reaction* spreadsheet). These were then manipulated to:

- convert displacements to forces transmitted through bearing supports by applying bearing stiffnesses. A similar process was used to convert axial displacement to thrust and angular displacement at the forward end of the shaft to torque.
- change the frame of reference from propeller fixed to hull fixed (ie rotating with the force system). This was done by adding the appropriate time dependant angle to each force component in the plane of the propeller disc, and recasting these as vertical and horizontal forces with respect to the hull. This process is illustrated in Figure 23 and Figure 24. Here the time window from 0.02 to 0.06 seconds covers one revolution of fully developed force application at the rotational speed of 25 Hz. Figure 23 shows the vertical and horizontal forces at the aft bearing during this time period before the change of reference frame; Figure 24 shows them referenced to the hull. Thrust and torque were not affected by this process.

Further analysis was carried out to determine the behaviour of the system under the influence of the time varying loads and this led to the next stage in the development of a

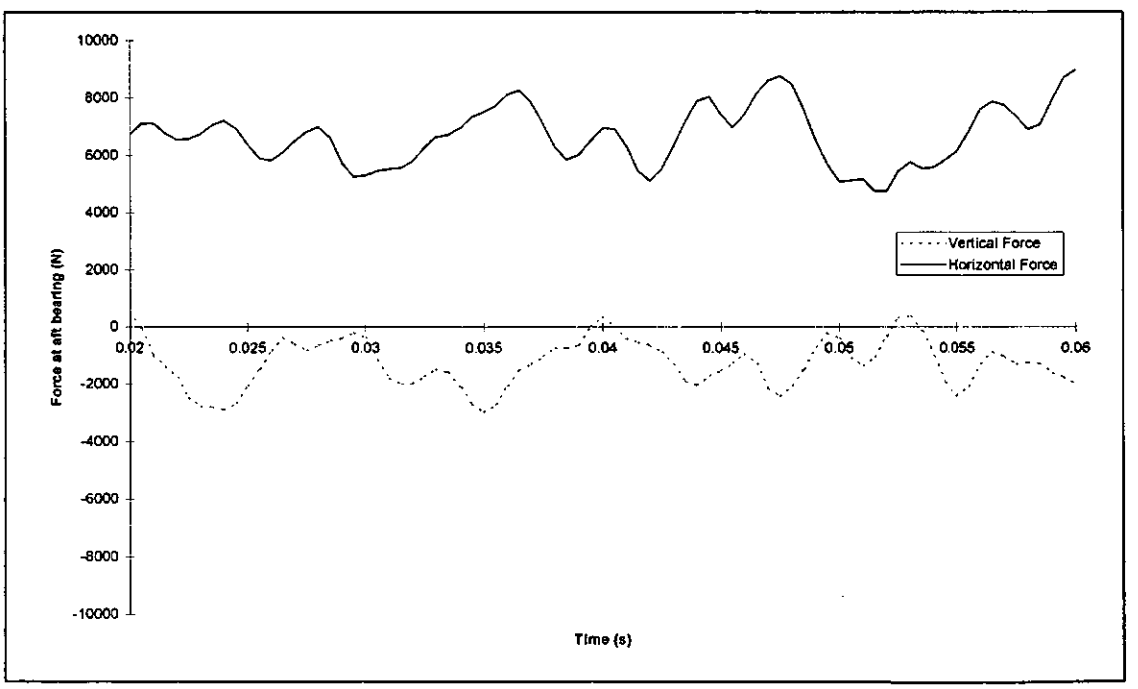

Figure 24. Force Variation at Aft Bearing (frame of reference fixed to hull).

more realistic load profile.

3.6.3. Development of Transient Model (No. 2 - "Spike" Load at a Constant Radius)

Clearly the picture painted in the previous section is simplistic. Rotational speed is not a single fixed speed but will vary over the working range, and will coincide at various points with system resonances, though not at the design speed if the system is well designed. Damping will occur, to a small extent internally within the structure and also externally due to viscous forces on the propeller. Centripetal stiffening of the blades will occur, especially at high speeds, and Coriolis forces may be an issue, as the propeller, on the overhung shaft, rotates while the shaft vibrates, thus giving a variable eccentric motion. Finally, and of major importance, the simple load profile used previously is inadequate. This is clear from the fact that the mean vertical force was found to be close to zero because of the symmetry of the loading about the vertical centre-line; similarly the moment about a vertical axis is also small. Practice shows a significant vertical force and vertical moment (measured by Rose et al (1993)) which point to asymmetric loading - a high blade lift on the side where blades enter the water which then reduces towards the exit. This is also supported by Allison (1978) who measured the pressure at a point on the blade of a SPP, and observed a considerable peak as the blade entered the water. The effect is less marked in experiments by Olofsson (1996), who measured forces on a single blade of a SPP by mounting it on a flexure unit. This was probably because of the relatively low immersion (30%) which he used.

It is also apparent that the precise nature of the load profile is significant to the vibrational performance of the system. This is because the profile shape - the gradient of the rises and falls and the extent of any constant load periods - governs the distribution across the frequency range of the input energy which excites the system. The interaction between

these frequencies and system resonances has a direct bearing on the size and frequency of the system vibrations.

3.6.3.1. Experimentally Derived Load Profile

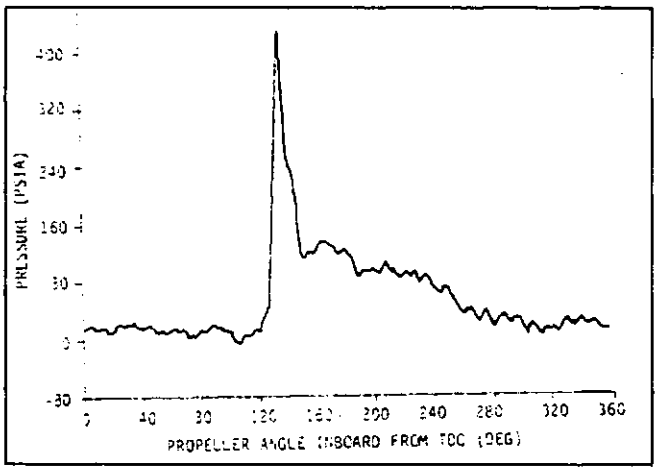

Figure 25. Pressure Measurement at 55% Radius, 60% Chord (from Allison (1978)).

The pressure peak measured by Allison is shown in Figure 25. This measurement was made at 55% radius, 60% chord on a full scale (8 ft diameter) controllable pitch SPP and clearly shows a steep rise in pressure as this part of the blade impacts the water.

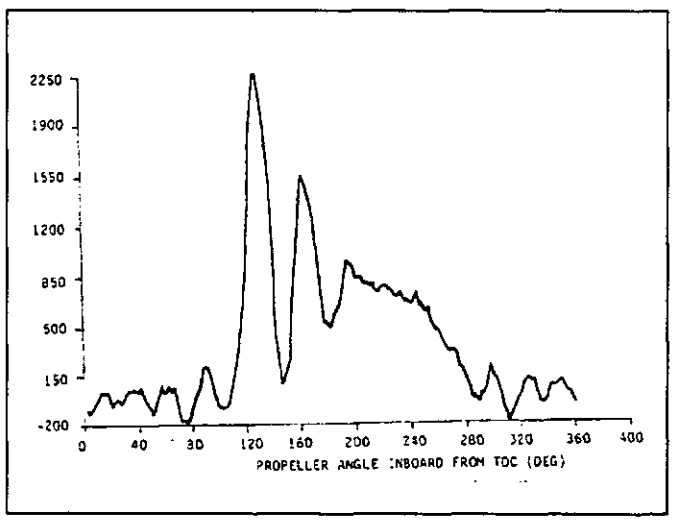

Figure 26. Measured Strain at Blade Root (from Allison (1978)).

This peak is not predicted by any of the theory so far developed, and consequently the small quantity of experimental evidence available has to be relied upon.

The cumulative effect of all such pressure peaks leads to a total force on the blade which also rises to a peak, though this is now spread over a wider angle of rotation. This is demonstrated by a root strain measurement made by Allison (Figure 26) which is indicative of the total blade load and shows the initial rise and fall followed by a more gradual tailing off. Superimposed on this a substantial vibration load (estimated at approximately 280 Hz) due to blade flexing can be seen.

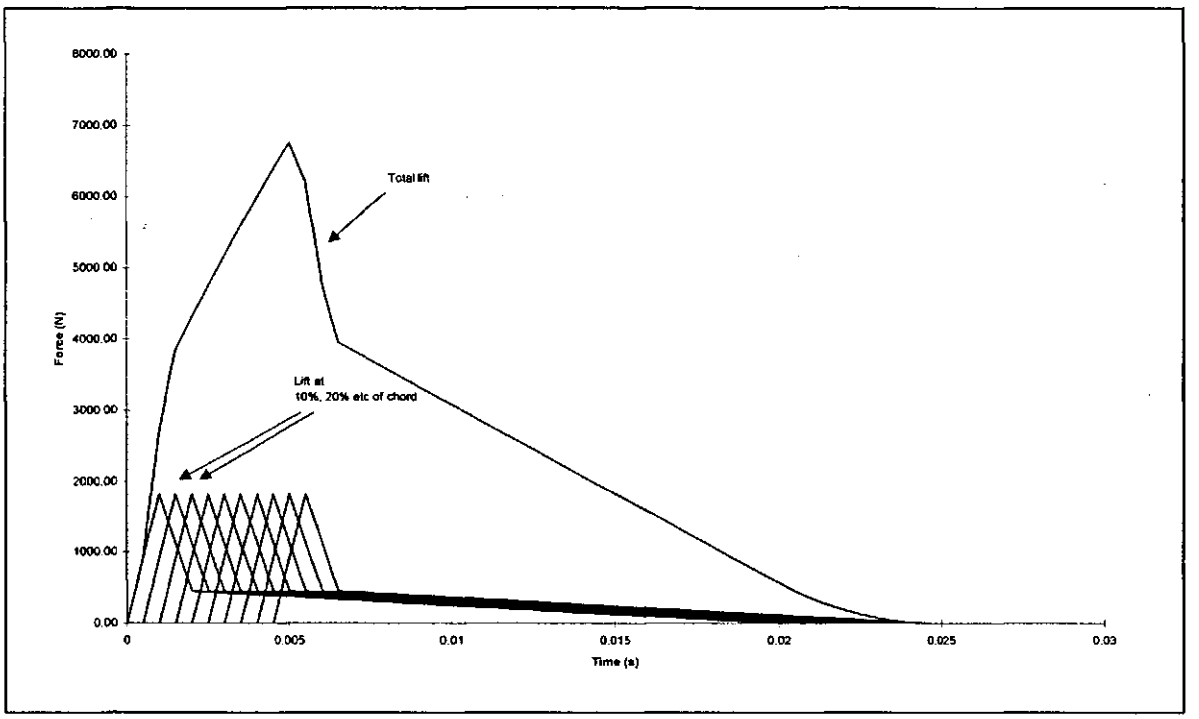

Figure 27. Aggregate of Forces using Measured Pressures.

To arrive at a more realistic load profile, the pressure peak measured by Allison was assumed to apply at each node point across the blade at 50% radius. Therefore this profile was summed for each point, time-shifted to allow for rotation (Figure 27). The load pattern thus produced was then scaled to give the same average thrust as previously used.

The resulting load history for the propeller, referenced to the hull and expressed as the force set applied at the hub is shown in Figure 28.

From this it can be seen that the vertical force and steering moment have non-zero values, since the load is now rotationally non-symmetric. One other effect of this more realistic profile is that the horizontal input force becomes time-varying.

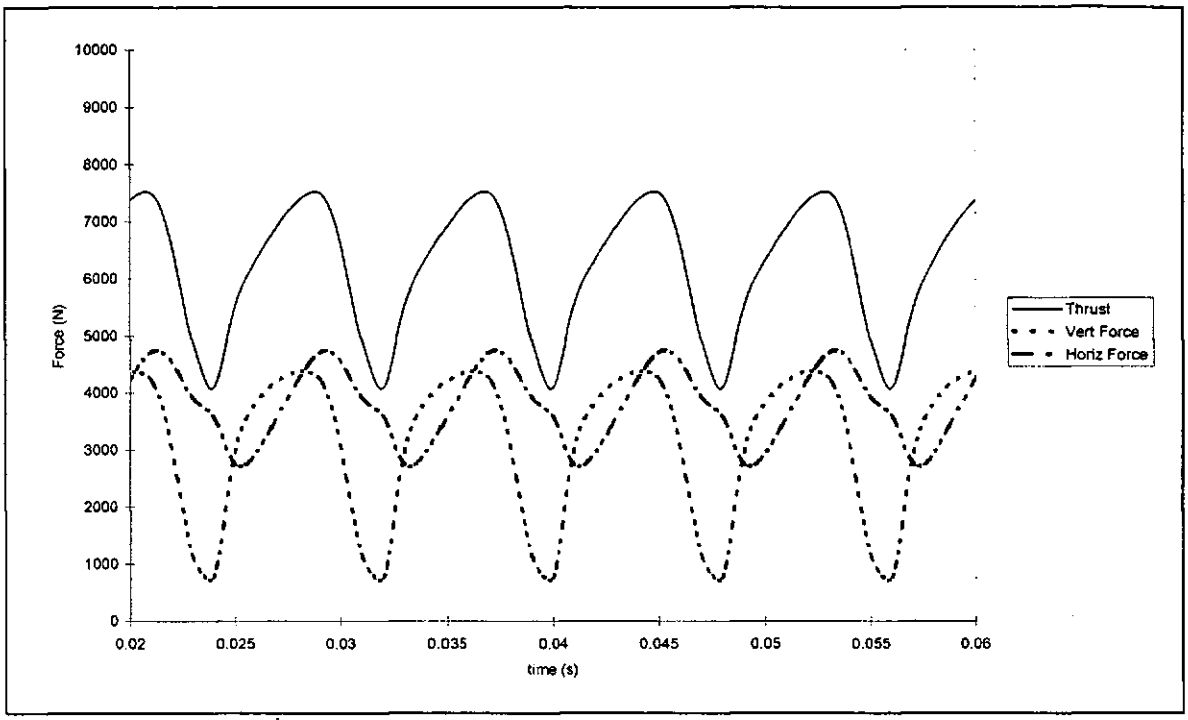

Figure 28. Effective Hydrodynamic Forces.

This load was then coded as a PAFEC "FORCING" module, with the force applied to the node at the centre of area of each blade.

3.6.3.2. Influence of System on Input Forces

The hydrodynamic forces applied to the propeller may be conveniently resolved into a set of 3 forces and 3 moments applied at the hub (Figure 29). These forces produce reactions at the supports which, if the system is fully rigid, may be calculated from simple force and moment resolution at each time-step. With a non-rigid system, PAFEC was used to predict these reactions which have now been modified by inertia forces. In order make a convenient comparison, the reaction forces at the supports which were output from the PAFEC model were resolved at each time-step to determine a hub force/moment set. This is equivalent to the set which *would be needed* at the hub of a rigid system to produce the same effect at the supports as the actual hydrodynamic forces acting on a non-rigid system.

This "modified input" may then be directly compared with the actual hydrodynamic input, also expressed as a 6 component set at the hub.

The output from PAFEC is shown in Figure 30 and Figure 31. The following are evident:

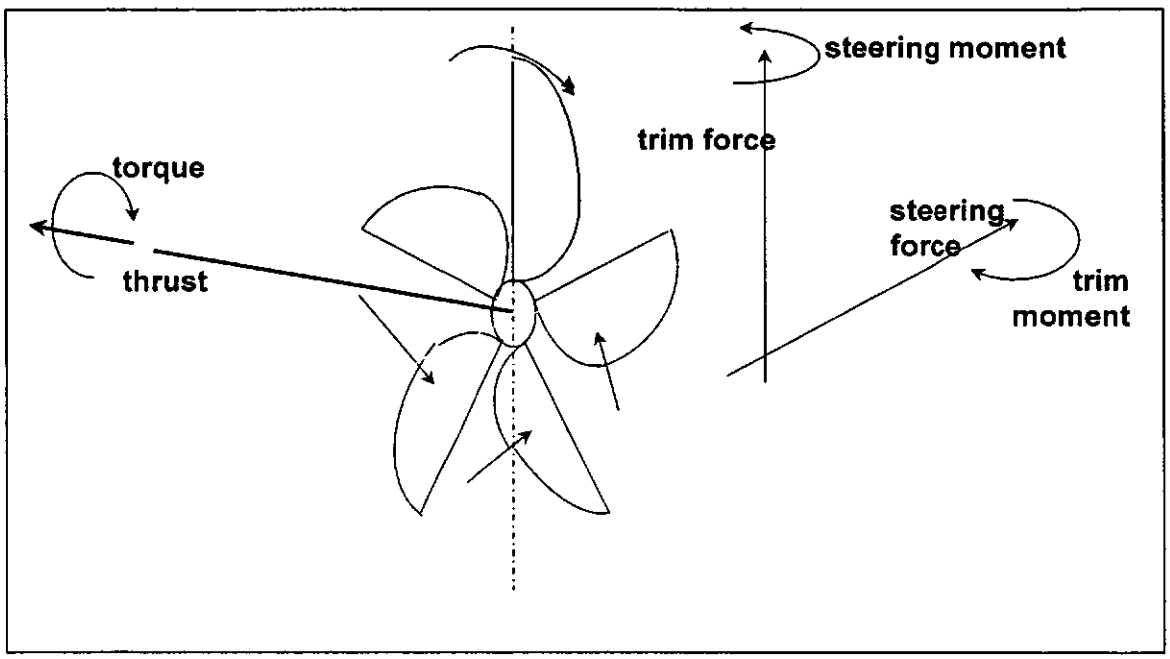

Figure 29. Six Components of Propeller Force / Moment.

- the thrust follows the input force closely with the blade passing frequency being dominant, but superimposed quite strongly upon this are 2nd and 4th harmonics.
- side and vertical forces are significantly amplified and are dominated by higher harmonics of blade passing frequency.
- steering and trim moments are dramatically amplified, and bear little resemblance to the input values.
- torque maintains approximately the same value as the input but is now dominated by the frequency of the first torsional mode of the shaft.

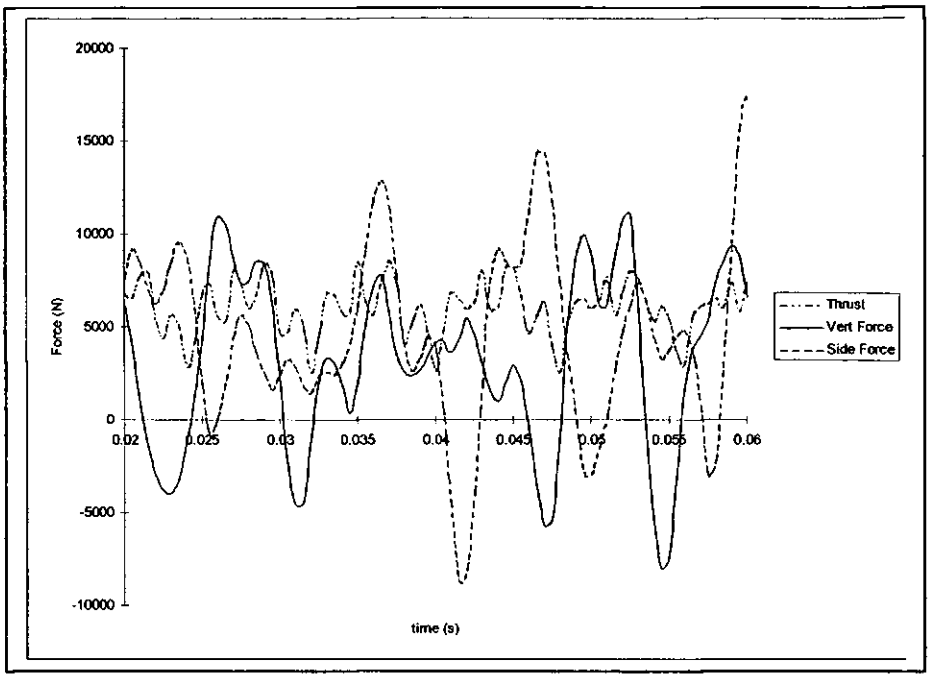

Figure 30. Effective Forces due to Hydrodynamics and Inertia.

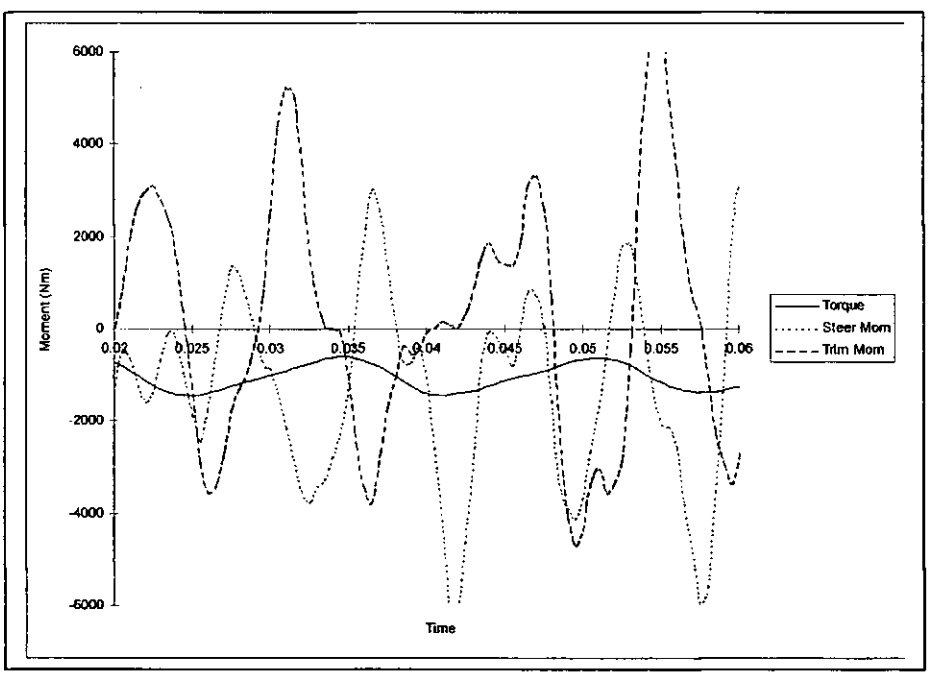

Figure 31. Effective Moments due to Hydrodynamics and Inertia.

The peak loads predicted from this analysis are significantly in excess of steady loads, and a preliminary investigation into the stresses induced by these loads shows that values approaching the fatigue endurance limit of the material are reached.

Furthermore an initial estimate has been made of the size and nature of the forces transmitted through the bearing housings to the hull. These values are of importance from the point of view both of hull fatigue and of passenger comfort.

3.6.4. Further Development of the Transient Model (No. 3 - "Spike" Load, Distributed)

The transient model which has been developed uses experimentally derived data, in terms of the peak pressure which is applied to any point on the blade, and provides an adequate input to the FE model. This permits a comparative study of shaft configurations. However it is limited since the load profile at only a single representative radius is considered. Thus no account may be taken of blade shape and configuration.

In order to refine the approach, the application of pressures to node points across the entire blade surface was considered. This was implemented in Visual Basic, using a time step procedure. The propeller was fixed and the waterline was modelled as rotating around the hub, sweeping across a stationary blade. An offset between propeller centre and waterline was included to allow for the effect of different immersions. It was assumed with this model that the waterline was cleanly cut at both entry and exit by the blade (Figure 32). The method is summarised as follows:

- the blade geometry file is accessed to determine the position of each node. From these, the direction cosine of the surface at each node is calculated.
- at each time step, each node is examined to determine whether it is always dry, immersed for the full revolution or immersed for part of one.

- if dry, then the pressure at that node is set to zero;
- if always immersed, it is set to the time-based mean pressure given by the load profile;
- if partially wet, then the angle through which that node has turned in water is determined. The magnitude of the pressure exerted at that point is then calculated by interpolation of a point load profile based upon Alison's (1978) measurements. Since the experimental data is limited, this profile is expressed only as a function of the angle turned by a node in water and not of either radial or chordwise position. It would be a simple step to include these latter dependencies if the data became available.

- the nodal forces are determined by applying the pressures to the area of the element surrounding each node. These are then resolved into axial, vertical and horizontal

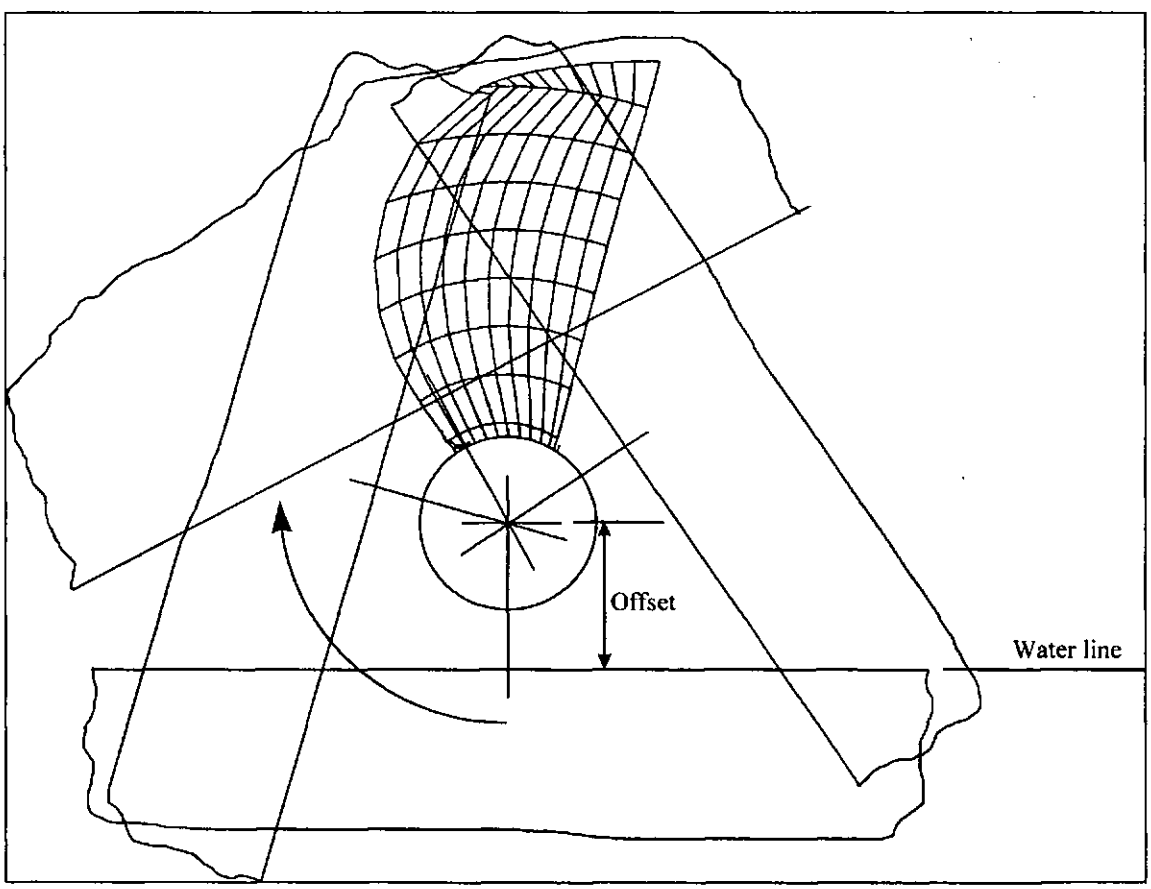

Figure 32. Schematic Showing Waterline Sweeping Across Stationary Blade.

components relative to the fixed propeller and integrated across all blades for each time step.

- the frame of reference is changed from the fixed propeller to the moving water surface, and therefore to the vessel.
- instantaneous values of thrust, vertical and horizontal force are normalised on mean thrust.

The code was run as an Excel macro, with one full revolution divided into 128 time steps to facilitate the later use of Fast Fourier Transforms. It was also linked to a harness code which ran it for a range of immersions. Typical results from this, showing the variation of both mean loads and rms values with immersion are shown in Figure 33.

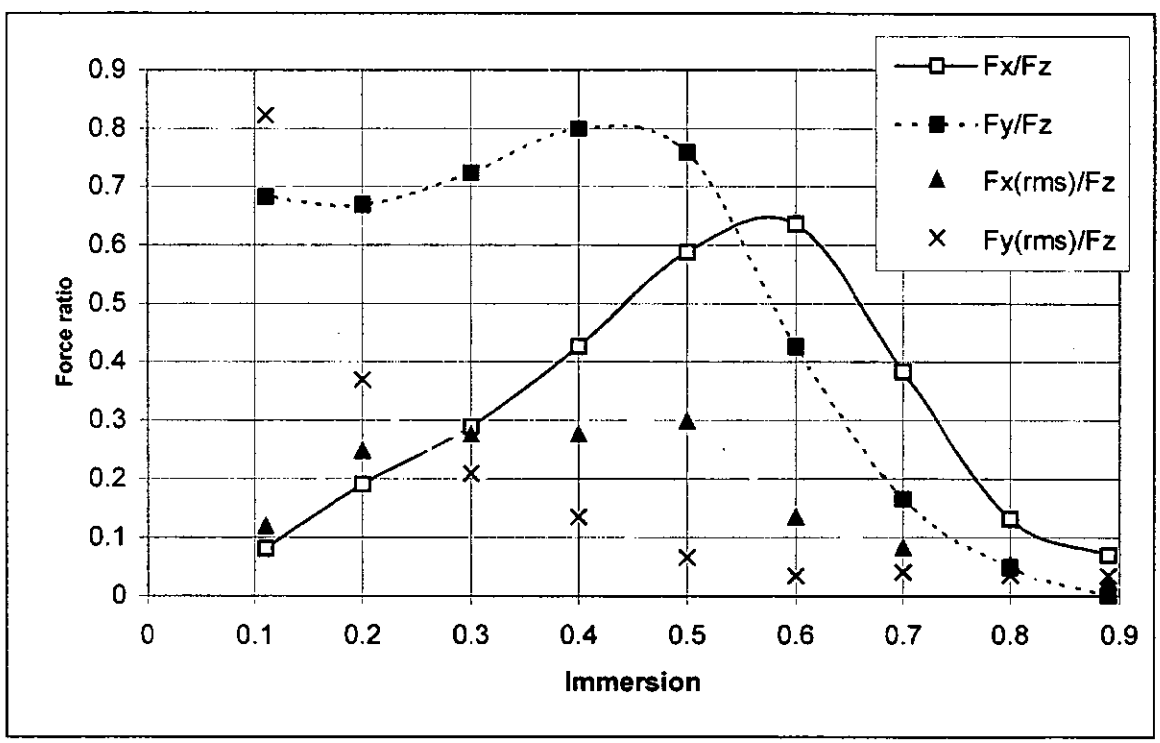

Figure 33. Propeller Forces (normalised against thrust) vs Immersion (F_x – vertical, F_y – horizontal, F_z – thrust).

The model which has been developed is a useful tool in the comparative study of geometric effects on transient loading. It is particularly instructive to view the results in the frequency domain to determine the effect upon each blade rate harmonic of changes in propeller configuration.

The propeller used for the first trial of this model was of 250 mm diameter with a P/D of 1.52, 4 blades and disc area ratio of 68%, chosen because detailed drawings were available. The skew of the blade was configured so that the trailing edge was radial (Figure 34 (a)).

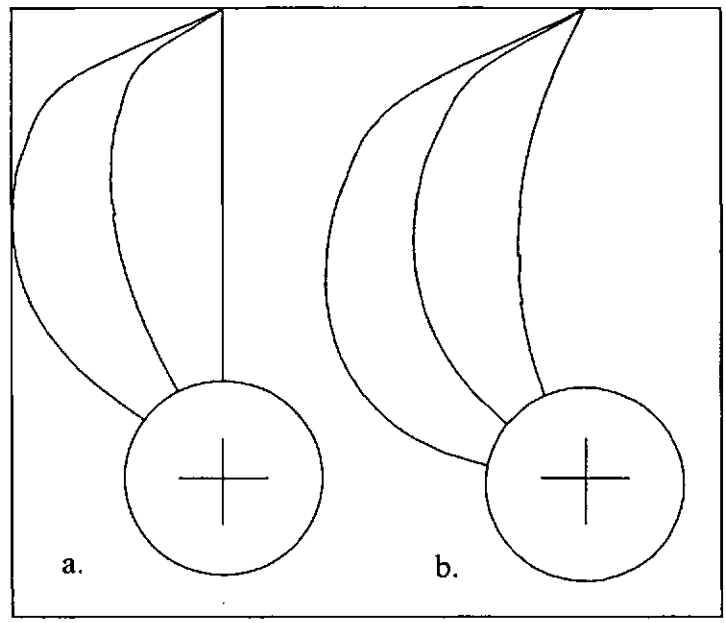

Figure 34. Standard (a) and High Skew (b) Blades.

3.6.4.1. Mean Load Results

In Figure 33 forces are normalised against the thrust at the relevant immersion so that comparisons may be drawn with other work. It is evident from the figure that vertical components of force are low at low immersion since blade lift forces are directed almost horizontally; at high immersion they are balanced for blades on each side of the vertical centreline and they peak at approximately 60 % immersion. Vertical components approach the tangent of pitch angle at the blade tip for low immersion, are also balanced for high immersion and peak at approximately 45% immersion.

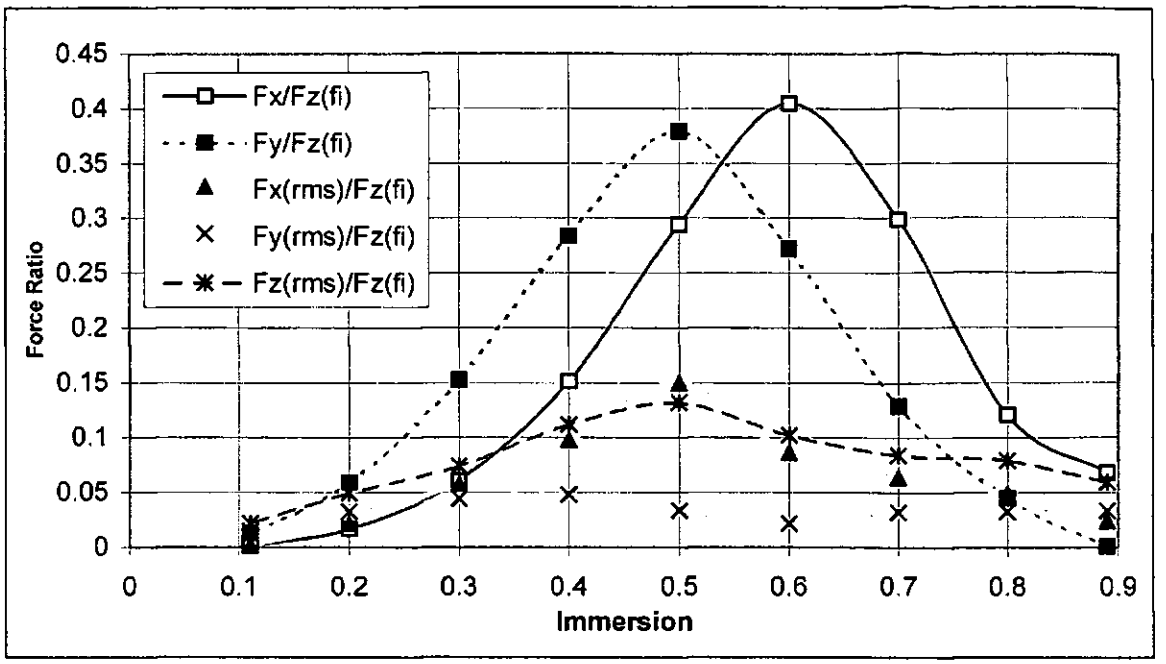

Figure 35 Propeller Forces (normalised against thrust fully immersed) vs Immersion.

Clearly, when immersion is low, the thrust is also low and thus the values scaled to mean thrust at that immersion do not give the clearest picture of when peak absolute loads arise. Consequently Figure 35 shows the forces scaled to the mean thrust that would be produced if the propeller were fully immersed; peak values occur for vertical and horizontal forces at 60% and 50% immersion respectively.

Vorus (1991), in work described previously, uses a theoretical approach to determine mean vertical, horizontal and thrust loads. The propeller which he used to demonstrate his method was of diameter 394 mm, P/D 1.43, with 3 blades and disc area ratio 52.8%.

Rose and Kruppa (1991) and Rose et al (1993) provide experimental results for these mean forces. The measurements of the latter were made at a variety of shaft inclination angles and presented against K_q/J^5. Consequently, in order to make a comparison, values were transformed from vessel related (*T_c (thrust), F_{vc} (vertical), F_h (side)*) to shaft related (*F_z (axial), F_x (perpendicular to shaft: up), F_y(perpendicular to shaft: side)*) (see Figure 36); the data was also manipulated in order to plot against advance coefficient. Figure 37 shows the variation in F_x/F_z and F_y/F_z with advance coefficient from Rose et al's results for the

configuration closest to the propeller used in this work: diameter = 250 mm, P/D = 1.6, 4 blades, disc area ratio = 80%. Immersion for this data was 47% and shaft inclination was 8^0.

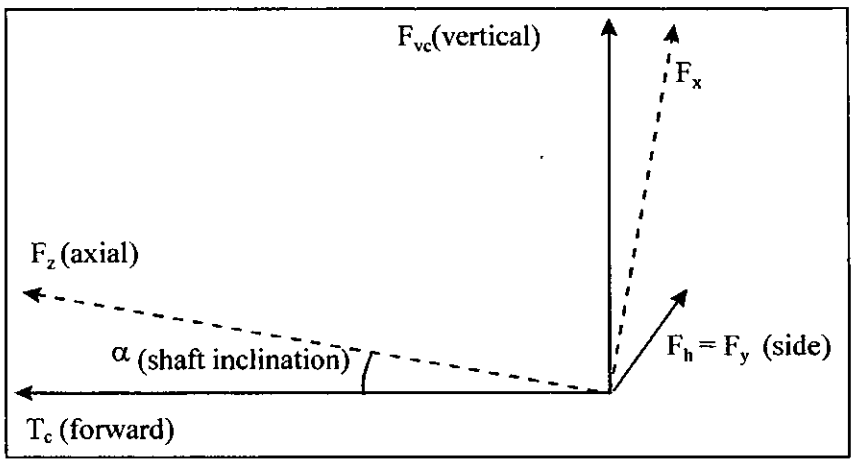

Figure 36. Axes Related to Craft (T_c, F_{vc}, F_h) and Shaft (F_z, F_x, F_y).

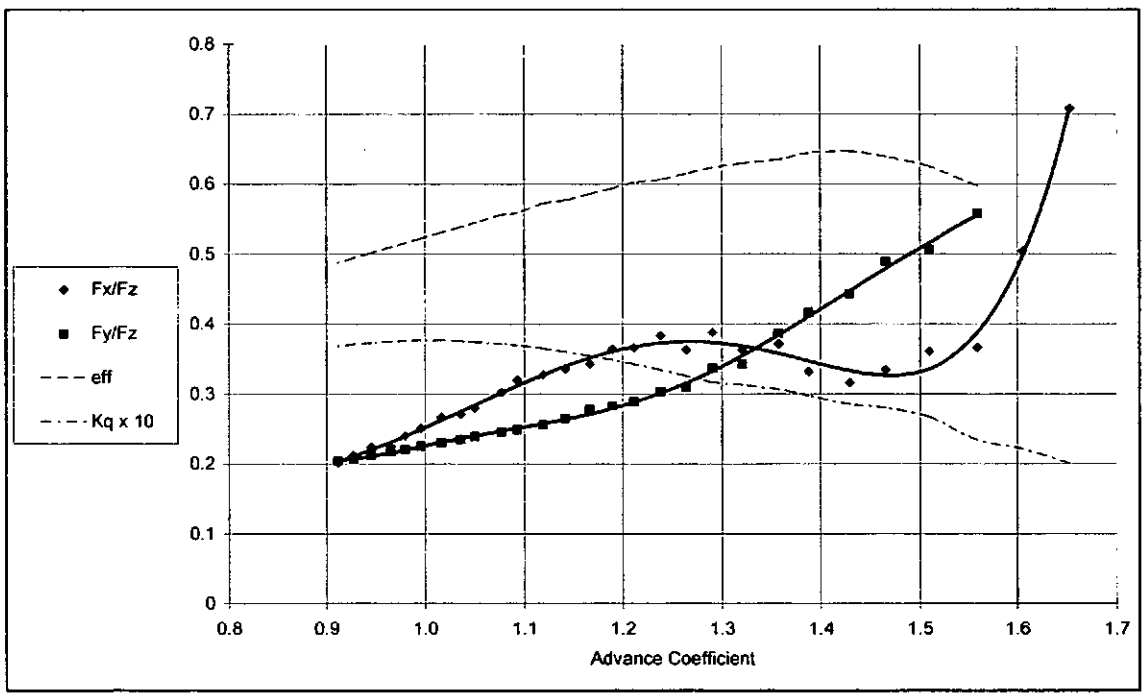

Figure 37. Side and Upwards Force Ratios (from Rose et al (1993)).

A comparison of mean loads is given in Table 3. These values show wide discrepancies. Vorus assumes that constant lift is produced while the blade is submerged; this is then modified using lifting line theory to allow for changes in angle of attack resulting from

shaft yaw and inclination. However, experimental evidence (Alison (1978)) clearly shows that blade surface pressures, and therefore lift forces are strongly influenced by transient flows and the proximity of the free surface, producing a highly non-axisymmetric lift profile as blade sections pass through the water. It is this which is responsible, in large measure, for the high side and vertical forces, even when yaw and inclination are zero. An attempt to model this asymmetry has been made in this work, which distinguishes it from that of Vorus, and gives results which are closer to the experimental evidence. However, lack of data concerning the spatial variation on the blade surface of the transient pressure profiles makes this model a simple one at present.

Table 3. Comparison of Force Ratios.

	This work Theory 50% immersion P/D = 1.52	Rose & Kruppa Experiment 47% immersion P/D = 1.6	Vorus Theory 50% immersion P/D = 1.43
F_x/F_z	0.59	0.2 to 0.4 (0.33 at max eff'y)	0.11
F_y/F_z	0.76	0.2 to 0.5 (0.45 at max eff'y)	0.01

In comparison with the experimental results, clearly this work over-predicts the F_x and F_y forces by a significant amount. Furthermore no allowance is made in the model for variations with advance coefficient. This factor would not only modify the angle of attack, and thus the lift distribution on the blade, but it would more importantly change the operating regime. As the operating point moves from lightly loaded and therefore partially ventilated, to heavily loaded and fully ventilated, this would also cause of change of lift distribution across the blade.

Observation of a propeller in operation makes another point clear; in practice the water surface is ill-defined in terms of both its position and its nature. As advance coefficient falls, so the blockage effects of the ventilated blades causes a pressure field upstream of the

propeller which raises the surface. Thus an immersion nominally measured as 50% becomes significantly more under some conditions. Also spray at the surface makes the transition from water to air indistinct, with an indeterminate quantity of water carried above the surface by the propeller. These factors make the modelling process an uncertain one and result in the differences between theoretical and experimental results. It can be seen from Figure 33 that vertical and horizontal force fall rapidly as immersion is increased above 50%; thus if the nominal immersion of 50% were in fact nearer to 65%, then values would be closer to the experimental figures.

3.6.4.2. Unsteady Load Results

The characteristics of the time varying forces - the frequencies and amplitudes of the dominant contributions and the aggregate time varying load imposed on the drive system - are key considerations in the design process. They depend on propeller shape (profile,

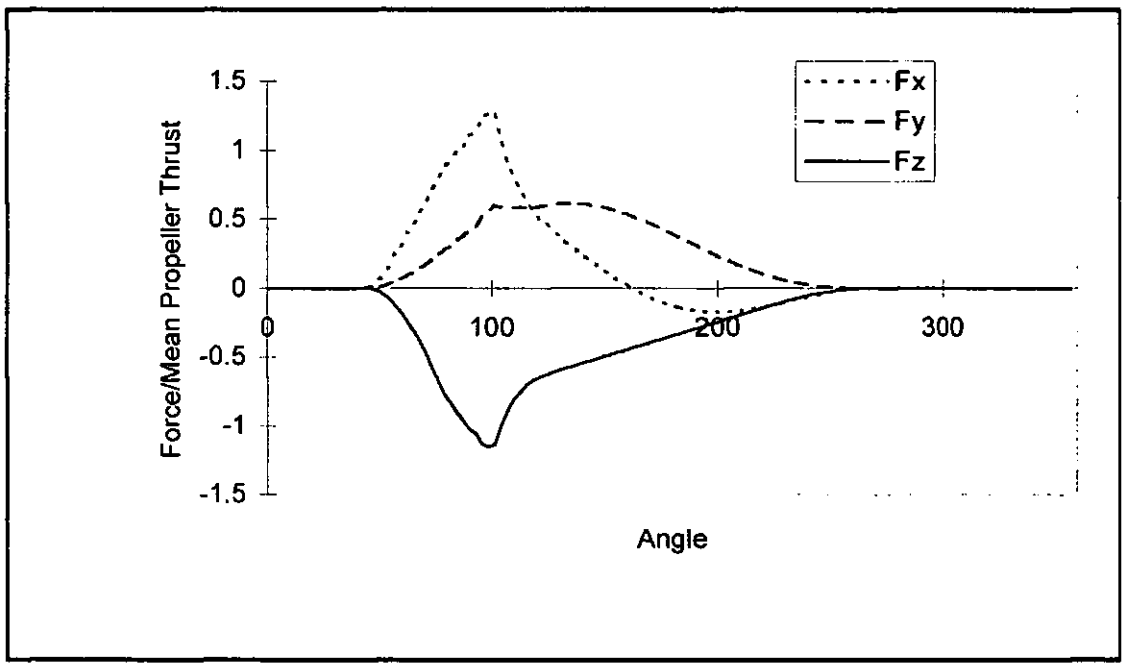

Figure 38. Forces for Single Blade (immersion = 50%).

skew, rake, pitch, number of blades), configuration (inclination, yaw, immersion) and operating conditions (advance coefficient, cavitation and Froude numbers). A comparative analysis of the effects of several geometric factors has been undertaken using this model.

Number of Blades. The output from this transient load model for a single blade is shown in Figure 38, in which forces are scaled to mean thrust. Thrust and vertical force rise rapidly to their maximum values, as a result of the rapid rise in surface pressures as flow is established during the entry phase of the transient. The vertical force then undergoes a reversal as the blade approaches the exit surface, although the rise and fall of this force are not symmetrical since during the exit phase, pressures are lower; thus the net effect is an upwards vertical force. Horizontal force changes more slowly, since the components in this direction are small as the blade enters and leaves the water.

Two propellers with 4 and 5 blades were investigated, using the same blade on each. Thus the disc area ratio was effectively increased by 25% by the addition of one blade, and overlap between blades was increased. A typical plot showing the integrated effect of 4 blades is given in Figure 39.

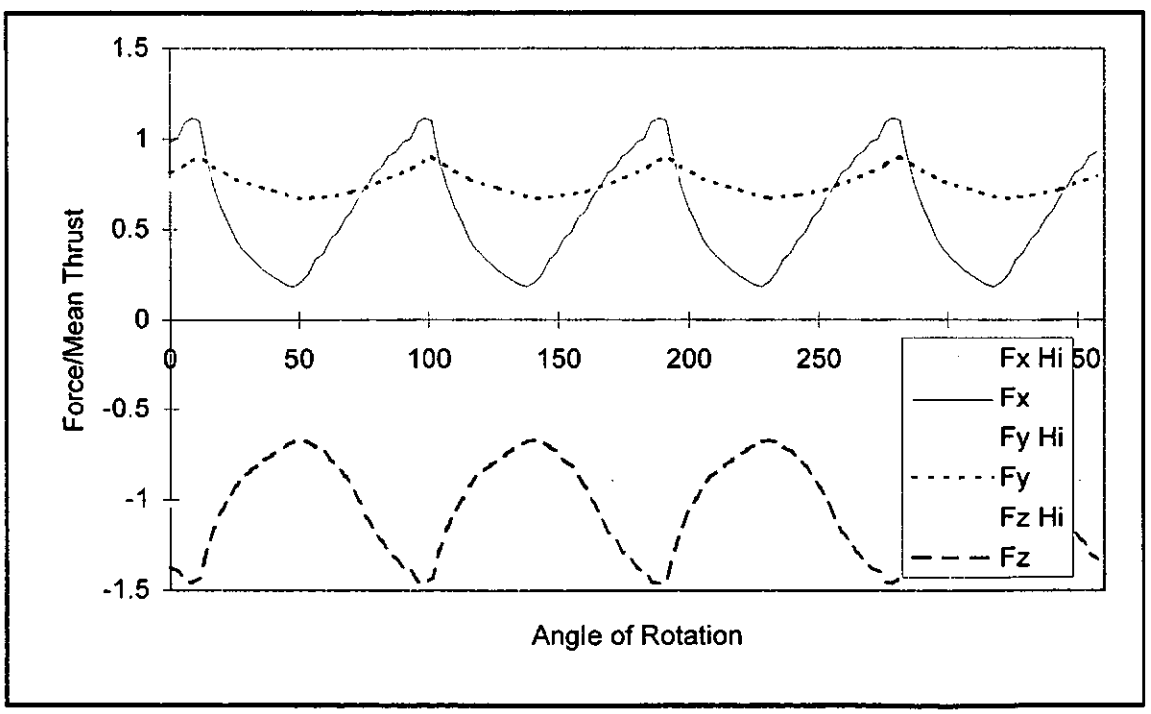

Figure 39. Comparison of Standard and High Skew (Hi) Forces (immersion = 50%).

The effect of increasing blade number is best quantified by the frequency spectrum of the output which shows the contribution to the total amplitude of each harmonic of blade rate Figure 40. From this it may be seen that an increase to 5 blades reduces the amplitude of the first harmonic from 0.36 to 0.26 of mean thrust. There are also reductions in other harmonics, though these make only a small contribution. Similar effects are observed with

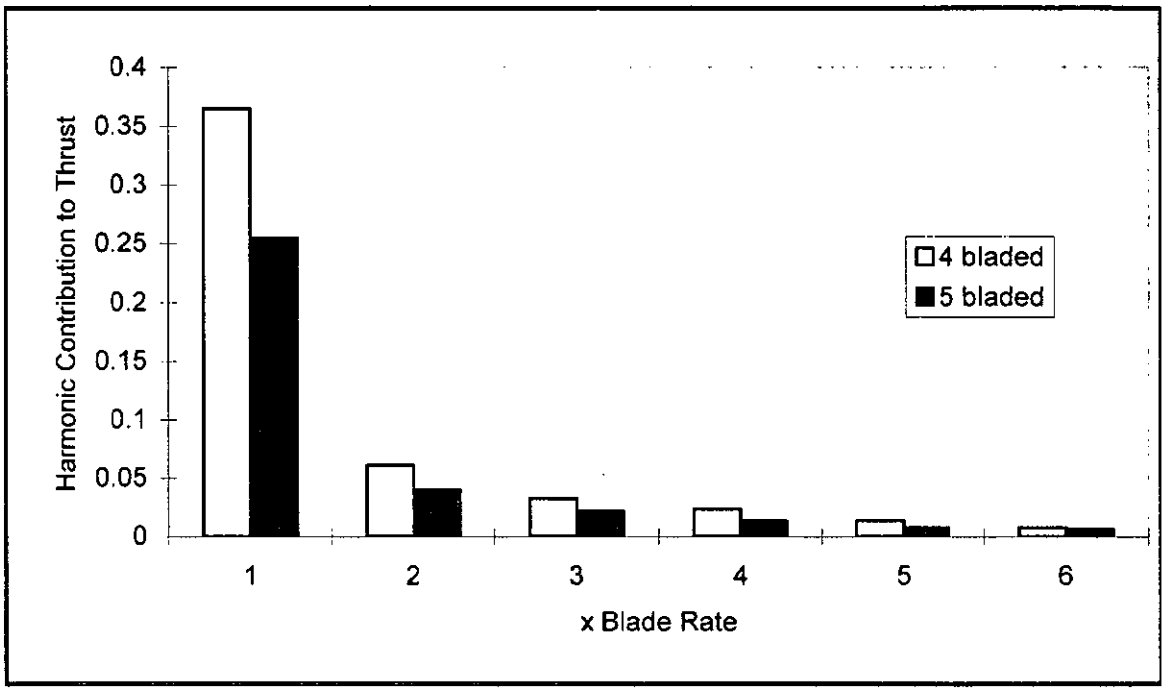

Figure 40. Harmonic Contributions of Thrust for 4 and 5 Bladed Propellers (immersion = 50%).

forces in the other co-ordinate directions.

Skew. Blade skew is one of the key variables used to control the level of vibration excited by the propeller. As the leading edge of the blade is swept back so the impact with the water is reduced; similarly sweeping back of the trailing edge can mitigate the effects of sudden removal of load as the blade leaves the water. However the use of skew must be treated with care, as the increasing asymmetry of the blade about its neutral axis leads to high stresses in the blade root. Also, while chord and disc area ratio may not change,

blades with high skew tend to take on a longer, more slender shape, with possible consequences as far as vibrational behaviour is concerned.

The load model was used to investigate two 4 bladed propellers, identical in pitch and disc area ratio; the first had conventional skew such that the trailing edge was radial. The second was swept by rotating the blade reference line back through an angle which varied linearly with radius from zero at the root to 0.5 radians at the tip. A schematic diagram of the two blades is shown in Figure 34.

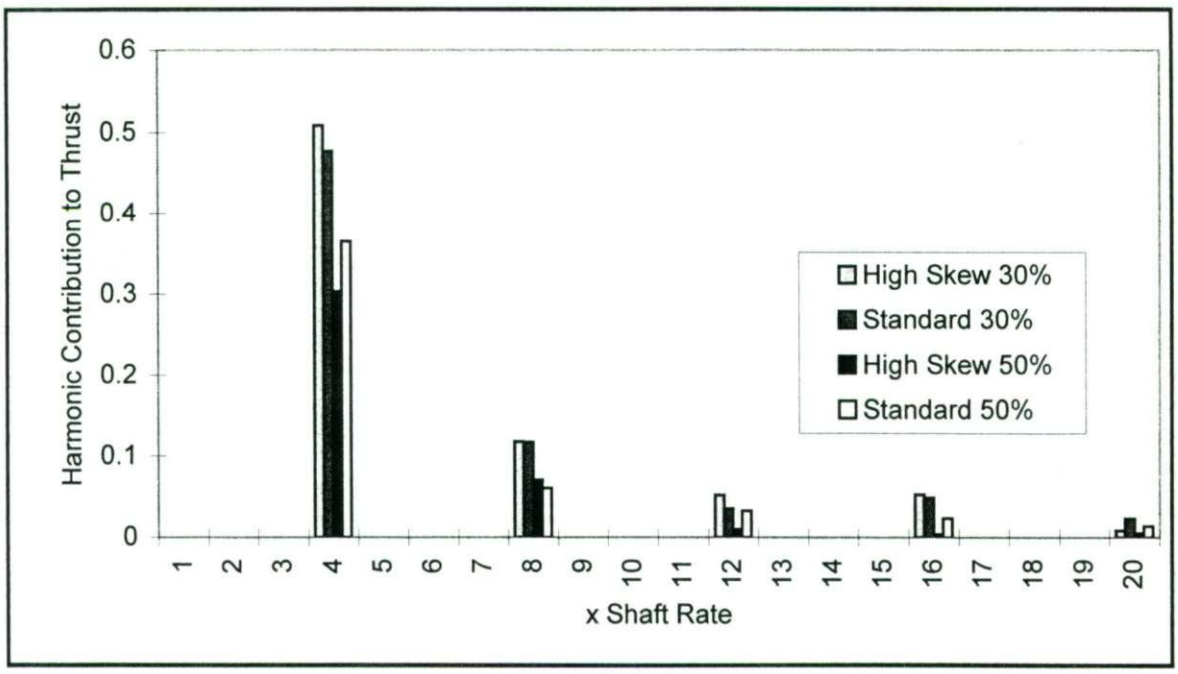

Figure 41. Harmonic Contributions to Thrust - Variation with Skew and Immersion.

The time dependant thrust, vertical and horizontal forces predicted by this model for 50% immersion in the cases of high and standard skew are shown in Figure 39. It is clear, firstly that horizontal force is almost steady. This was commented on when the simpler load models were analysed and supports the theory developed by Vorus (1991). Comparing the standard and high skew cases, it may be observed, as expected, that increasing skew has a beneficial effect on the amplitude of the fluctuating forces. This may be quantified more

easily with reference to the Fourier coefficients of the data. It can be seen from Figure 41 that, for 50% immersion, the increase in skew leads to a reduction in the thrust amplitude at blade rate from 0.36 of the mean value to 0.30. The second harmonic shows a slight increase, and remaining ones, while showing a decrease, are insignificant. The improvement is more marked for the vertical forces Figure 42, with a reduction in

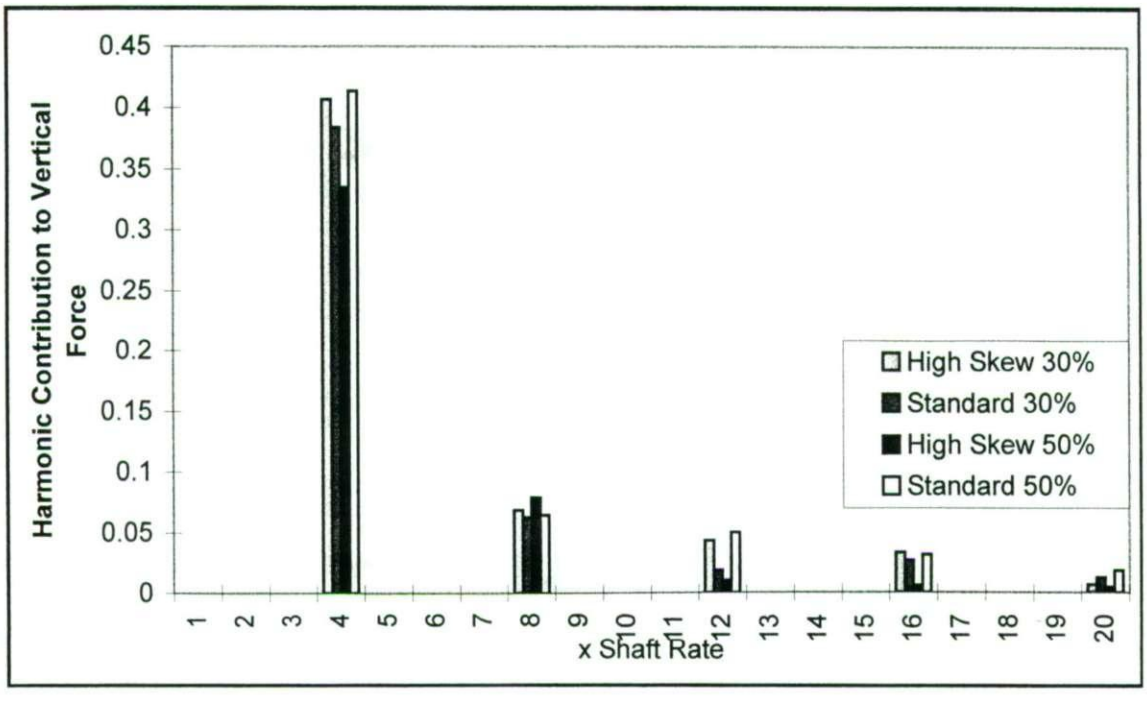

Figure 42. Harmonic Contributions to Vertical Force - Variation with Skew and Immersion.

amplitude from 0.41 of mean thrust to 0.33 in the first blade rate harmonic. It is also notable that the rate of rise in vertical force is significantly reduced in the high skew case, a point emphasised by the reduction in the higher harmonic contributions.

Immersion. At the design point, a propeller would operate at approximately 50% immersion. However there are wide variations in this figure, as payload, trim control, the effect of waves and start up conditions all have an influence. Consequently, the effect of immersion was investigated using this model by firstly determining the magnitude of the vibrational energy as immersion changed. Figure 33 shows this by giving the rms values of vertical and horizontal forces, normalised against thrust. Horizontally, these relative values

are highest at low immersion (since thrust is low); vertically they are almost constant between 25% and 50% immersion, peaking slightly at 50%. As with mean forces, a more realistic picture of the highest cyclical loads imposed on the system is given in, where the divisor is the constant value of fully immersed thrust. Here it can be seen that the thrust and vertical force fluctuations peak at 50% immersion, while horizontal values reach their maximum at 40%.

To examine the effect of immersion in more detail, a comparison was made between the 30% and 50% immersion cases for both the standard and the highly skewed blade. A contrast between the forces for the standard blade is shown in Figure 43, from which two features are clear. Firstly the marked fluctuation in horizontal force at low immersion is evident; referring the standard blade harmonic contributions of Figure 44, the reduction in immersion causes the blade rate contribution to increase in amplitude from 0.09 to 0.29 of mean thrust. Secondly the shape of the load profiles change, particularly that of thrust

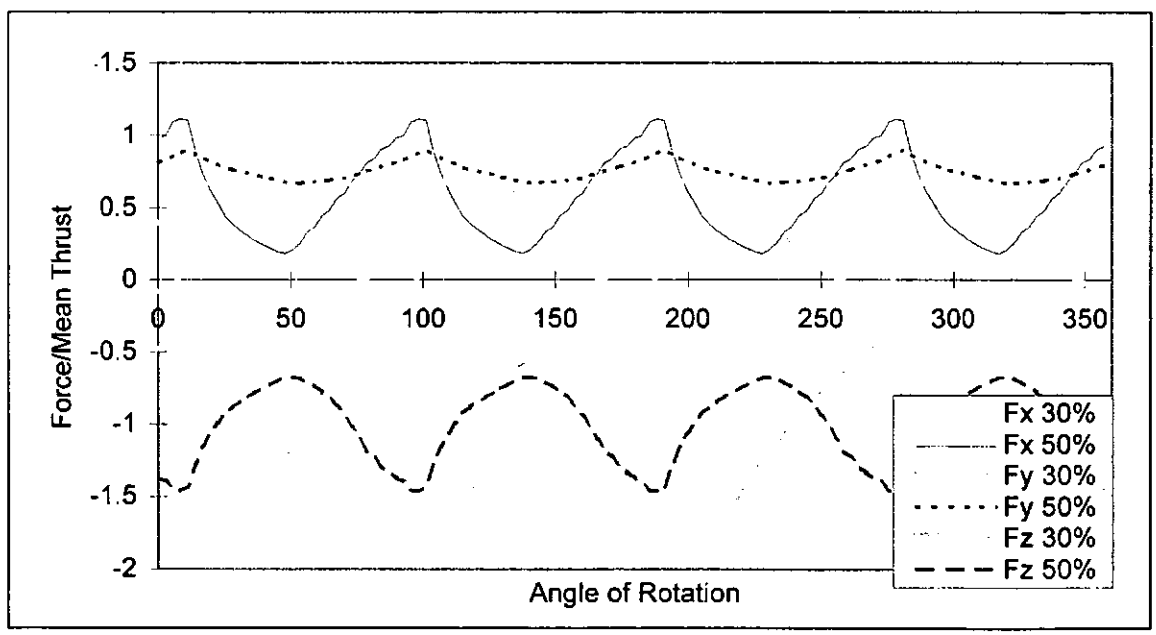

Figure 43. Comparison of Immersions for Standard Blade.

which has a more marked peak. Referring to the standard blade lines for thrust in Figure

41, there is not only a significantly higher blade rate amplitude for the lower immersion, but also an increase in the 2nd harmonic.

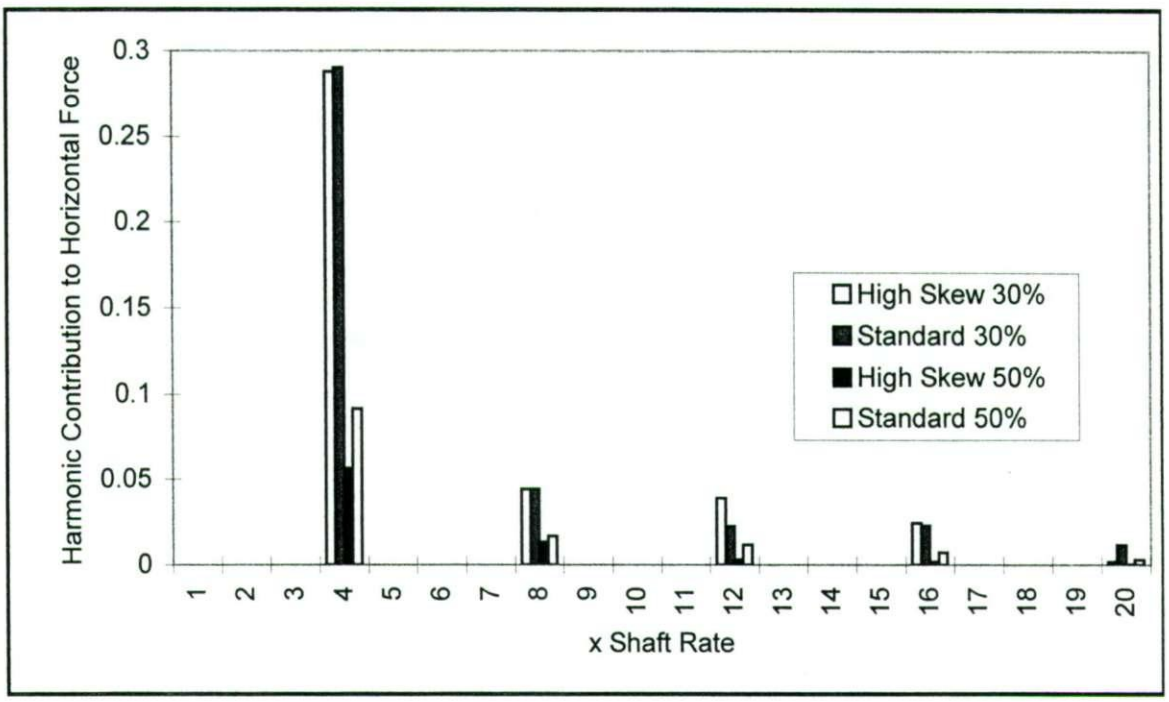

Figure 44. Harmonic Contributions to Horizontal Force - Variation with Skew and Immersion.

Turning to the effect of skew when immersion is reduced, Figure 41 shows that increasing blade skew actually increases the amplitude of thrust when operating at low immersion. A similar effect is also found with vertical forces (Figure 42).

3.6.5. Summary of Transient Loading

A transient loading model has been developed from the experimentally derived "spike" load applied at a constant radius (no. 2). This is sufficient to apply a representative time-varying load to each propeller blade in turn in order to use FEA to assess the response of the system.

The distributed "spike" load model (no.3) may be used to make a comparative assessment of the effect of geometry changes. The limitations of this model are that:

- while the blade surface pressure at a point varies with angle turned by that point, no variation in this transient profile is allowed for in either the radial or chordwise directions;
- variations in transient pressure profile resulting from changes in operating conditions are not allowed for. It would be expected that, as advance coefficient and therefore blade section angle of attack varies, so the surface pressure profile would vary. Furthermore, changes in profile would also be expected as the operating regime changes from partially ventilated to fully ventilated;
- blades are assumed to cut a well defined surface cleanly.
- it would be difficult to incorporate this model in the FEA since the transient load input would be required for every time step at every node point across each blade.

These limitations make any prediction of absolute values unreliable, as shown by the comparison with experimental results. However, if used as a comparator to determine the relative effect of changes in geometry and configuration of a propeller, it is proposed that this method provides a useful tool. Using it, an estimate may be obtained of the way in which mean horizontal and vertical forces vary with geometry; also of changes in the size and nature of the fluctuating components of thrust, horizontal and vertical forces.

4. DESIGN AND COMMISSIONING OF TEST RIG, AND EXPERIMENTAL PROCEDURE

At the outset of the project, it was intended to use the cavitation tunnel at the Defence Evaluation and Research Agency (DERA), Haslar, Gosport. However, early tests showed that this would not be viable because of the difficulty of achieving a level free surface without standing waves, and of obtaining high enough velocities when running with a free surface.

This chapter describes the rationale adopted in the design of a test rig to operate in the alternative facility, a Circulating Water Channel (CWC), also at DERA.

4.1. Facility at DERA

The CWC is equipped with a hood which permits evacuation of the air above the water surface, thus allowing for scaling of cavitation number. It is also sufficiently wide to allow for a range of yaw angles to be tested, and for blockage effects to be small when testing model propellers of 250 mm diameter. In summary, it provides:

- working section width of 1.2 m;
- clearance from water surface to hood of 0.89 m
- advance velocity of 0 - 6 m/s (see later comments under "Commissioning");
- pressure down to 3500 N/m^2 (see later comments under "Commissioning")
- capability for viewing and photography from most directions below the waterline

4.2. Test Rig Parameters

4.2.1. Model Propeller Diameter

Based on a review of previous work, an assessment was made of good working practice for testing SPPs. As may be seen from Table 1 most models tested to date have been in the region of 250 mm diameter. After discussing the matter with DERA, 250 mm diameter

models were considered to be suitable, having insignificant channel blockage effects, even when the yaw angle was set to an extreme angle.

4.2.2. Advance Coefficient and Scaling

Working practice at the DERA has been to use rotational speeds up to 1800rpm. Although this is lower than speeds used by some other workers (2500 rpm by Rose and Kruppa (1991) and Rose et al (1993), 3000 rpm by Olofsson (1996)) it is considered sufficient to cover most of the working range.

Advance coefficients (J) and maximum velocities covered by previous workers are:

0 - 1.3,	6.4 m/s	by Hadler and Hecker (1968),
0.7 - 1.6,	8 m/s	by Rose et al (1991 & 1993),
0 - 1.45,	approx. 4.7 m/s	by Ferrando (1996)
0.4 - 1.3,	12 m/s	by Olofsson (1996).

Testing across the full range of J values is desirable: at low J since designers need high load data to predict starting performance, at high J for design speed conditions, and in the transition region since this is where particular vibration problems may occur. Olofsson (1996) notes that cavitation and Froude numbers play a significant role at low J and at transition. Therefore, if possible, full scale σ and Fr numbers should be achieved in these regions.

At full speed, a typical vessel (50 kts, 0.5 m diameter propeller) has σ and Fr of 0.3 and 11.6 respectively, and a design advance coefficient, depending on propeller pitch, in the region of 1.2. To recreate the cavitation requirement at model speed, using the maximum advance velocity of 6 m/s, a reduced atmospheric pressure of 0.054 bar is required. Modelling of advance coefficient requires a rotational speed of 1200 rpm. These conditions may be achieved in the CWC. However, the Froude number under these conditions is only

3.8, substantially less than the 11.6 required. Fortunately, Olofsson states that in this partially ventilated region, Froude effects are negligible provided Fr>4, a condition which is almost satisfied in the test channel at 6 m/s.

Testing at lower values of J while keeping σ fixed may be achieved by increasing rotational speed up to the maximum of 1800 rpm (J = 0.8). Below this the advance velocity needs to be reduced, while reducing atmospheric pressure to its minimum of 0.035 bar (at which J = 0.64); clearly any reduction in advance velocity will cause a reduction in Froude number, and thus a further divergence from full scale conditions. Further reductions in advance coefficient may only be achieved by reducing velocity still further, which will cause increasing discrepancies in σ.

In conclusion, high values of rotational speed and motor power would be required to simulate full scale σ at low J. Even then, Froude number would not be scaled correctly. The added expense of attempting to achieve true scaling is not considered justifiable in terms of the extra data that would be made available.

4.2.3. Inclination

Shaft inclination is closely tied to propeller rake and plays an important role in determining the forward thrust, thrust variations during a propeller rotation and the vertical force which in turn influences vessel trim. Shaft inclinations used by previous workers are:

4^0, 8^0, 12^0 by Rose et al (1991 & 1993),
4^0, 6^0, 8^0 by Ferrando (1996),
0 - 5^0 by Olofsson (1996).

Feedback from industry and the literature shows that the most commonly used value is in the region of 7^0. The test rig will accommodate inclinations from 4^0 to 8^0.

4.2.4. Immersion Ratio

Immersion ratios used previously are:

33% - 60%	by Hadler and Hecker (1968),
30%, 47.4%, 58%	by Rose et al (1991 & 1993),
40% - 80% (and fully submerged)	by Ferrando (1996),
33%	by Olofsson (1996).

In operational vessels, values are in the region of 50% and less except when starting. The test rig configuration will permit up to 50% at all inclinations, and more at higher inclinations. Inclination and immersion will be independently variable (not the case with Rose et al (1991 & 1993)).

4.2.5. Yaw

Yaw is significant in determining side force, and has an effect on force variations and propeller efficiency. The effect of yaw has been investigated by Olofsson (1996) who used values in the range $0\text{-}30^0$; also by Alder and Moore (1977). The test rig will accommodate values in the range $0\text{-}15^0$.

4.2.6. Torque and Force Magnitudes

Using the K_q-J curves which have been collated (Figure 8), with the rig operating at its maximum speed (6m/s, 1800 rpm, giving J=0.8) the highest torque likely (from the peak of Ferrando's upper curve) is assessed as 50 Nm; at this point the thrust produced is some 880 N. However, conditions for this were extreme at 80% immersion, and since Ferrando comments that his rig restricted him to 392 N thrust and 14.7 Nm torque, it is clear that he did not obtain these results at full speed.

More realistic figures come from Rose et al (1993); their peak torque for P/D=1.6, IR=58% occurs at J=1.05. If V=6 m/s (for which n=1370 rpm) then Q_{max}=22 Nm; if efficiency is taken to be 50%, then the corresponding thrust is 260 N.

At this point vertical and horizontal forces may also be found from their results; $F_v/T=0.55$, $F_h/T=0.08$. Thus $F_v=143$ N and $F_h=21$ N. It should be noted that as immersion falls F_h/T rises, but there is also a fall in thrust and therefore little overall change in side force.

4.2.7. Vibration Forces

By taking Olofsson's (1996) results for a single blade and summing to simulate the composite force on a 4 and 5 bladed propeller, the nature of the vibration forces expected was investigated. From this it was found that the following approximate time varying force ranges and frequencies would be superimposed on the steady thrust value:

- blade striking frequency: 0.1 x thrust, 0 - 150 Hz depending on n;
- blade vibration (water): 0.04 x thrust, small contribution, 550 /850 Hz depending on fully or partially ventilating condition and blade material;
- blade vibration (air): small contribution, 1100 Hz depending on blade material.

4.3. Available Test Rigs

Two possible rigs were viewed at the DERA;

- the unsteady force module models the stern of a submarine. While it would take the measurements required, it is larger in diameter than the model propeller and if situated immediately upstream, it would disturb the flow severely in the test region. If placed downstream of the propeller, it would be submerged in order to achieve the correct shaft inclination and would obstruct the flow in the channel, probably modifying the surface level at the propeller.
- a rig used for ship model testing had substantial mass suspended on the flexure units and would not therefore have the dynamic response required.

A purpose made rig was decided upon.

4.4. Rig Design

4.4.1. Layout

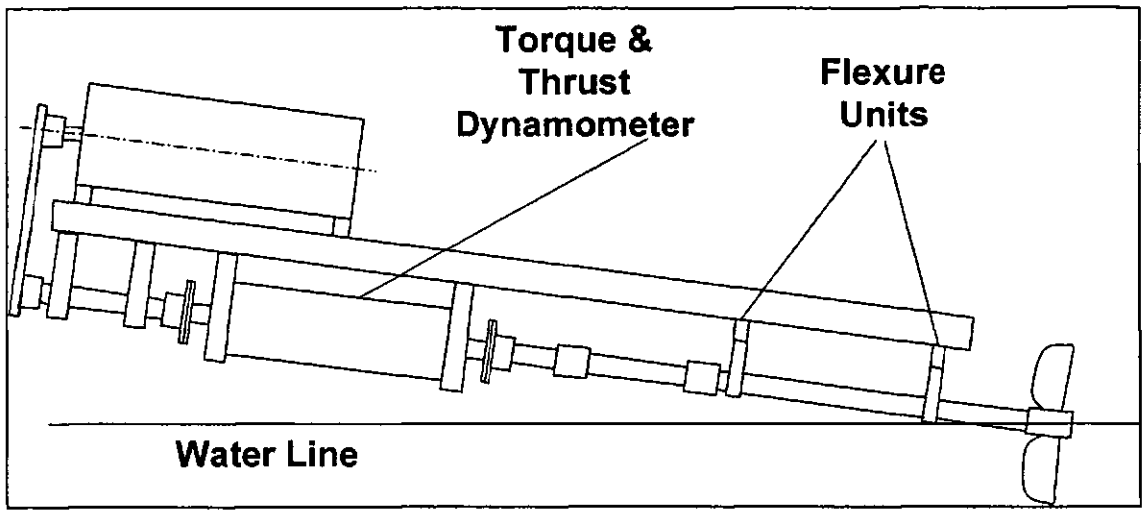

Figure 45. Rig Layout.

The rig layout is shown in Figure 45. This has the principal advantages that

it is sufficiently low to fit within the pressure hood at inclinations up to 12^0,

it is not submerged and the mass suspended on the gauges is kept low to give satisfactory dynamic response.

4.4.2. Force and Moment Measurements

The three components of force and the three components of moment acting on the propeller may be related directly to the six measurements taken from the rig (vertical and horizontal forces at each bearing, torque and thrust). For the rig dimensions proposed and given the expected force levels of 22 Nm (torque), 260 N (thrust), 143 N (vertical) and 21 N (horizontal), then if moments are ignored initially, magnitudes of measured values are expected as:

Q: 22 Nm

T: 260 N

F_{x1} 215 N

F_{x2} 72 N

F_{y1} 32 N

F_{y2} 11 N

Turning to the effect of moments, Rose and Kruppa give M_x/RT and M_y/RT of order 0.25 and 0.3 respectively. These modify the reaction forces above by 33 N, 33 N, 27 N and 27 N respectively. These are measurable differences and show that the effects of force and moment are distinguishable using the proposed system.

4.4.3. Torque and Thrust Dynamometer

A Kempf and Remmers torque and thrust dynamometer, measuring a maximum thrust of 2.2kN is used. Preliminary tests carries out at the DERA indicate that this will measure the dynamic data required in the 0-150 Hz range.

4.4.4. Flexure Design

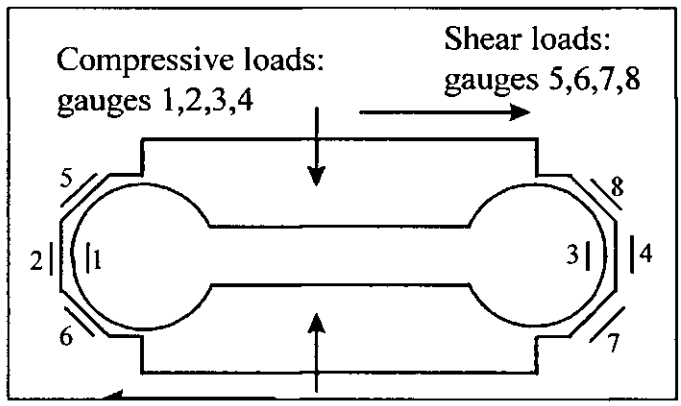

Figure 46. Schematic of Flexure Unit.

4.4.4.1. Principle

The flexure units chosen, shown in Figure 46, have been used previously for the measurement of machine tool cutting forces. By connecting the 8 strain gauges in two separate full bridges, independent measurements of force in the compressive/tensile and shear directions may be made. Pure compressive/tensile loads give theoretical zero strains at positions 5,6,7 &8, while pure shear give zeros at 1,2,3 & 4. Any small cross-coupled

strains which do occur tend to be self-cancelling because of the way in which the bridges are connected.

4.4.4.2. Theory

Theory for the gauges was derived using energy methods assuming the flexure ends approximated to a simple ring. This gave an indication of the influence of the key physical dimensions and allowed an initial design to be determined which gave a satisfactory compromise between high sensitivity and high stiffness. Aluminium was chosen so that the width the flexure could be increased while keeping measurement sensitivity fixed, thus increasing the rigidity in the direction perpendicular to the face.

4.4.4.3. FE Model of Flexure

A flexure with the dimensions calculated was modelled using PAFEC, which allowed strains to be assessed at the strain gauge positions under both direct load and shear; also deflection of the top surface relative to the bottom, allowing stiffness to be determined, and the 1^{st} and 2^{nd} mode vibration frequencies when a given mass was placed on the gauge (approximating to a simple spring-mass system comprising a flexure and half of the propeller and shaft assembly). This process demonstrated that finite element modelling of the restraints and loads was critical, and led to the upper and lower surfaces being increased in thickness in order to distribute imposed loads. It also allowed refinement of the key dimensions.

4.4.4.4. Prototype tests

A prototype was manufactured and tested using dead-weights in the compressive and shear directions. Results showed high linearity, little cross coupling or hysteresis and good discretisation (4.98 μV/N in compression with 0.23 μV/N registering on the shear bridge, and 6.93 μV/N in the shear direction with 0.1 μV/N registering on the compression bridge). When loaded in shear with an offset from the horizontal centre line, a small

variation in the cross-coupled signal to the compression bridge was observed, depending on the size of the offset.

Comparison of sensitivities and deflections between theory, PAFEC and practice showed significant differences, particularly in deflection due to compressive load. However, the critical parameters, recorded strain under compression (least sensitive) and deflection under shear (least stiff) are in sufficiently good agreement to give confidence in the design process.

4.4.4.5. Final design

The flexure units and propeller/tail-shaft assembly were analysed as a system to assess vibration behaviour, using both a simplified theoretical model and PAFEC. In the light of this it was evident that the system's first resonant mode, a twisting motion of the shaft in a horizontal plane, resonated in the region of the blade striking frequency; using an AB2 propeller, and a coupling of equivalent mass at the other end of the shaft, theory (assuming a rigid shaft) gave n_{horiz}=103 Hz, while PAFEC (allowing shaft flexibility) gave n_{horiz}=92 Hz). It was therefore decided that the gauges should be stiffened by increasing wall thickness, accepting that sensitivity would be reduced. Furthermore, it was calculated that the use of an aluminium propeller would reduce suspended mass and raise the resonant frequency to an estimated 180 Hz. Final key flexure dimensions are:

inner radius	6.5 mm
width	19 mm
wall thickness at strain gauges	3 mm
material	2618A Aluminium

In spite of these measures, it was not possible to raise this resonant frequency to a value even approaching the blade resonant frequency, and it was accepted that, while vibration data below 150 Hz could be measured, forces due to blade inertia at upwards of 500Hz will not be measurable using this rig. Further work will be needed to assess whether loads at

these frequencies significantly influence the design of a drive system and, if so, to devise an alternative strategy for measuring them.

4.4.4.6. Maximum stress

To ensure that failure of the flexures does not occur, maximum stresses were assessed; under normal working loads it was confirmed that they are well within the material proportional limit, and also well below the endurance limit, meaning that fatigue loading in the flexures is not an issue. Nevertheless, it was considered prudent to incorporate a safety bracket in the design to retain the shaft in the event of failure so that damage to the CWC pumps would not ensue.

4.4.5. Tail-shaft Design

4.4.5.1. Diameter

Initially a 20 mm diameter shaft was planned. However, initial calculations, and then PAFEC suggested that the shaft would resonate in bending at below 150 Hz. It was therefore decided to increase the diameter to 30 mm, thus removing this problem. The first torsional mode was checked as was the possibility of shaft whirling, but neither were found to be a problem.

4.4.5.2. Length

In deciding upon the length of the shaft, a long overhang between aft bearing and propeller would have been desirable to keep the bearing clear of the water and avoid disturbing the flow. However it was found that a value greater than 150 mm adversely affected the lowest resonant frequency. The 300 mm spacing between flexures was fixed in order to keep overall length short, and thus ensure adequate headroom beneath the hood at large inclination, while not being so short as to degrade vibration characteristics.

4.4.5.3. Propeller fitting

In consultation with Teignbridge propellers, a parallel bore keyed propeller boss was chosen to allow for easy removal of the propeller.

4.4.5.4. Maximum stress

Maximum shaft stress under combined torsional, bending and compressive loads were determined and found to be well within both the material yield stress and the endurance limit.

4.4.6. Bearings

Journal bearings using PTFE, Tuffnol or similar inserts are commonly used at the DERA for similar applications, and are specified for this rig. They have the advantage that insert and housing thickness is small. Consequently any disturbance caused to the flow as the aft bearing becomes immersed at low inclinations is small. There is concern about lubrication, as the bearings rely on spray, but if this becomes a problem, particularly for the forward bearing, a water feed to the bearings will be devised.

4.4.7. Couplings

A Cardin shaft will be used to transmit torque and thrust between dynamometer and propeller. This is a configuration currently used at the DERA and problems are not

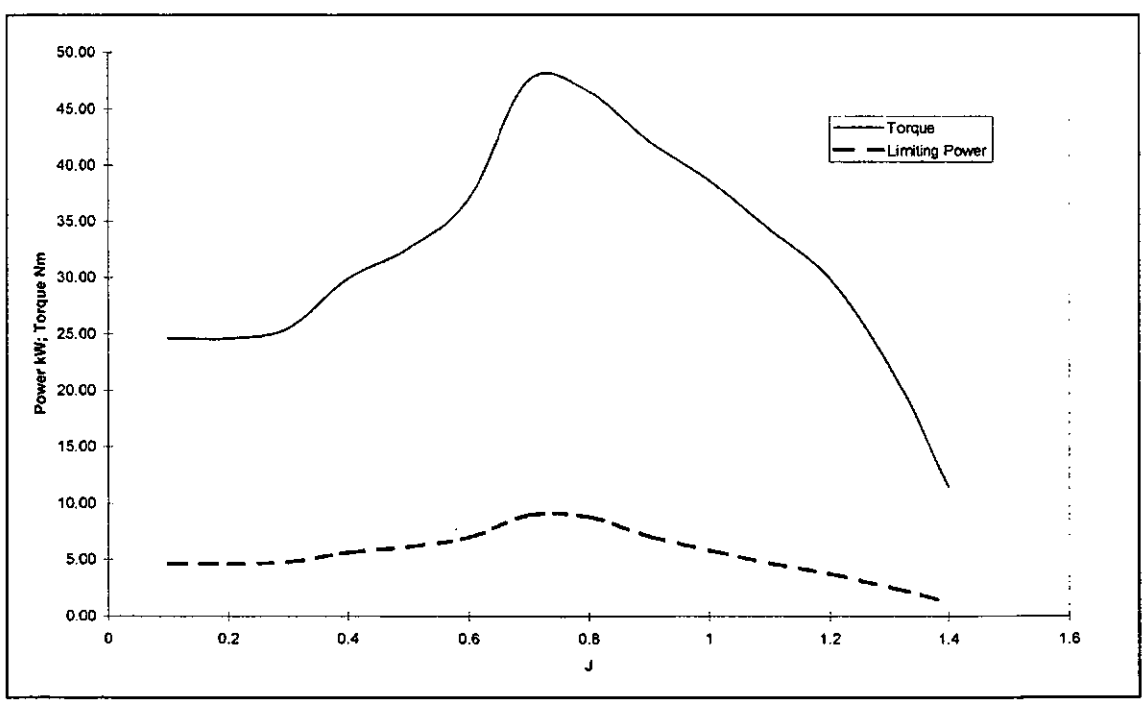

Figure 47. Torque and Power Curves for Rig.

envisaged provided misalignment is kept small.

4.4.8. Motor

Using the collated K_q-J curves (Figure 8), power versus advance coefficient curves (Figure 47) have been constructed, assuming:

$0 < J < 0.8$: motor speed of 1800 rpm, variable V,
$J > 0.8$: variable motor speed, V = 6 m/s.

From this a maximum power value of 9kW was determined, with a torque of 50 Nm. As discussed earlier, it is unlikely that these figures would be needed, since they were produced at high immersion; however it would be useful to have the flexibility of such a motor.

Motor cooling was considered to be a problem, as, at the low operating pressure under the hood, cooling air is scarce. Hydraulic, pneumatic and submersible (water cooled) electric motors were investigated as alternatives. A submersible electric motor was chosen since this was the most convenient power source for the isolated condition under the hood. This was specially constructed to ensure that the vacuum conditions did not draw lubricating oil out of it, and it was significantly over-rated to avoid the need for cooling water.

4.4.9. Rig Orientation

As commented previously, the rig will accommodate a range of inclinations, yaws and immersions. Remote hydraulic adjustment, as used by Olofsson is considered unnecessarily expensive, and manual adjustments using winches and lock bolts are to be used.

4.4.10. Instrumentation

In addition to the force and torque measurements described above, the test facility is equipped with the following:

- Shaft speed measurement (from torque-thrust dynamometer)

- Water velocity measurement (mean value and traverse)
- Stroboscopic photography
- 7 channel data logger (4 resistance bridges, torque, thrust, shaft speed)
- Air pressure measurement

4.4.11. Fair water plate

In order to ensure a smooth, predictable water surface, a flat plate was originally proposed, placed at the surface ahead of the propeller, as used by Rose & Kruppa (1991) and Rose et al (1993). Experience subsequently showed that the water surface was well behaved with no standing waves and a stable level, so the plate was not fitted.

4.5. Summary of Experimental Rig

The principal rig parameters to which the rig was designed were:

Maximum advance velocity	6 m/s
Maximum rpm	1800
Propeller diameter	0.25 m
Advance coefficient range	0 - 1.4
Yaw angle range	$0 - 5^0$
Inclination angle range	$6^0 - 12^0$
Immersion ratio range	0 - 50 % at all incl's; up to 80 % at high incl's
Air pressure	down to 3500 N/m^2
Max motor power	9 kW
Max motor torque	50 Nm

4.6. Rig Calibration, Commissioning and Operational Limitations

4.6.1. Measurement Equipment

A general view of the test rig is shown in Figure 48 and others are given in Appendix C. When it had been mounted in the circulating water channel, power and data cables were

led through air tight glands to the motor controller and data logging equipment. The latter comprised a signal amplifier producing a gain of 1000 which fed into a ProSig analogue to digital converter, and then into a PC running ProSig software which was used to view, process and record the data. Data was collected simultaneously, using an internal clock, across seven channels: vertical and horizontal forces on each of the two flexure units, torque, thrust and a tachometer signal giving 60 oscillations per revolution which was used to determine shaft speed when the results were processed.

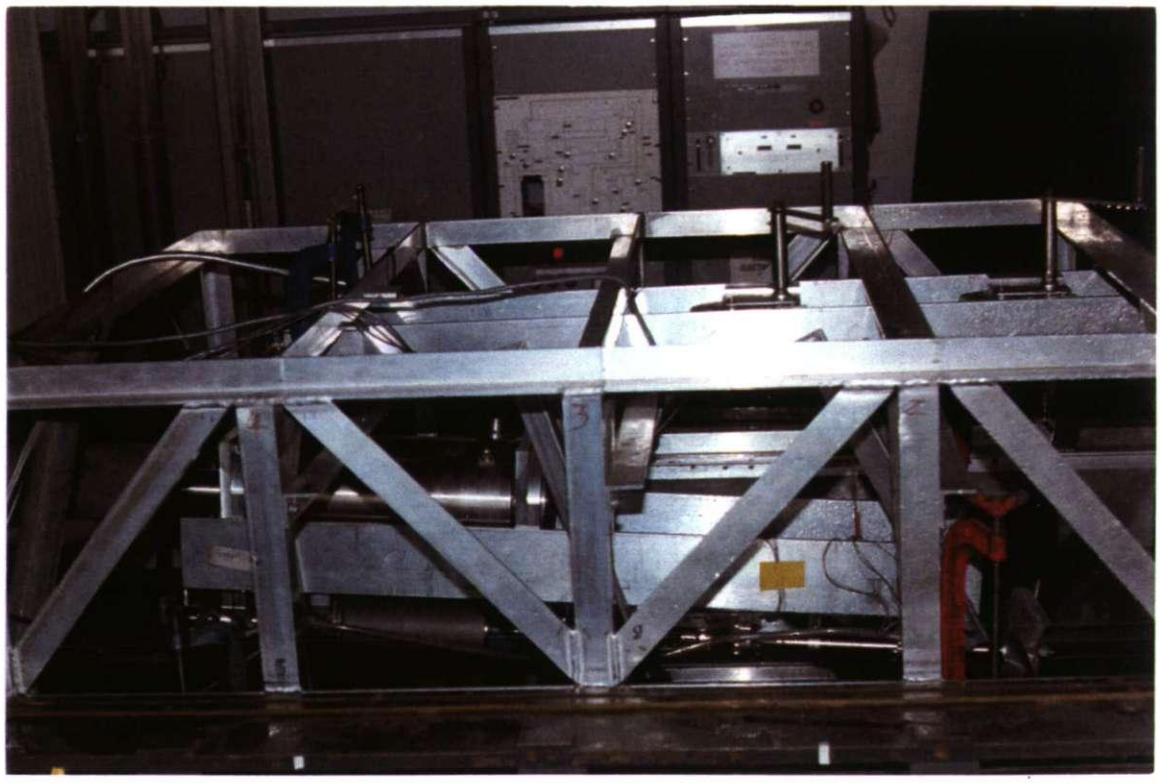

Figure 48. Test Rig General View.

Considerable electrical noise was observed when the system was first set up, emanating from both the propeller motor and the CWC pump motor. The latter was particularly troublesome since it was an old thyristor controlled unit which imposed a large number of spikes on the signal, almost completely masking it. It was found that this was predominantly transmitted through the mains supply for the building and was largely eradicated by using a mains filter for all equipment. Noise from the propeller motor was reduced by careful earthing of casing and screen cables, taking care not to create earth

loops which had a serious effect on datum values. A software low pass filter with a cut off frequency set at 2500 Hz was implemented.

The highest shaft speed to be used was 30 Hz, and thus the maximum blade striking frequency for a 5 bladed propeller was 150 Hz. In order to resolve this and its low harmonics, and provide sufficient data points to permit averaging, a sampling rate of 4000 Hz was chosen with a sample time of 0.5 seconds. This would yield a frequency resolution of 2 Hz and a time domain resolution of 2.7^0 of shaft rotation which were considered to be sufficient.

Rotational speed was set for each run by using the motor speed dial readings. These were calibrated against a hand held tachometer in order to facilitate the setting of test run

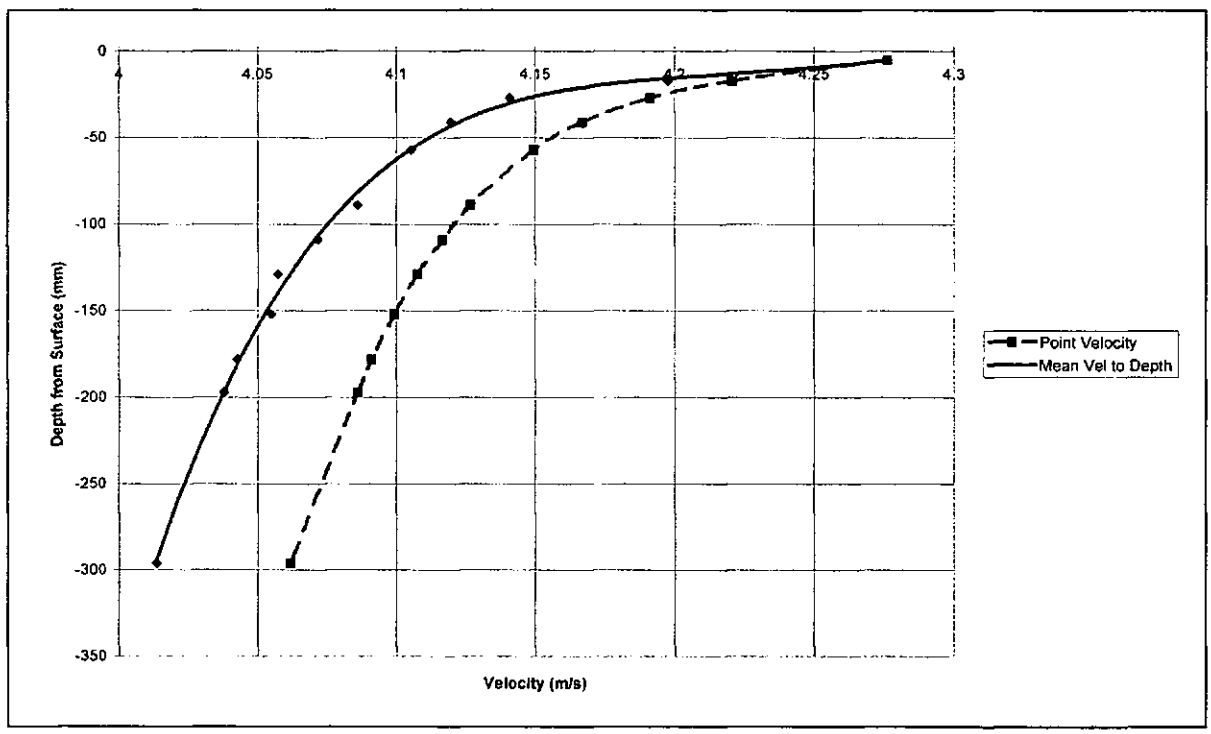

Figure 49. Velocity Traverse for the Circulating Water Channel.

conditions; however accurate measurement of speed was derived from the tachometer data channel during post processing of the signals.

Advance velocity was set using a calibration chart which had previously been produced for the channel. This was checked against readings from a pitot-static tube traverse, carried out as part of the calibration procedure. From the results of this traverse, shown in Figure 49, it can be seen that velocity is slightly higher at the surface as a result of the injection hood in the CWC, but the velocity variation over the propeller semi-disc is less than ±3%. A mean velocity over the top 125 mm was used in calculations.

Ambient pressure within the hood was measured using a vernier mercury manometer.

4.6.2. Calibration

The flexure units had previously been checked in the laboratory for linearity shortly after they were manufactured. When fitted to the rig, they were calibrated in-situ using dead weights as follows. Thin mono-filament cable was attached to the shaft forming a bridle

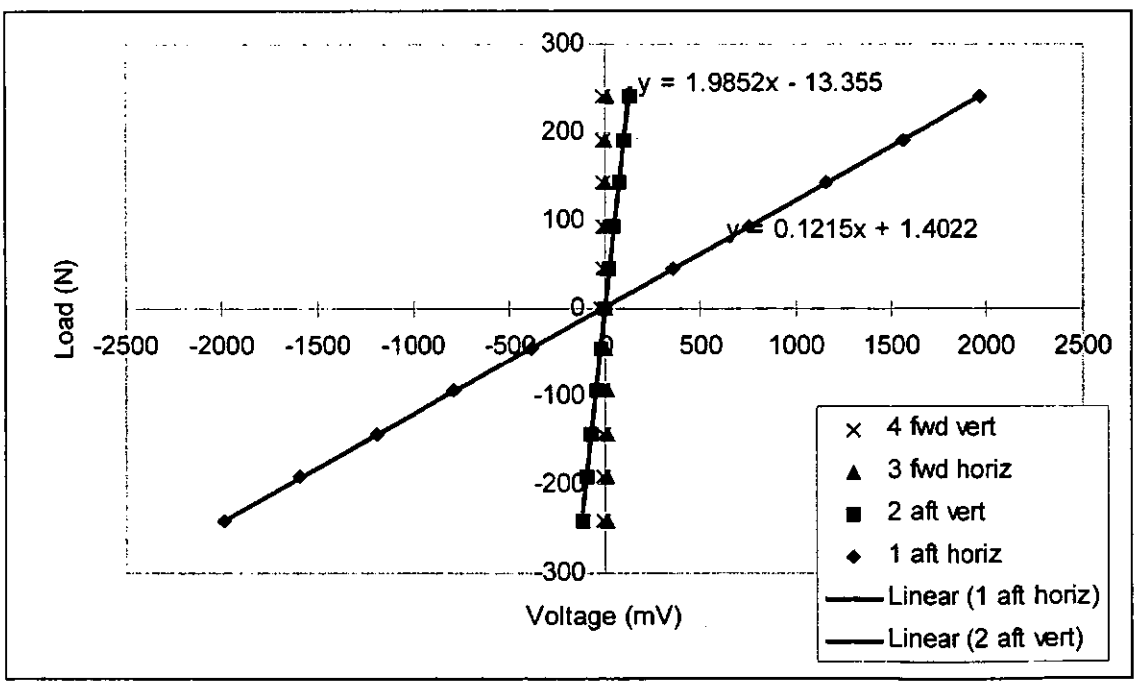

Figure 50. Calibration Curve for Flexure Unit (aft unit, horizontally loaded, positive force to starboard).

across the bearing housing, and weights were attached to the string pulling either directly downwards, or, using a low friction pulley, horizontally. With this arrangement, the force was transmitted to the flexure at its longitudinal centre and on the shaft centre line. For each flexure, loads were applied horizontally to starboard and port, and vertically downwards, loading and unloading in steps to a maximum of 25 kg. At each step, the signal for each of the four flexure channels was recorded. A typical calibration curve is shown in Figure 50. In this case load was applied horizontally at the aft flexure. It can be seen that the horizontal signal for this flexure bears a linear relationship to the load. Signals at the forward flexure were negligible. However there was a small linear variation in the vertical signal as horizontal load was applied. The gradients of the lines were recorded as the flexure calibration coefficients (eg C_{ahv} = load (N) applied to horizontal channel to achieve unit signal (mV) on vertical channel, aft flexure) and relationship was derived to allow for the cross coupling between the channels.

The flexure force measurements are related to forces and moments applied at the propeller.

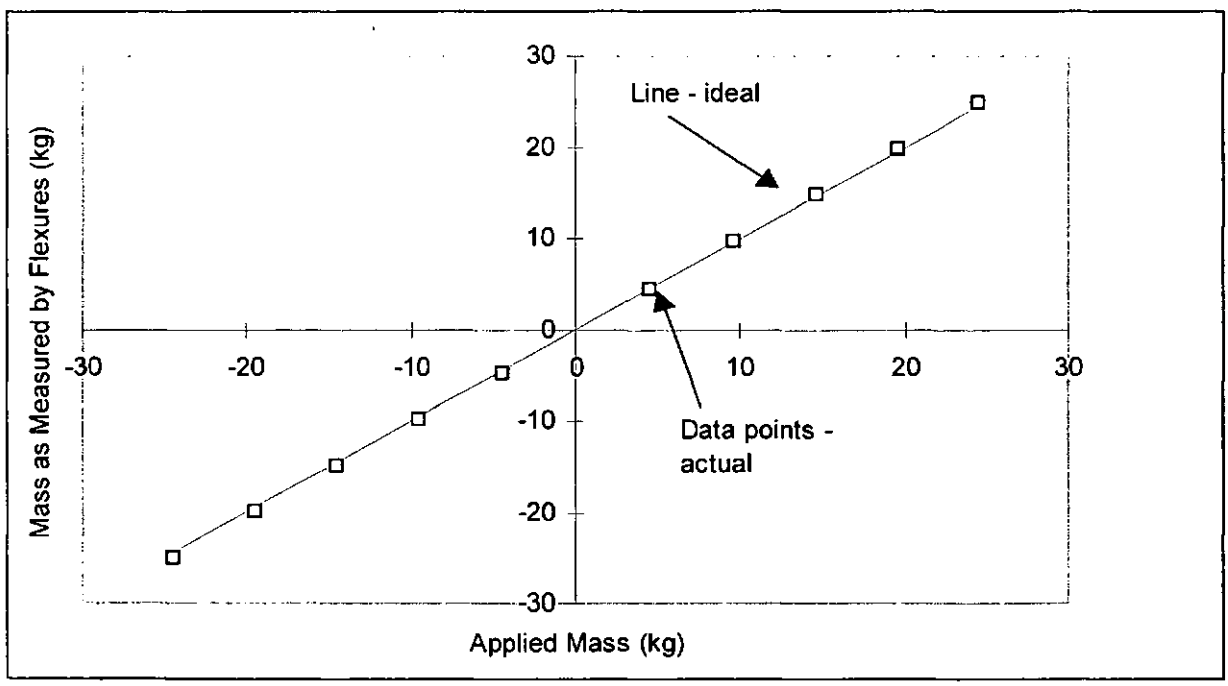

Figure 51. Calibration Check by Loading at the Propeller.

To check the calibration, the rig was loaded horizontally and vertically at the shaft shoulder against which the propeller would be mounted. For each load increment, each flexure signal was recorded. Using the calibration coefficients previously measured and the channel cross coupling relations, predictions of the load were then made to check against the actual load applied. Typical results from this procedure are shown in Figure 51

The torque and thrust dynamometer was also calibrated with dead weights using a purpose made rig.

4.6.3. Limitations

4.6.3.1. Test Conditions

Based on previous experience with the Circulating Water Channel which had shown that a pressure of 3500 Pa and a speed of 6 m/s was achievable, the minimum cavitation number for the operation of the rig was projected as 0.1. Initial runs showed that both pressure and speed were optimistic values. After extensive work on the CWC to seal leaks a pressure of 8000 Pa was achieved. As far as speed was concerned, advance velocities were limited due to excessive aeration of the water. At higher speeds, the rooster tail from the propeller impinged on the back wall of the hood, and was deflected back to the propeller; also, a significant amount of air became entrained in the water and its bulk increased, raising propeller immersion and exacerbating the problem.

The rig was repositioned as far upstream in the channel as possible to permit the greatest distance downstream for the wake to settle and the maximum advance velocity for continuous running was found to be 4 m/s. While very brief excursions above this were possible, the system quickly became unstable. The result of these figures was that testing

over the operating range of the propellers was found to be possible at a minimum cavitation number of 0.8.

The only available data which allows an estimate of the effect of cavitation number is presented by Rose & Kruppa (1991). Here K_t and K_q results are shown for cavitation numbers of 3, 0.5 and 0.3. In the partially ventilated region, K_t and K_q are approximately 10% higher at $\sigma = 0.5$ compared with 0.3. Efficiency predictions are some 3 percentage points higher. There is no effect when the blade is fully ventilated.

4.7. Experimental Testing

4.7.1. Propellers Tested

The propellers used for the programme were typical 'cleaver' profiles, with a sharp leading edge and a pronounced trailing edge cup. Four propellers, shown in Figure 52, were tested. Each was of 250 mm diameter with pitch: diameter ratio of 1.5. All blades had the same area and the variables were the number of blades (one 5 bladed, and three 4 bladed propellers were used) and skew. The 5 bladed and one of the 4 bladed propellers had radial

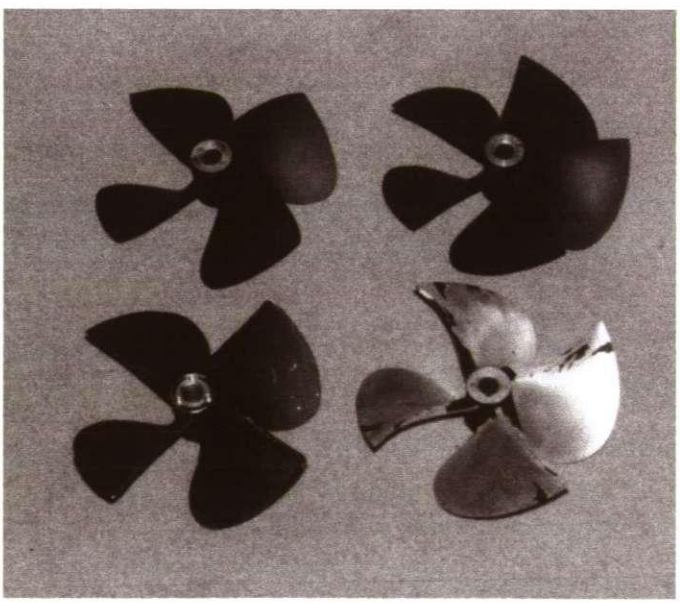

Figure 52. Propellers Tested.

trailing edges, while the remaining propellers had their trailing edges skewed forward and backwards by 0.1D at the tip.

4.7.2. Procedure

When immersion, inclination and yaw had been set, the static water level was marked on the glass side panels. The hood was positioned on its rubber seal, water speed was set to a low value and the vacuum pumps started. Considerable care was required throughout testing to ensure that pressure was balanced between the converging inlet section and the working section of the channel; failure to do this caused an accumulation of air in the converging section which raised the water level at the propeller.

When the correct pressure had been reached, the water speed was set to zero and allowed to settle so that the datum value on each signal channel could be recorded. This was done with the propeller motor power supply energised (but with the propeller stationary) as it was found that this influenced the datum levels. Water speed was then set at the test value required; this had to be done in small increments to avoid surge, and the propeller speed was also increased incrementally, approximately at zero-load values so that the water did not become too aerated. Adjustments were made if necessary to the floor level and to the control flap at the exit of the working section to ensure that the water was level without significant standing waves and propeller immersion (measured from the water level in the far field, away from propeller disturbance) was at the correct value. In fact, adjustments required were very small.

Measurements for each advance coefficient were recorded by raising the propeller speed to the appropriate value, running the data logger and then reducing speed quickly back to the no-load value. Operating in this way, the aeration of the water was minimised, but it was

still necessary periodically to allow the water to settle, and to adjust the pressure balance as described earlier.

When a set of measurements had been taken, the channel and propeller were again stopped and datum values were recorded. Several of the runs were duplicated during the test programme to ensure repeatability.

4.7.3. Data Processing

Data was converted to ASCII format for portability between computers. Several MathCad routines were written to process this data, carrying out the following:

- determination of datum values;
- determination of running speeds;
- calculation, point by point during time history, of propeller forces and moments from flexure measurements;
- determination of mean performance;
- synchronous averaging of transient load data, to remove non-periodic noise;
- transformation of transient data to frequency spectra;

In order to allow for the frequency response of the system when determining the excitation forces at the propeller, the frequency response function between the propeller and the flexure signals was measured. This was done experimentally using an impact hammer applied to the shaft just forward of the propeller. The response function was then applied to the frequency spectrum of the signals obtained over the lower range of frequencies; at higher frequencies, the response had high noise levels and was considered to be inaccurate. The modified frequency spectrum, and associated phase data were reconstructed into a time history for visual analysis.

4.7.4. Errors

A sensitivity analysis was carried out to establish the influence that error in each measurement has on the final results. The lateral force at the propeller is calculated from forces measured at the forward and aft flexures, which in turn are a voltage measurement multiplied by a calibration constant which itself is experimentally determined.

Calibration constants were measured by loading up, then down, and then rechecking, and a high degree of correlation was achieved. Analysis of the regression shows errors to be in the region of 0.5%. Mean forces were measured by taking 2000 data points during a 0.5 second time interval. By considering the peak to peak range of these voltage readings and the number of data points taken, the error in the mean at each flexure was calculated to be in the region of 0.5%. By determining the relative contribution of each of these errors to the force at the propeller, it was estimated that calibration and voltage measurement errors led to an error band of around ±1.5%. Calculation of moments at the propeller included one further set of parameters: the spacing of the flexures and position of the propeller relative to them. Initially this caused a problem because the width of the bearing housings led to uncertainty, but by checking back through the calibration figures, and since it was known that the dead-weight calibration did not impose a moment at the propeller, effective lengths could be determined. It was considered that these were accurate to within ±1 mm, and this led to estimated errors in the moments of ±10%.

The other key source of potential error was measurement of the datum voltages before and after each run (a run comprised the recording of data at each of nine rotational speeds). Despite much work on the electronics, particularly identifying earth loops and waterproofing connectors, it was found that, on occasions, there was significant drift during a run. Where this was considered excessive, the run was repeated. Observation indicated that the datum values changed steadily with time, rather than erratically, and

therefore datum values were linearly interpolated between the pre- and post-readings to obtain values for each speed within a run. Using this strategy, it is estimated that for the more heavily loaded speeds, contribution to overall errors resulting from this were in the region of ±3% for horizontal forces and ±8% for vertical. However, at the lowest speed where measured forces were small, the resulting error could be as high as ±6% for horizontal and 24% for vertical force, since this force was negligible at this speed. For torque and thrust, the figures are ±2% and ±1% at high load, but ±7% and ±4% at low load. These last figures make calculation of efficiency, which includes both torque and thrust errors, unreliable at low load.

5. PRESENTATION AND DISCUSSION OF EXPERIMENTAL RESULTS

5.1. Mean Propeller Performance

5.1.1. General

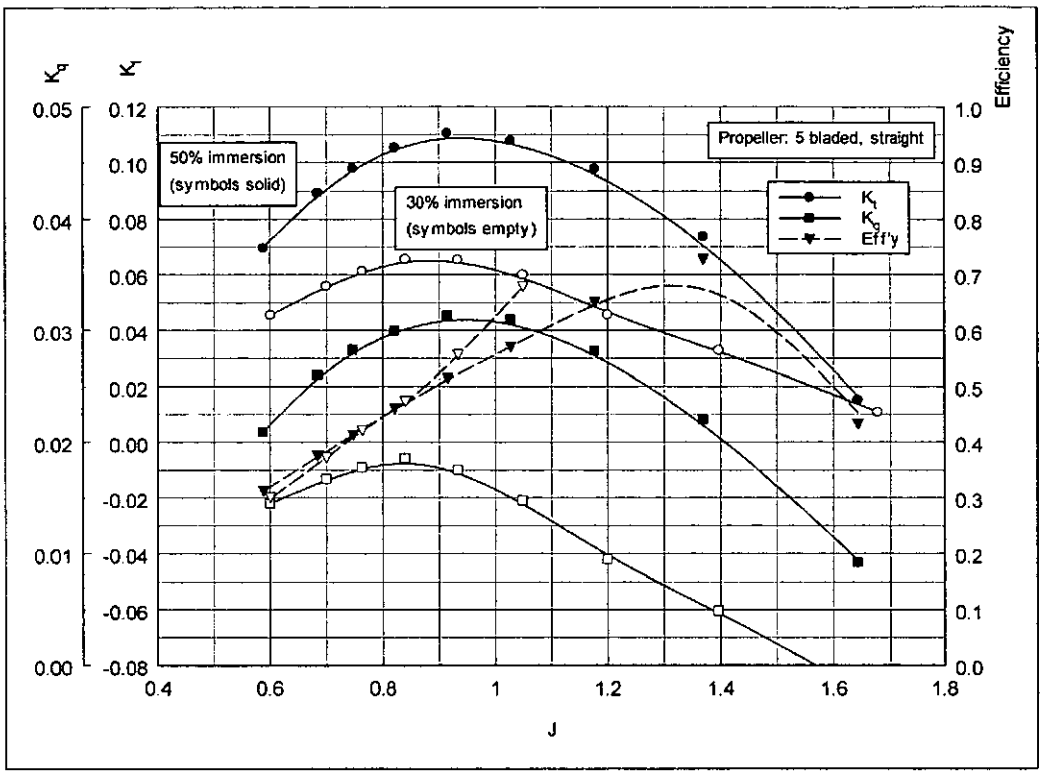

Figure 53. Typical Performance Curves.

Mean performance results are presented in Appendix A, showing comparisons between propellers, immersions, and angles of yaw. Representative summaries of these results are reproduced in this discussion.

Typical propeller performance criteria are shown plotted against advance coefficient in Figure 53. This is representative of the majority of results obtained and clearly shows the maxima achieved in K_t and K_q, a feature of SPPs. This is significantly different to non-cavitating conventional propellers for which the K_t and K_q curves would be expected to

rise steadily as J is reduced. The peak values correspond to the transition region in which ventilation begins to cover the entire back of the blade. The maxima for K_t and K_q occur at approximately the same point, but this does not coincide with the point of maximum efficiency, which occurs at a much lighter load. Since at these light loads, measurement errors were proportionately higher, the efficiency values here are subject to relatively large error bands, and considerable scatter was observed. However, from those propellers that show coherent results down into the lightly loaded region, peak efficiencies in the region of 70% were measured.

The existence of the maximum thrust condition has a large impact on the design process. This is because a propeller designed for optimum efficiency may produce insufficient thrust under start-up conditions, at low advance coefficient. This is particularly critical as the vessel goes through the displacement-planing mode transition.

The face pitch-diameter ratio for all propellers is 1.5; however the zero load points occur at advance coefficients a little above 1.6. This implies that the effective pitch-diameter ratio is higher than 1.5, which is attributed to the significant effect of cupping on the face at the trailing edge.

Results are also presented in terms of the customary design coefficients, K_t/J^2 and K_q/J^5, parameters that avoid the need for a priori knowledge of the speed and diameter respectively. Figure 54 is a typical plot of K_t/J^2, showing the upper limit in the region of 0.2 for 50% immersion, which is characteristic of surface piercing propellers. This effectively represents the limiting mean pressure imposed on the disc, again a result of ventilation, which limits the suction side pressure of the foil to atmospheric. (To put this into context, the equivalent thrust-loading coefficient for a conventional propeller designed

to avoid cavitation would be in the region of 2.9). The effect of immersion can also be clearly seen in Figure 54, with thrust falling as the effective disc area is reduced.

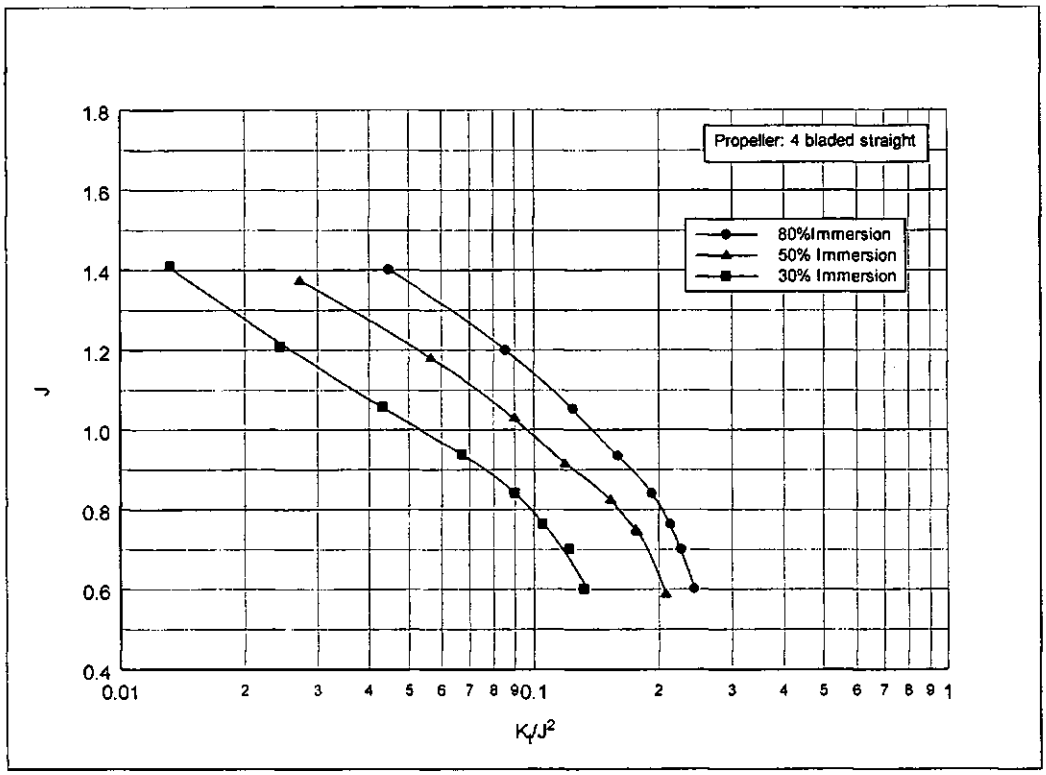

Figure 54. Advance Coefficient vs Thrust Coefficient – Effect of Immersion.

Side and vertical forces and moments occur in all propellers because of wake fluctuations. However, they are particularly pronounced in surface piercing propellers, which could be viewed as operating in a wake of extreme fluctuations, as blades pass through the water-air interface and the reasons for these supplementary forces have been examined in a previous section. Their magnitudes may most easily be seen by presenting the force coefficients over the range of advance coefficients, as shown for a typical case in Figure 55. In general the horizontal and vertical forces rise and fall with thrust, although the positions of the maxima are not precisely coincident. It is believed this occurs because in the transition region a varying amount of blade surface is ventilated as J changes, which varies the position of the centre of lift on each blade. Thus, because of the blade camber, the direction of the lift force relative to the blade chord also varies.

Moments about the horizontal transverse axis (trim or "bow-up" moments), which result from the centre of thrust being below the propeller centre line, also vary in similar fashion,

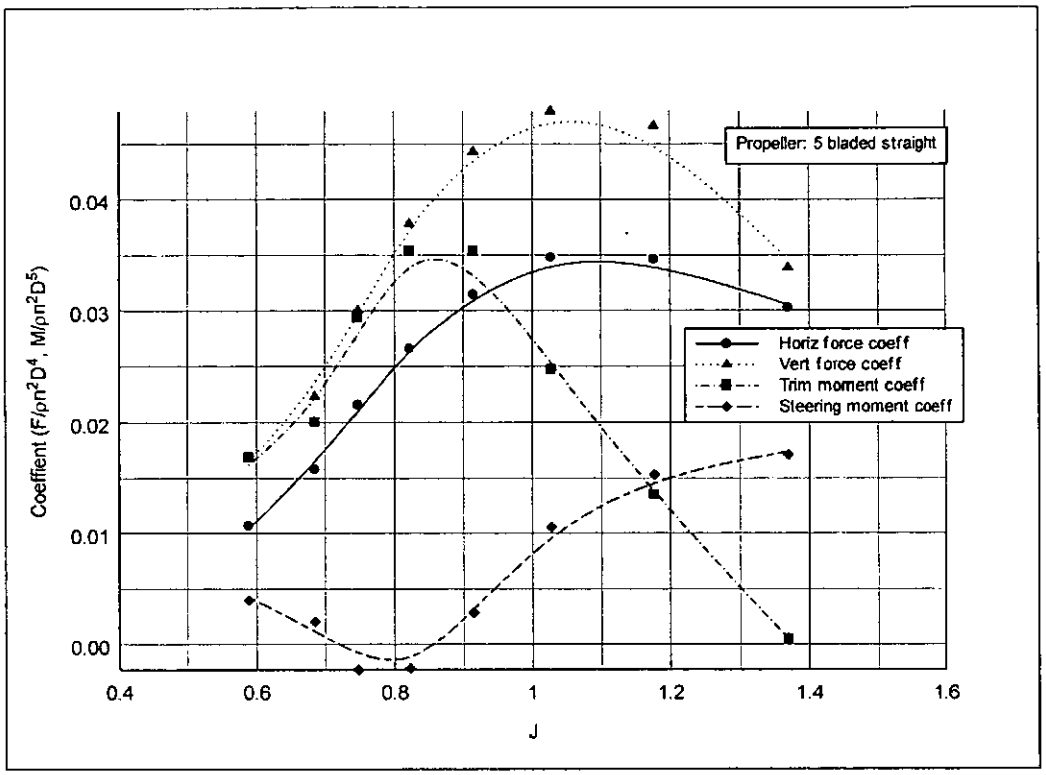

Figure 55. Vertical & Horizontal Force & Moment Coefficients for 5 Bladed Propeller.

with a maximum in the transition region. Moments about the vertical axis (steering moments) are more variable, but typically for 50% immersion, they fall to a minimum in the transition region and rise rapidly as the partially ventilated region is entered.

Supplementary forces and moments will be examined more closely by normalising over thrust when comparisons between propellers and operating conditions are presented.

5.1.2. Comparison between Propellers and Immersions

A summary of the principal tests carried out is given in Table 4. Cavitation number for all tests was approximately 0.8. The 4 bladed straight propeller was also run at 50%, 4^0 in order to establish the effect of inclination at a given immersion, which was found to be negligible.

Table 4. Summary of Tests Carried Out.

Propeller	immersion: 80% inclination: 8^0 yaw: 0^0	immersion: 50% inclination: 8^0 yaw: 0^0	immersion: 30% inclination: 4^0 yaw: 0^0	immersion: 50% inclination: 8^0 yaw: 15^0
5 bladed, straight trailing edge		✓	✓	✓
4 bladed, straight trailing edge	✓	✓	✓	✓
4 bladed, forward skewed trailing edge		✓	✓	✓
4 bladed, backward skewed trailing edge		✓	✓	✓

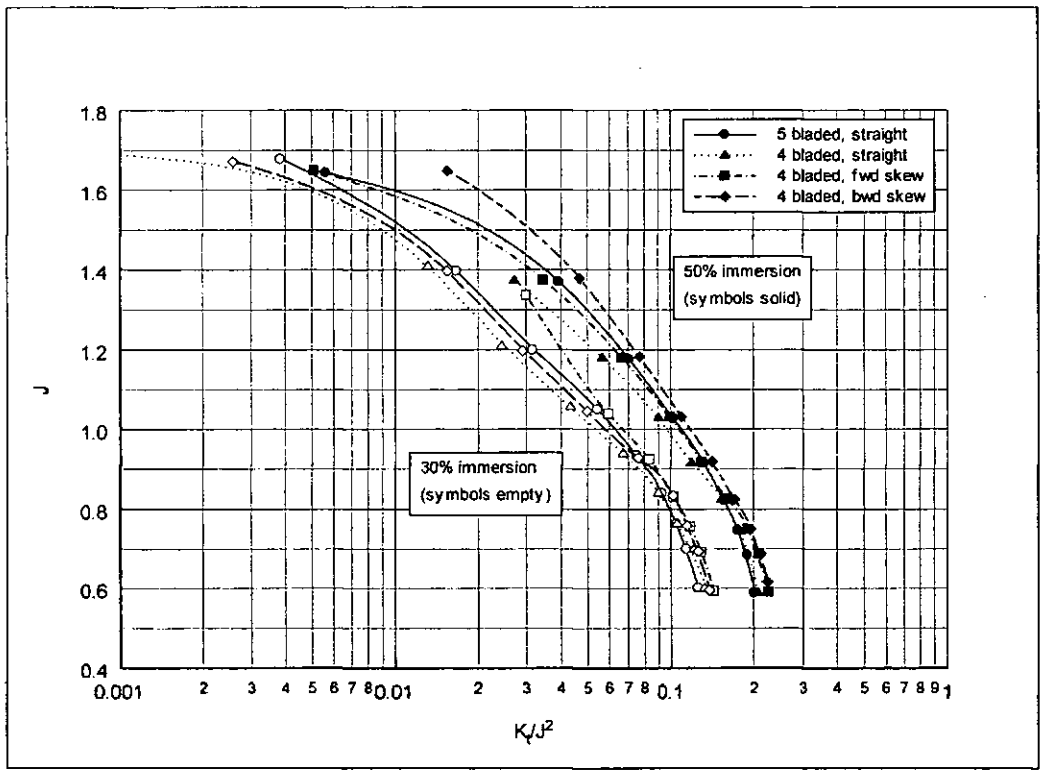

Figure 56. Advance Coefficient vs Thrust Coefficient – Effect of Propeller & Immersion.

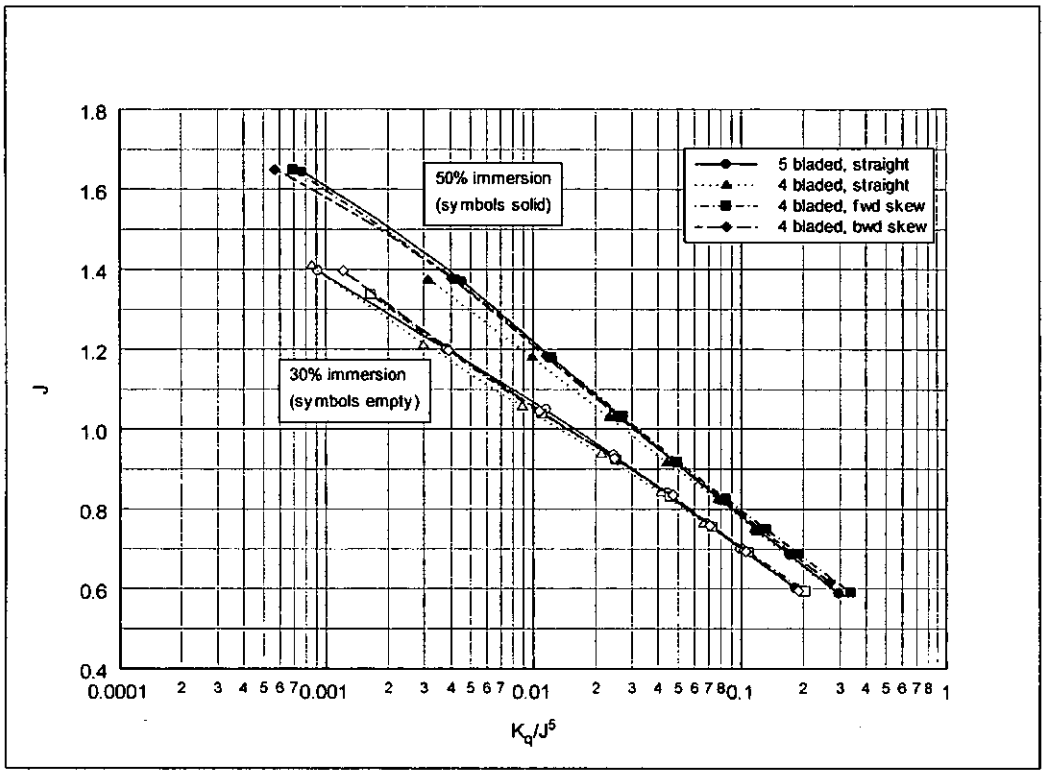

Figure 57. Advance Coefficient vs Torque Coefficient – Effect of Propeller & Immersion.

Thrust, torque and efficiency performance charts are shown in Figure 56 to Figure 58. The five-bladed propeller shows consistently slightly higher thrust and torque and a slightly higher efficiency. Of the four bladed propellers, the back-skewed case shows a slightly better efficiency, but other differences between them are marginal. Immersion clearly has an influence, with a demarcation between the three groups of curves at 50% and 30% on the torque and thrust charts, but, surprisingly, negligible differences in efficiency.

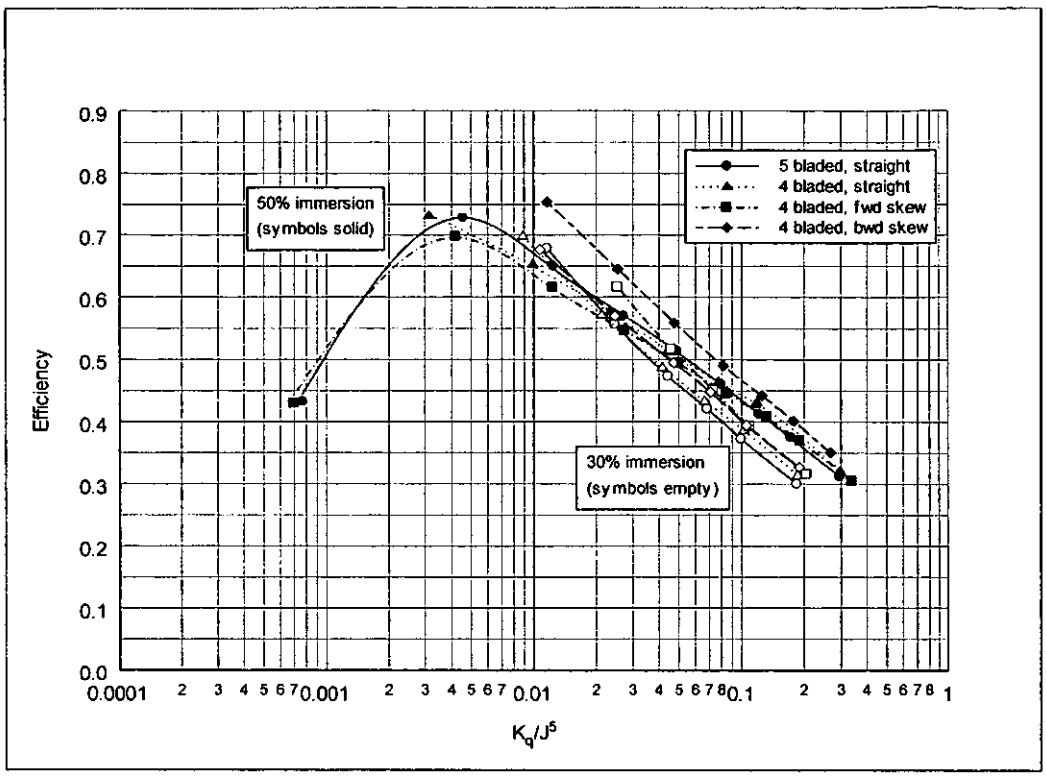

Figure 58. Efficiency vs Torque Coefficient – Effect of Propeller & Immersion.

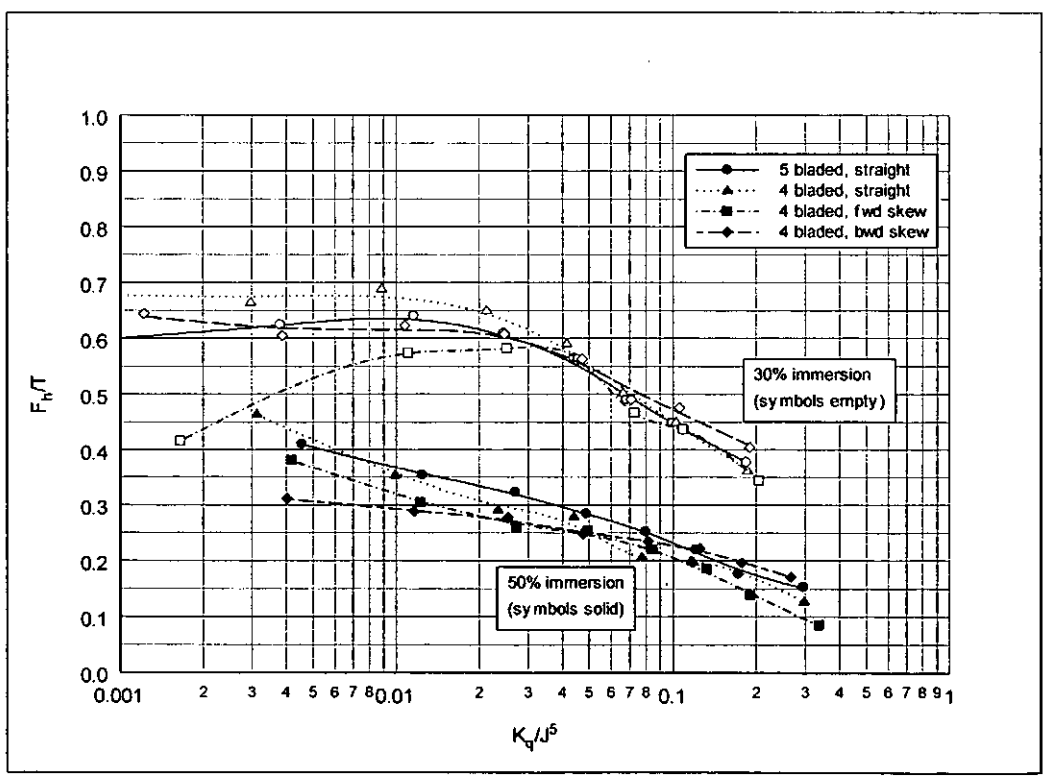

Figure 59. Horizontal Force vs Torque Coefficient – Effect of Propellers & Immersion.

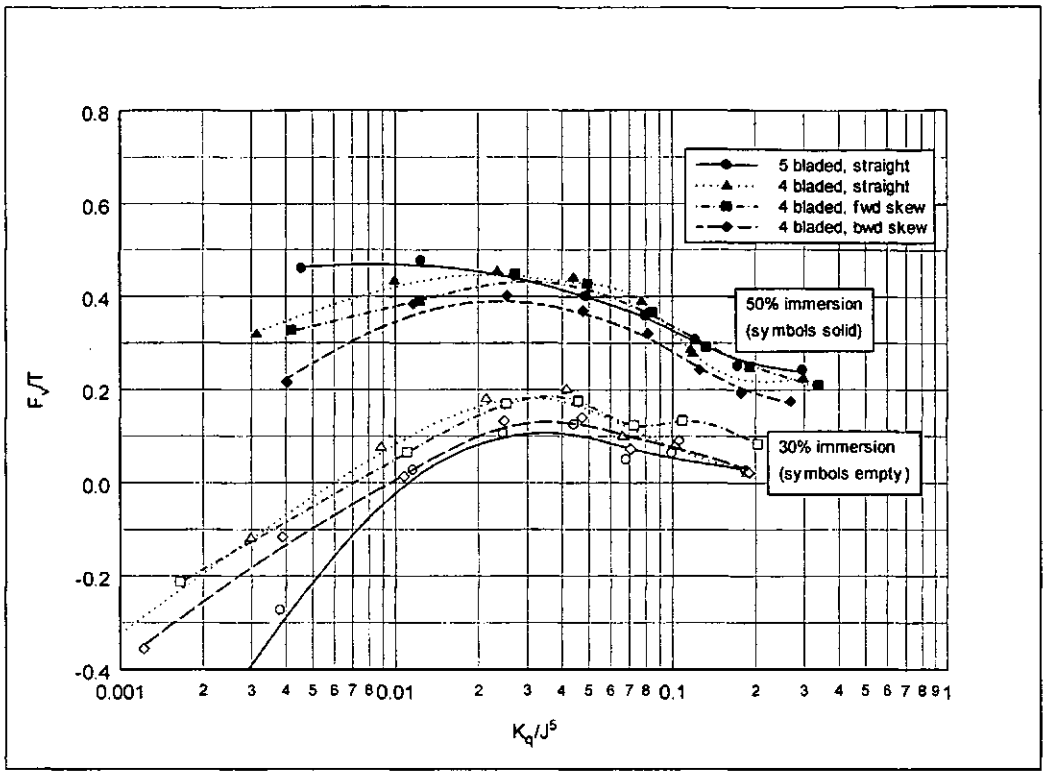

Figure 60. Vertical Force vs Torque Coefficient – Effect of Propellers & Immersion.

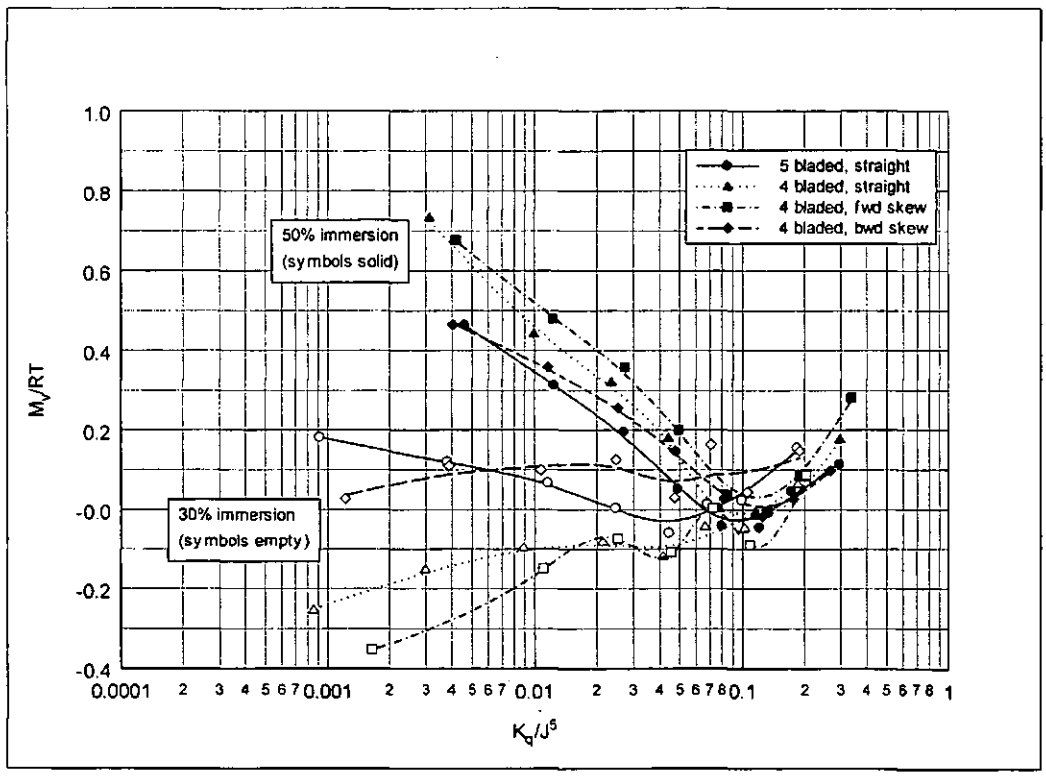

Figure 61. Steering Moment vs Torque Coefficient – Effect of Propellers & Immersion.

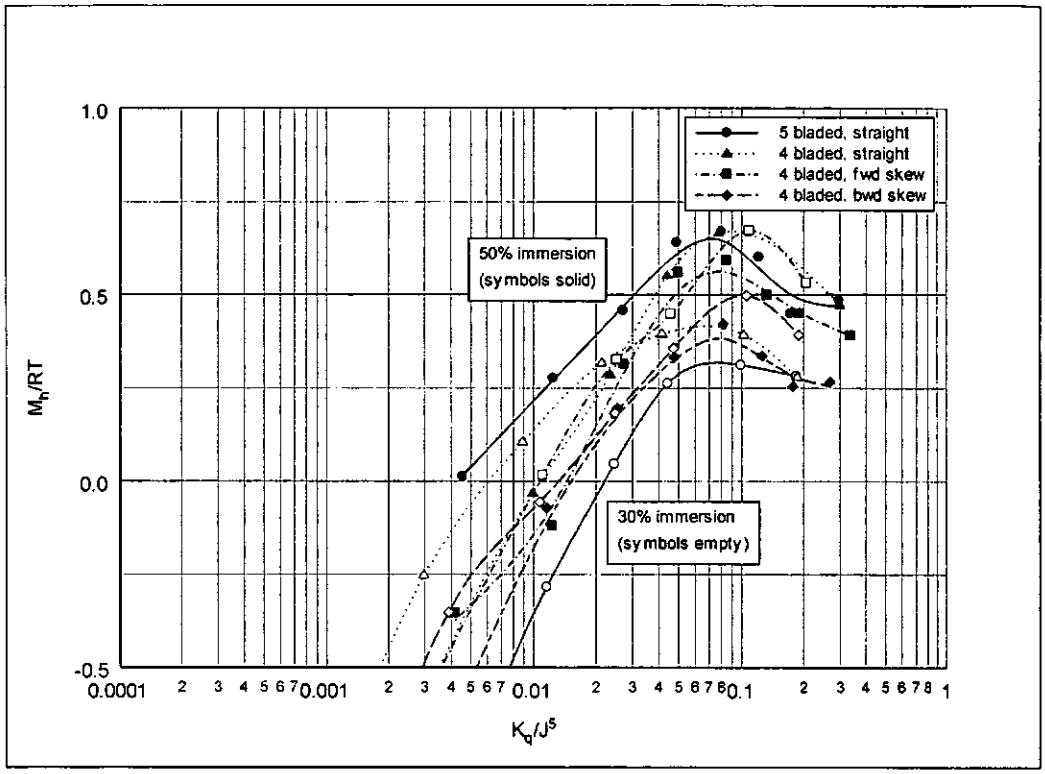

Figure 62. Trim Moment vs Torque Coefficient – Effect of Propellers & Immersion.

Horizontal and vertical forces, normalised on thrust, are shown in Figure 59 and Figure 60. Differences between propellers are small, although there are divergences in horizontal forces under lower loads at low immersion. The horizontal force ratio is significantly higher at low immersion. This is because, as the thrust producing section of the blades moves out towards the tips, the circumferential component of the lift forces are increasingly directed to starboard for a right handed propeller. At 80% immersion, it was found that the normalised horizontal force is low at light loads (unsurprising since for the fully immersed case in a uniform flow it would be zero). However it does rise to values close to the 50% case at high loads; this is an indication of the extent to which the water surface immediately upstream of the propeller is disturbed, with a "pressure bulge" increasing the effective immersion above the nominal 50% value.

Vertical forces are generally directed upwards and are at their maxima for 50% immersion. At 30% immersion, values are low (since circumferential lift components are largely horizontal); indeed they are directed downwards at low load, probably because of the amount of spray directed upwards. At 80% immersion, values are generally lower than the 50% case over the mid-range but coincide elsewhere, again reflecting the extent of the water surface disturbance.

Moments about vertical and horizontal axes are shown in Figure 61 and Figure 62. They are normalised by the product of radius and thrust, and are therefore the offsets from the centreline at which the thrust acts, expressed as fractional radii. For the vertical axis case, values are at their highest for 50% immersion, the centre of thrust being offset to starboard (the side on which blades strike the surface). This results from the higher transient lift forces incurred as flow is established when blades enter the water, followed by lower forces as the partial ventilation bubble becomes established. As load is increased, the offset is reduced until it is close to zero when the blades are fully ventilated. This implies very little asymmetry, about the vertical axis, in application of the lift force under these conditions.

All propellers exhibit a small rise in offset as load is further increased. For the 30% case, offsets are small, sometimes negative. Here, the position at which the ventilation bubble becomes established is a key factor in determining the position of the centre of thrust. For the 80% case, there is a marked variation across the load range, with the offset becoming negative in the fully ventilated region.

Considering moments about the horizontal axis (measuring offsets of the centre of thrust below the shaft), it would be expected that the value for 30% immersion should be greater that at 50%; however there is little difference between immersions. The dominant effect

here is ventilation at the blade root. This renders this part of the blade less effective as a producer of lift, thus maintaining the centre of thrust the same distance below the shaft line even though immersion changes from 30% to 50%.

5.1.3. Effect of Shaft Yaw

It has been proposed that a yaw angle may be usefully applied to the propeller shaft in order to direct the vector sum of the thrust and side force in the forward direction (Olofsson 1996, Rose & Kruppa 1991, Rose et al (1993). This would have the effect of augmenting the thrust, and thus enhancing propulsive efficiency, while minimising the side force. However, the potential benefits must be examined in the light of possible loss of efficiency due to hydrodynamic effects. The four propellers were tested at 50% immersion, 8^0 inclination at yaw angles of 10^0 and 15^0 for comparison with the zero yaw case. Results are presented with parameters expressed both relative to the shaft and relative to the vessel

Results for a typical propeller (4 bladed, straight) are shown below. The thrust relative to the shaft (shown in Figure 64, plotted against J for clarity) was reduced by the yaw angle, since the effective pitch of the propeller was reduced for much of the blades' sweep through the water by the re-orientation about the vertical axis. For the other propellers this was true across the operating range; for this one there appears to be a changeover in the transition region, with a reduction at lighter loads but an increase when fully ventilated, although the effect is marginal.

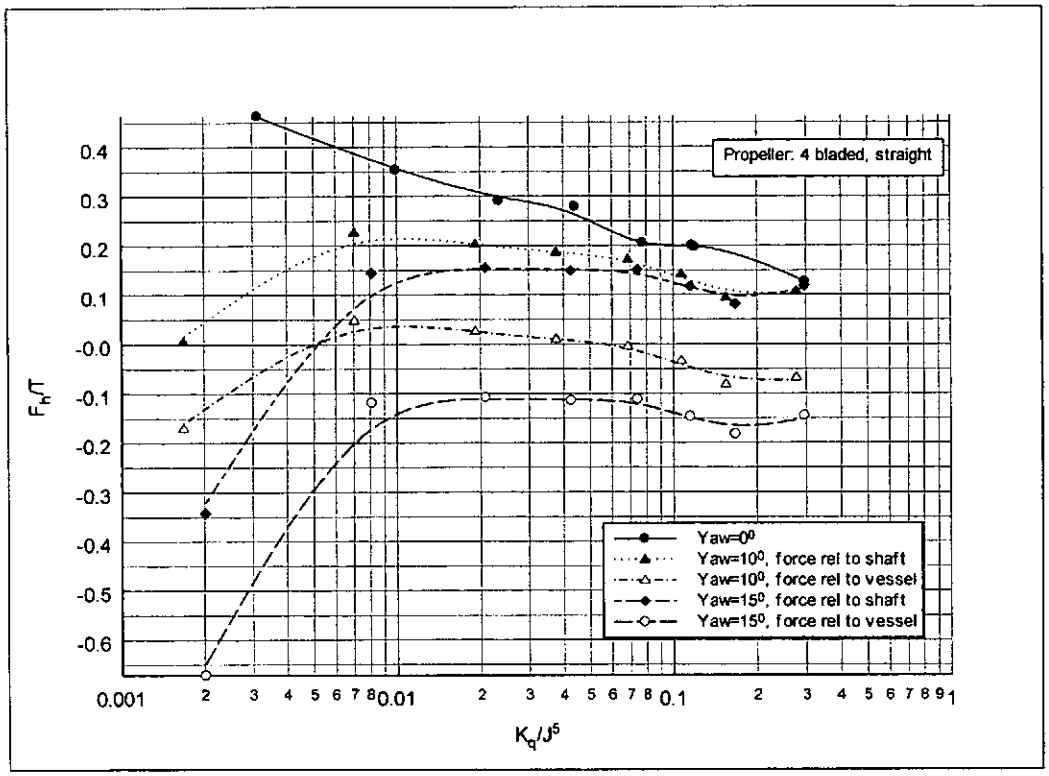

Figure 63. Horizontal Force vs Torque Coefficient – Effect of Yaw.

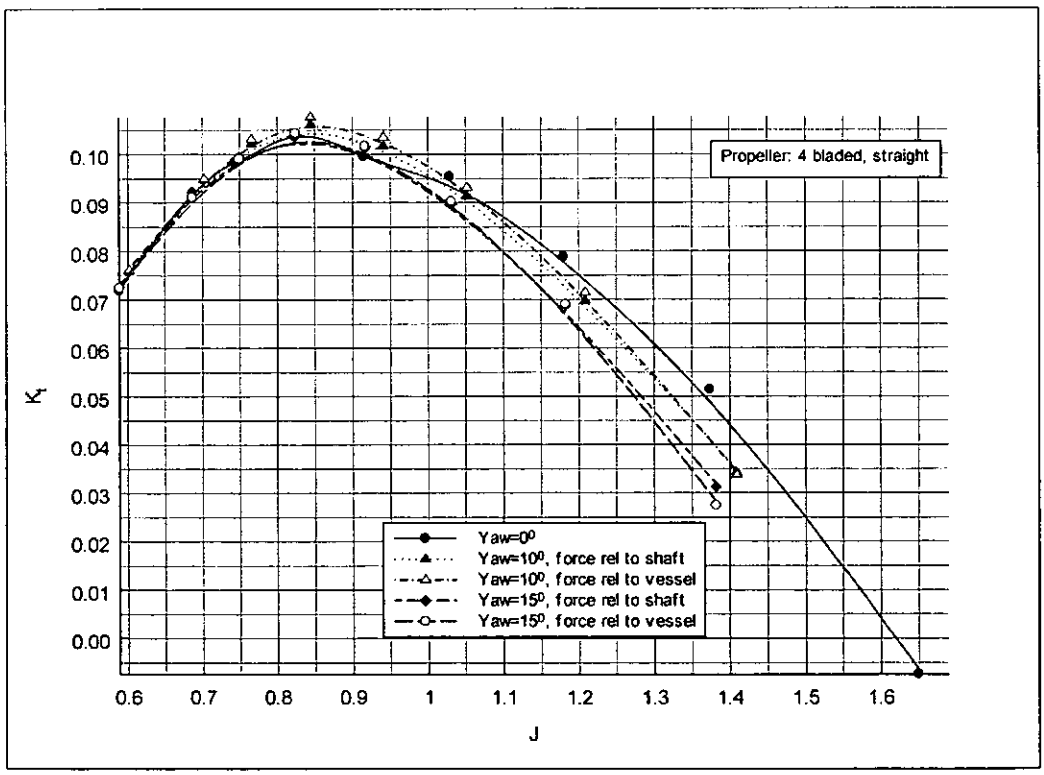

Figure 64. Thrust Coefficient vs Advance Coefficient – Effect of Yaw.

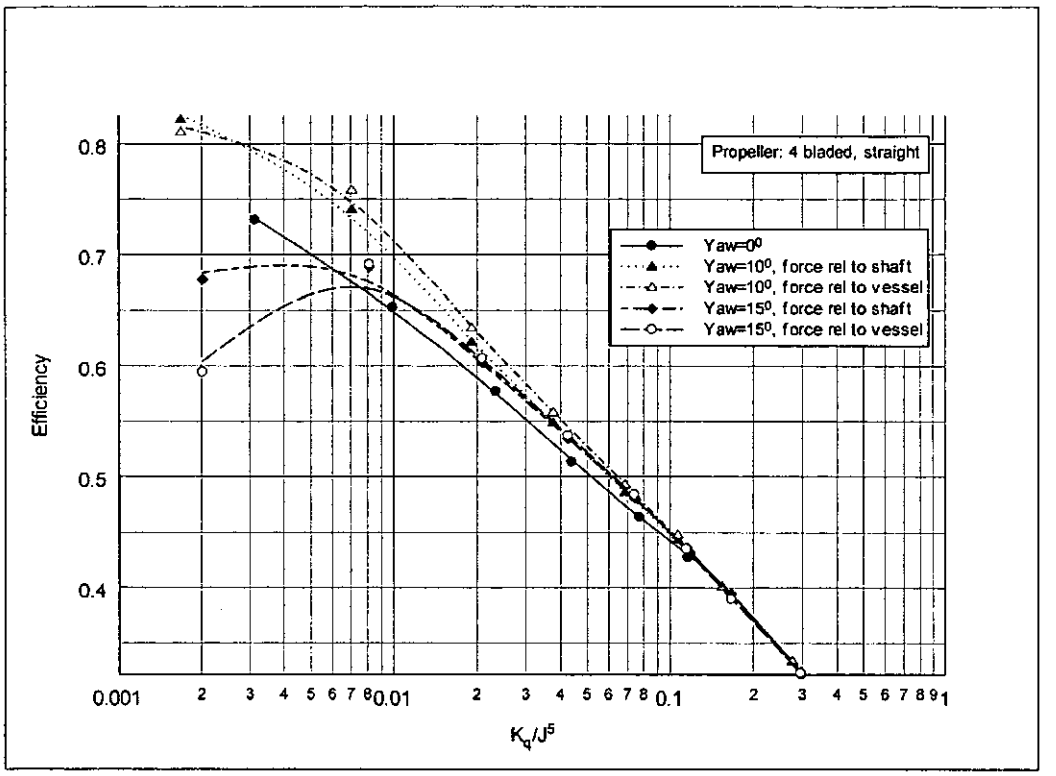

Figure 65. Efficiency vs Torque Coefficient – Effect of Yaw.

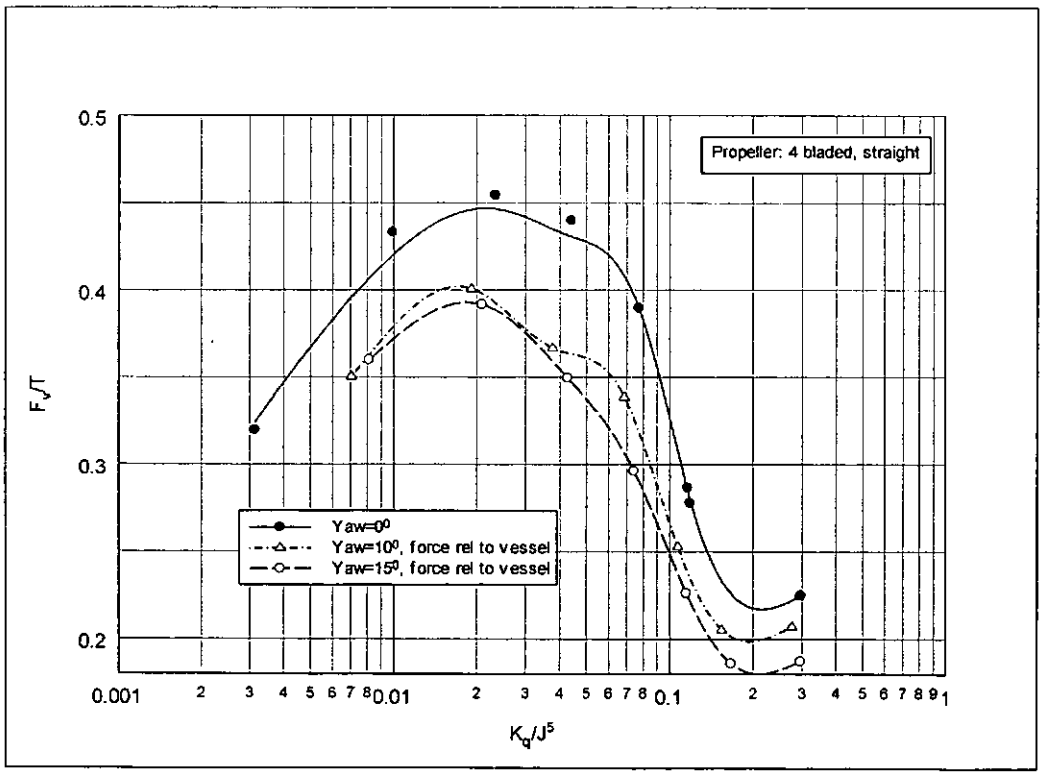

Figure 66. Vertical Force vs Torque Coefficient – Effect of Yaw.

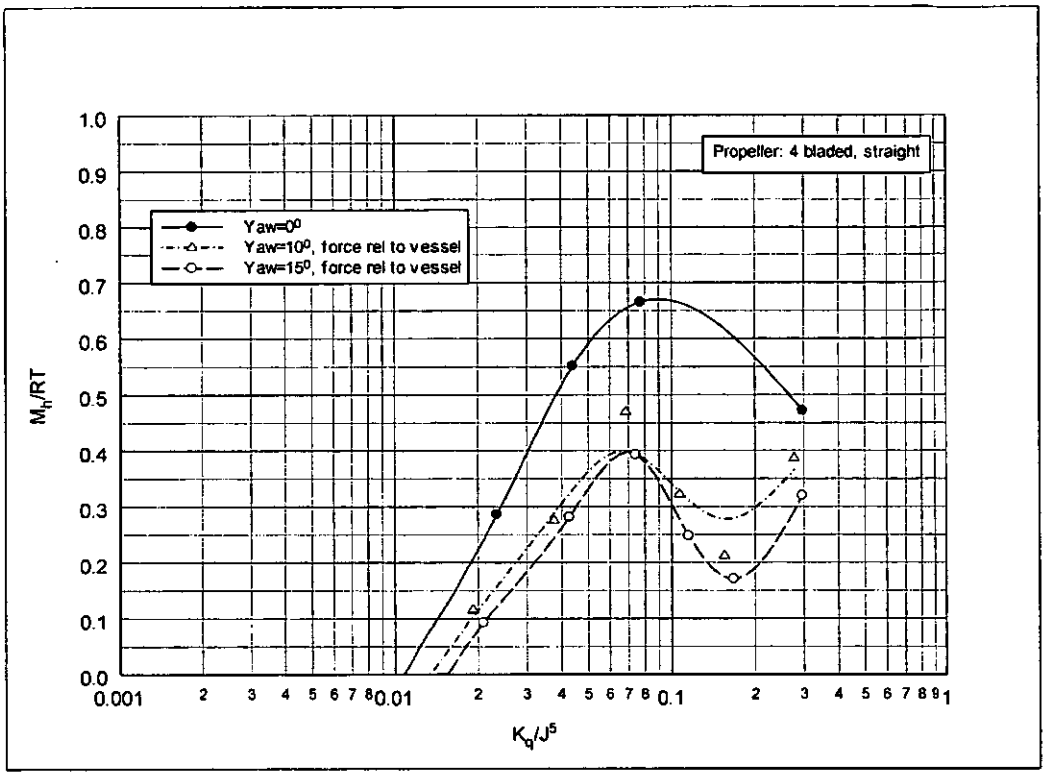

Figure 67. Trim Moment vs Torque Coefficient – Effect of Yaw.

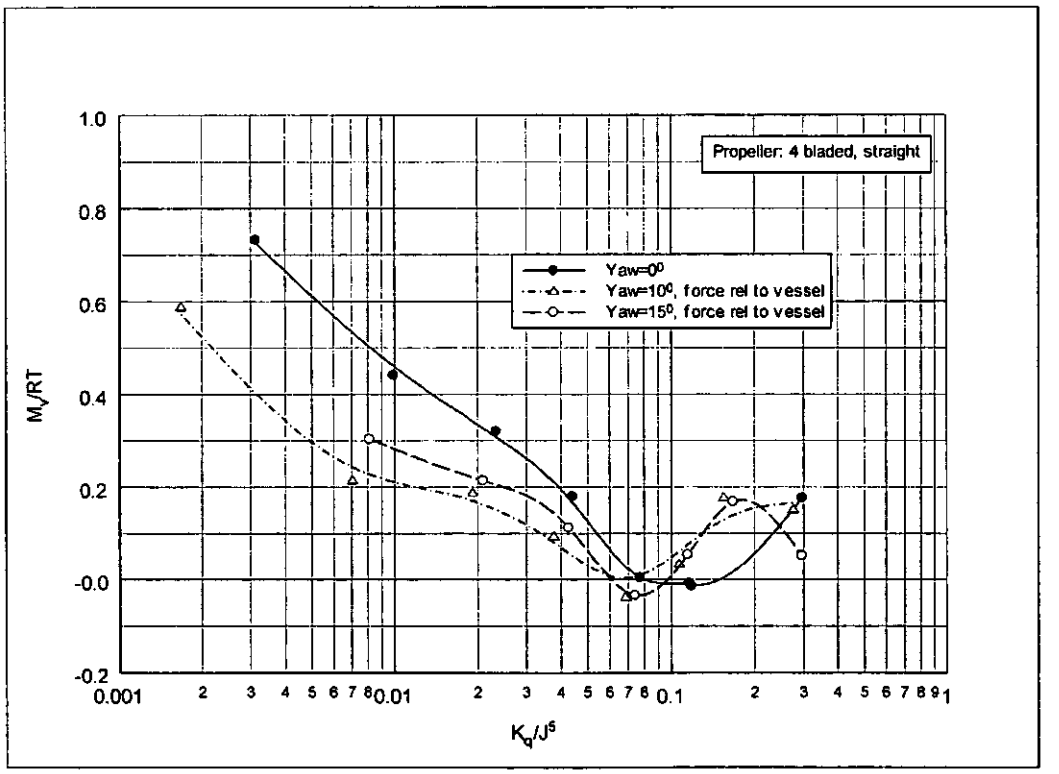

Figure 68. Steering Moment vs Torque Coefficient – Effect of Yaw.

From Figure 63 which shows the horizontal forces, it can be seen that these values also reduce (relative to the shaft) due to the effective pitch reduction. From this figure the contribution to thrust may be calculated; at 10^0 the added thrust would be approximately 3.5% ($\approx 0.2 \sin 10^0$) while at 15^0 the figure is 3.9%. These changes are accompanied by small changes in torque, again because of the pitch effect, and the net result is a small increase in propulsive efficiency (Figure 65). However, although the nature of the effect can be seen using these results, the actual change in efficiency is within the error band and a definitive figure would be inappropriate. It can also be seen from Figure 63 that horizontal forces relative to the vessel are reduced significantly because of the opposing effect of the sideways component of thrust when the shaft is yawed. Indeed, at 15^0 yaw, the horizontal force relative to the vessel is reversed.

It is of interest to note the results for the other supplementary forces. Figure 66 to Figure 68 show a reduction in all three, resulting from the pitch effect. It is also worth commenting that the similarity between the shapes of lines for each force indicates good consistency for the tests, which were interspersed with complete shut downs of the channel and removal of the hood in order to change propellers or yaw angles.

5.2. Transient Results

5.2.1. General Principles

Before discussing individual time histories, it is important to establish some general principles:

- force values presented have been normalised by the mean thrust in each case, torque by mean torque and moments by the product of radius and mean thrust.
- transient forces are calculated relative to the shaft, not the vessel; thus upward forces, for example, are referred to as trim forces (rather than vertical) and do not contain a

contribution from thrust due to shaft inclination, or vice versa; the same principle applies to sideways forces (yaw forces) when shaft yaw is involved.

- a propeller acts as an integrator of the forces produced by each underwater blade element. Thus:
  - the yaw and trim *components* of lift force on each wetted blade element are added. Hence, the total yaw force is influenced by the fact that the components are small for those blade elements entering and leaving the water, and reach a maximum as they pass beneath the shaft. Conversely, the trim force components are a maximum as the elements enter and leave the water and are a minimum as the blade passes beneath the shaft.
  - in the cases of torque and thrust, the relevant components of the elemental lift forces concerned are circumferential and axial respectively, and thus the net effect is simply additive over all wetted blades.

5.2.2. Time Histories

A typical set of time histories is shown in Figure 69 to Figure 71, with a full set for advance coefficients of 1.37, 1.03 and 0,82 presented in Appendix B. These J values relate to conditions close to the maximum efficiency point, the approach to transition and the maximum thrust point respectively, while avoiding critical resonant frequencies of the test rig.

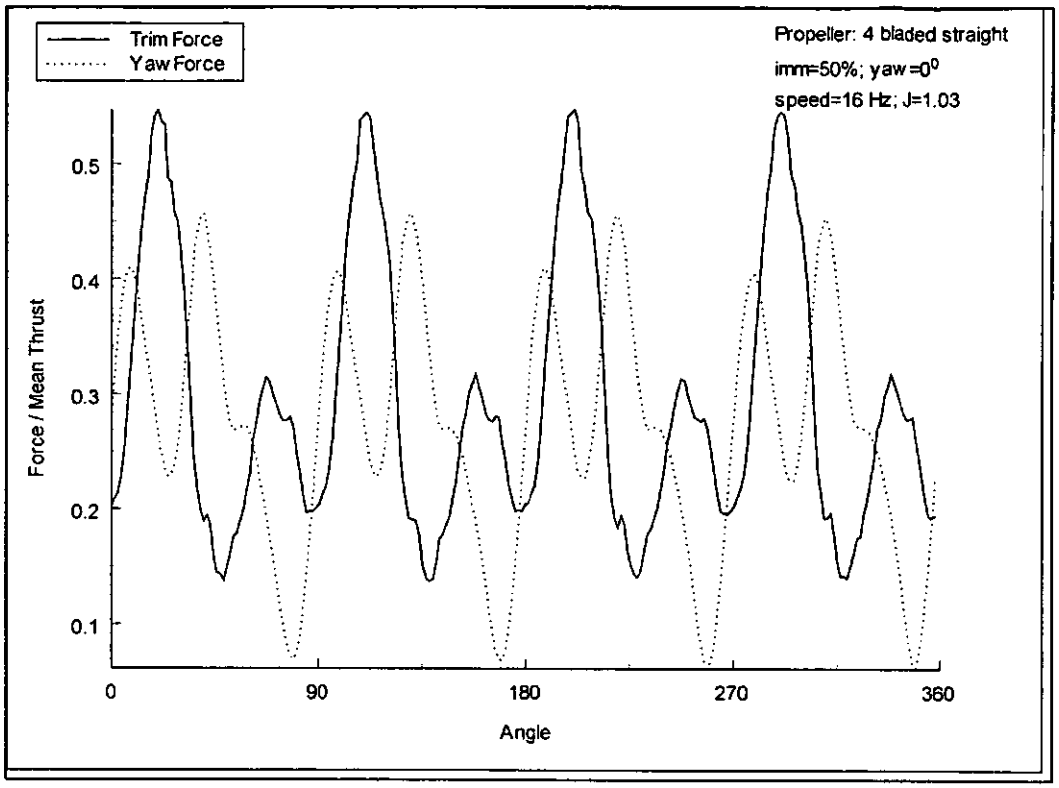

Figure 69. Typical Time Histories for Trim and Yaw Force.

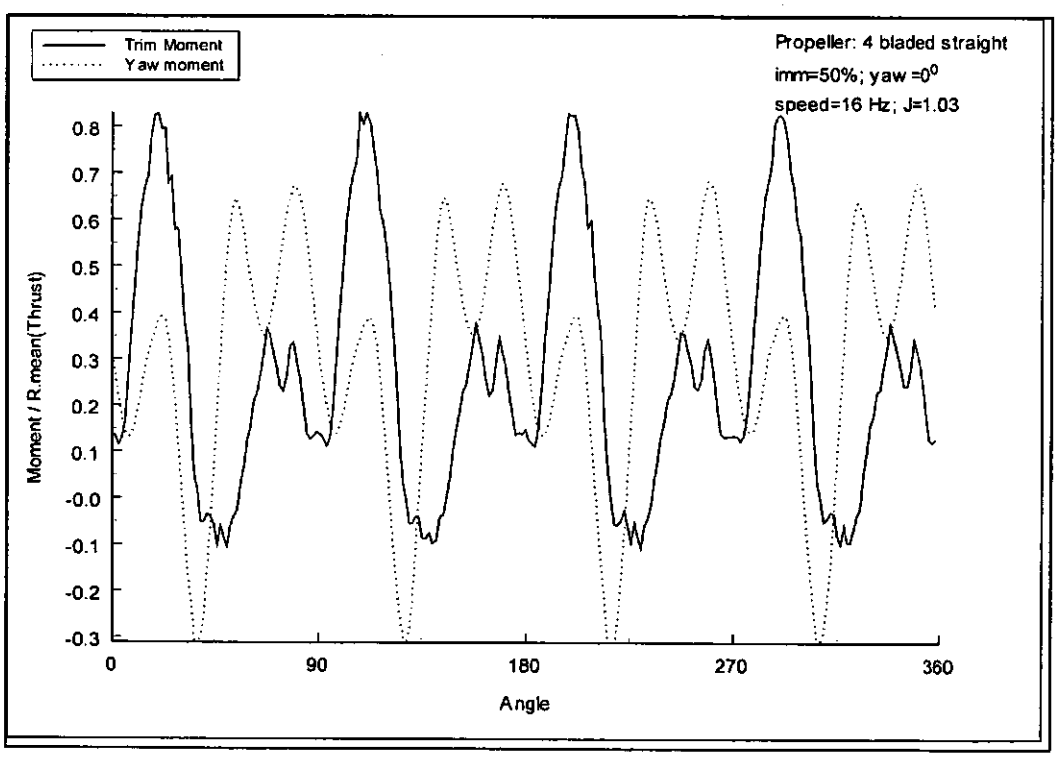

Figure 70. Typical Time Histories for Trim and Yaw Moments.

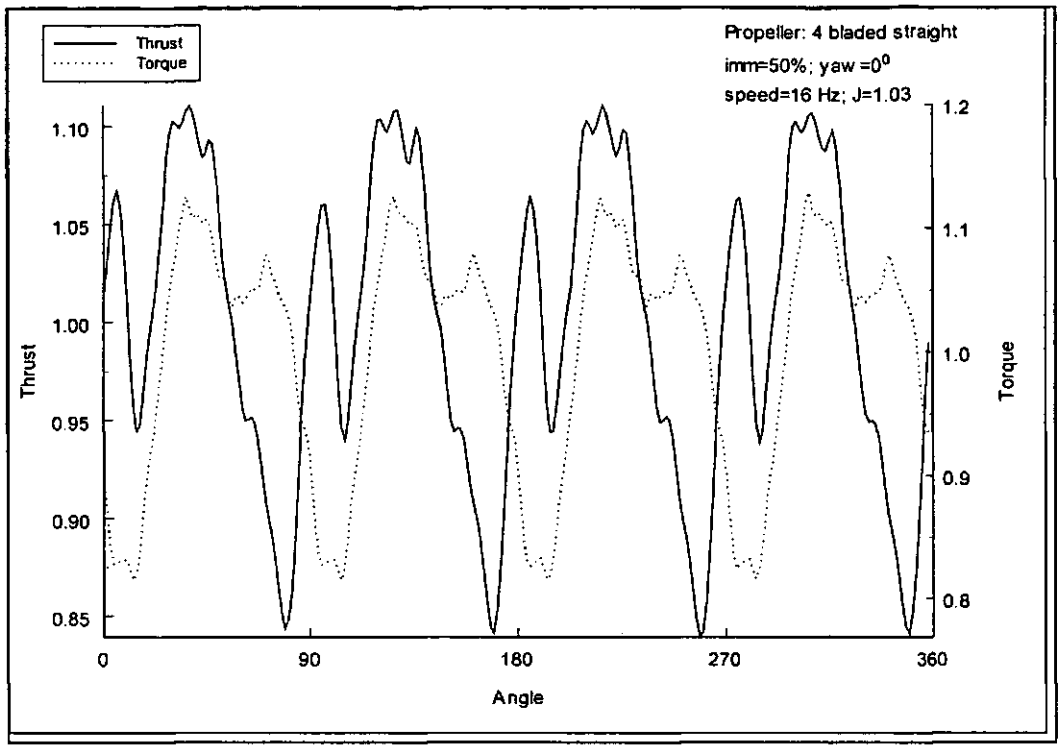

Figure 71. Typical Time Histories for Thrust and Torque.

From these traces, the pulsing of each force as blades impact the water is clearly visible. Trim forces show a marked peak for all propellers at 50% immersion, especially at lighter loads. At the higher load, the amplitude reduces, reflecting the local elevation in water level and higher aeration of the water, making the initial impact less distinct. Yaw forces, which are less dominated by the initial impact, generally have lower amplitudes at the low load condition. At high loads, however, the transients evidently persist to the point where blades reach the bottom of their swings. Consequently lift forces remain high to the point where yaw components are significant and amplitudes are thus increased.

Thrust also shows distinct pulsing, frequently with a double pulse for each blade. This effect is evident at several operating speeds and, since no resonant frequencies could be detected at the blade rates in question, this effect must be hydrodynamic in origin. There are certainly distinct differences between thrust histories for each blade shape. This would

indicate that the relative rates of rise and fall of lift during the steep transients as blades enter and exit the water, which are dependent on blade shape, are critical in determining the thrust history. A double pulse for a blade would, then, be explained as a rapid rise as a blade impacts, followed immediately by a sharp fall as the leading edge of a blade exits, with an associated break down of the flow field, followed by a rise as the flow field becomes further established around the entering blade. The five bladed propeller shows less tendency towards this type of behaviour, since with an odd number of blades, the entry and exit transients do not occur almost simultaneously, as is the case with an even number. The torque curves generally follow the same pattern as thrust, although they are not an exact mimic as might be expected if conditions were slowly varying, since non-linearities are introduced by the large and rapid variations in the lift-drag ratio of the foil sections during the transients.

The trim and yaw moments show the most complex variations, as these depend not only on the fluctuations of thrust, but also on the movements of its effective point of action on the propeller disc. Thus, for example, as a blade impacts the water, the thrust increases, but the fact that the increase arises from the blade near to the surface means that the centre of action rises and moves outwards on the entry side. Thus the yaw moment increases since both the force and radius at which the force acts increase. However, with the trim moment, force increases while radius decreases. The situation is further complicated by the blade that exits the water, and it is difficult to relate these various conflicting effects to the time histories.

5.2.3. Comparison of Propellers

To enable comparisons to be made between different propellers, and between immersions, the root mean squares of fluctuations from the mean are presented. In each case, although there are some discrepancies, the trend is clear; the magnitudes of the force ratios remain constant at high loads, and start to rise as load is reduced and operation moves into the partially ventilated region. This is in accord with the theory, discussed in section 2.2, concerning the relative insensitivity of fully ventilated foil sections to changes of angle of attack. Figure 72 and Figure 74 show how the trim and yaw force fluctuations vary for each propeller across the operating range; torque, thrust and moments are shown in Appendix B.

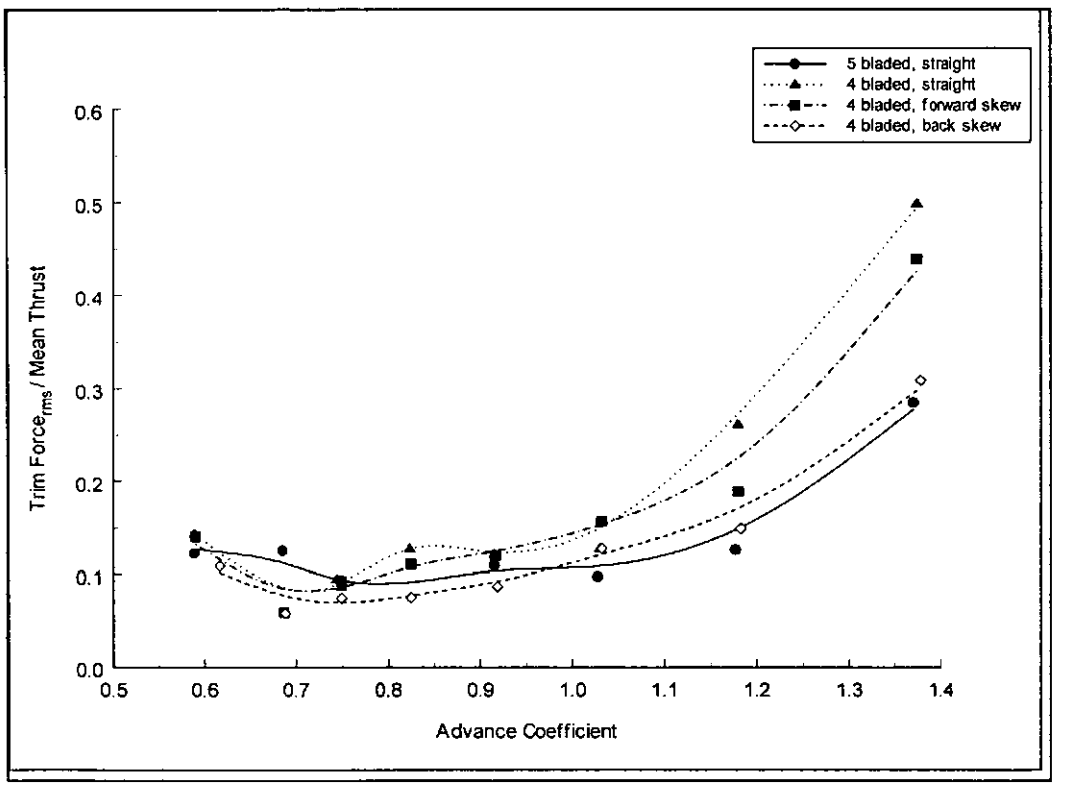

Figure 72. RMS Values of Trim Force Fluctuations – Effect of Propeller.

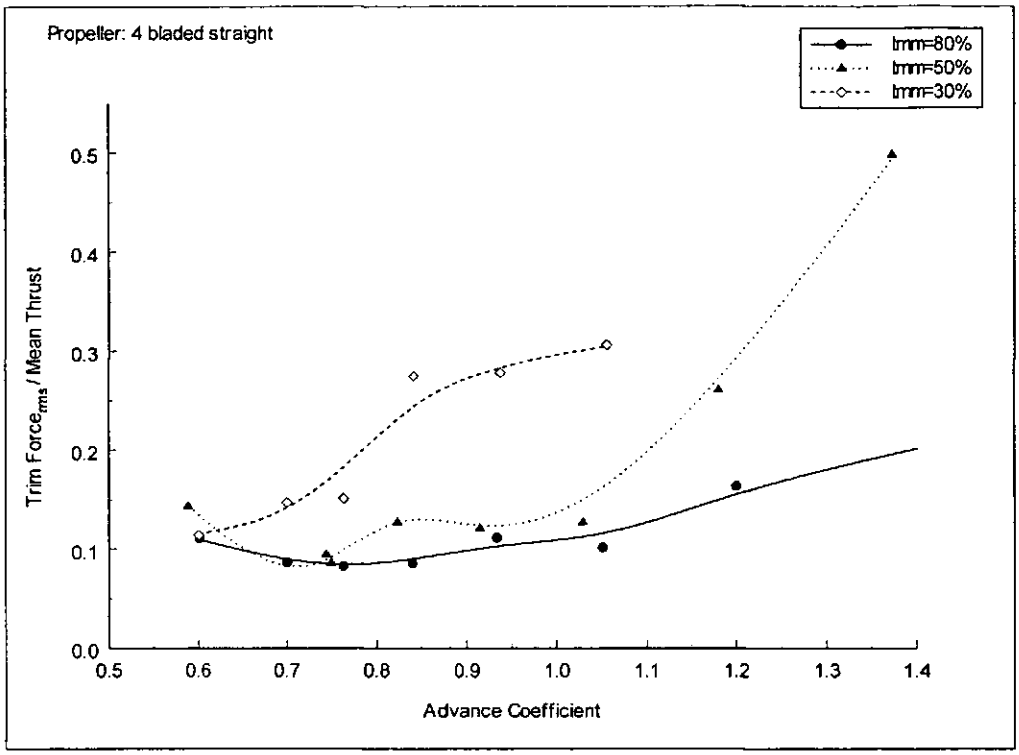

Figure 73. RMS Values of Trim Force Fluctuations – Effect of Immersion.

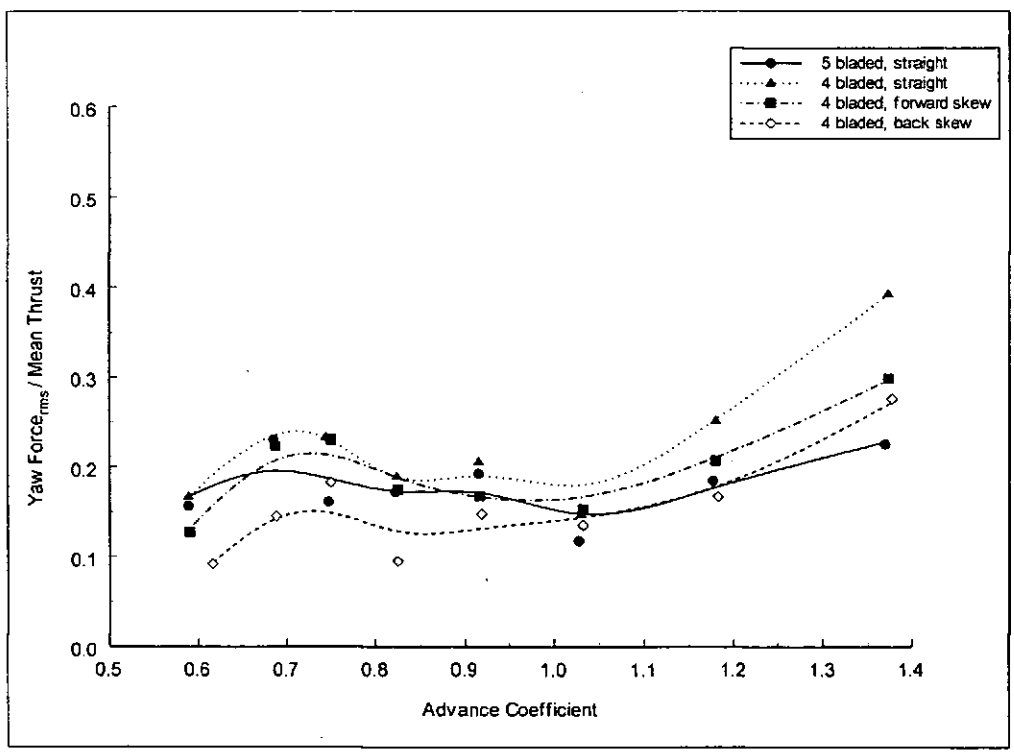

Figure 74. RMS Values of Yaw Force Fluctuations – Effect of Propeller.

There are markedly reduced amplitudes in the case of the back skewed, compared with the other four bladed propellers, and it is better generally than even the five bladed propeller. Clearly, the skew has the effect of the reducing impact forces because the flow field is established incrementally across the blade span. Comparing the five bladed propeller with the 4 bladed straight (which has an identical blade profile), amplitudes are, as expected, lower with the 5 bladed, with the difference becoming more marked as load is reduced.

5.2.4. Comparison of Immersions

The difference between immersions is brought out clearly in Figure 73. The 30% immersion case has significantly higher fluctuation: mean thrust ratios, which generally rise steadily as load is decreased. These higher fluctuations are also clear on the time histories, with more discrete pulses in the yaw direction, since only the ends of blades are impacting the surface and there is less interference between adjacent blades. Also, as expected, the 80% immersion case shows lower fluctuations, as blade forces are maintained around a much greater proportion of the arc.

5.2.5. Frequency Spectra

The frequency spectra relating to the time histories are presented in Appendix B; Figure 75 to Figure 77 show typical spectra. In these, the normalised magnitudes are presented for each frequency line. In most cases, clear peaks exist at harmonics of blade rate, with the dominant values being at first and second harmonics, usually some contribution at the third and little above that. Intermediate lines also exist at shaft rate and multiples thereof. This is possibly the result of slight imbalance of the propellers, although they were statically balanced and checked by running out of water, showing only small shaft rate amplitudes. A more likely reason is small differences between blades, a factor not detectable on the time histories because of the syncronous averaging process.

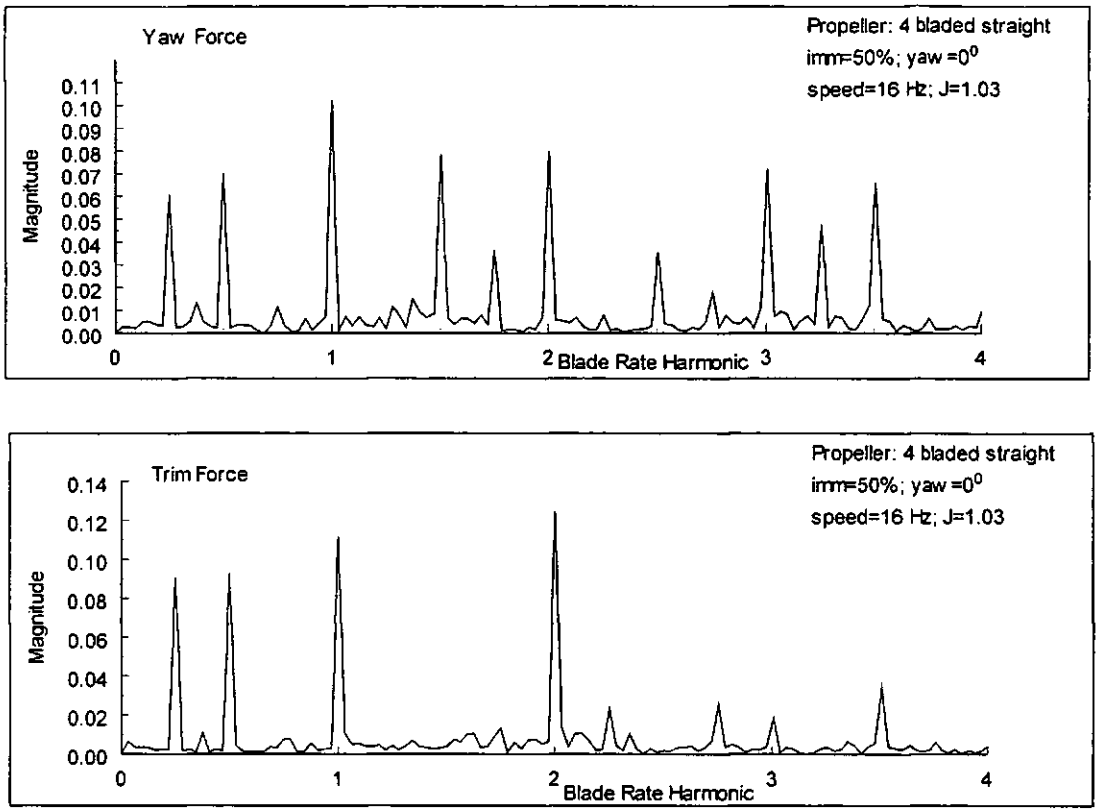

Figure 75. Typical Frequency Spectra for Yaw and Trim Force.

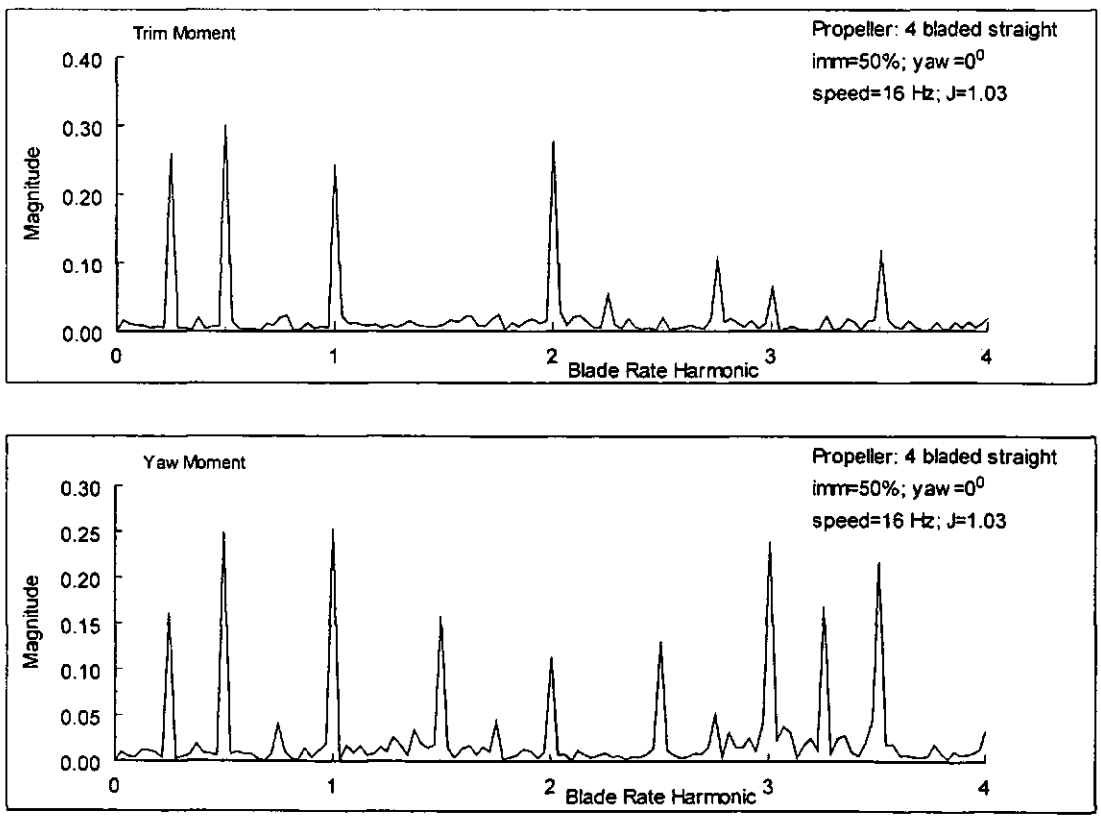

Figure 76. Typical Frequency Spectra for Trim and Yaw Moments.

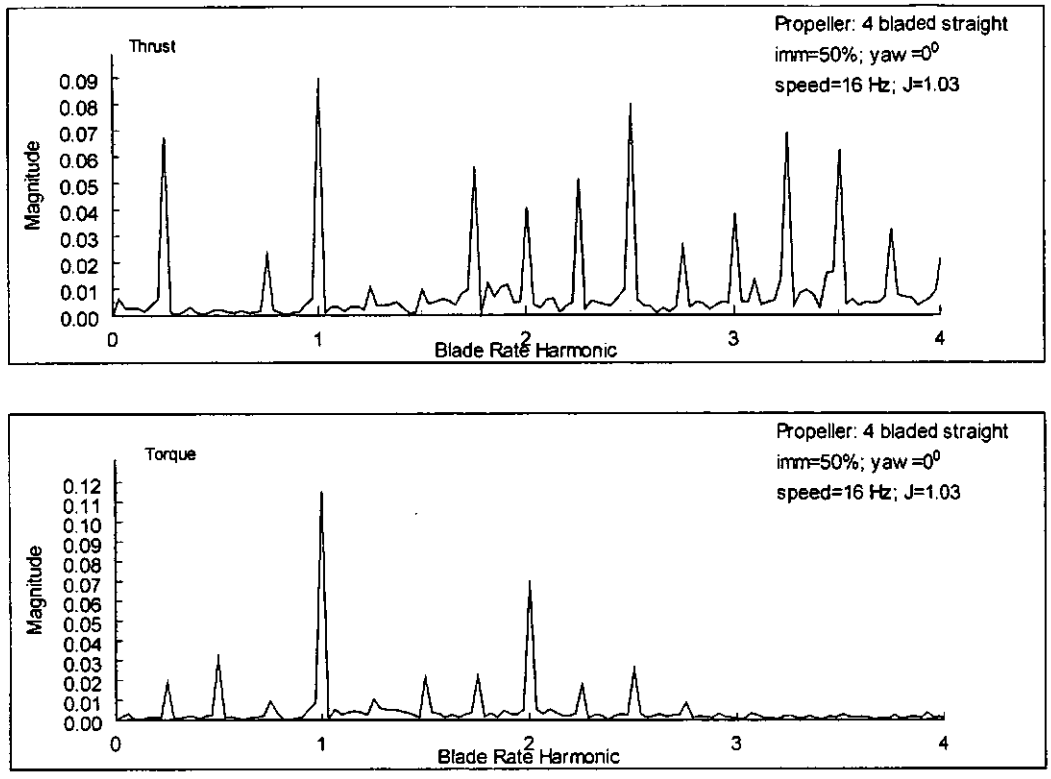

Figure 77. Typical Frequency Spectra for Torque and Thrust.

The comments made above when comparing propellers, concerning relative magnitudes of the vibrations, are also evident from the spectra. However, one further detail is available with the data presented in this way – the distribution of vibration energy across the frequency range. Most notably, in the case of the back skewed propeller, the dominant frequency lines are considerably lower than with the other propellers, but the lesser lines tend to be higher, the energy being spread across more frequencies.

5.2.6. Effect of Yaw

Finally, the effect of shaft yaw may be seen in Figure 78 and Appendix B. It was observed in the discussion on mean loads that the forces when the shaft was yawed were much reduced as a result of a decrease in the effective pitch. The effect on fluctuations is, at high loads, an equivalent one, as seen from the fact that the normalised values for 15^0 of yaw are close to the values for zero yaw. At lighter loads, the yawed case shows higher levels of normalised force fluctuations. Under these conditions, the water surface is more distinct, and the angle of attack at entry is high, compared with the bottom of the blade's swing

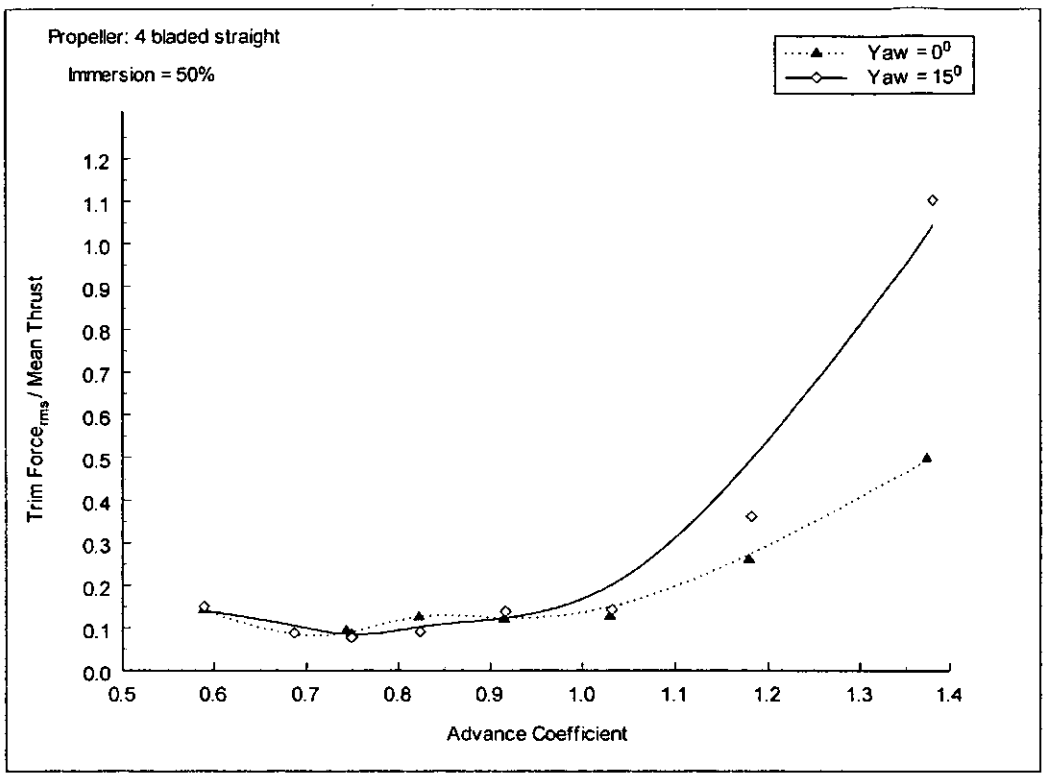

Figure 78. RMS Values of Yaw Force Fluctuations – Effect of Yaw.

where it is effectively reduced by the yaw angle. Hence, the effect of the impact forces is high, relative to the low mean forces being produced.

5.3. Comparison of Experimental Results with Numerical Model

The purpose of the numerical model developed in section 2 is to predict the nature of the fluctuating forces exerted at the propeller. The model assumed that the blades were operating fully ventilated, so that all the lift force was produced by the pressure face, and was based on a routine which integrated an experimentally derived surface pressure transient across the blade. It is intended that it may be used as a comparator, so that, given mean force components and a blade profile, the amplitude and nature (eg. the rate of increase of force on each pulse) of the forces may be estimated. Different blade profiles may then be compared.

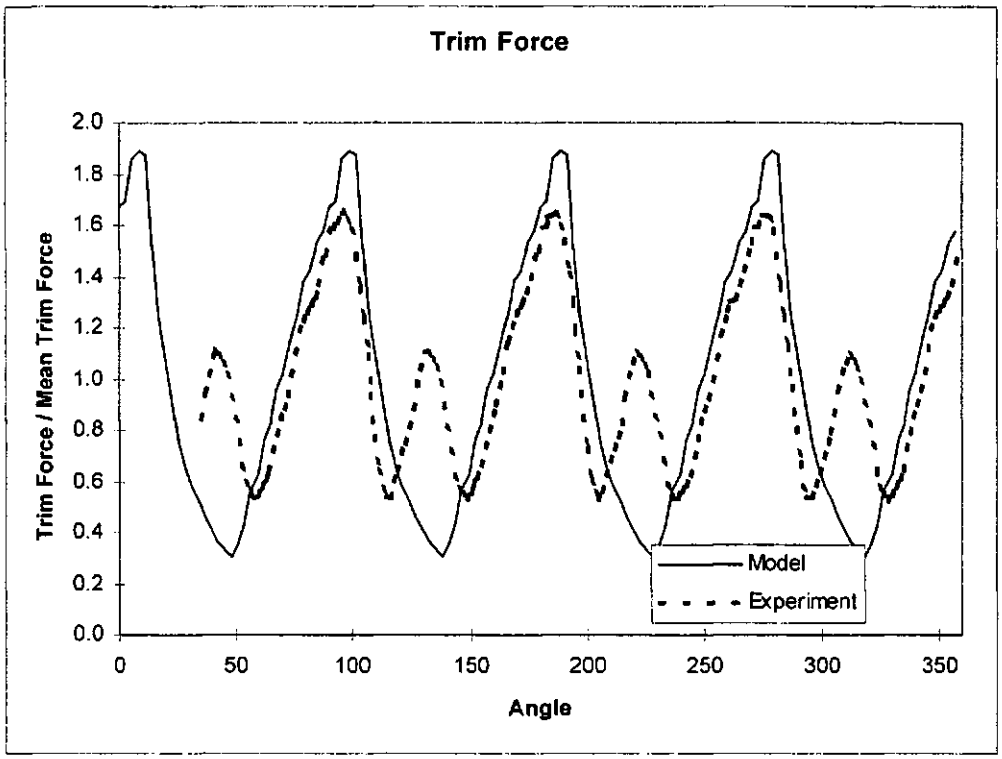

Figure 79. Trim Force Comparison between Numerical Model and Experiment.; Straight Trailing Edge; J = 0.91; immersion = 50%.

Figure 79 shows a comparison, for trim force at 50% immersion, between the model and the experimental results at an advance coefficient for which the propeller is just fully ventilating, but is not so low that the water surface is significantly modified. The force has been normalised by the mean trim force, not the mean thrust as has been used previously. This is because it was found that the model does not predict well the relationship between mean thrust and the other components of mean force. However, it can be seen from the figure that if the fluctuations are related to the mean force under consideration, then there is a reasonable correlation. The rate of increase of force for the pulse is well predicted, and the maximum values are within 15%. The added pulse in the experimental curve is accounted for by the way in which the ventilation bubble forms and then partially collapses, an effect which it was not possible to include in the model. The comparison for thrust at an immersion of 30% is shown in Figure 80, and this also shows a good degree of correlation.

Comparisons for the other force components were also examined, as was a different blade profile, and while there is some correlation, most cases are less distinct, being complicated

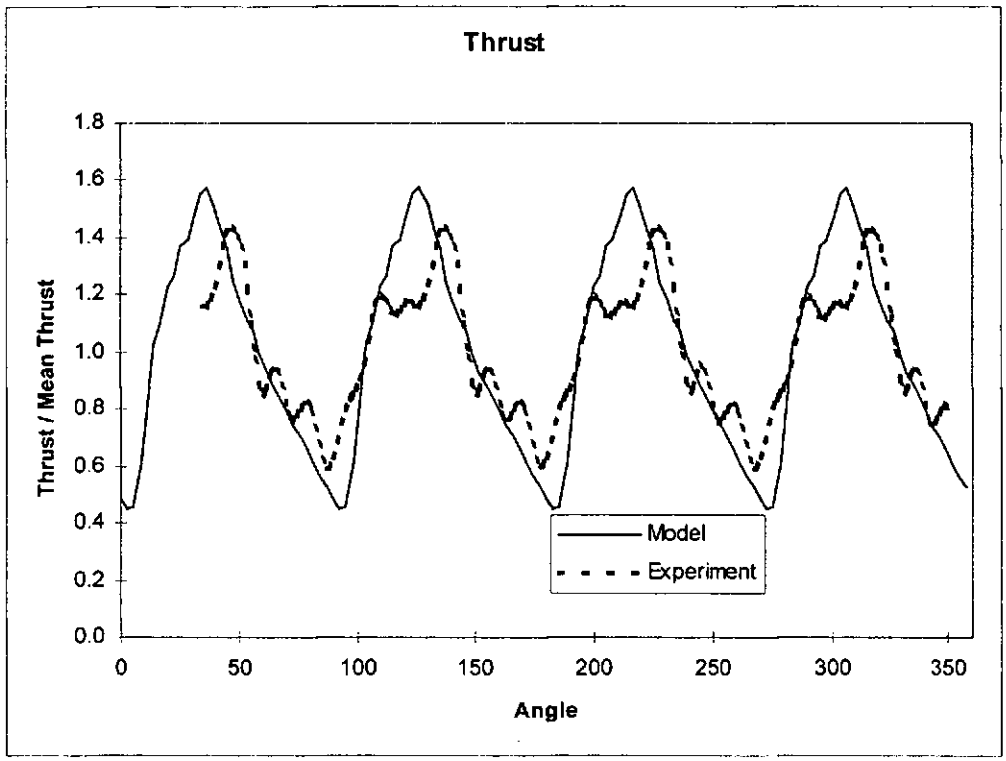

Figure 80. Thrust Comparison between Numerical Model and Experiment.; Straight Trailing Edge; J = 0.91; immersion = 30%.

by experimental effects such as bubble collapse, water aeration and modification of the surface level upstream of the propeller. In view of the relative simplicity of the numerical model, the limited correlation described above does encourage the refinement of the model in future work.

6. DESIGN METHODOLOGY

6.1. Introduction

The magnitudes of trim and yaw forces applied to the propeller have considerable impact on shaft design. Rose et al (1993) demonstrate a calculation which accounts for the stresses imposed by the mean values of these forces, combined with torque and thrust, which leads to an estimate of shaft size based on the Von Mises failure criterion.

However, this analysis accounts for neither the alternating nature of the mean loads as the shaft rotates, nor the peak loads arising from the blades impacting the water. It is now possible, in the light of this work, to refine the design process.

6.2. Detailed Design Process

This work has approached the problem from the direction of both finite element analysis and experimental measurement of the fluctuating forces imposed on the propeller-shaft system.

The finite element work modelled the propeller in some detail. It led to the conclusion that the flexibility and dynamic behaviour of the blades (and added mass due to surrounding water) have little impact on the stress condition in the shaft. Thus a simplistic model of the propeller, as a lumped mass with appropriate moments of inertia about its three axes, is sufficient. The shaft is modelled as a simple beam, supported on springs representing cutlass bearings. A modal analysis may first be carried out, using an initial estimate of shaft diameter, to establish resonant frequencies, and thus ensure that normal operation does not coincide with these. For realistic sizes of shaft, this behaves as a rigid body. Thus it is the spring support stiffnesses which dominate these frequencies; shaft diameter has a relatively minor effect through the mass term. Damping is included as modal damping, with a value of damping ratio of 0.05 (as discussed in section 2.5.4) for all modes.

For the appropriate advance coefficient, the mean force and moment values may be determined from Appendix A, and the time histories from plots similar to those presented in Appendix B. The trim and steering forces and moments need to be transformed so that they relate to the rotating shaft as shown in Figure 81.

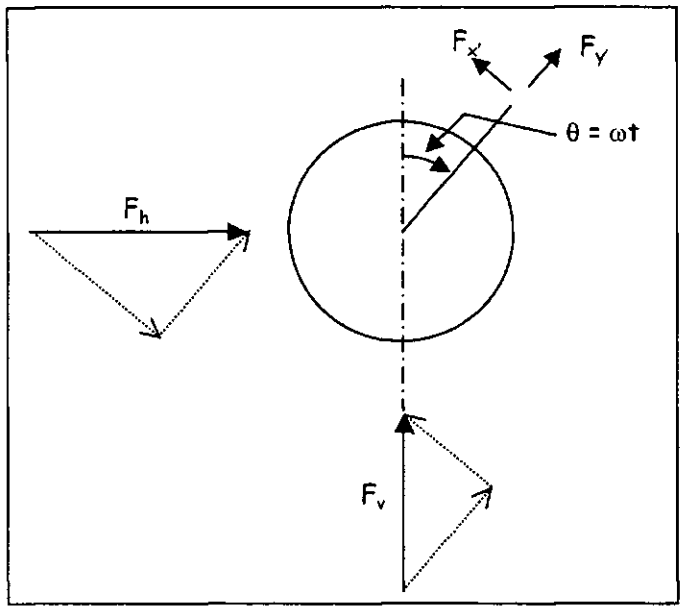

$$\begin{vmatrix} F_{x'} \\ F_{y'} \end{vmatrix} = \begin{vmatrix} F_h \\ F_v \end{vmatrix} \cdot \begin{vmatrix} \cos\omega t & -\sin\omega t \\ \sin\omega t & \cos\omega t \end{vmatrix}$$

$$\begin{vmatrix} M_{x'} \\ M_{y'} \end{vmatrix} = \begin{vmatrix} M_h \\ M_v \end{vmatrix} \cdot \begin{vmatrix} \cos\omega t & -\sin\omega t \\ \sin\omega t & \cos\omega t \end{vmatrix}$$

where a prime indicates a frame of reference rotating with the shaft

Figure 81. Transformation from Craft based to Shaft based Axes.

The set of transient forces and moments are applied to the centre of the propeller boss in the FE model which is run as a transient time-marching analysis. The output transient may then be examined to identify the peak values of maximum stress reached. Since the shaft is rotating, the mean value of stress which it experiences is zero, and thus only alternating stresses need to be included in the fatigue analysis. The S-n curves for the proposed material would be used to establish the maximum allowable stress for the infinite life condition, allowing as usual for factors such as stress raisers and surface finish. The shaft diameter may then be modified if necessary.

6.3. Design Example

In order to demonstrate the process, an example has been chosen of a typical propeller-shaft system currently in operation. Essential details are given in Table 5.

Table 5 . Details of Propeller Shaft System used in Design Example.

Propeller:	
diameter	1.04 m
pitch:diameter ratio	1.52
mass (estimated)	115 kg
polar 2nd moment of area	5.37 kg m^2
lateral 2nd moment of area	3.80 kg m^2
Shaft:	
diameter	105 mm
material	TEMET25
elastic modulus	200 Gpa
density	7800 kg/m^3
forward bearing	ball / thrust
aft bearing	cutlass
cutlass bearing stiffness (estimated)	30 MN/m
centre prop to centre cutlass bearing (estimated) (z_0)	345 mm
Craft	
Advance coefficient (estimated)	1.2

6.3.1. Calculation Using Mean Forces

Using the Von Mises yield criterion proposed by Rose et al (1993),

$$\sigma_{max} = \sqrt{\sigma_{b\,max}^2 + 3\tau_{max}^2}$$

where

$$\sigma_{b\,max} = \frac{32}{\pi D^3} M_{b\,max}^2$$

$$M_{b\,max} = \sqrt{(M_v + F_h z_0)^2 + (M_h - F_v z_0)^2}$$

$$\tau_{max} = \frac{16}{\pi D^3} Q$$

together with mean values of the forces and moments taken from experimental results, the following values were calculated:

Max bending moment, $M_{b\,max}$	8860 Nm
Max bending stress, $\sigma_{b\,max}$	77.9 MPa
Max shear stress, τ_{max}	32.3 MPa
Max Von Mises stress, σ_{max}	95.9 MPa

This lies well within the 0.2% proof stress value of 500 MPa for this material.

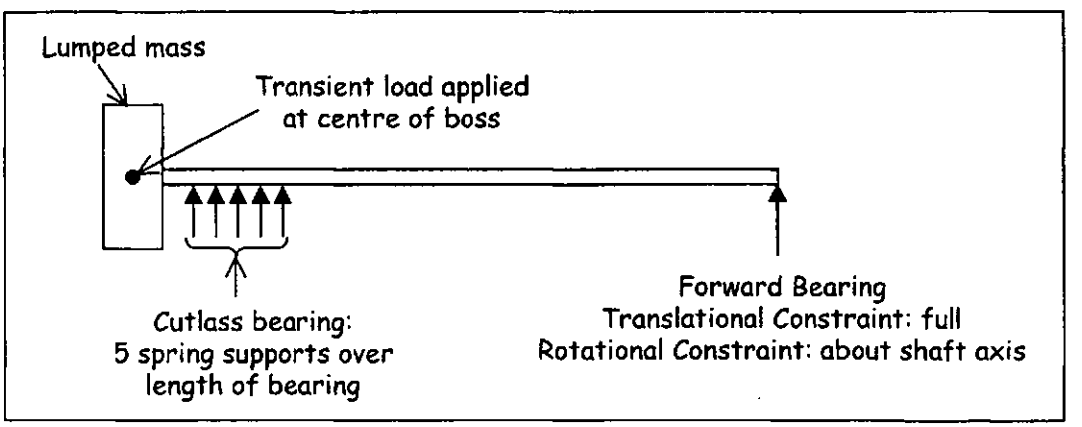

Figure 82. Schematic of FE Model.

6.3.2. Calculation Using Transient Forces

The FE model was created as shown in Figure 82, and loaded at the boss centre with the transient forces and moments derived from the experimental results for the appropriate

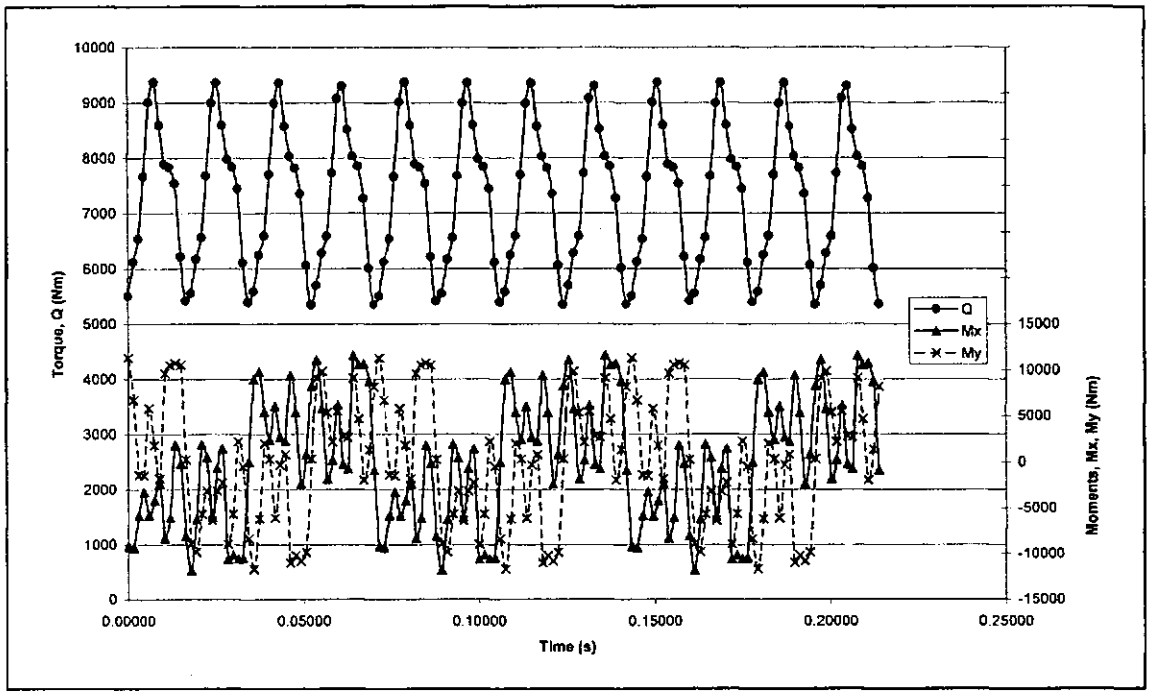

Figure 83. Transient Moments Input to FE Model.

advance coefficient. These forces and moments are shown in Figure 83 and Figure 84. The output of the maximum fibre stress in the shaft, at a point in the centre of the cutlass bearing where the maximum bending moments were found to occur, is shown in Figure 85. On checking the natural frequencies, it was found that first occurred at 43 Hz, close to three times the shaft rate, and this gave unacceptably high peak values. Consequently, for the purpose of this exercise, the bearing stiffness was changed upwards to raise the first natural frequency to 47 Hz. Figure 85 shows the result for six full revolutions during which the excitation force was applied, followed by a further period which demonstrates the effect of the damping used. The excitation period was ample to overcome the start-up transient. The stress plotted is not that at a particular point on the circumference of the shaft, but rather the maximum and minimum stresses occurring at that time step at any point around the circumference. Examination of the components of these stresses has

shown that they are dominated by bending stresses, with those due to torsion being an order of magnitude smaller, and those from axial and shear forces being negligible. Consequently it is reasonable to assume that the stress at any given point on the shaft reverses about a zero mean value. Further investigation was carried out to establish the relative contributions to shaft stress of the imposed forces and the dynamics of the system, by making the mass and inertias of the propeller negligible. From this it was found that the system dynamics were responsible for approximately 12% of the induced peak stresses.

It can be seen from Figure 85 that there are several peak stresses occurring in the region of ±200 MPa (over 8% of points lie outside the ±200 MPa band). Data for this material show that the fatigue strength at $2x10^7$ cycles, when tested in 3% NaCl is 430 MPa for un-notched bar and 230 MPa for notched bar. Taking the un-notched value, and including correction factors for surface (0.8) and size (0.7), the fatigue strength becomes 240 MPa. The peak stresses in excess of 200 MPa, which would be increased by stress concentration

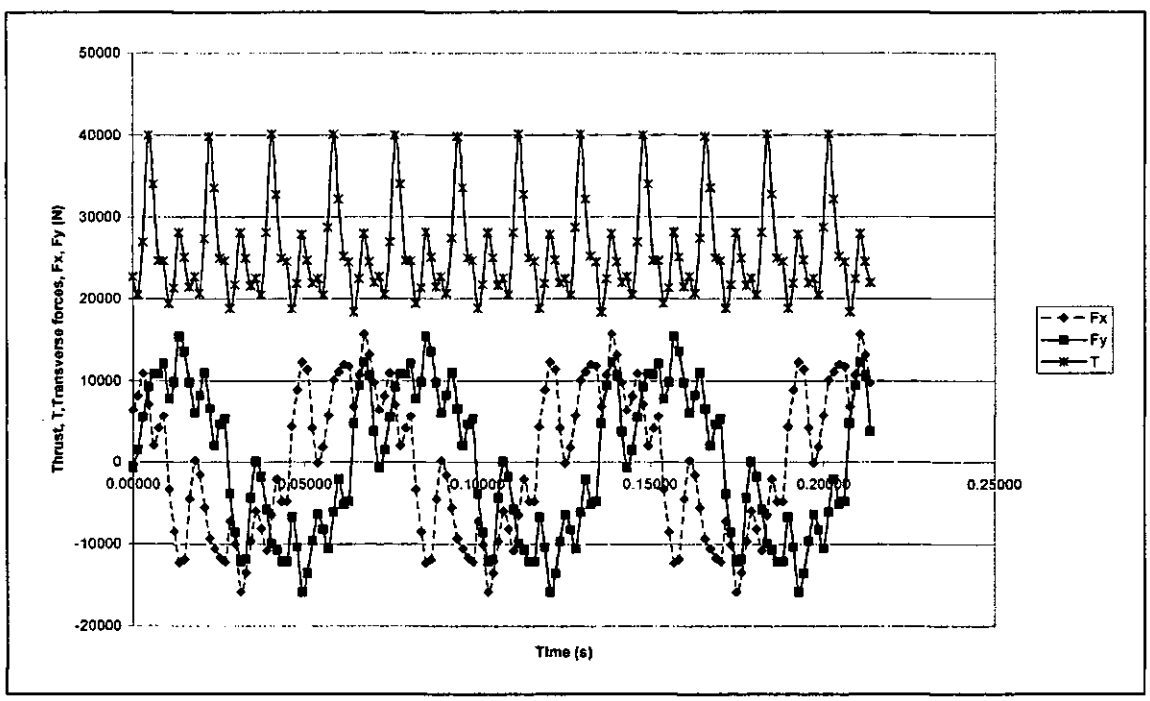

Figure 84. Transient Forces Input to FE Model.

factors not discussed here, would be judged to be too close to this 240 MPa limit.

The forgoing calculation was for design point operation. Inspection of the thrust coefficient in Appendix A (figure A1) shows that if vessel speed were to be lower while shaft speed remained at the design value (under start up conditions for example), reducing J from 1.2 to 0.9, then a peak value of K_t would be attained. This would increase thrust by some 35% and other forces similarly. The amplitude of vibration can be seen, from rms values of fluctuations in Appendix B (figures B127 ff), to reduce a little as the blade fully ventilates, but the overall effect is a substantial increase in the reversing stresses imposed on the shaft. Thus, under these conditions, the stress would significantly exceed the fatigue limit.

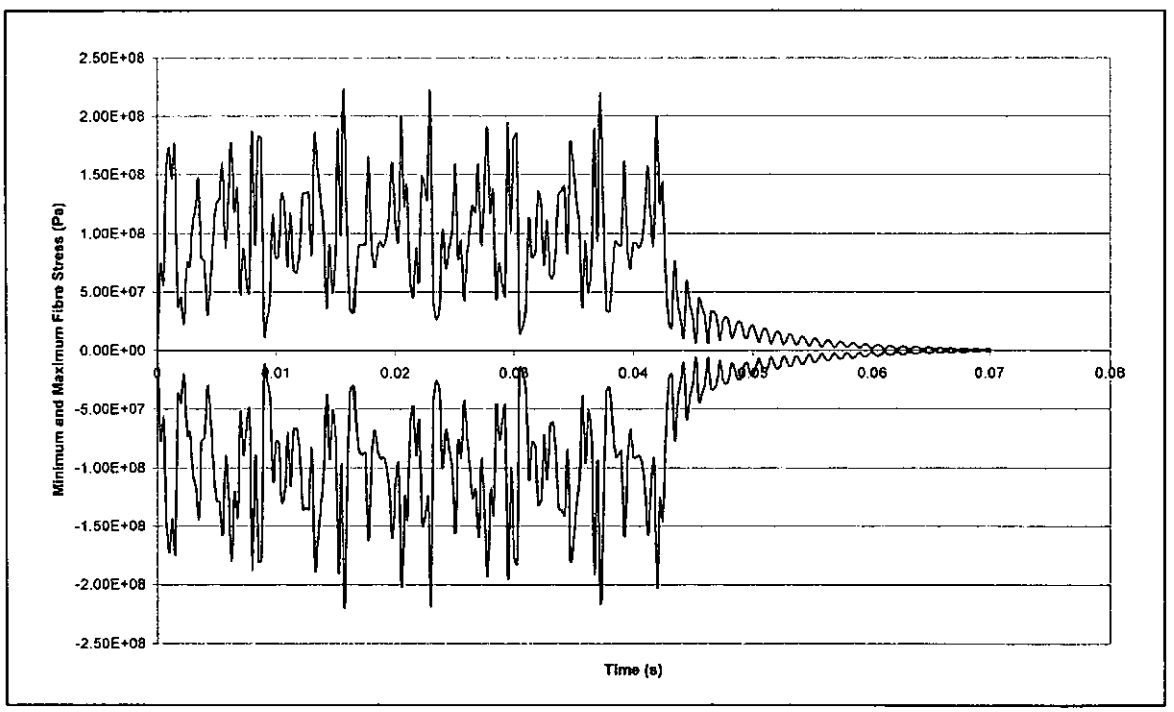

Figure 85. Output from FE Model – Maximum and Minimum Fibre Stress at Centre of Cutlass Bearing.

7. CONCLUSIONS AND RECOMMENDATIONS

7.1. Conclusions

This project has approached the problems associated with surface piercing propeller drive systems from several standpoints. The individual elements of the project are as follows.

- A test facility for surface piercing propellers now exists at DERA Haslar. This has involved the design and commissioning of a test rig capable of operating at low pressure, not only over a range of inclinations and immersions, but also at a range of yaw angles, a feature not previously available to experimentalists. Whereas most conventional propeller test facilities are equipped to measure only the mean values of torque and thrust, this rig is designed to measure trim and steering effects in addition, and is capable of recording force and moment time histories, rather than simply mean values. The circulating water channel, not previously used for propeller testing, was shown to be a suitable facility for surface piercing propellers, and it is consequently now being considered for the testing of waterjets. The rig ran reliably during the testing phase, and although experience showed that it had some limitations as a result of spray, vacuum limits and data-logging, it nonetheless produced a consistent set of useful data.
- Mean and time varying data have been gathered for four propellers, covering differences in number of blades, skew, immersion and yaw. This data clearly quantifies the key role played by immersion, from the point of view both of the magnitude of the mean load and the nature of the impact forces which become relatively significantly higher at low immersion. Immersion is a parameter which may not be entirely under the designer's control, but is something which may have a major impact on propeller performance. Examination of the effects of blade shape has shown the value of back-skewed blades in reducing the amplitude of fluctuating forces, a predictable result when one considers the similar effect on conventional propellers operating in an asymmetric

wake, but a result which is now supported by quantified evidence for surface piercing propellers.

- A semi-empirical loading model has been developed which provides a means of assessing the effect of changes in propeller geometry on the amplitudes of the fluctuating forces. This model takes an experimentally measured pressure transient at a point on a blade, and by integrating this across the surface of all blades, allowing for changes in direction of the lift force both across the blade surface and as the shaft rotates, it calculates the time histories of thrust, steering and trim forces. While there is modest agreement under certain conditions between this model and experimental results, it is not sufficiently sophisticated to accurately predict performance over the range of operation. However, the model does provide a valuable tool for the comparison of propeller profiles, since from the geometry files for the propellers in question, comparative time histories may be calculated, and thus the amplitudes and frequencies of vibrations may be assessed.
- A transient finite element technique has been used to model the propeller-shaft system. It has been found that the dynamic behaviour of the blades has little impact on the shaft stresses, and thus in practice a much simplified model of the propeller is sufficient. This FE model was developed using semi-empirical transient loads applied to each blade. However, it has led to a design methodology in which the experimentally measured set of transient forces and moments may be applied to a simplified FE model of the propeller, shaft and bearings. Thus the maximum peak stresses may be calculated and compared with the fatigue behaviour of the material. In a typical example, it has been shown that, although a mean stress calculation predicts a satisfactory shaft stress condition, the transient analysis predicts significant peak stresses which would lead to fatigue failure.

Taken together, these strands now help to provide a deeper insight into the complexities of the design of surface piercing propeller systems.

7.2. Recommendation for Further Work

With increasing interest in surface piercing drives as a propulsion option, both for conventional high speed vessels and those with air-lubricated hulls, there is a need for further data to permit designers to undertake a more certain design process. There is also a need for systematic development of the propeller, based on a fundamental understanding of the hydrodynamics, and of the installation, with respect particularly to the interaction between hull and propeller.

The direct progression from this work is to carry out further testing to establish data, both mean and transient, for a methodical series of propellers. In order to use the same test facility, renovation would be required to permit operation at the full design vacuum for the channel, so that cavitation numbers may be accurately modelled. A spray collection and dissipation system would also be required, which would permit operation at higher velocity. Finally, the data logging equipment needs to be refined, with particular attention paid to cable runs, screening and earthing, in order to eliminate signal drift and improve accuracy.

Working practice with surface piercing propellers has shown the importance of the cup on the face of the blade. This has the effect of increasing the propeller pitch, and its size is usually a matter of trial and error. A deeper understanding of the influence of the cup on hydrodynamics would undoubtedly be of benefit. This would come from both further testing and theoretical studies, making use of Computational Fluid Dynamics (CFD). The latter has not been attempted in any detail because of the difficulty caused by the two phase flow, and the establishment of the correct size and position of the ventilation bubble. Once

CFD techniques have been developed, they would replace the semi-empirical transient model in this work and would become a crucial design tool in determining efficient, low vibration blade shapes. In the meantime however, the type of model used here remains useful but needs refining, using more experimentally derived data on the spatial and temporal distribution of pressure across the blades.

Further work on the finite element model of the propeller blade would be of benefit in establishing both its static and dynamic behaviour, and could lead to a more efficient design with thinner sections in critical areas.

Finally, the experimental work has been carried out in a flow channel in which the velocity profile is nearly uniform. To achieve a higher level of accuracy, calculations based on these results would need to be modified to account for boundary layer formation on the hull. While there is considerable data on wake fraction for conventional craft, there is little for the type of craft that use surface piercing propellers, particularly taking into account the effect of trim tabs, angle of trim and the shape of the transom or tunnel. This would be a fruitful area for further research.

8. REFERENCES

Acompara, B. (1995), SM Racer: Design and Operation of on of the World's Fastest Monohulls. Marine Technology; v32, n3.

Alder, R.S. and Moore, D.H. (1977), Performance of an Inclined Shaft Partially Submerged Propeller Operating over a Range of Shaft Yaw Angles. NSRDC Report SPD 802-01

Allison, J.L. (1978), Propellers for High Performance Craft. Marine Technology. v15, n4, pp335-380.

Brandt, H. (1972), Modellversuche mit Schiffspropellern an der Wasseroberflache. Dissertration. TU Berlin.

Ferrando, M. and Scamardella, A. (1996), Surface Piercing Propellers: Testing Methodologies, Results Analysis and Comments on the Open Water Characteristics. Proc Small Craft Symposium, Ypsilanti, Michigan.

Furuya, O. (1985), A Performance Prediction Theory for Partially Submerged Ventilated Propellers. Jnl Fluid Mechanics; v151, pp311-335.

Hadler, J.B. and Hecker, R. (1968), Performance of Partially Submerged Propellers. Proc 7th ONR Symposium on Naval Hydrodynamics, Rome.

Harris, C.M. (Ed) (1996), Shock & Vibration Handbook. 4th edition. McGraw-Hill.

Hecker, R. (1973), Experimental Performance of a Partially Submerged Propeller in Inclined Flow. SNAME Spring Mtg; Lake Buena Vista, Florida.

Hylarides, S. (1978), Model Tests on Hydrodynamics of Propeller Blade Vibrations. Propellers '78 Symposium, SNAME, Virginia.

Kamen, P. (1998), Surface Piercing Propellers. www.well.com/user/pk/SPAprofboat.html (from Professional Boatbuilder Magazine).

Keller, M. (1995), Full-Scale Measurements on a Ventilated Propeller. Proc FAST 95, Lubeck-Travermunde, Germany, v2, pp991-1002.

Kruppa, C.F.L. (1972), Testing of Partially Submerged Propellers. Proc 13th ITTC Report of Cavitation Cttee, Berlin & Hamburg, Appendix V, v1.

Kruppa, C.F.L. (1992), Aspects of High Speed Propulsion. STG International Symposium on Propulsors & Cavitation, Hamburg, pp1-11.

Kruppa, C.F.L. (1992), Testing Surface Piercing Propellers. Marin Workshops on Advance Vessel Station Keeping, Propulsor-hull interaction & Nautical Simulators, Wageningen.

MER (1993), Propulsion of Fast Ferries. Marine Engineers Review, December 93; pp 29-33.

Milne-Thomson, L.M. (1960), Theoretical Hydrodynamics. 4th edition Macmillan.

Motor Boat and Yachting (1996), VSV 50.

Newman, J.N. (1992), Marine Hydrodynamics. MIT, p132 ff.

Olofsson, N. (1993), A Contribution on the Performance of Partially Submerged Propellers. Proc FAST '93, Yokohama, Japan, v1, pp 765-776.

Olofsson, N. (1996), Force and Flow Characteristics of a Partially Submerged Propeller. PhD Thesis; Chalmers Univ, Gotborg, Sweden.

Pike, D. (1997), Yacht has Powerboat Pedigree. Speed at Sea; v3, issue 2, May.

Radojcic, D.; Matic, D. (1997), Regression Analysis of Surface Piercing Propeller Series. Nav & HSMV Intl Conf, Naples.

Rose, J.C. and Kruppa, C.F.L. (1991), Methodical Series Model Test Results. Proc FAST '91, Trondheim, Norway, v2.

Rose, J.C., Kruppa, C.F.L. and Koushan, K. (1993), Surface Piercing Propellers - Propeller Hull Interaction. Proc FAST '93, Yokohama, Japan, v1.

Shaozong, L. and Hengshun, Z. (1988), An Experimental Study on the Performance of Partially Submerged Propeller. Int'l High Performance Vehicle Conference, Shanhai, China, CSNAME.

Speed at Sea (1997), News Section, v3, issue 2, May.

The Naval Architect (1996), Naval News Section, Feb.

Van Tassel, G.W. (1989), A Ventilated Tunnel/Surface Piercing Propeller Propulsion System. AIAA Intersoc Adv Marine Vehicles Conf, Arlington.

Van Tassel, G.W. (1992), Application of the Air Drive Ventilated Tunnel/Surface Piercing Propeller Propulsion System. Proc HPMV 92, Arlington.

Vorus, W.S. (1991), Forces on Surface Piercing Propellers with Inclination. Jnl Ship Research; v35, n3, pp 210-218.

Wang, D.P. (1977), Water Entry and Exit of a Fully Ventilated Foil. Jnl Ship Research; v21, pp44-68.

Wang, D.P. (1979), Oblique Water Entry and Exit of a Fully Ventilated Foil. Jnl Ship Research; v23, pp43-54.

Wang, G.Q., Jia, D.S. and Sheng, Z.B. (1992), Study on Propeller Characteristics Near Water Surface. Proc 2nd Symp on Propeller & Cavitation, Hangzhon, China, pp161-168.

9. NOMENCLATURE

A_e/A_0	propeller expanded area ratio
c	chord length
C_L	foil lift coefficient
D	diameter
E	Elastic modulus
F	force
{F}	force vector
Fr	Froude number $= \frac{V}{\sqrt{gD}}$
g	gravitational constant
h	thickness of water layer (from Wang's theory, Section 2.2)
IR or imm	immersion ratio $= \frac{\text{max immersed depth of propeller tip}}{\text{propeller diameter}}$ (see diagram)
J	advance coefficient $= \frac{V}{nD}$
K_q	torque coefficient $= \frac{Q}{\rho n^2 D^5}$
K_t	thrust coefficient $= \frac{T}{\rho n^2 D^4}$
m	mass
[M]	mass matrix
n	rotational speed, revs/sec
$\underline{n}$	normal vector
P	pitch
P/D	mean pitch:diameter ratio
p	pressure
p_{static}	static pressure
p_{vapour}	vapour pressure
Q	torque
r	radius (generally)
R	propeller tip radius
[S]	stiffness matrix
S	surface (integration over)

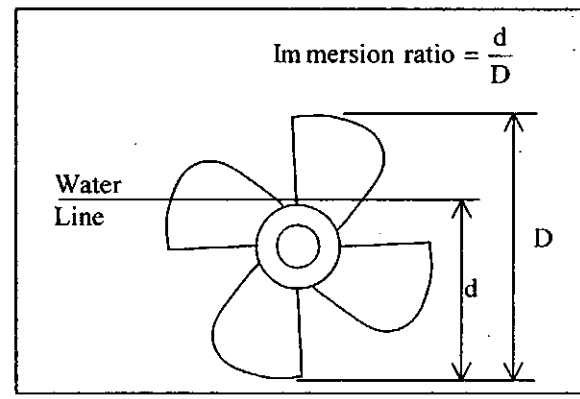

T	thrust (relative to shaft)
T_c	thrust (relative to craft)
t	time
{u}	displacement vector
U	body velocity
V	advance velocity
z_0	shaft overhang (propeller centre to aft bearing centre)
α	foil angle of attack
Δ	increment
λ	advance coefficient (from Wang's theory, Section 2.2)
ρ	density
σ	cavitation number $= \frac{p_{static} - p_{vapour}}{\frac{1}{2}\rho V^2}$
σ	direct stress (in section 6.3.1)
τ	shear stress
ϕ	potential function
ω	radiancy

Subscripts

c	relative to craft
h or y	yaw force directed along horizontal (side) axis (starboard +ve) or trim moment about that axis (bow up +ve)
v or x	trim force directed along axis perpendicular to shaft (upward +ve) or yaw moment about that axis (yaw to port +ve)
x1	upwards (relative to shaft) direction at aft bearing
y1	horizontal direction at aft bearing
x2	upwards (relative to shaft) direction at forward bearing
y2	horizontal direction at forward bearing
z	directed along shaft axis (+ve forward)

Appendix A. Mean Propeller Performance Data

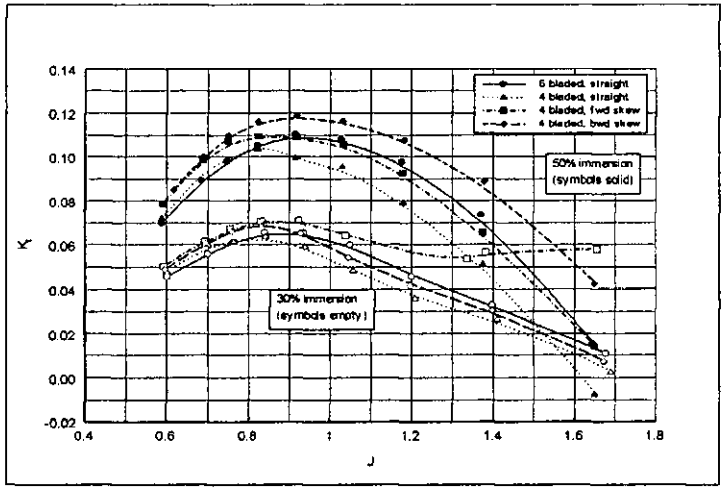

Figure A1. Comparison of Propellers and Immersions: Thrust Coefficient vs Advance Coefficient.

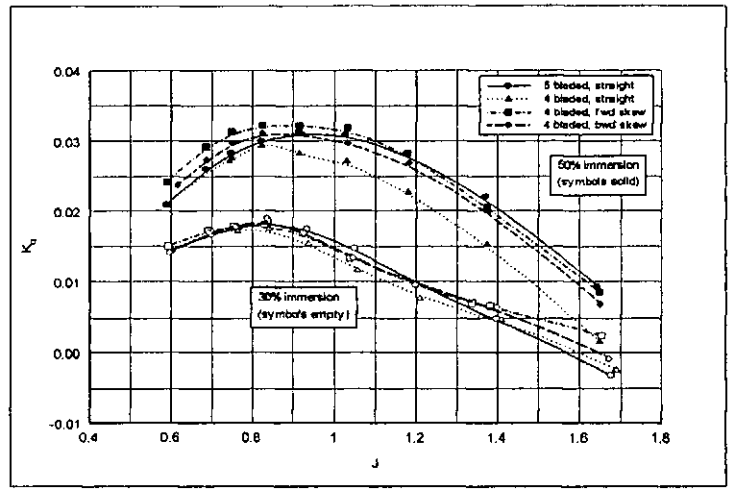

Figure A2. Comparison of Propellers and Immersions: Torque Coefficient vs Advance Coefficient.

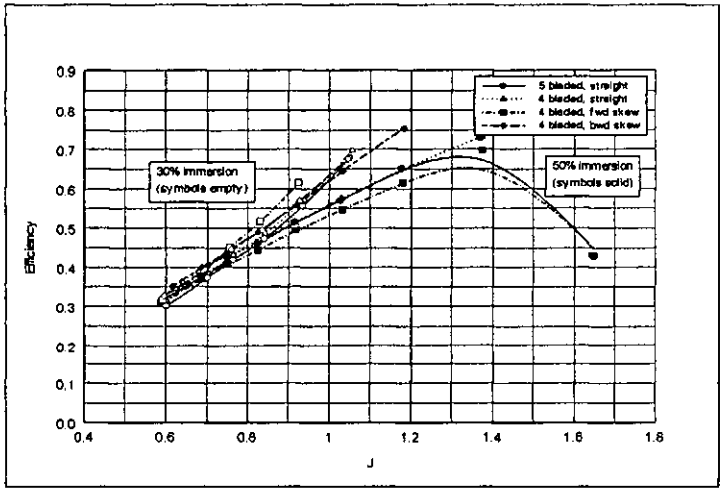

Figure A3. Comparison of Propellers and Immersions: Efficiency vs Advance Coefficient.

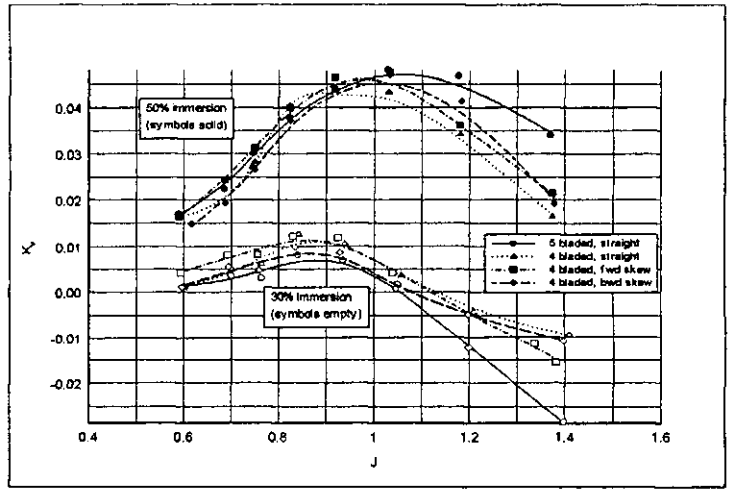

Figure A4. Comparison of Propellers and Immersions: Vertical Force Coefficient vs Advance Coefficient.

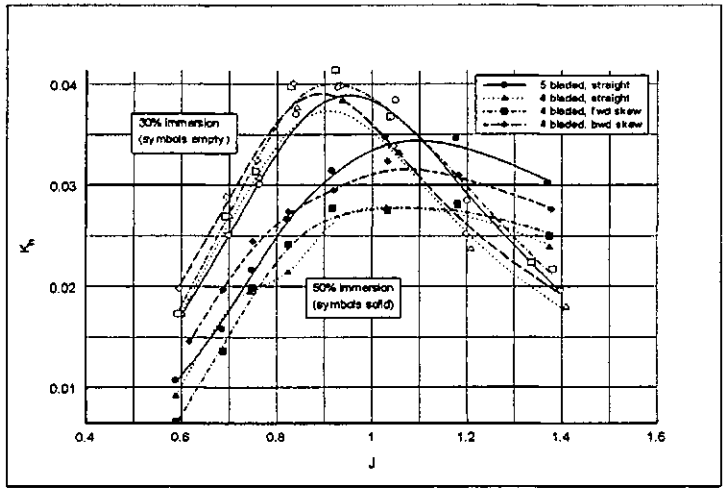

Figure A5. Comparison of Propellers and Immersions: Horizontal Force Coefficient vs Advance Coefficient.

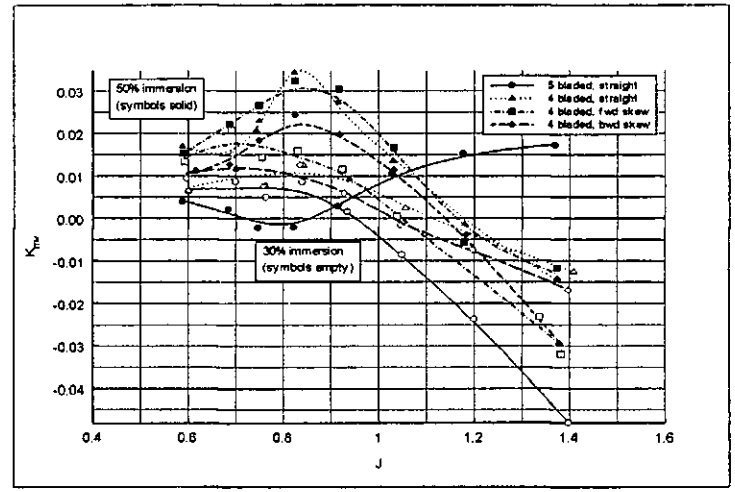

Figure A6. Comparison of Propellers and Immersions: Yaw Moment Coefficient vs Advance Coefficient.

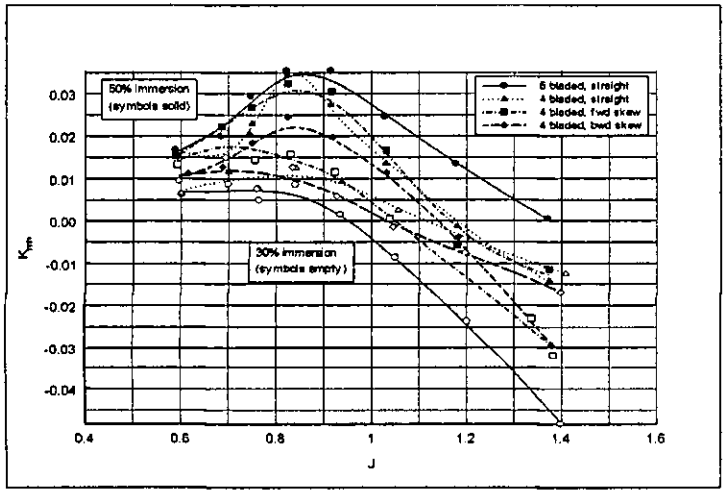

Figure A7. Comparison of Propellers and Immersions: Trim Moment Coefficient vs Advance Coefficient.

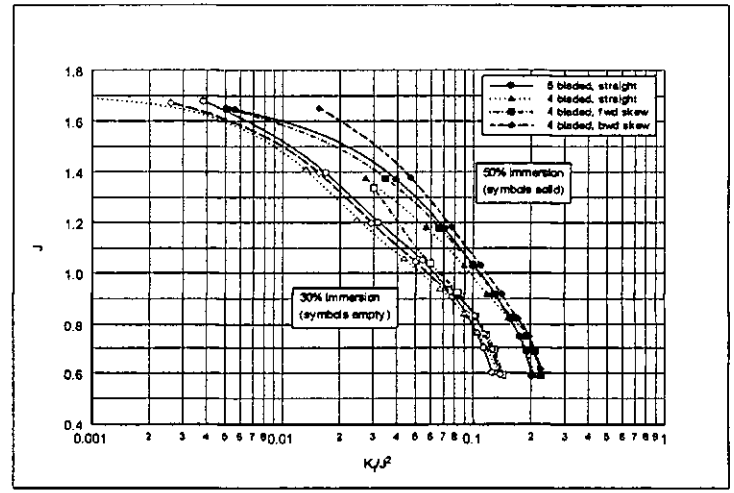

Figure A8. Comparison of Propellers and Immersions: Advance Coefficient vs K_t/J^2.

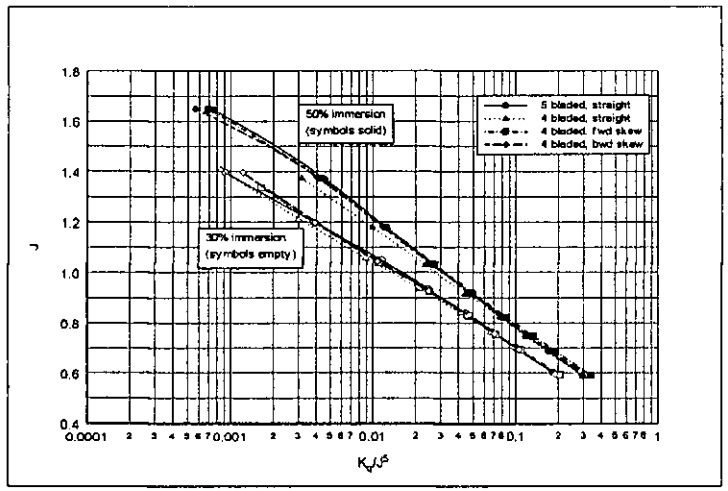

Figure A9. Comparison of Propellers and Immersions: Advance Coefficient vs K_q/J^5.

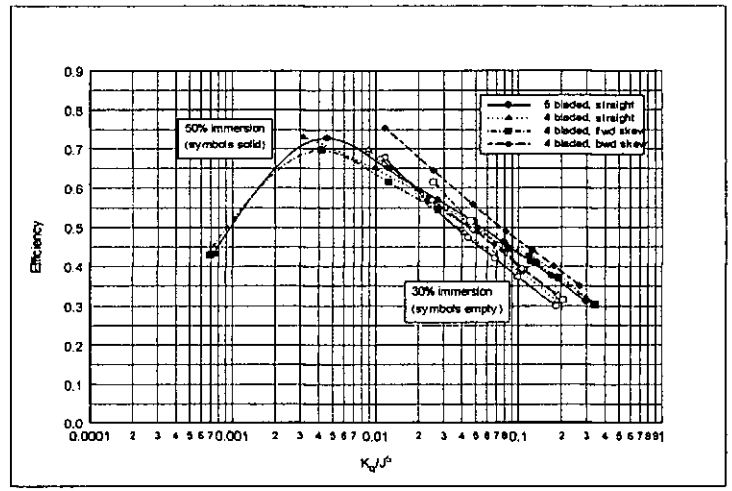

Figure A10. Comparison of Propellers and Immersions: Efficiency vs K_q/J^5.

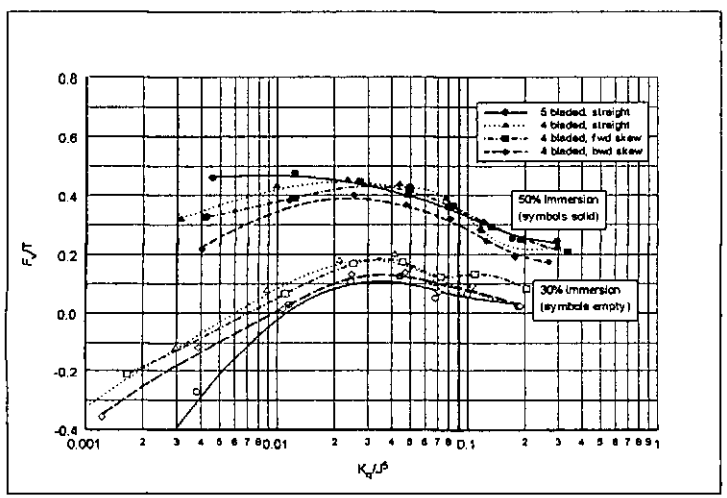

Figure A11. Comparison of Propellers and Immersions: Vertical Force vs K_q/J^5.

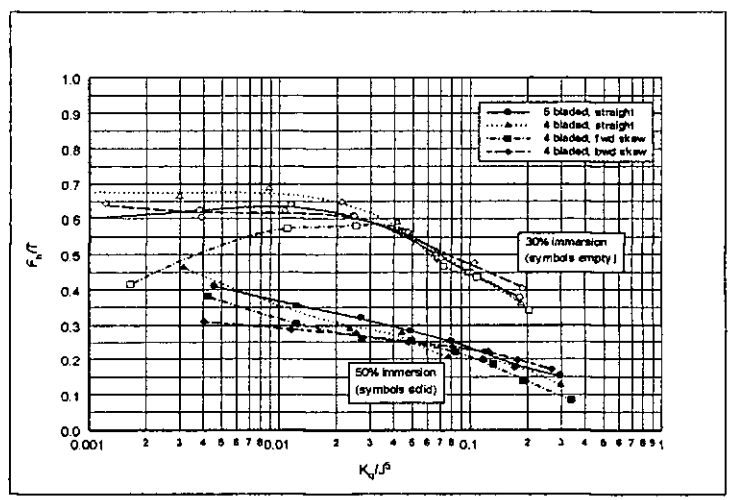

Figure A12. Comparison of Propellers and Immersions: Horizontal Force vs K_q/J^5.

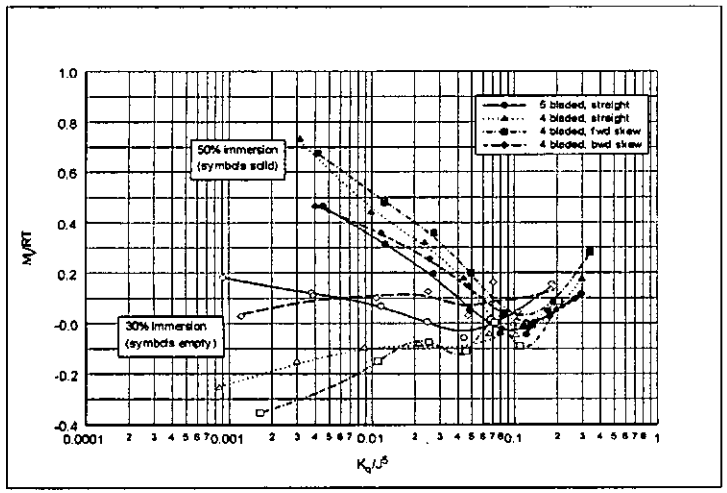

Figure A13. Comparison of Propellers and Immersions: Yaw Moment vs K_Q/J^5.

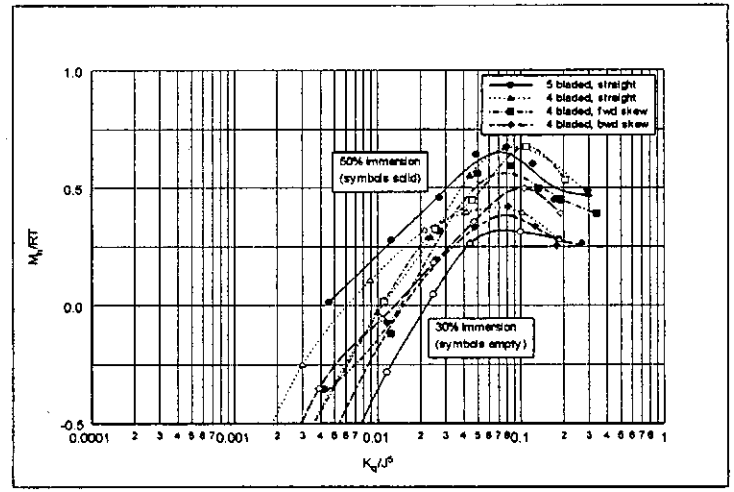

Figure A14. Comparison of Propellers and Immersions: Trim Moment vs K_Q/J^5.

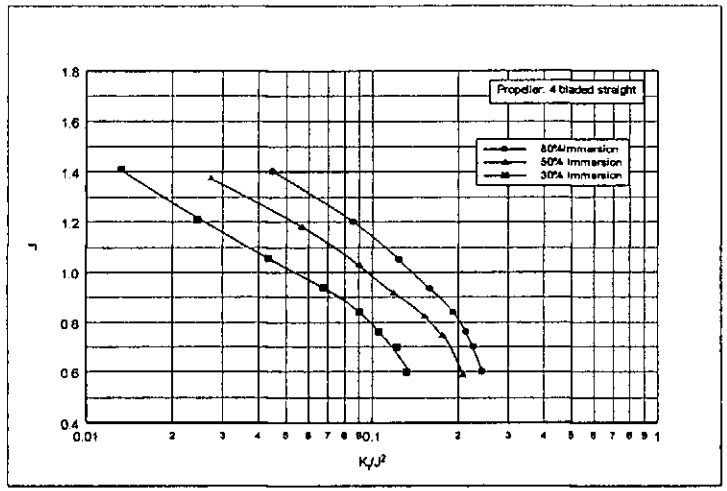

Figure A15. Effect of Immersion: Advance Coefficient vs Thrust Coefficient

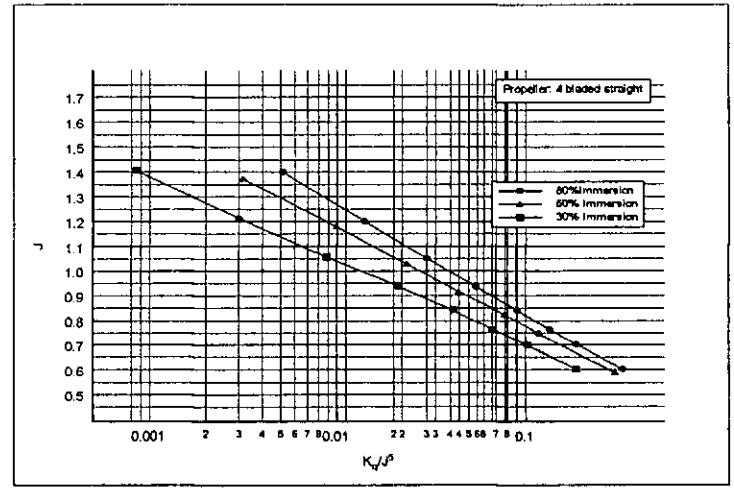

Figure A16. Effect of Immersion: Advance Coefficient vs Torque Coefficient

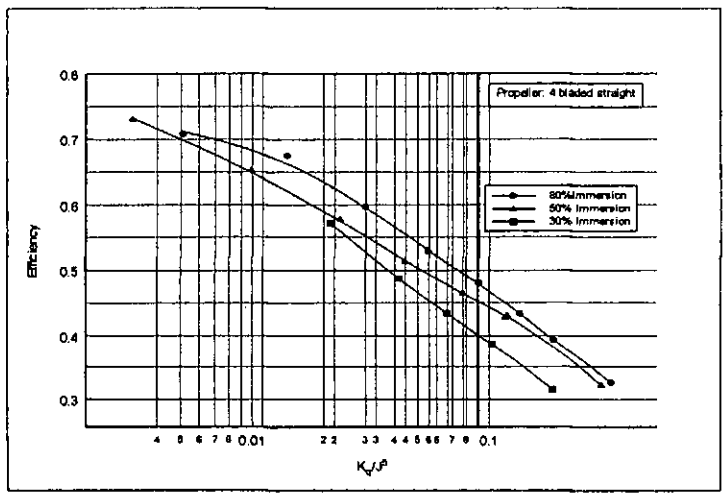

Figure A17. Effect of Immersion: Efficiency Coefficient vs Torque Coefficient

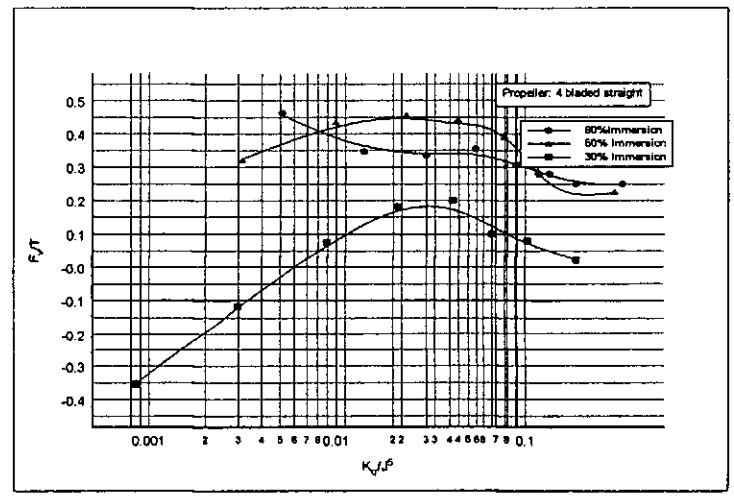

Figure A18. Effect of Immersion: Vertical Force Coefficient vs Torque Coefficient

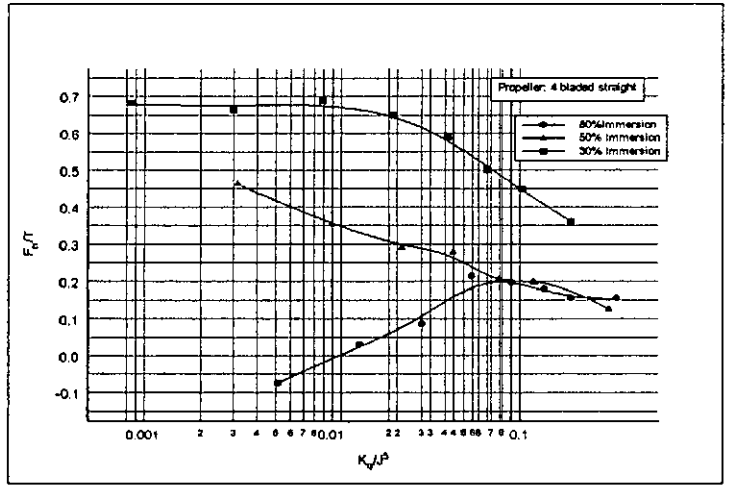

Figure A19. Effect of Immersion: Horizontal Force Coefficient vs Torque Coefficient

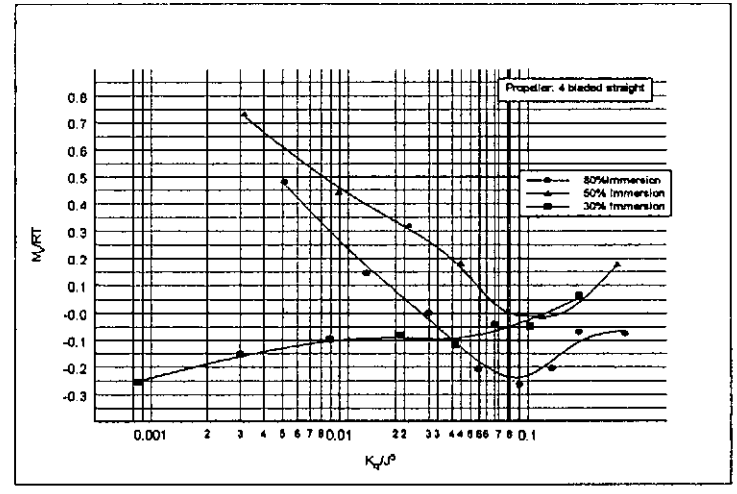

Figure A20. Effect of Immersion: Steering Moment Coefficient vs Torque Coefficient

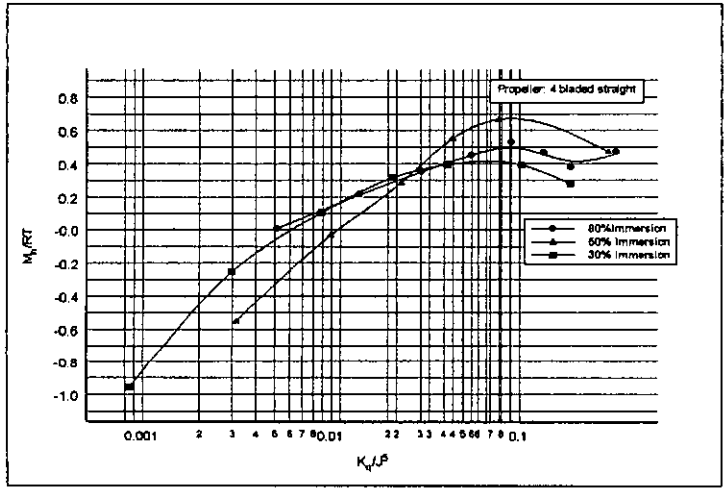

Figure A21. Effect of Immersion: Trim Moment Coefficient vs Torque Coefficient

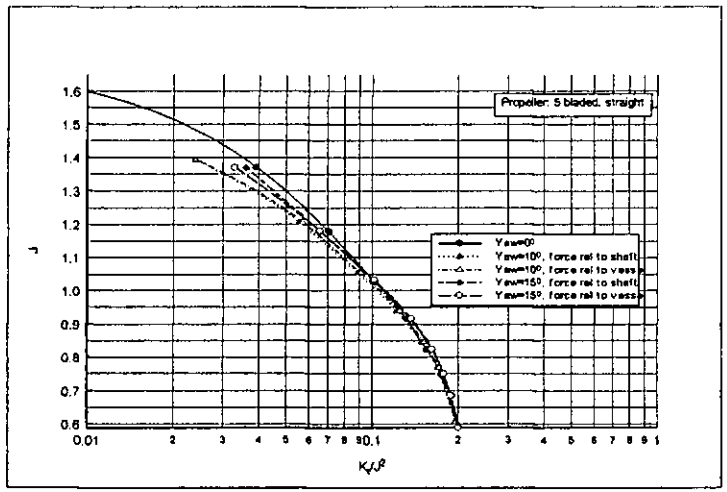

Figure A22. Effect of Yaw: Advance Coefficient vs K_t/J^2.

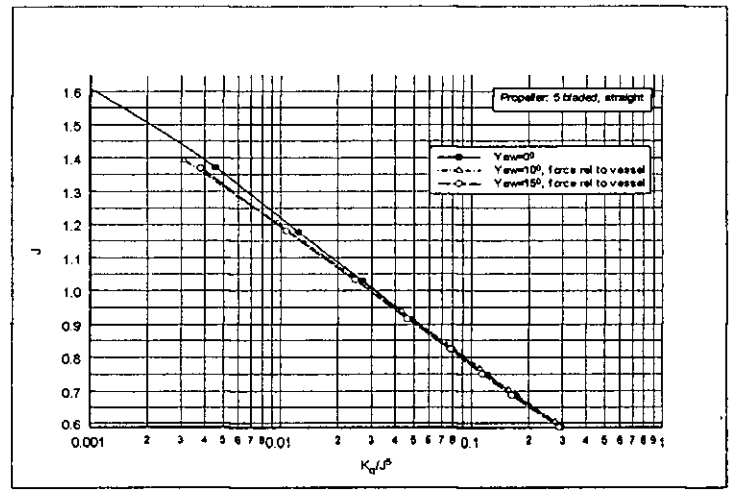

Figure A23. Effect of Yaw: Advance Coefficient vs K_q/J^5.

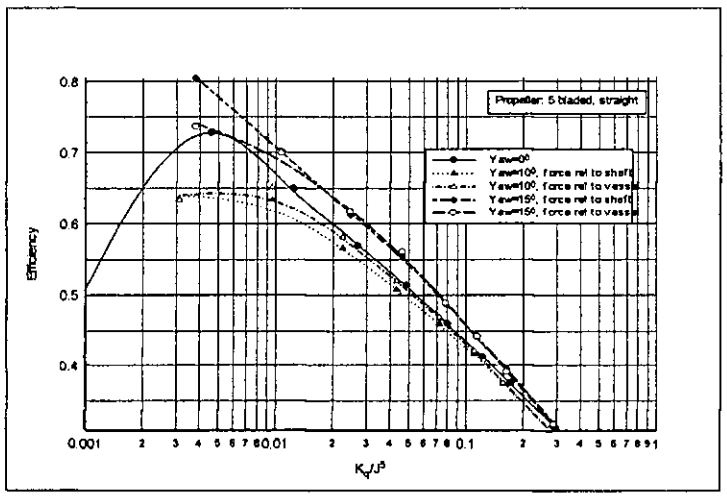

Figure A24. Effect of Yaw: Efficiency vs K_q/J^5.

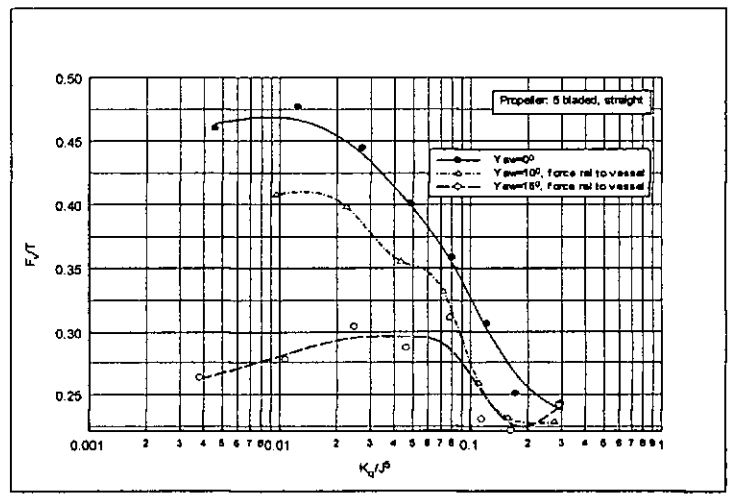

Figure A25. Effect of Yaw: Vertical Force vs K_q/J^5.

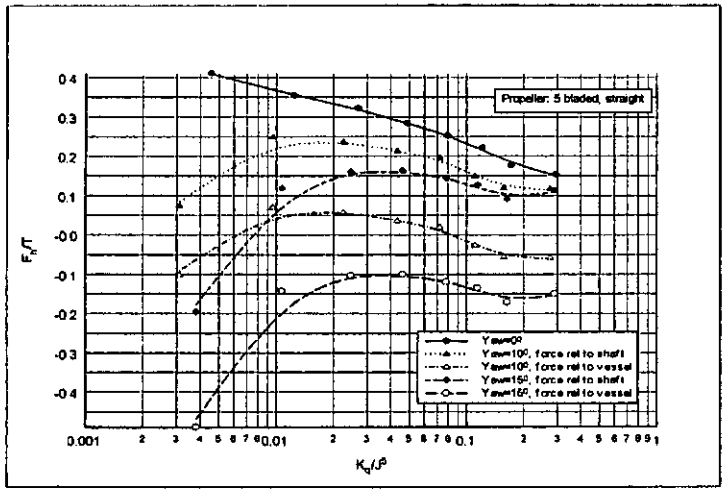

Figure A26. Effect of Yaw: Horizontal Force vs K_q/J^5.

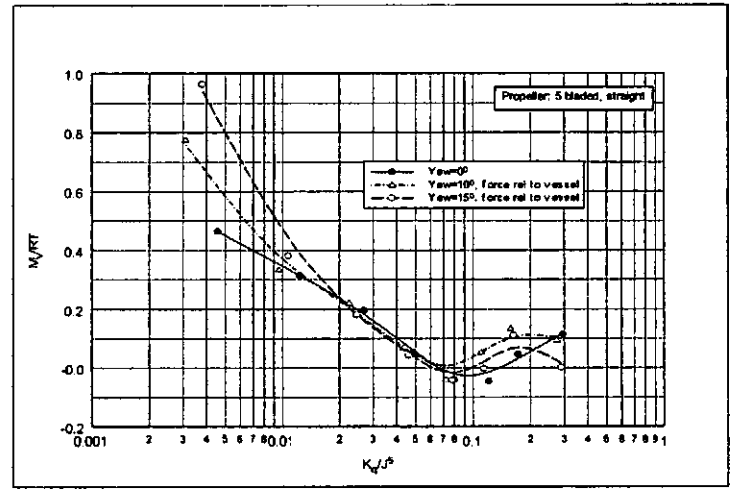

Figure A27. Effect of Yaw: Yaw Moment vs K_q/J^5.

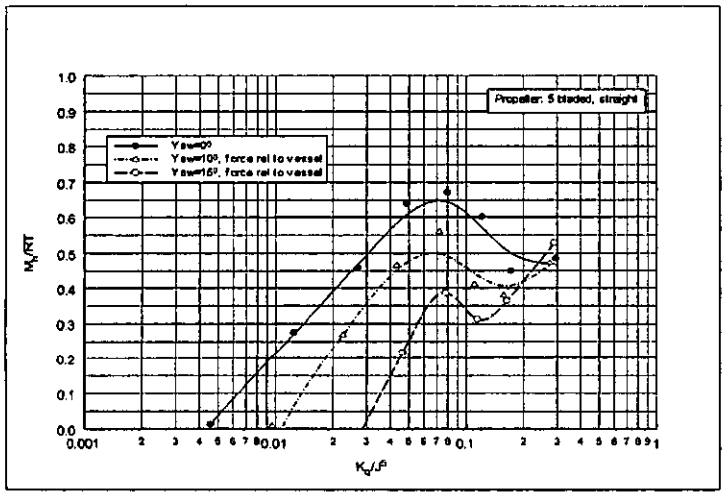

Figure A28. Effect of Yaw: Trim Moment vs K_q/J^5.

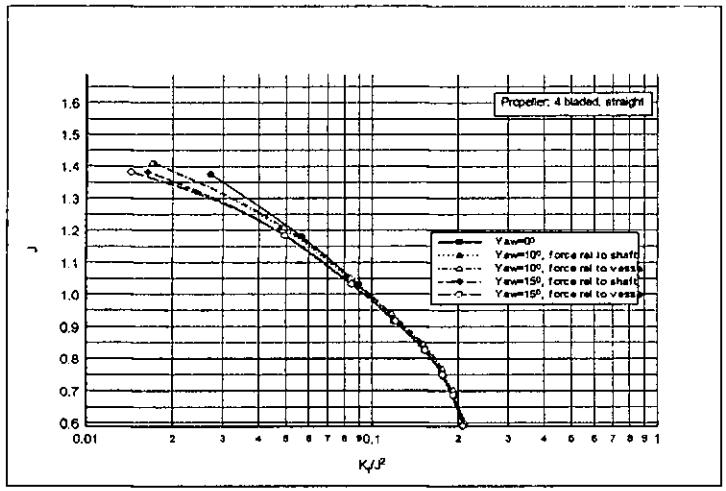

Figure A29. Effect of Yaw: Advance Coefficient vs K_t/J^2.

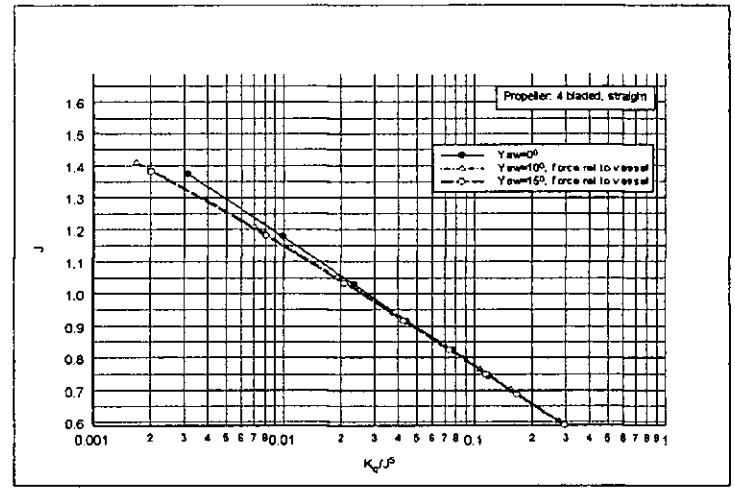

Figure A30. Effect of Yaw: Advance Coefficient vs K_q/J^5.

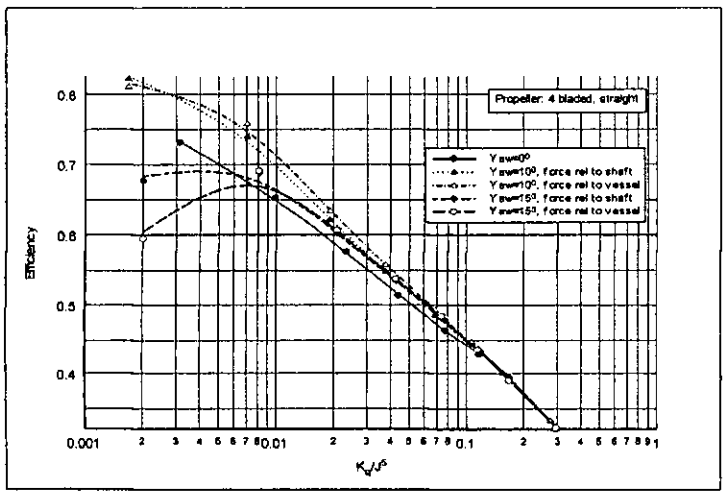

Figure A31. Effect of Yaw: Efficiency vs K_q/J^5.

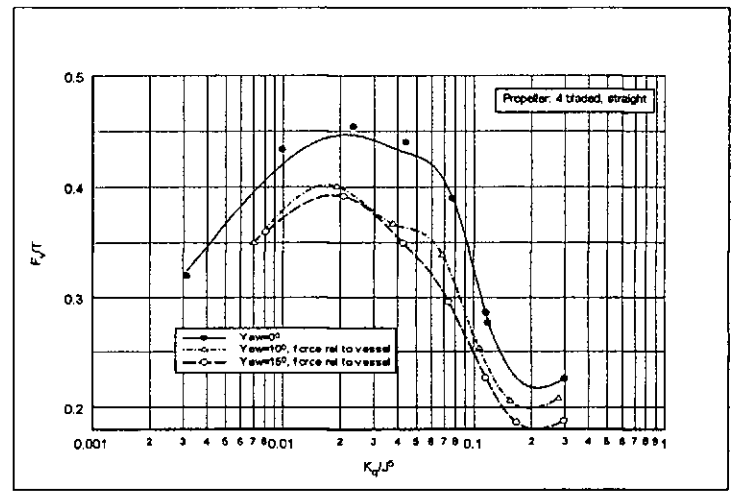

Figure A32. Effect of Yaw: Vertical Force vs K_q/J^5.

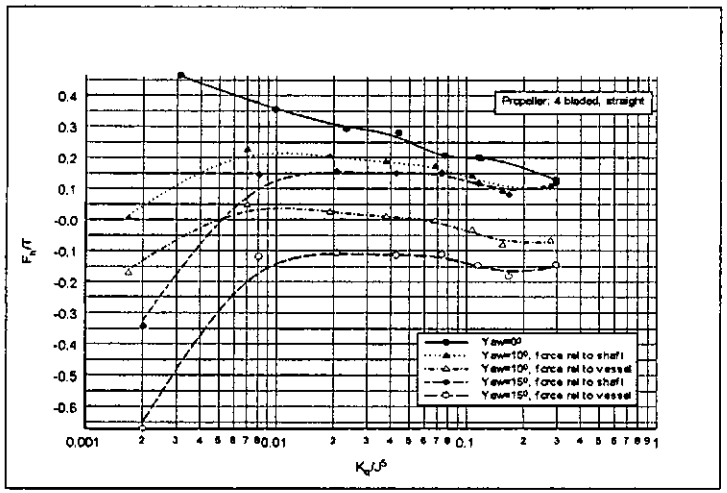

Figure A33. Effect of Yaw: Horizontal Force vs K_q/J^5.

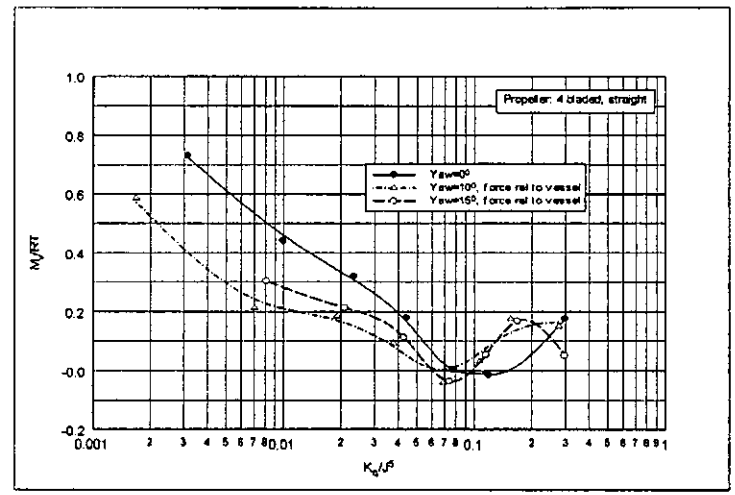

Figure A34. Effect of Yaw: Yaw Moment vs K_q/J^5.

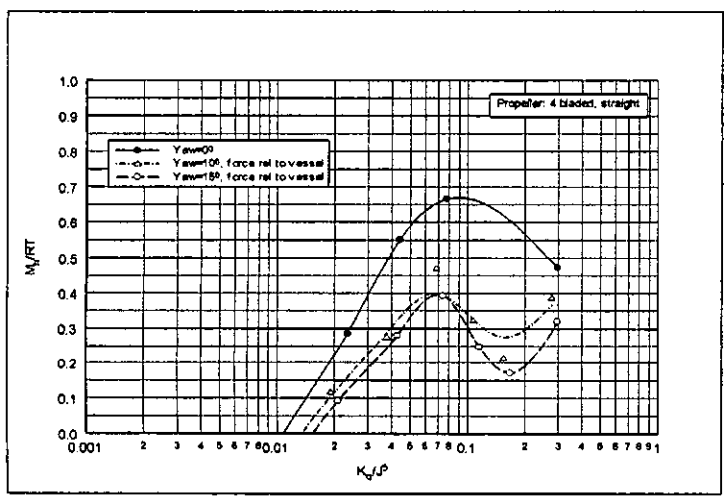

Figure A35. Effect of Yaw: Trim Moment vs K_q/J^5.

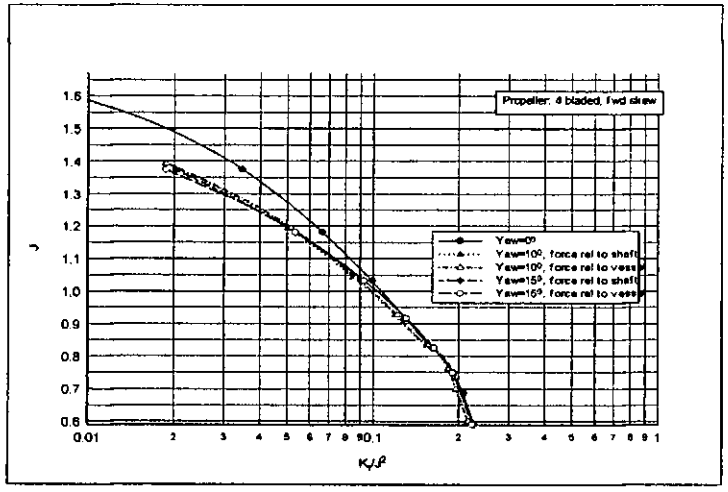

Figure A36. Effect of Yaw: Advance Coefficient vs K_t/J^2.

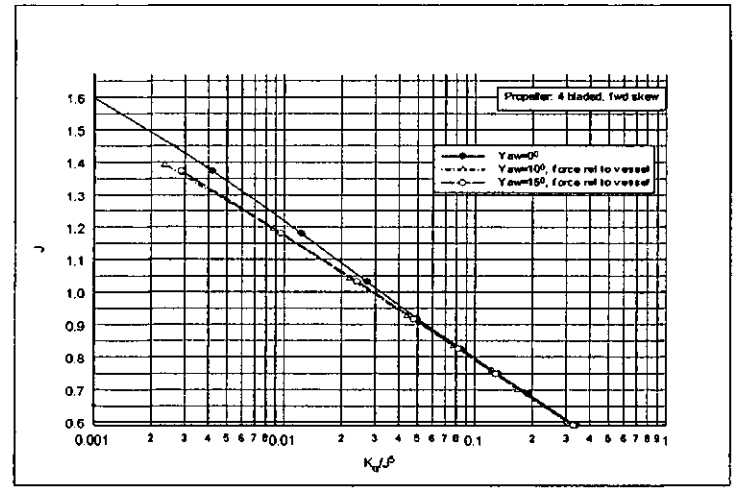

Figure A37. Effect of Yaw: Advance Coefficient vs K_q/J^5.

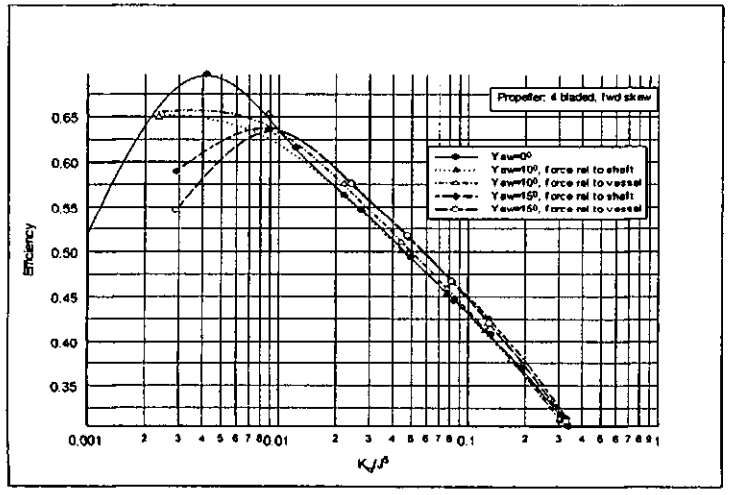

Figure A38. Effect of Yaw: Efficiency vs K_q/J^5.

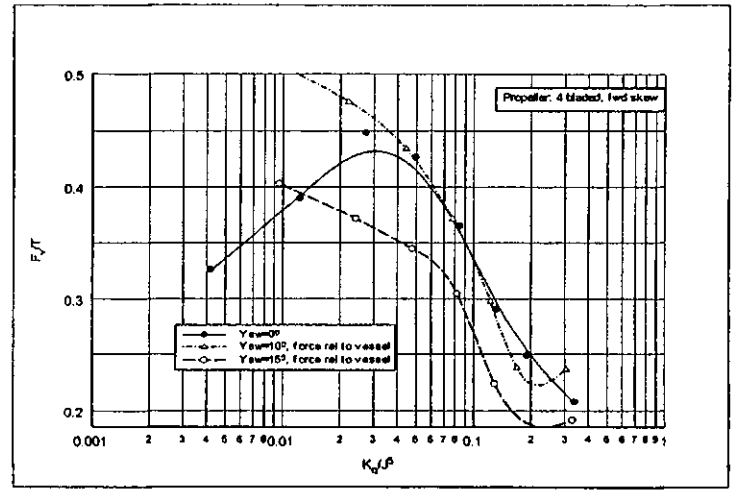

Figure A39. Effect of Yaw: Vertical Force vs K_q/J^5.

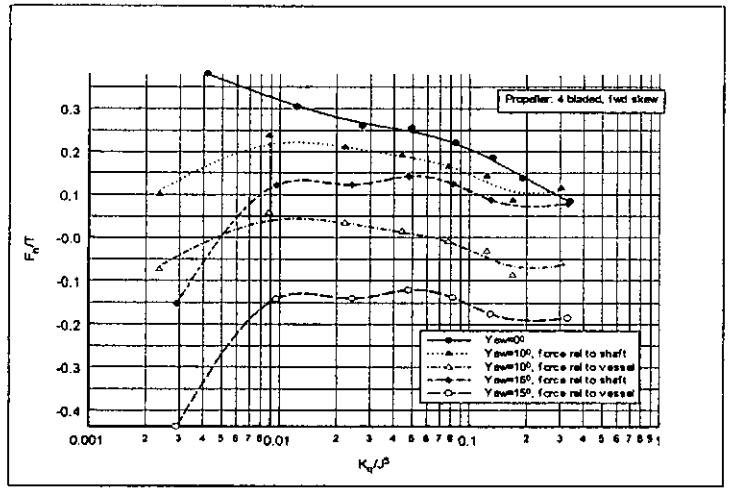

Figure A40. Effect of Yaw: Horizontal Force vs K_q/J^5.

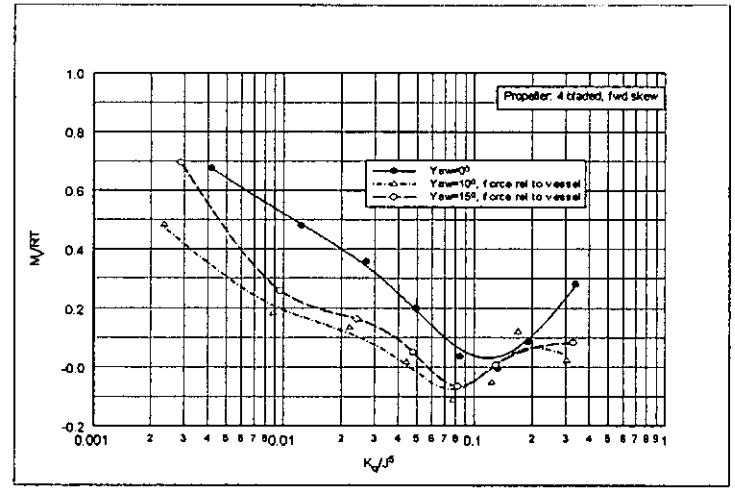

Figure A41. Effect of Yaw: Yaw Moment vs K_q/J^5.

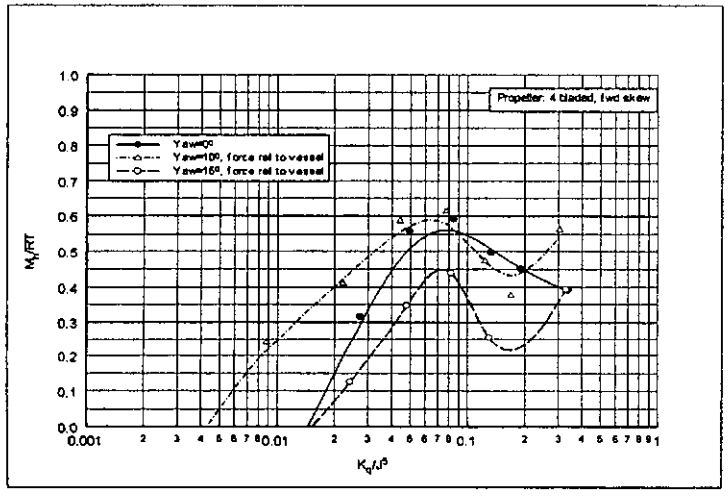

Figure A42. Effect of Yaw: Trim Moment vs K_q/J^5.

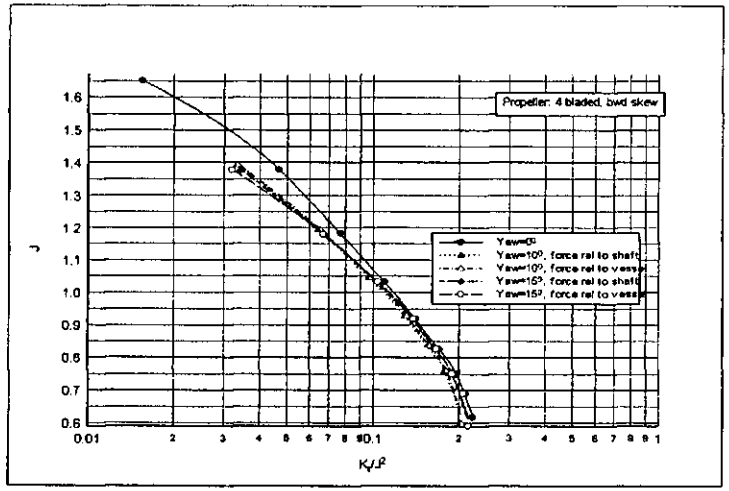

Figure A43. Effect of Yaw: Advance Coefficient vs K_t/J^2.

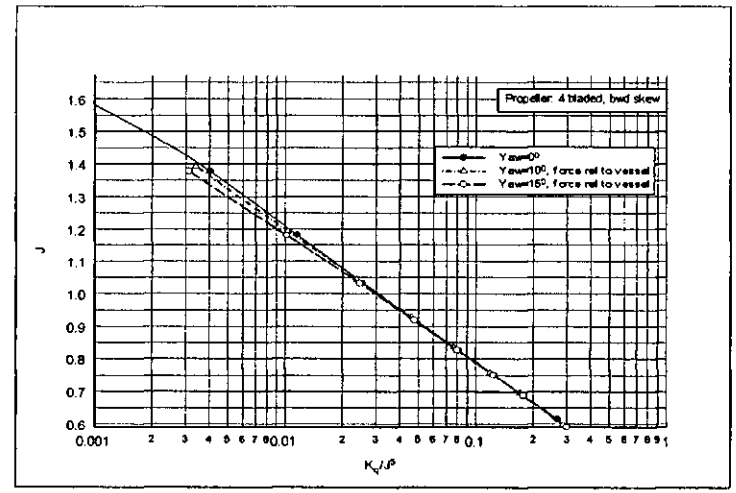

Figure A44. Effect of Yaw: Advance Coefficient vs K_q/J^5.

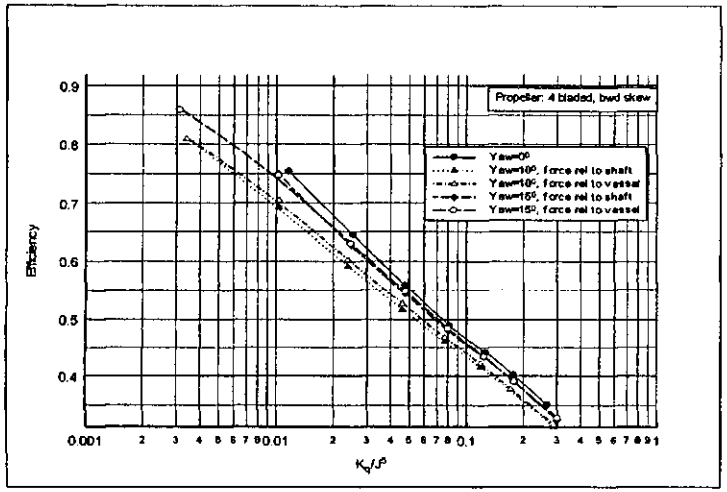

Figure A45. Effect of Yaw: Efficiency vs K_q/J^5.

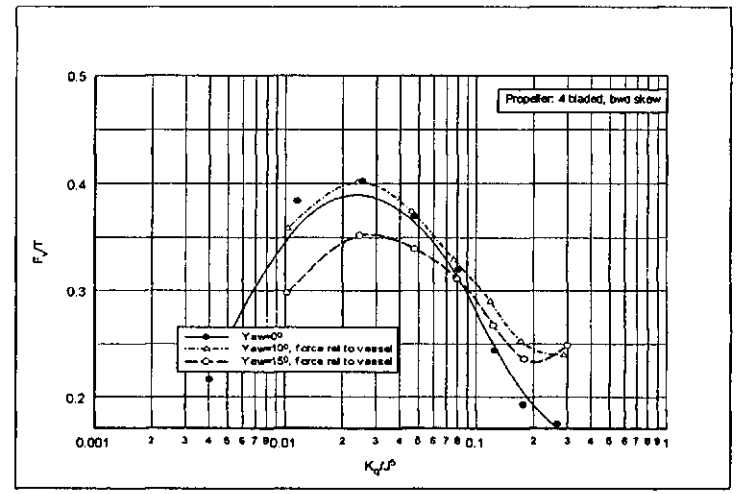

Figure A46. Effect of Yaw: Vertical Force vs K_q/J^5.

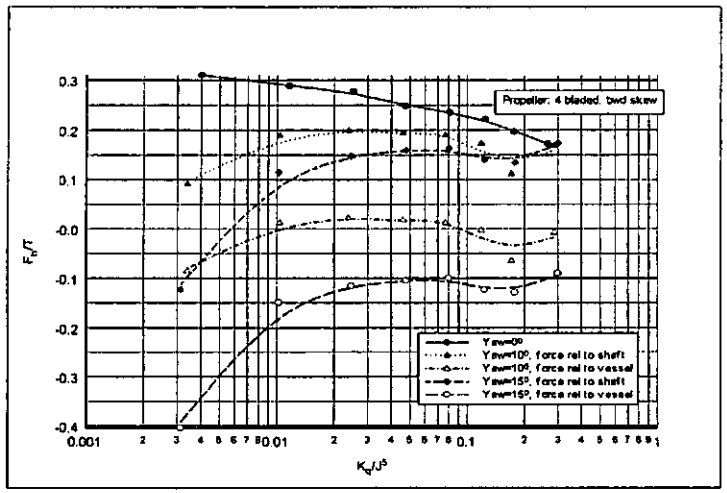

Figure A47. Effect of Yaw: Horizontal Force vs K_q/J^5.

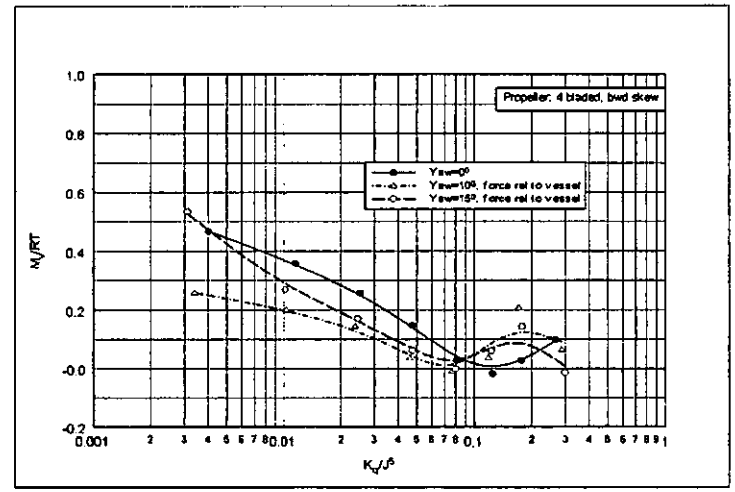

Figure A48. Effect of Yaw: Yaw Moment vs K_q/J^5.

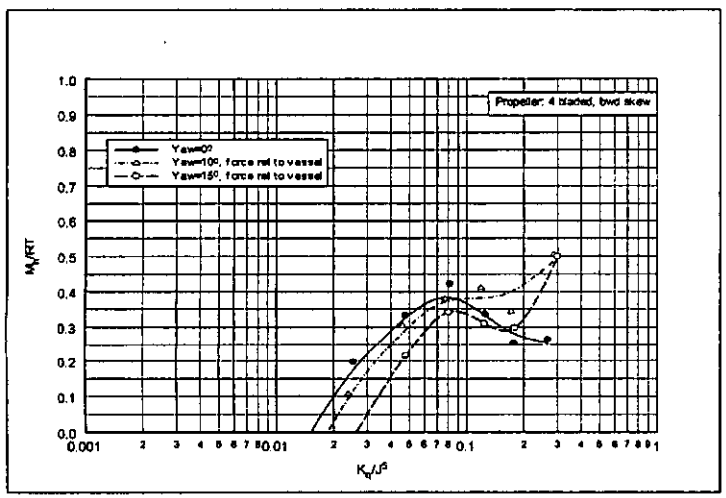

Figure A49. Effect of Yaw: Trim Moment vs K_q/J^5.

Appendix B. Transient Propeller Performance Data

figures

Time Histories – Trim and Yaw Force

Each propeller;	imm 50%; yaw 0^0;	B1 to B12
4 bladed straight TE;	imm 30%; yaw 0^0;	B13 to B15
4 bladed straight TE;	imm 80%; yaw 0^0;	B16 to B18
4 bladed straight TE;	imm 50%; yaw 15^0;	B19 to B21

Frequency Spectra – Trim and Yaw Force

Each propeller;	imm 50%; yaw 0^0;	B22 to B33
4 bladed straight TE;	imm 30%; yaw 0^0;	B34 to B36
4 bladed straight TE;	imm 80%; yaw 0^0;	B37 to B39
4 bladed straight TE;	imm 50%; yaw 15^0;	B40 to B42

Time Histories – Thrust and Torque

Each propeller;	imm 50%; yaw 0^0;	B43 to B54
4 bladed straight TE;	imm 30%; yaw 0^0;	B55 to B57
4 bladed straight TE;	imm 80%; yaw 0^0;	B58 to B60
4 bladed straight TE;	imm 50%; yaw 15^0;	B61 to B63

Frequency Spectra – Thrust and Torque

Each propeller;	imm 50%; yaw 0^0;	B64 to B75
4 bladed straight TE;	imm 30%; yaw 0^0;	B76 to B78
4 bladed straight TE;	imm 80%; yaw 0^0;	B79 to B81
4 bladed straight TE;	imm 50%; yaw 15^0;	B82 to B84

Time Histories – Trim and Yaw Moments

Each propeller;	imm 50%; yaw 0^0;	B85 to B96
4 bladed straight TE;	imm 30%; yaw 0^0;	B97 to B99
4 bladed straight TE;	imm 80%; yaw 0^0;	B100 to B102
4 bladed straight TE;	imm 50%; yaw 15^0;	B103 to B105

Frequency Spectra – Trim and Yaw Moments

Each propeller;	imm 50%; yaw 0^0;	B106 to B117
4 bladed straight TE;	imm 30%; yaw 0^0;	B118 to B120
4 bladed straight TE;	imm 80%; yaw 0^0;	B121 to B123
4 bladed straight TE;	imm 50%; yaw 15^0;	B124 to B126

RMS Values of Fluctuations vs Advance Coefficient

Each propeller;	thrust, & torque	imm 50%;	yaw 0^0;	B127 to B128
4 bladed straight TE;	thrust, & torque	each imm;	yaw 0^0;	B129 to B130
Each propeller;	trim & yaw force	imm 50%;	yaw 0^0;	B131 to B132
4 bladed straight TE;	trim & yaw force	each imm;	yaw 0^0;	B133 to B134
Each propeller;	trim & yaw moment	imm 50%;	yaw 0^0;	B135 to B136
4 bladed straight TE;	trim & yaw moment	each imm;	yaw 0^0;	B137 to B138
4 bladed straight TE;	thrust, & torque	imm 50%;	yaw 15^0;	B139 to B140
4 bladed straight TE;	trim & yaw force	imm 50%;	yaw 15^0;	B141 to B142
4 bladed straight TE;	trim & yaw moment	imm 50%;	yaw 15^0;	B143 to B144

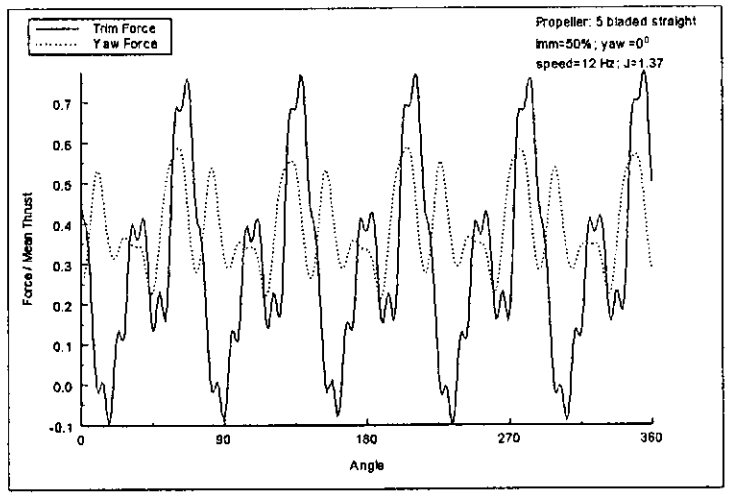

Figure B1

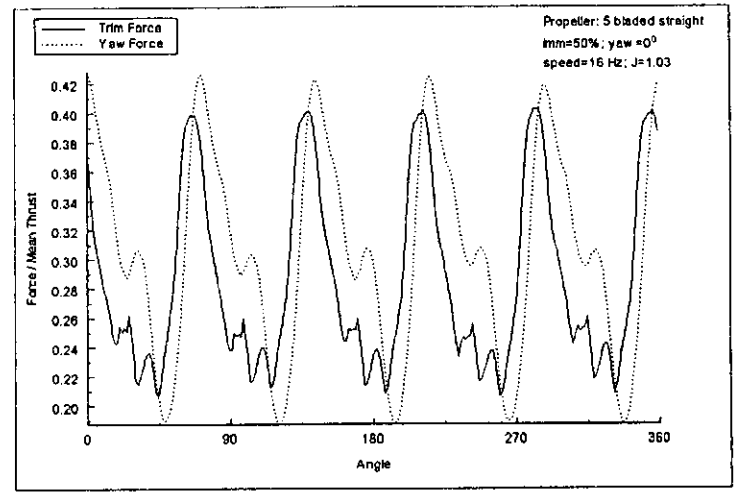

Figure B2

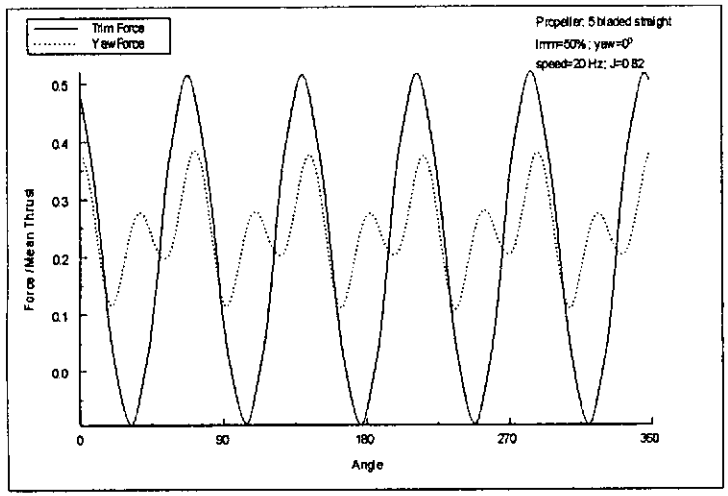

Figure B3

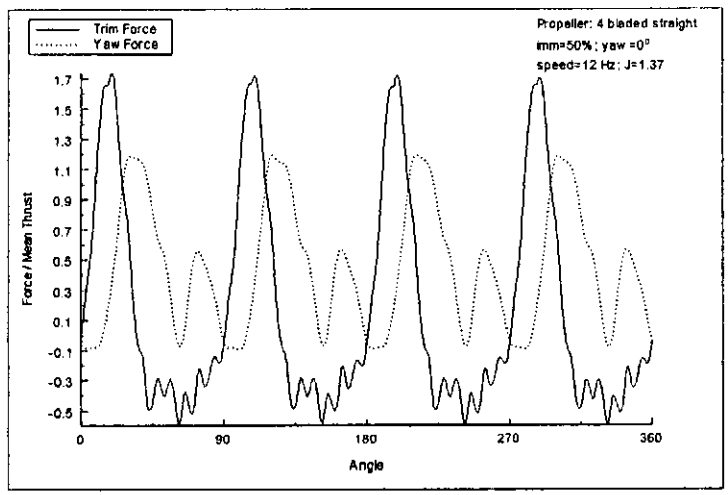

Figure B4

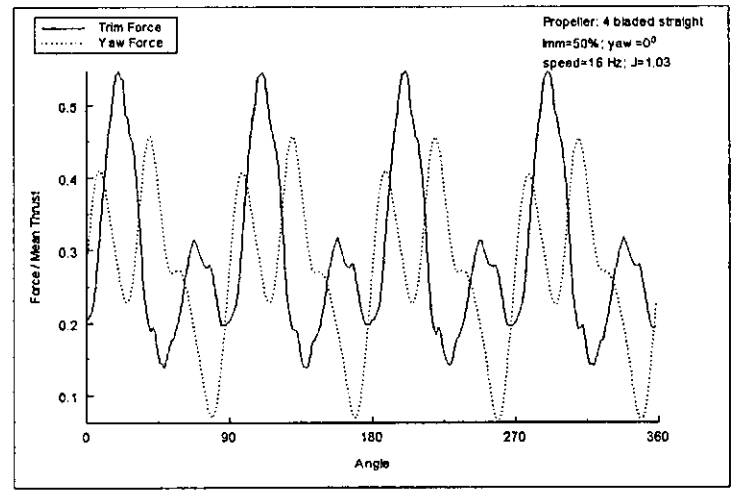

Figure B5

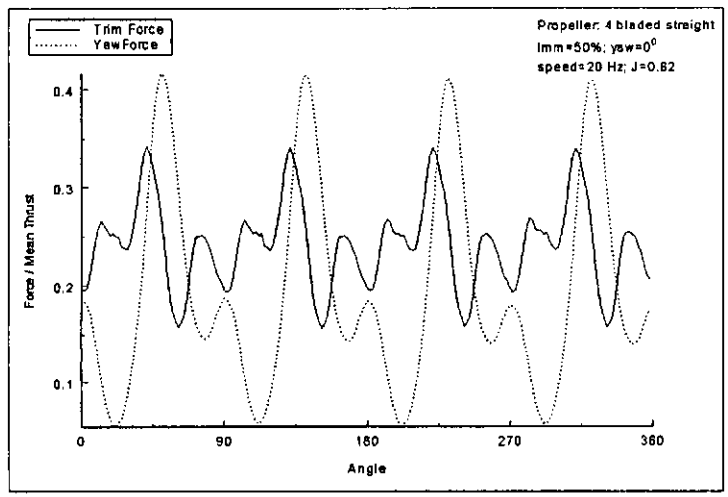

Figure B6

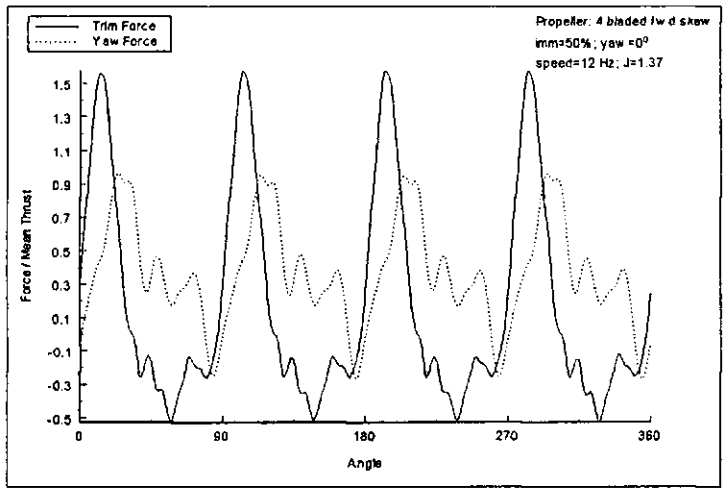

Figure B7

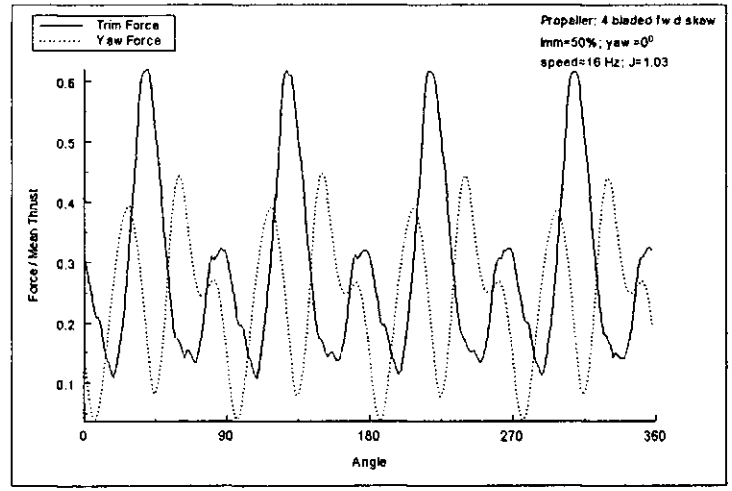

Figure B8

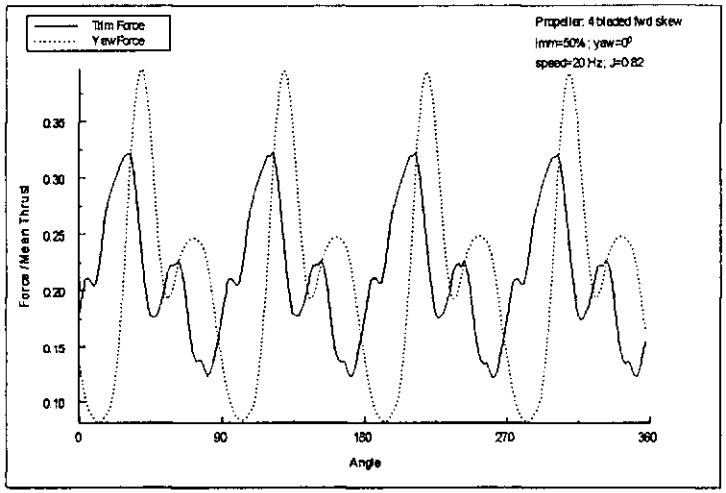

Figure B9

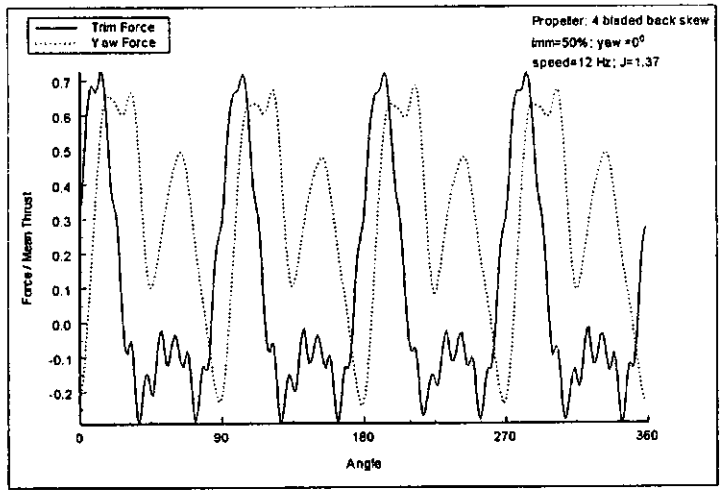

Figure B10

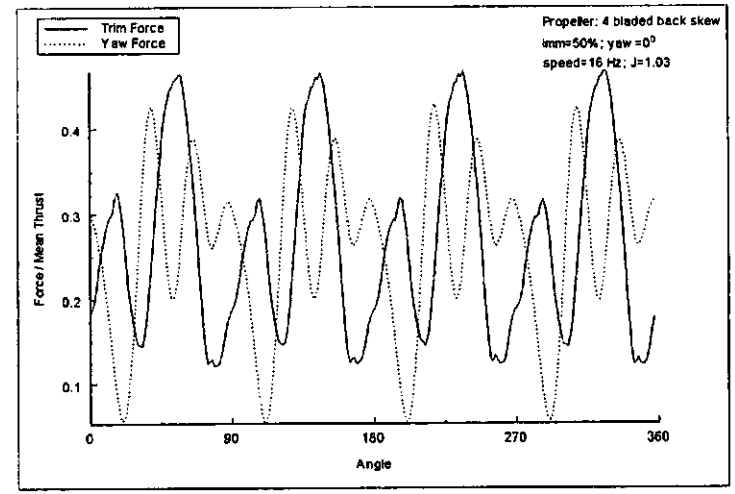

Figure B11

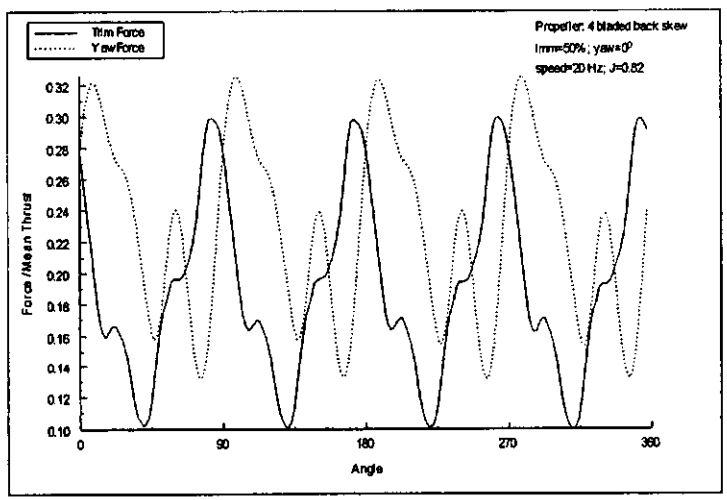

Figure B12

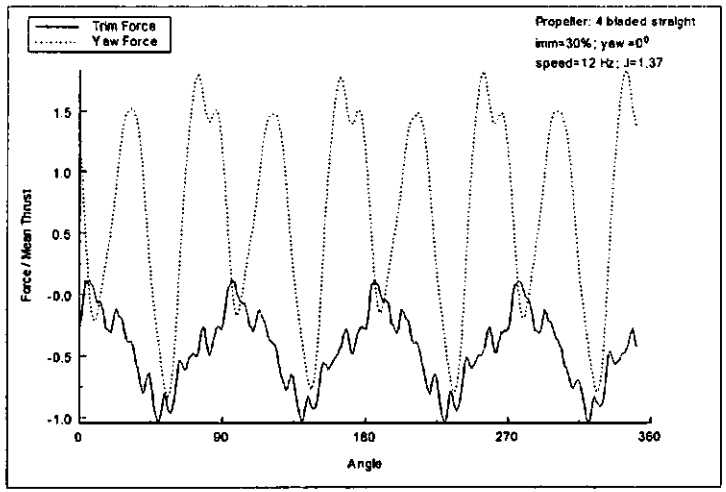

Figure B13

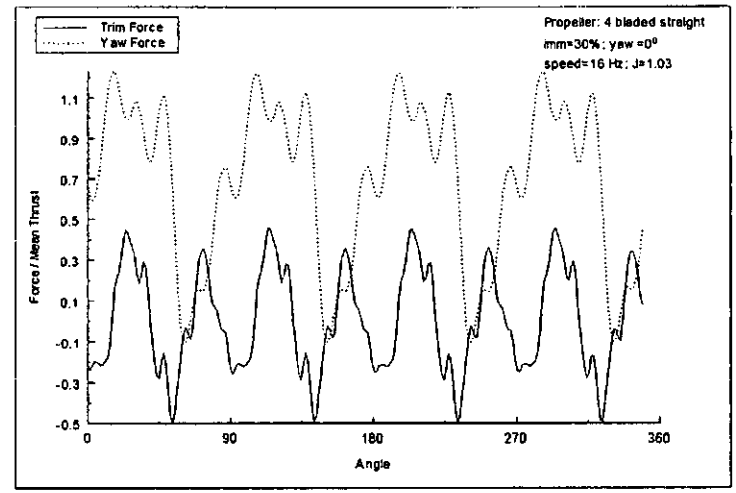

Figure B14

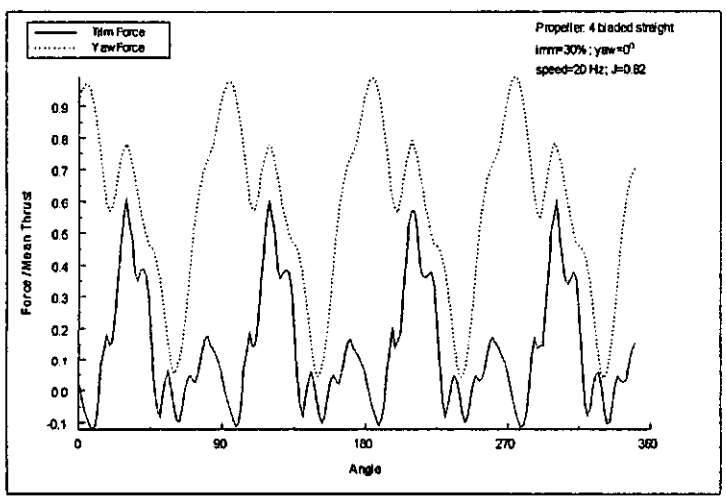

Figure B15

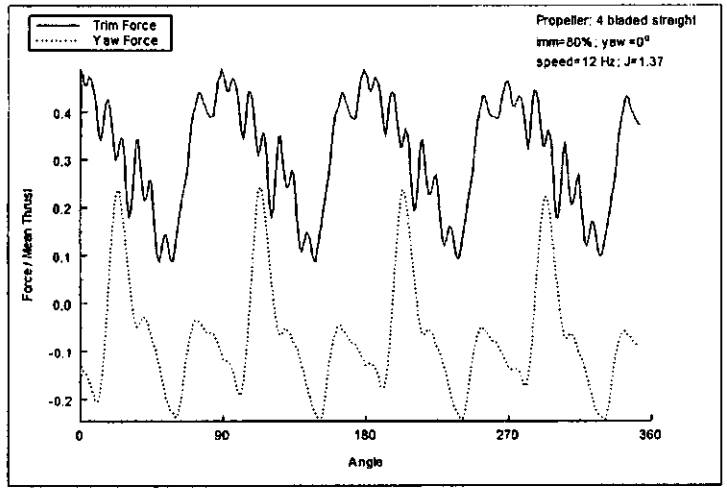

Figure B16

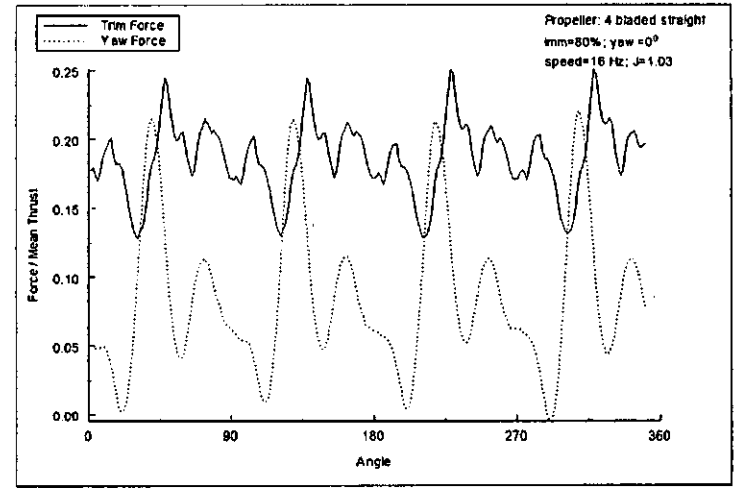

Figure B17

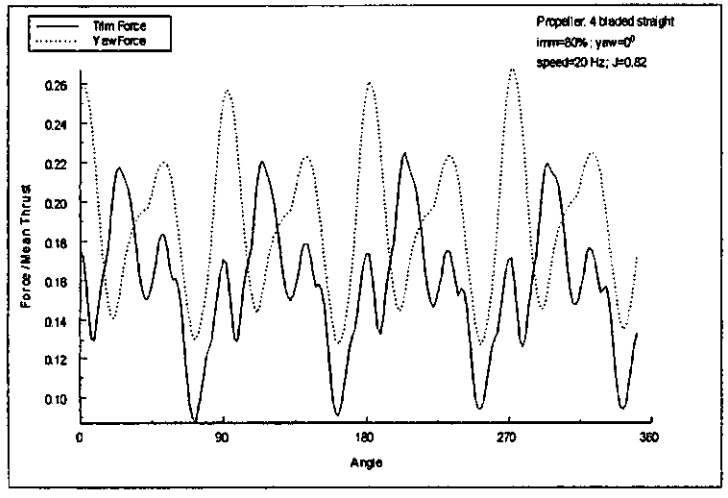

Figure B18

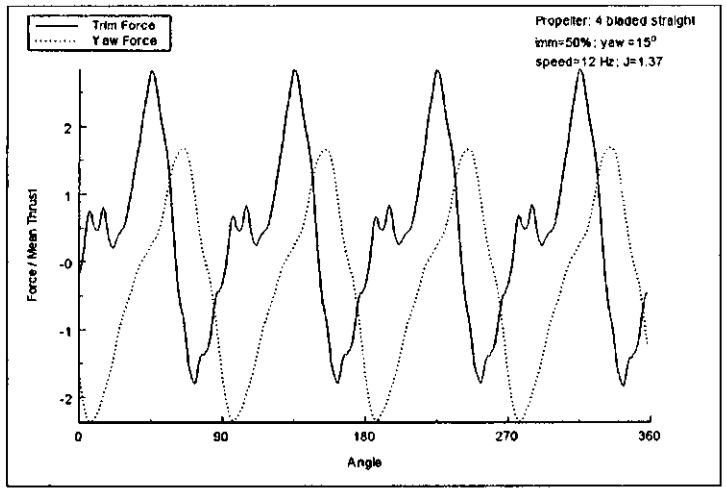

Figure B19

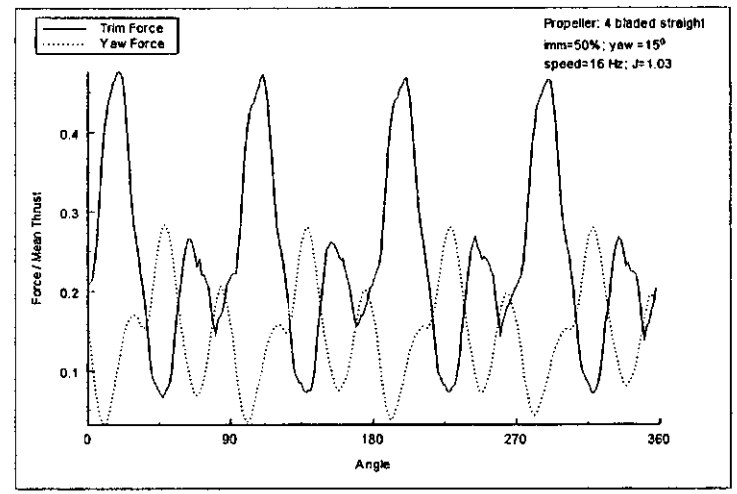

Figure B20

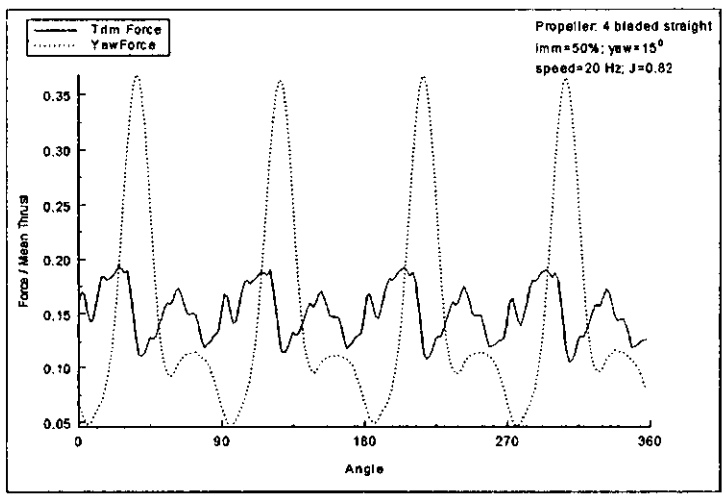

Figure B21

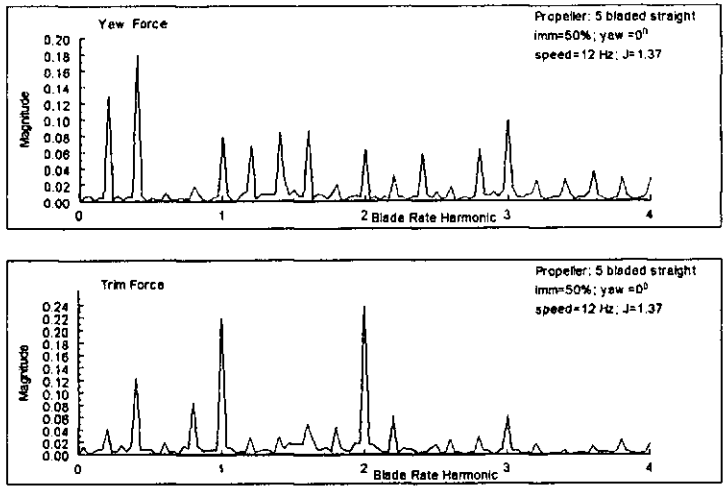

Figure B22

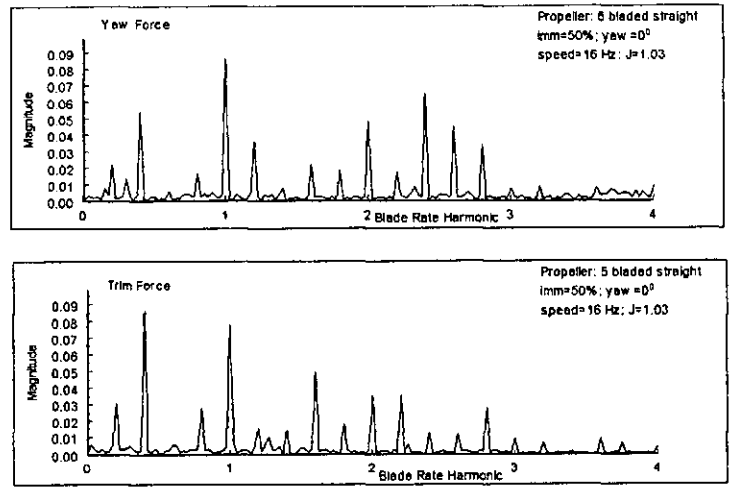

Figure B23

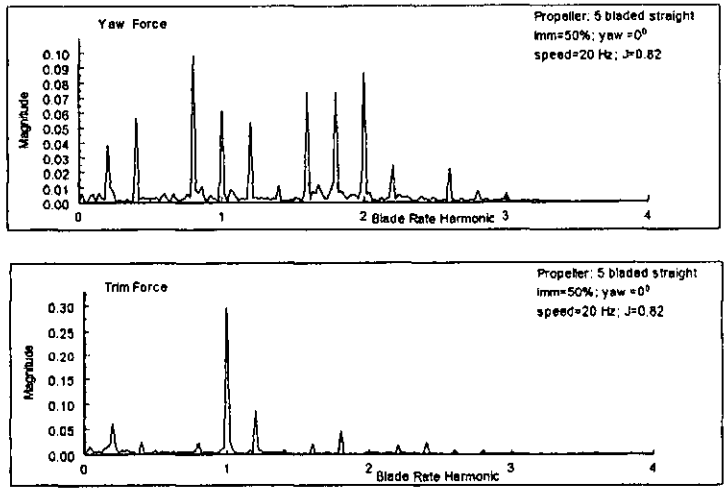

Figure B24

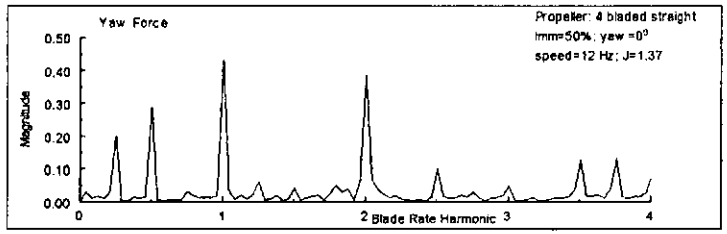

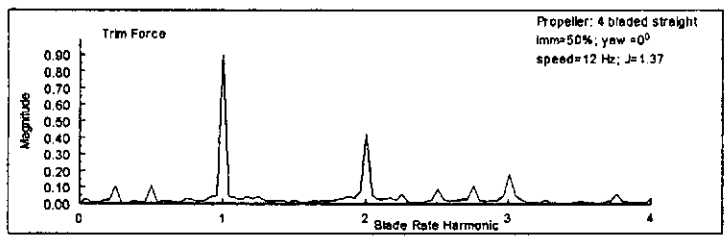

Figure B25

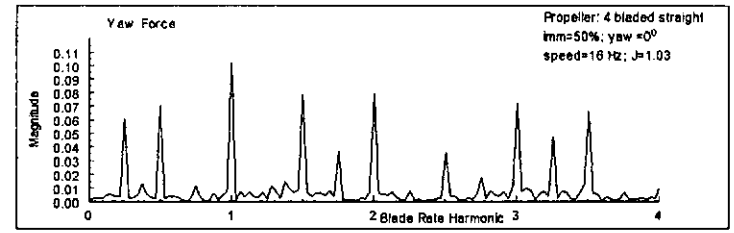

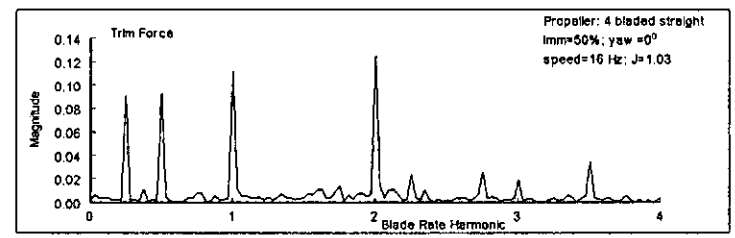

Figure B26

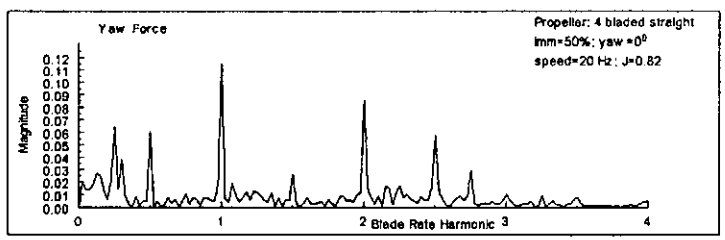

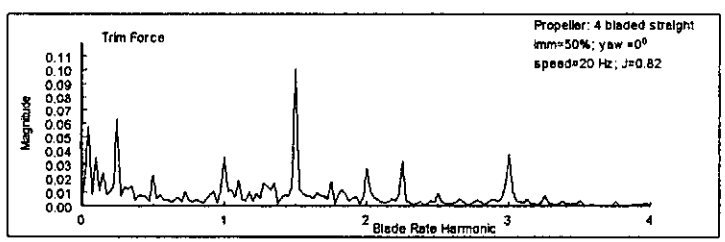

Figure B27

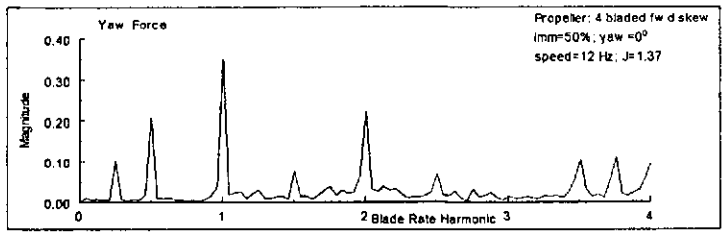

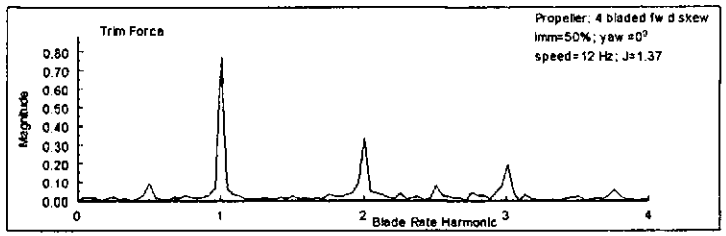

Figure B28

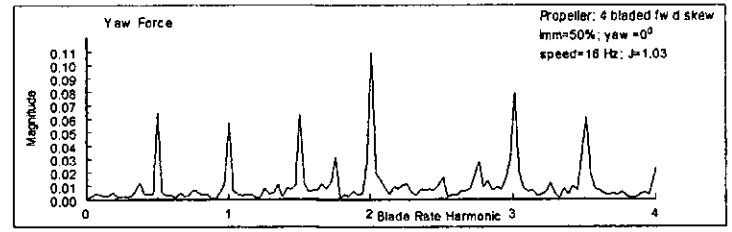

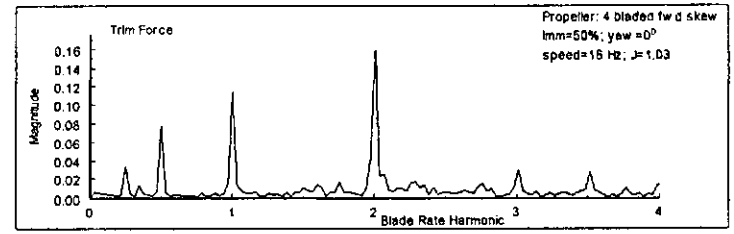

Figure B29

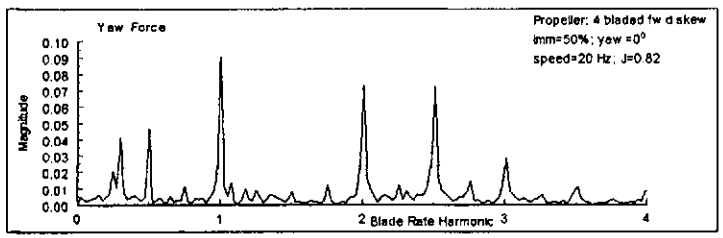

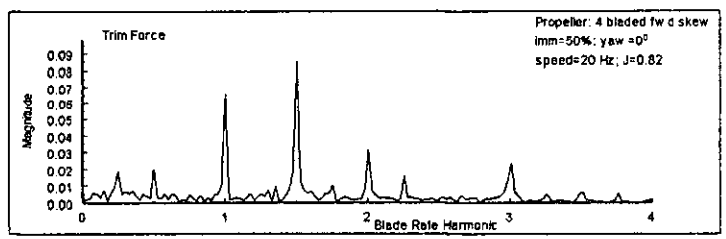

Figure B30

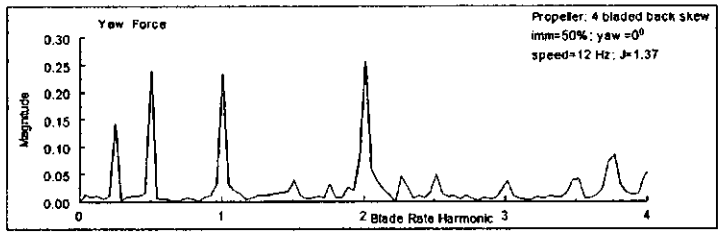

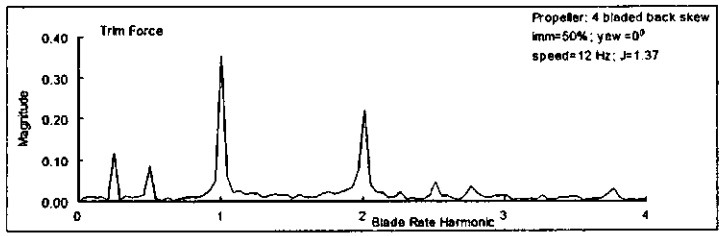

Figure B31

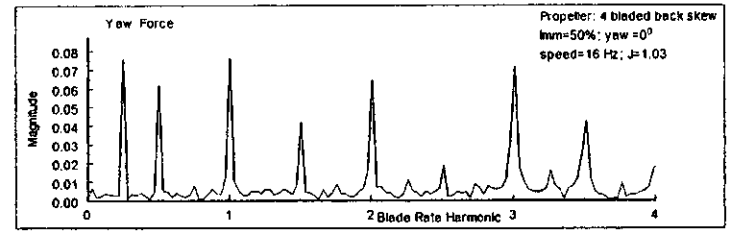

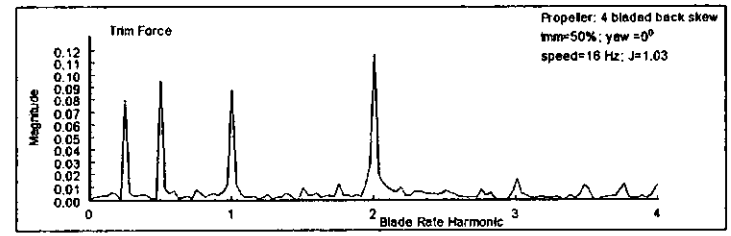

Figure B32

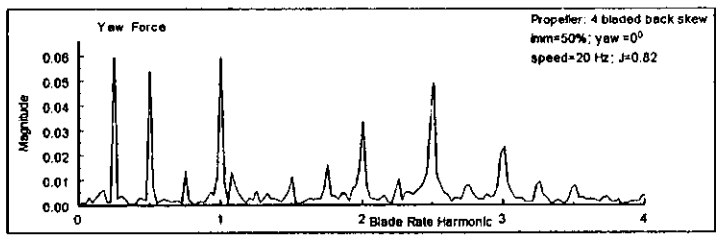

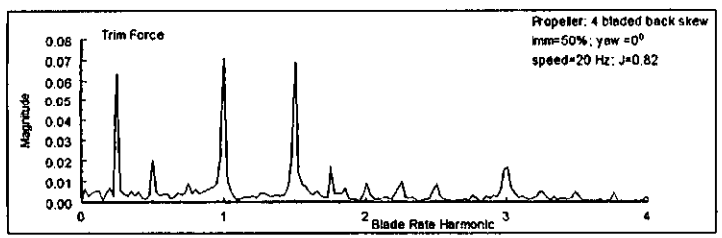

Figure B33

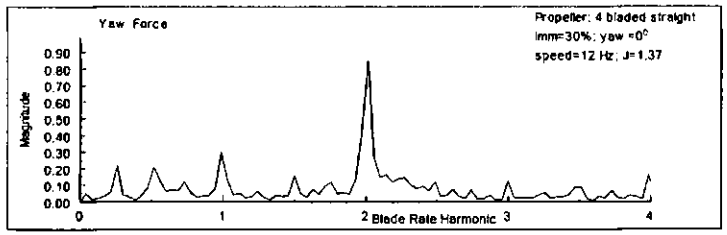

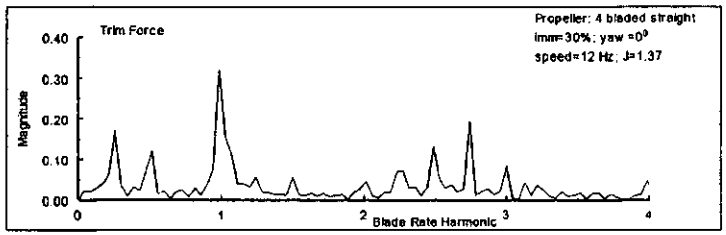

Figure B34

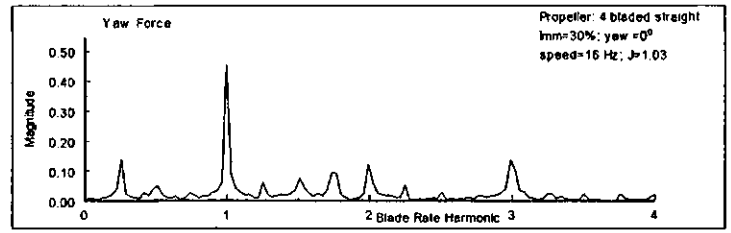

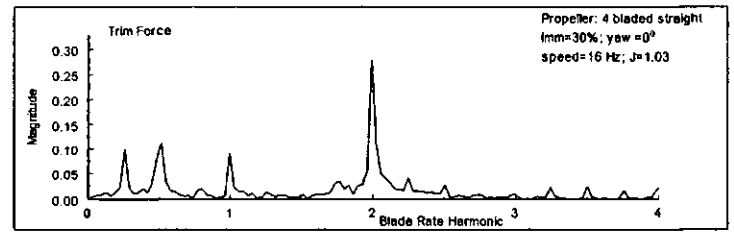

Figure B35

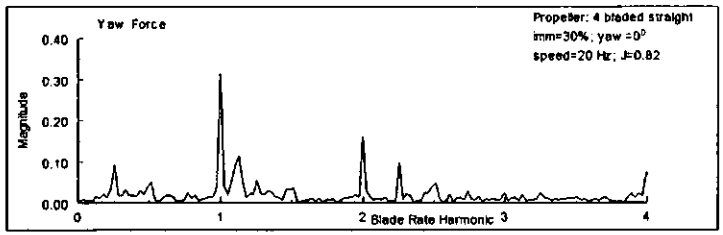

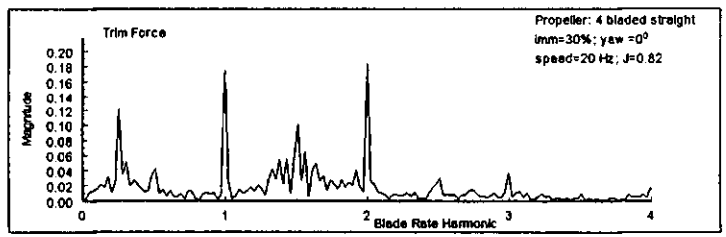

Figure B36

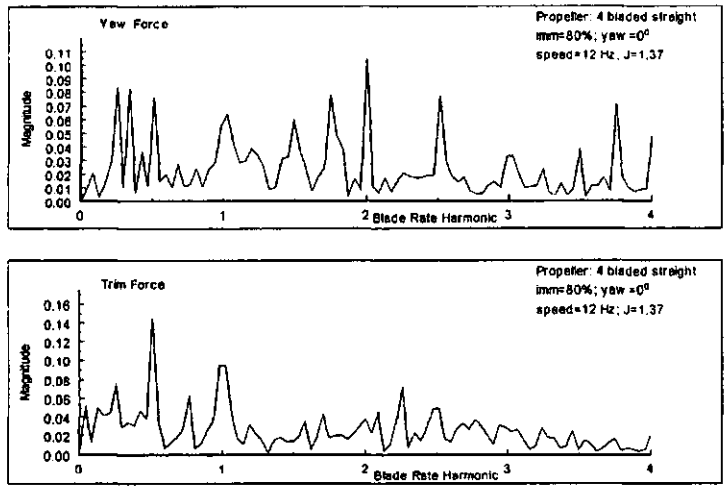

Figure B37

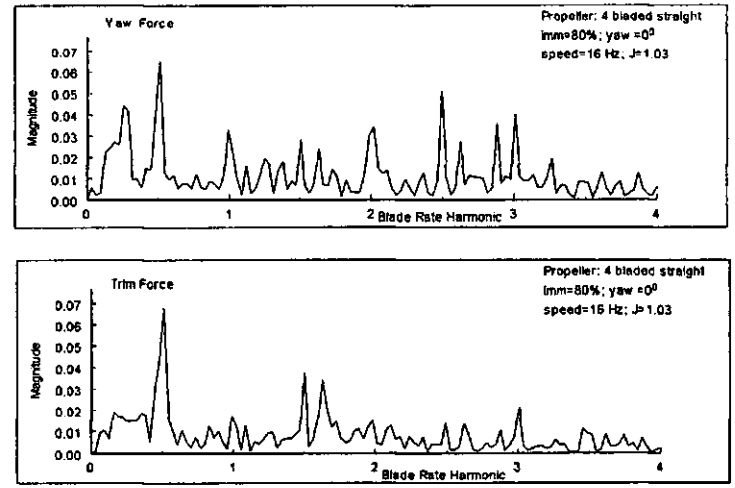

Figure B38

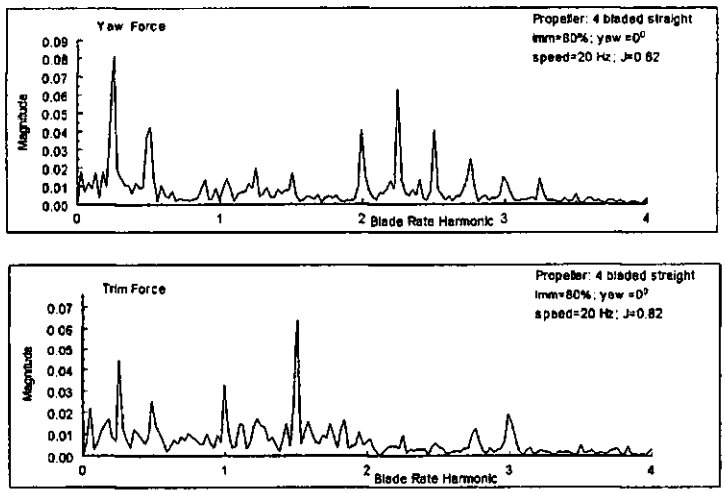

Figure B39

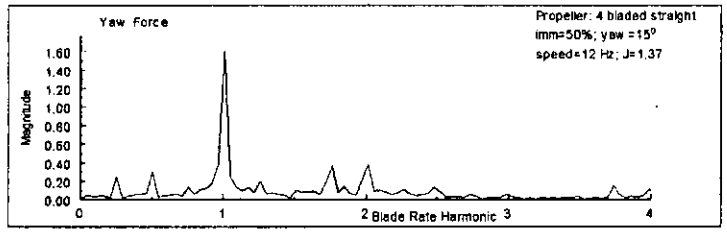

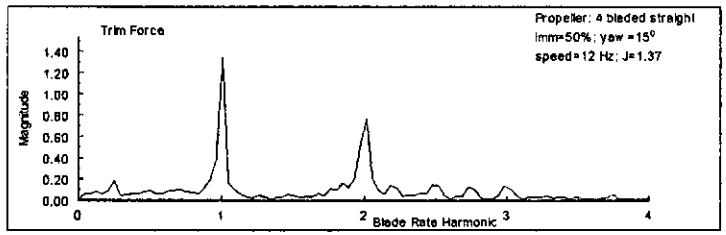

Figure B40

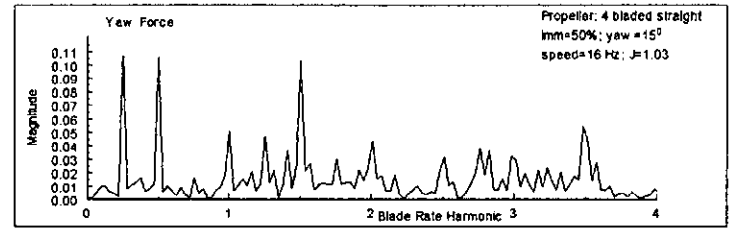

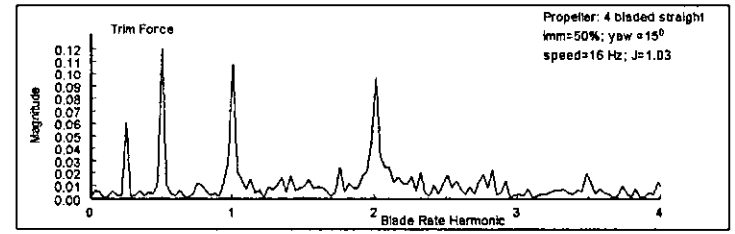

Figure B41

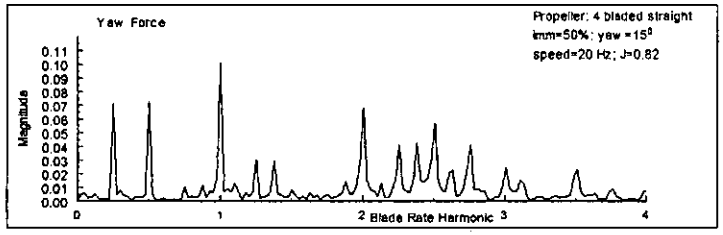

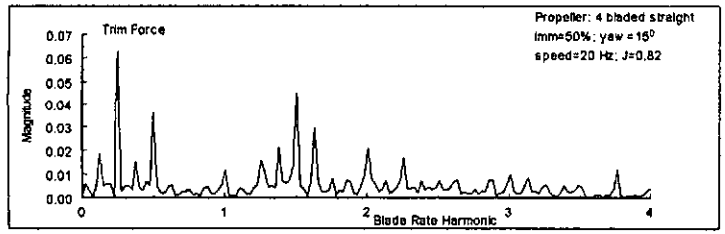

Figure B42

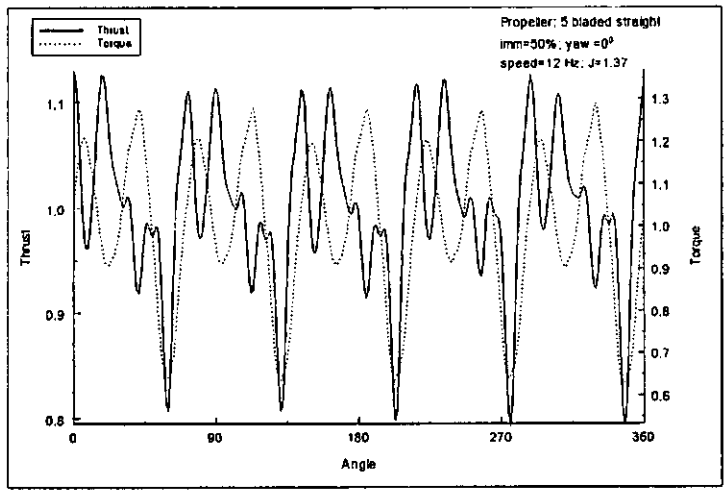

Figure B43

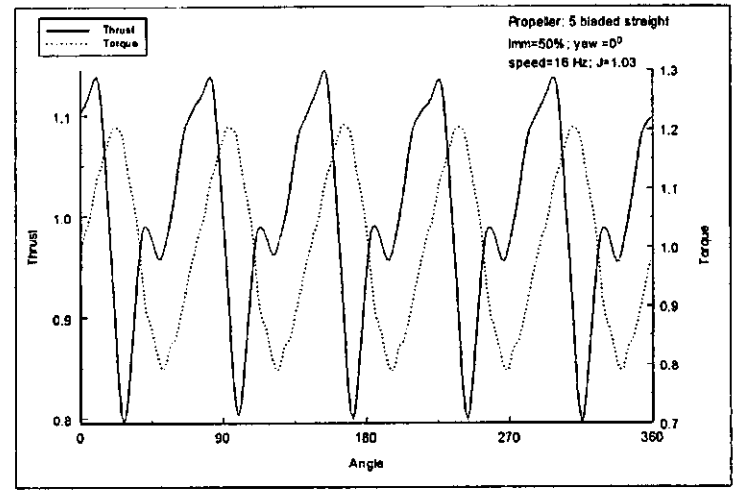

Figure B44

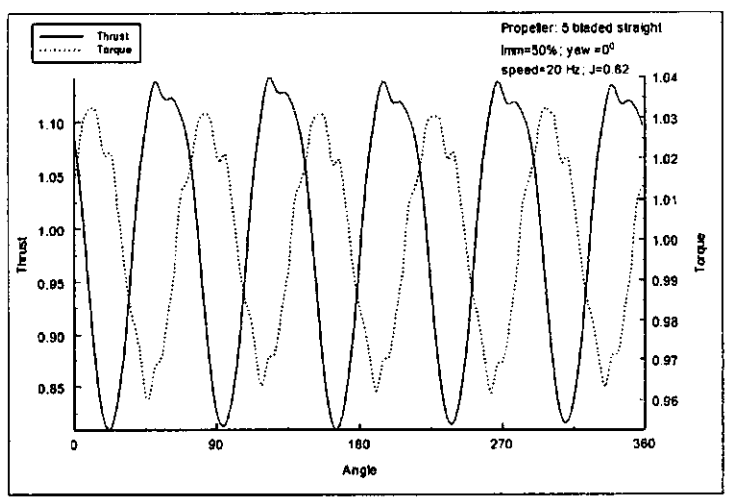

Figure B45

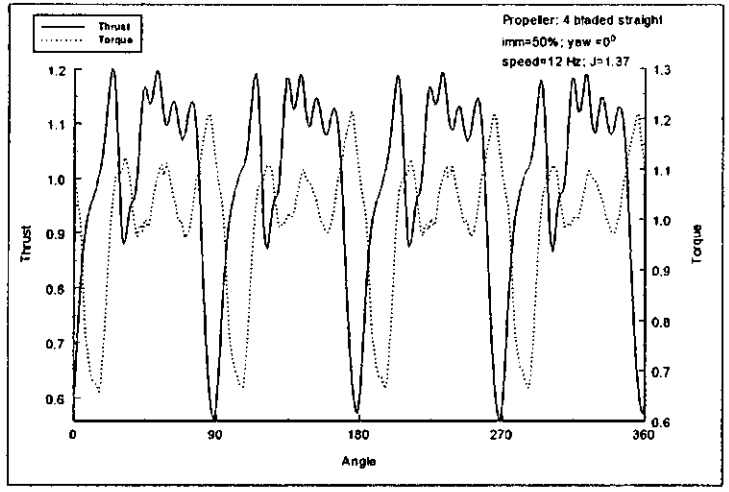

Figure B46

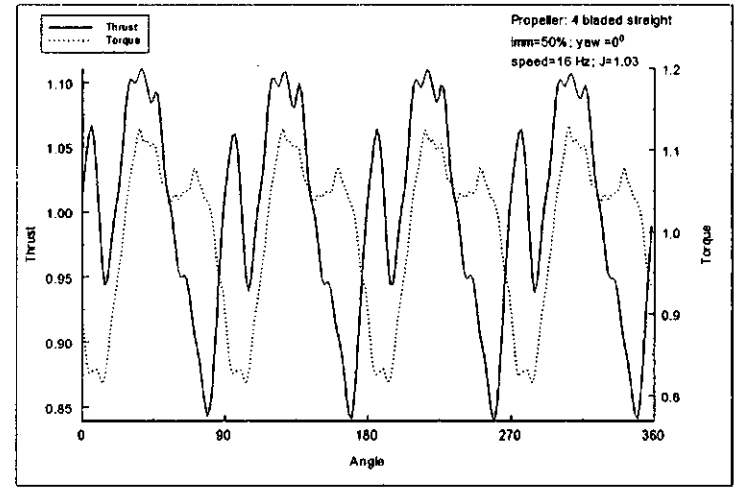

Figure B47

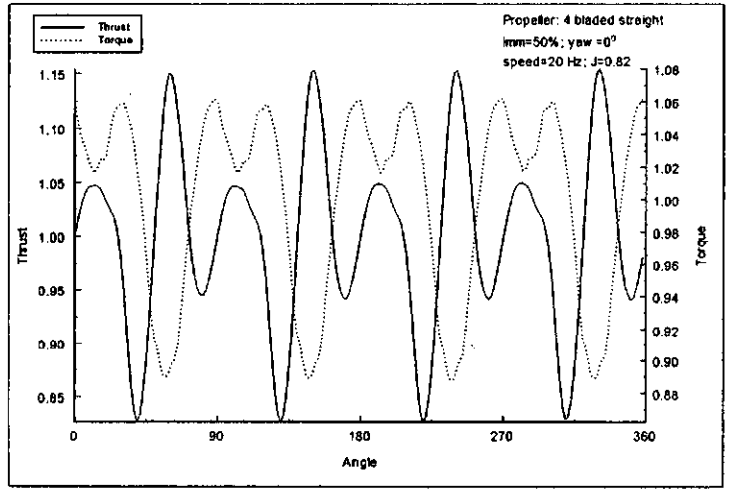

Figure B48

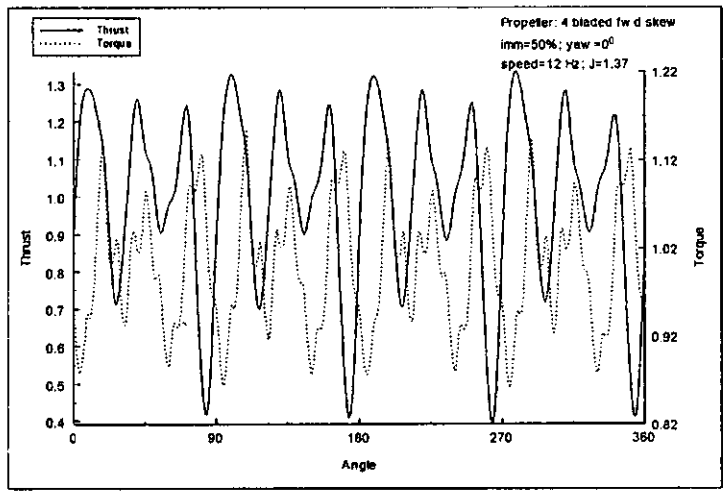

Figure B49

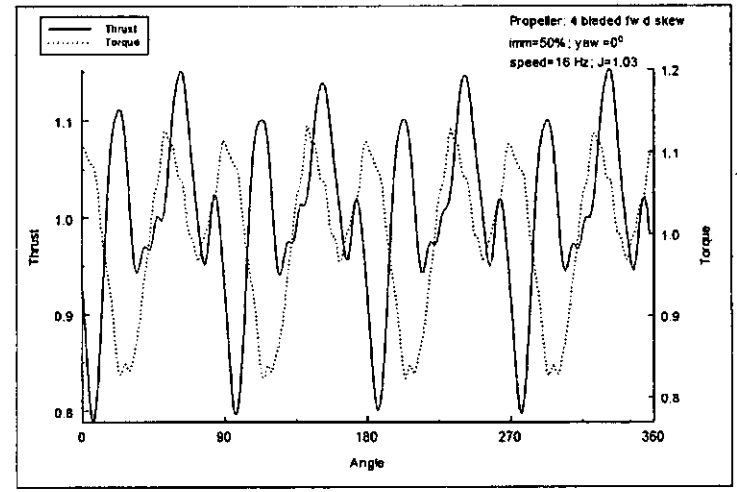

Figure B50

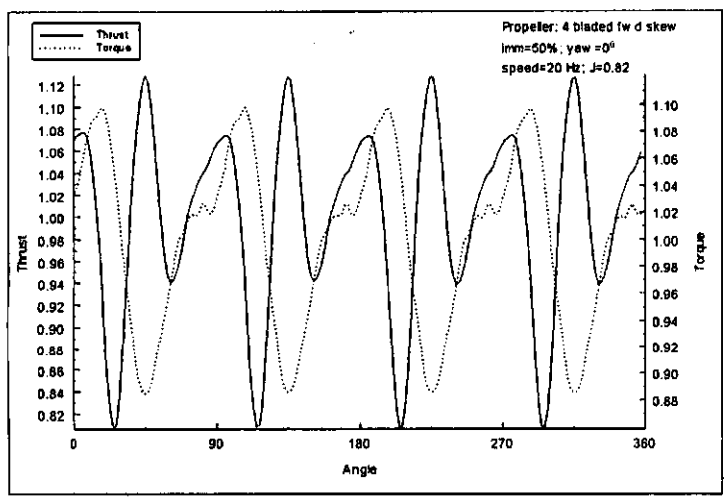

Figure B51

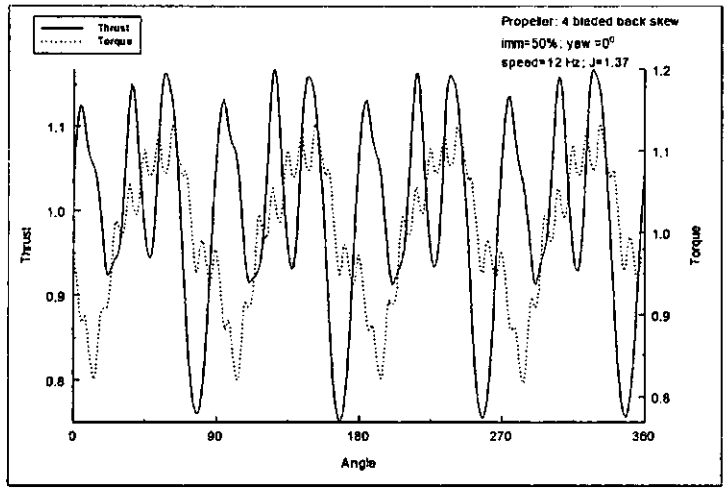

Figure B52

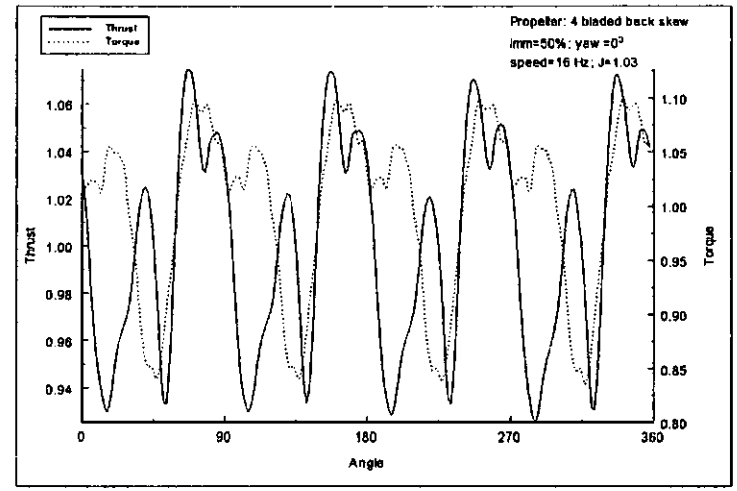

Figure B53

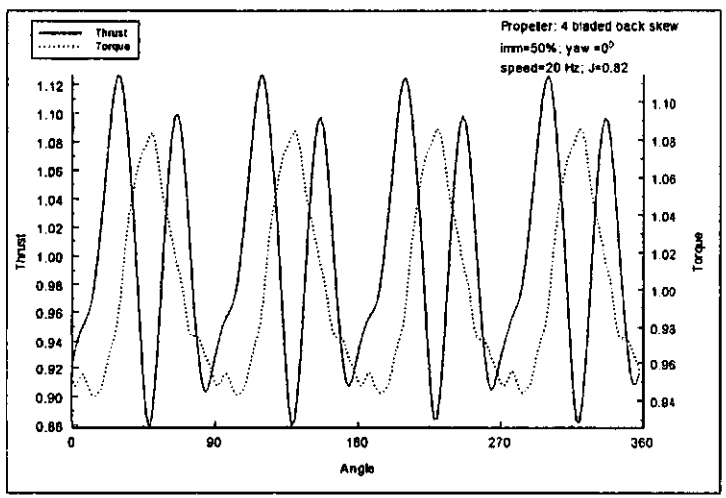

Figure B54

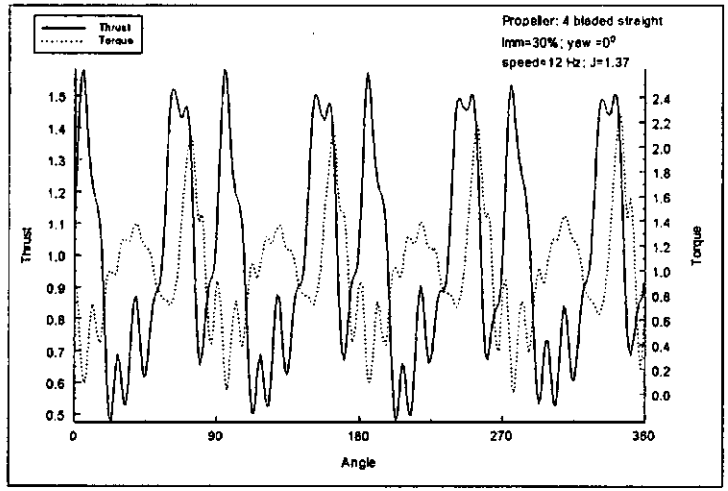

Figure B55

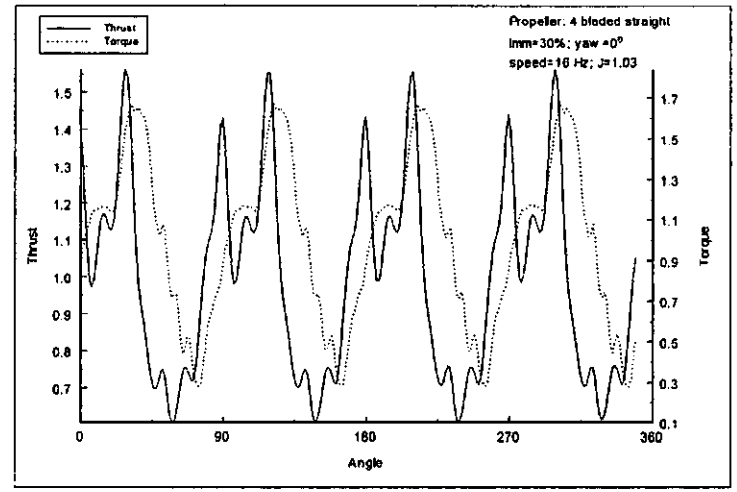

Figure B56

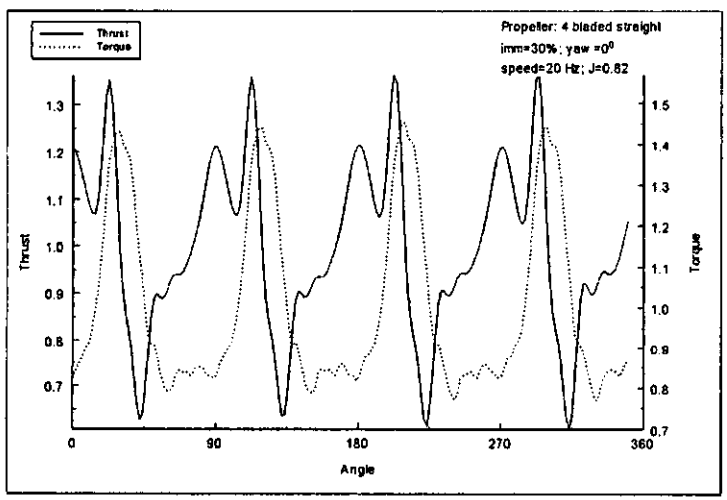

Figure B57

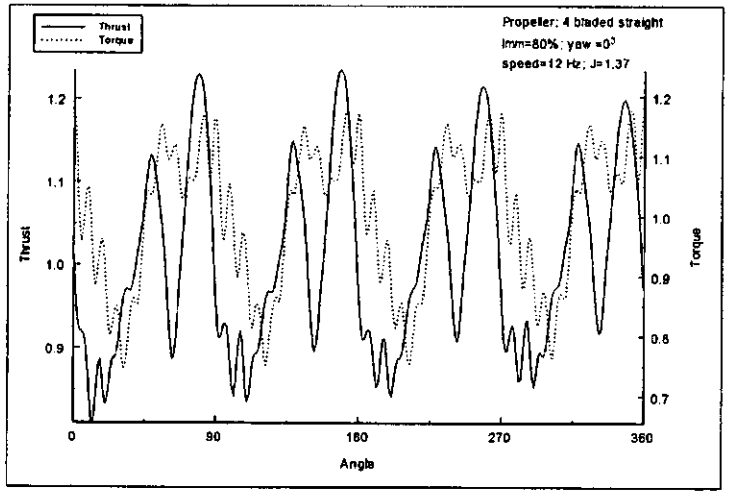

Figure B58

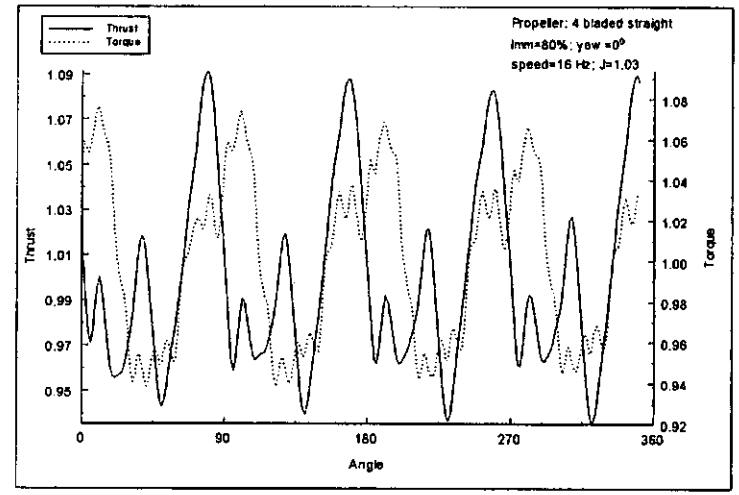

Figure B59

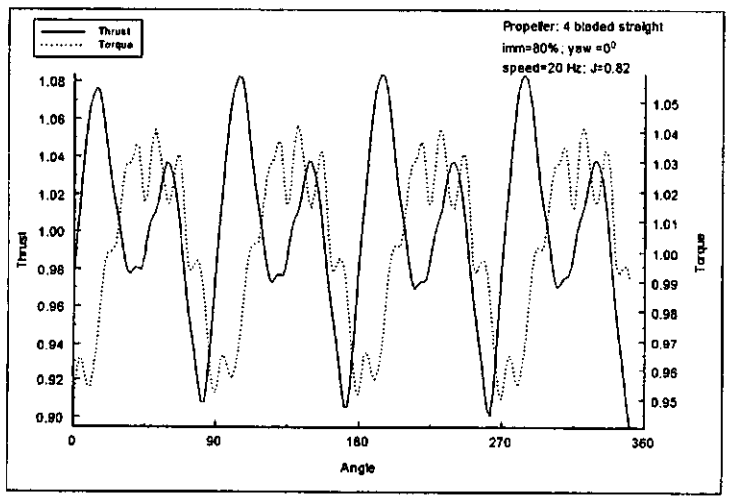

Figure B60

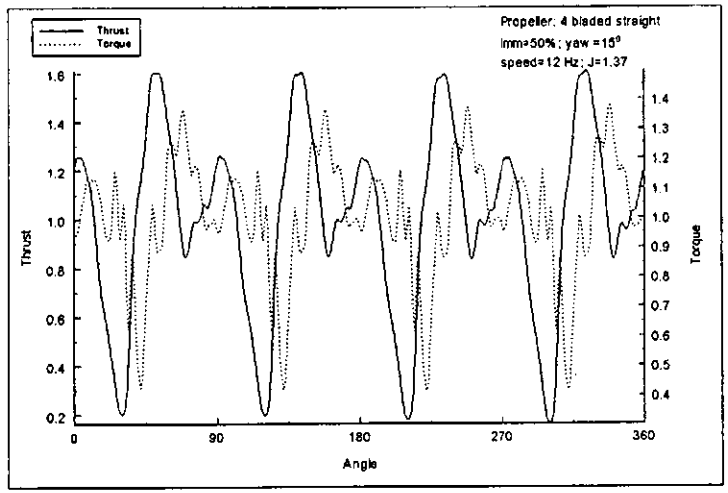

Figure B61

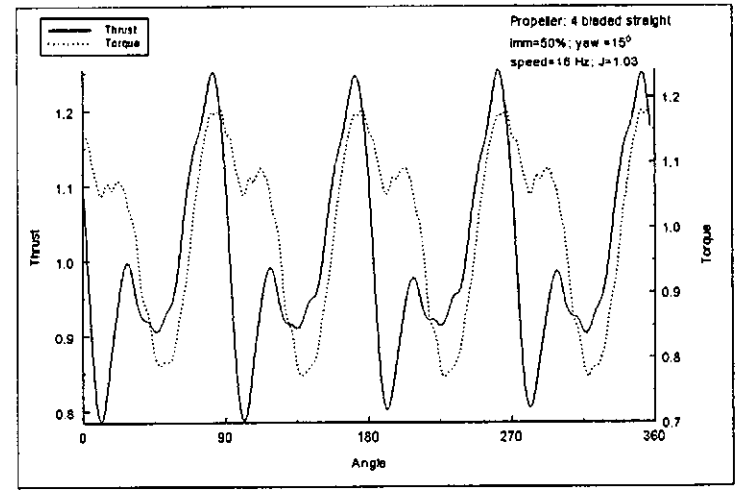

Figure B62

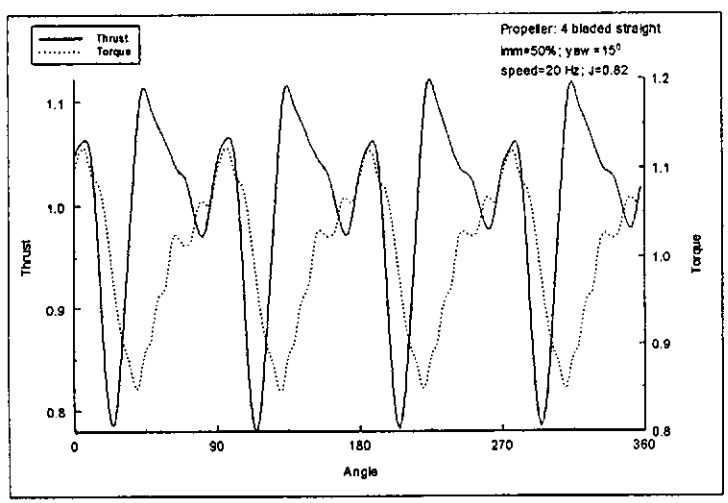

Figure B63

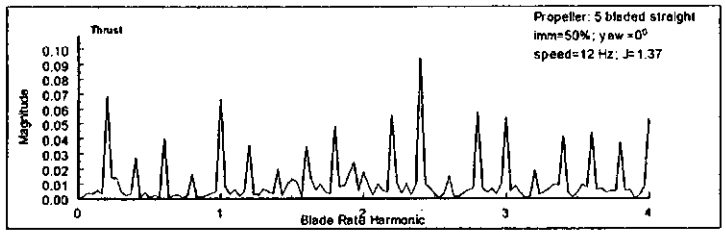

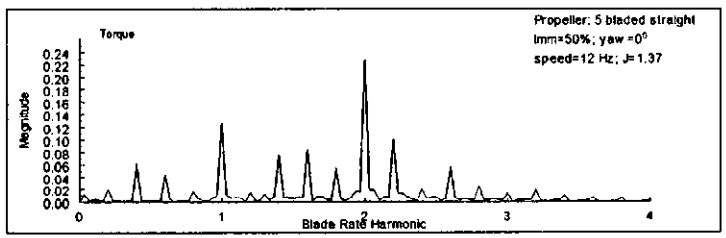

Figure B64

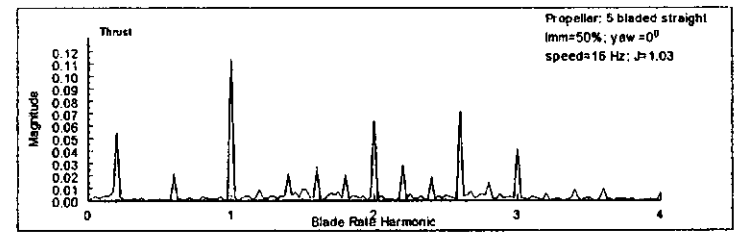

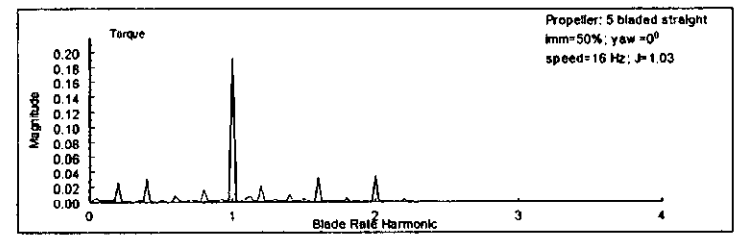

Figure B65

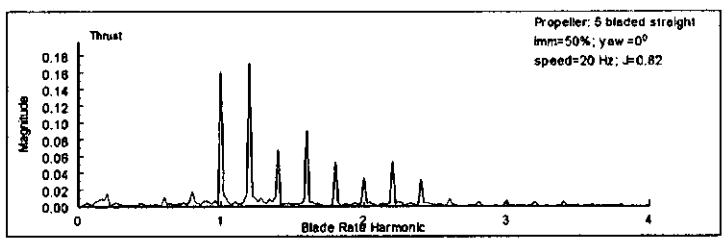

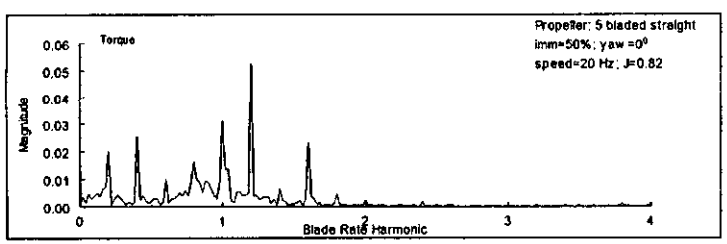

Figure B66

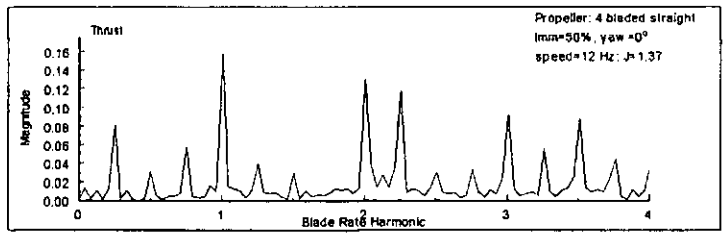

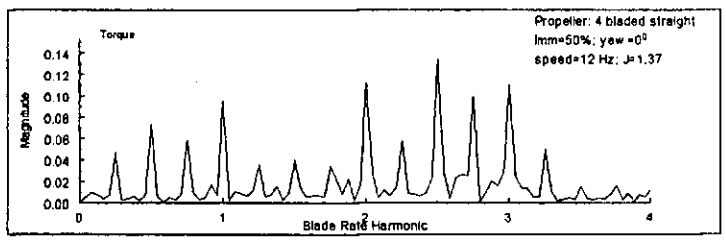

Figure B67

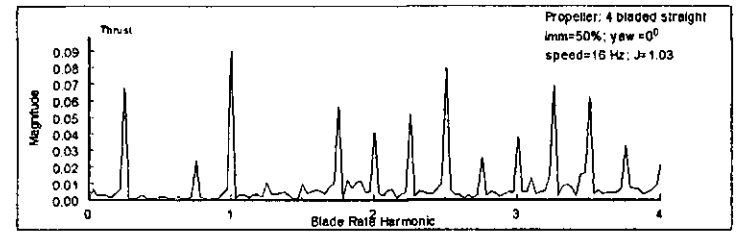

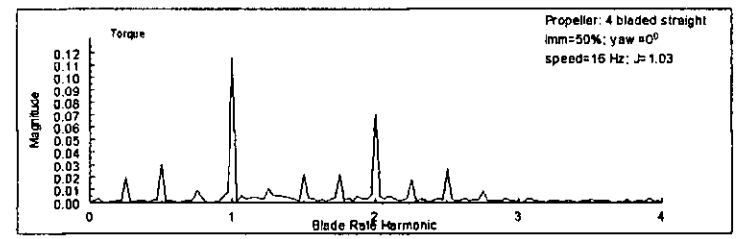

Figure B68

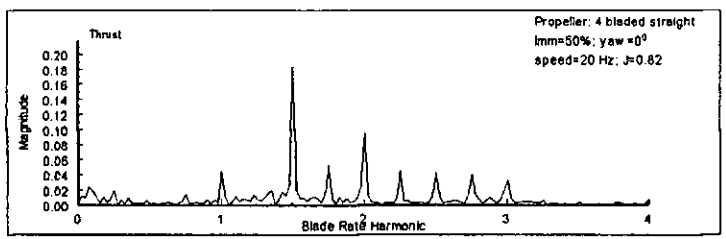

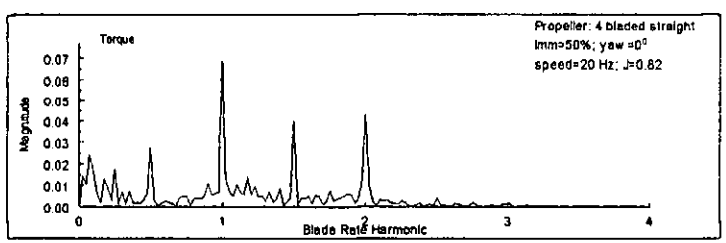

Figure B69

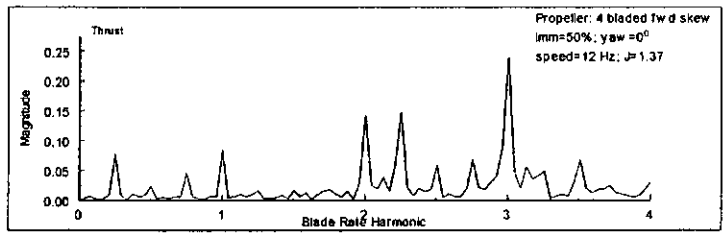

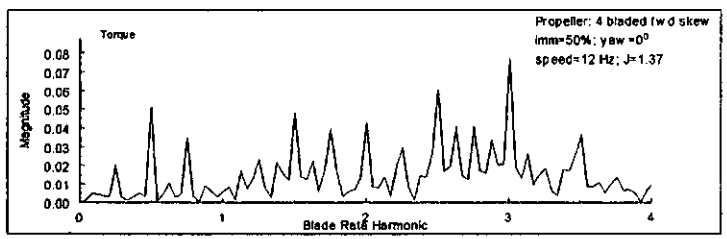

Figure B70

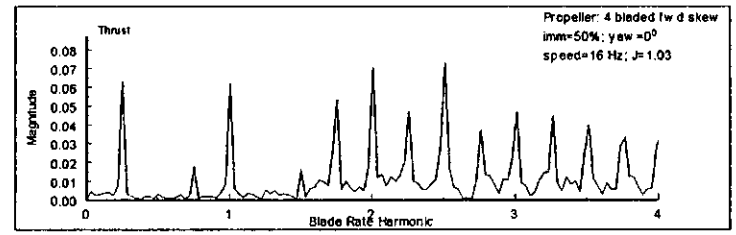

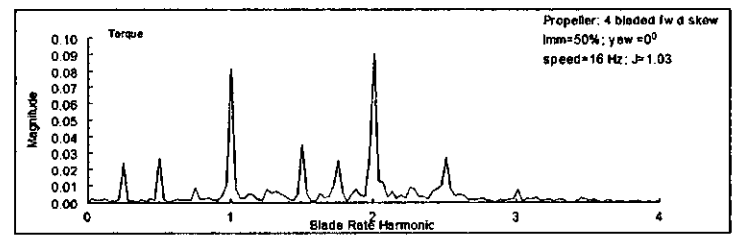

Figure B71

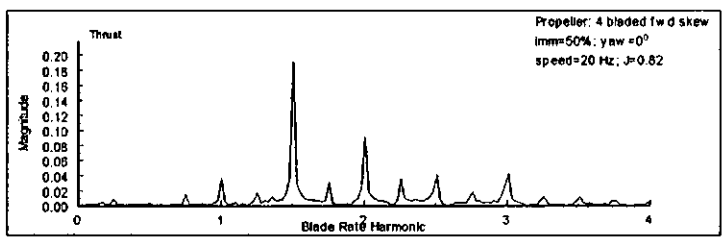

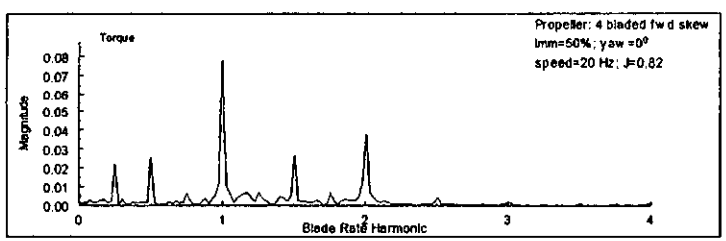

Figure B72

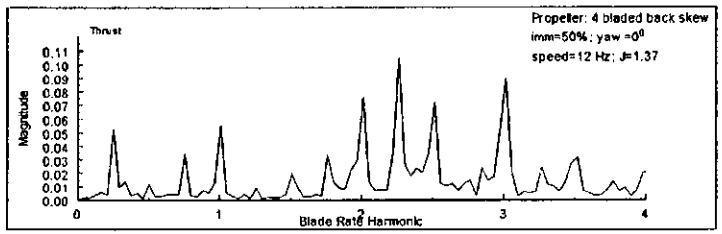

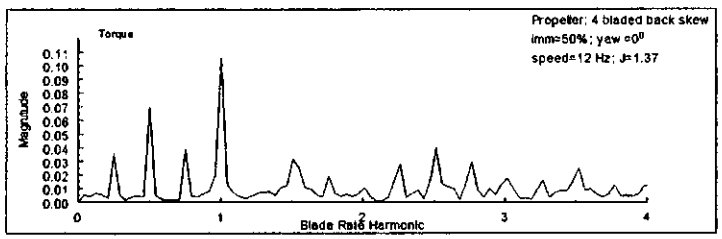

Figure B73

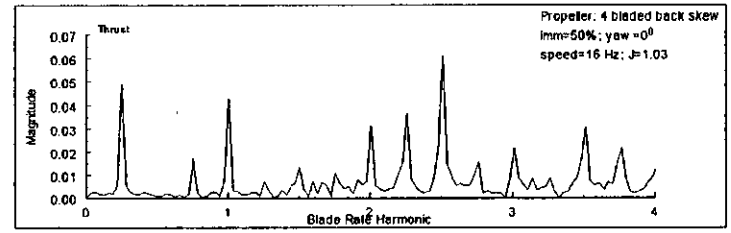

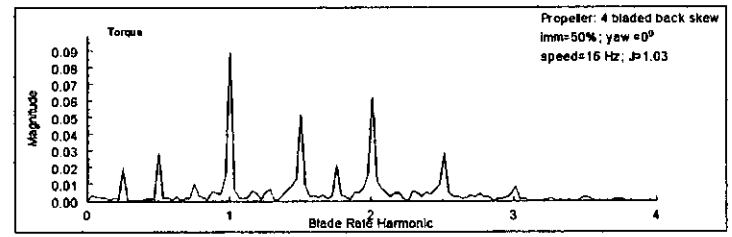

Figure B74

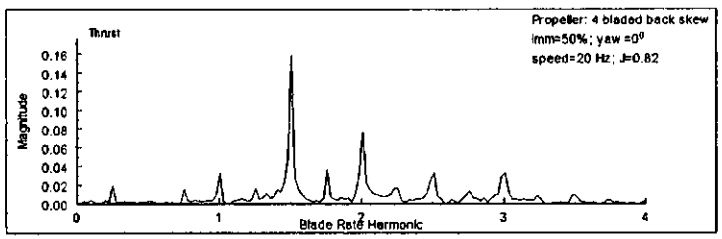

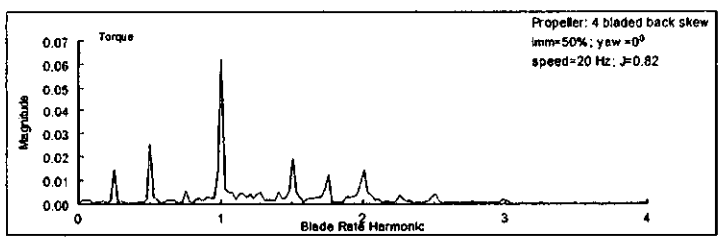

Figure B75

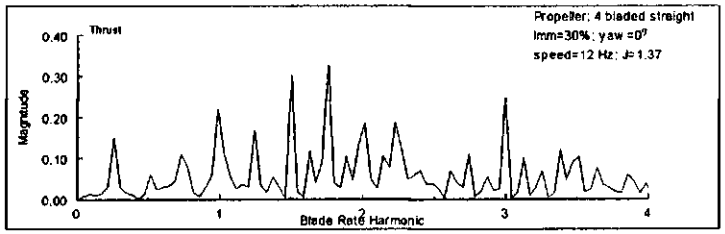

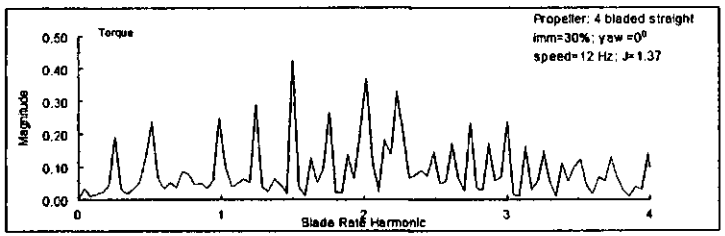

Figure B76

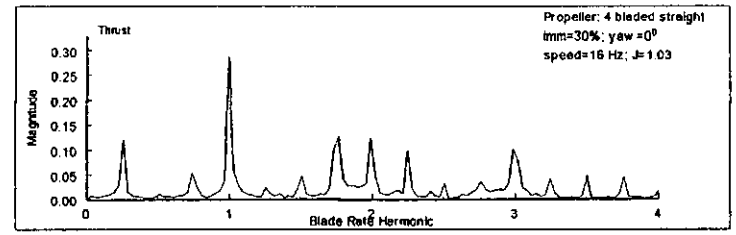

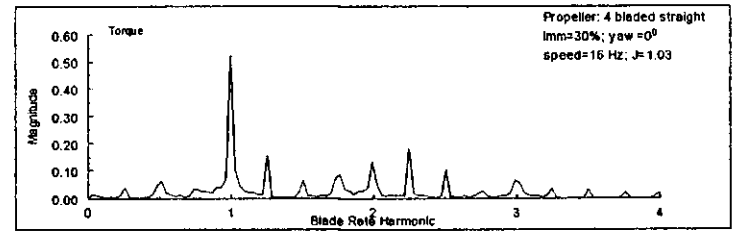

Figure B77

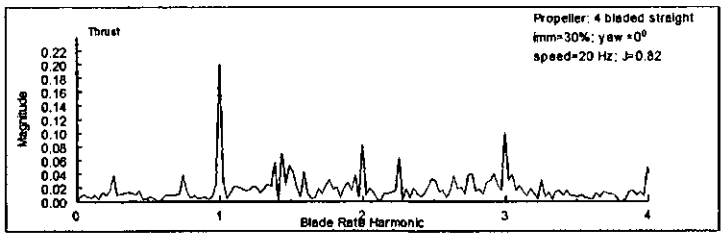

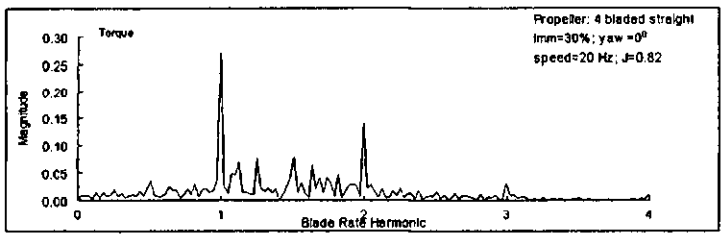

Figure B78

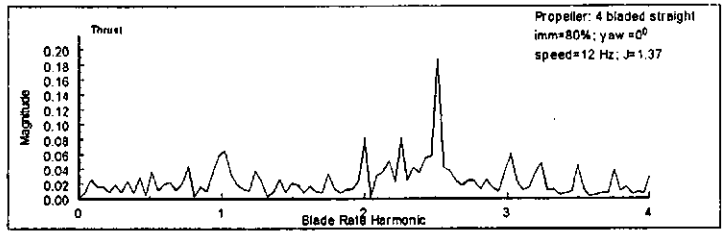

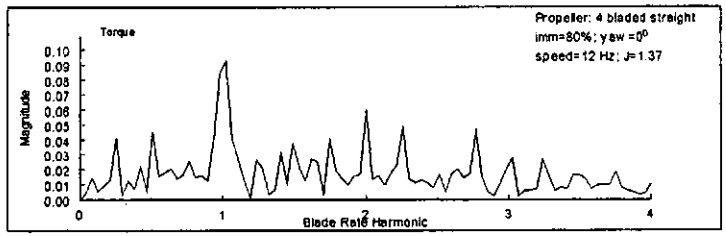

Figure B79

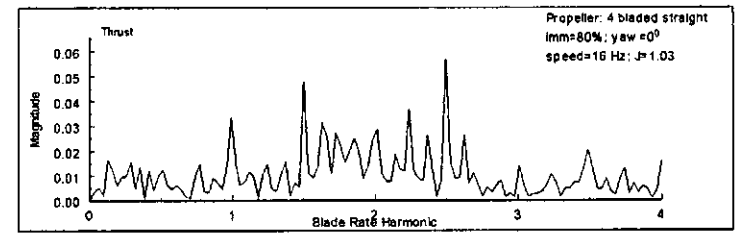

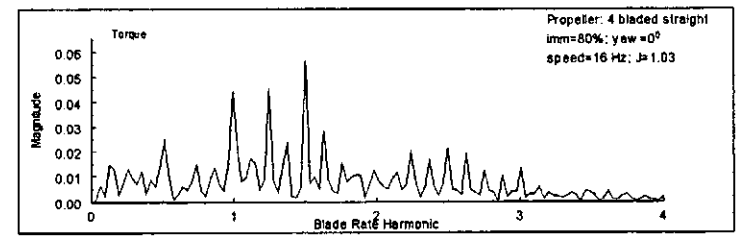

Figure B80

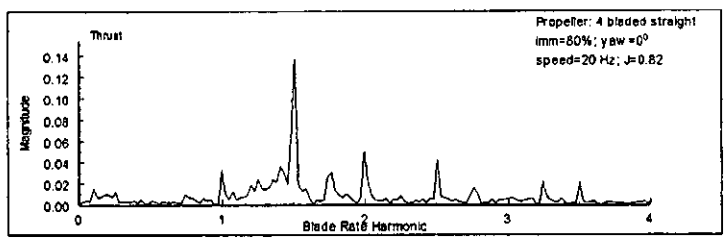

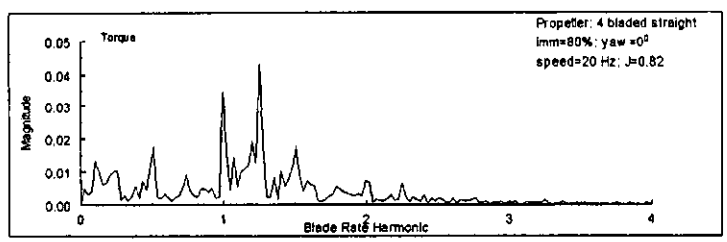

Figure B81

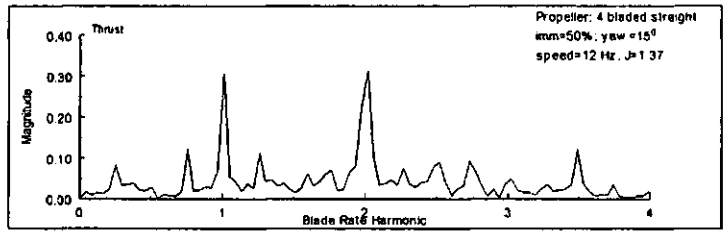

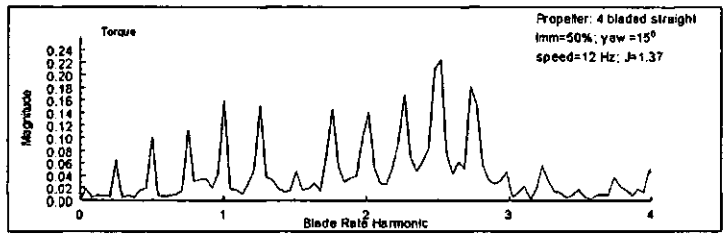

Figure B82

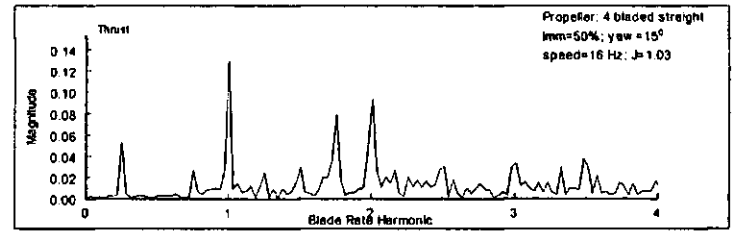

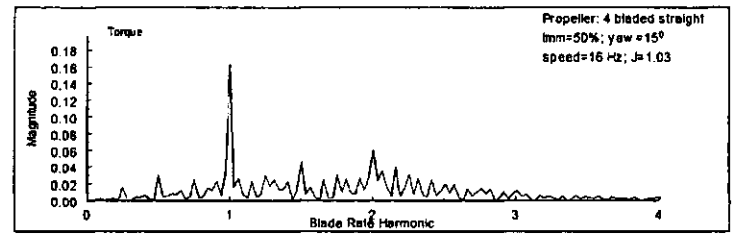

Figure B83

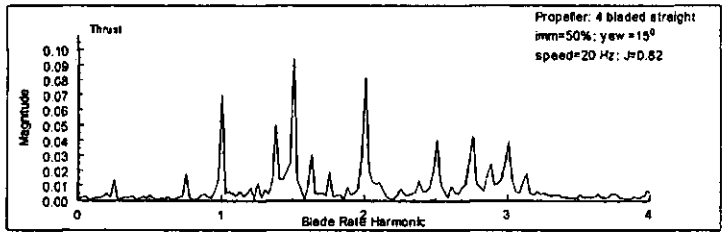

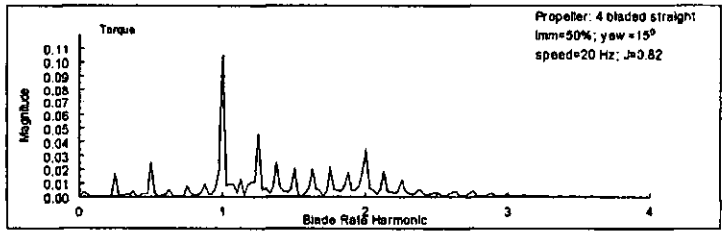

Figure B84

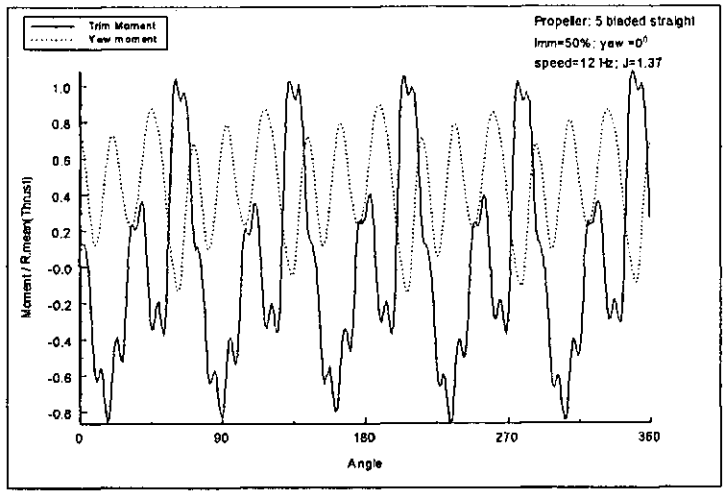

Figure B85

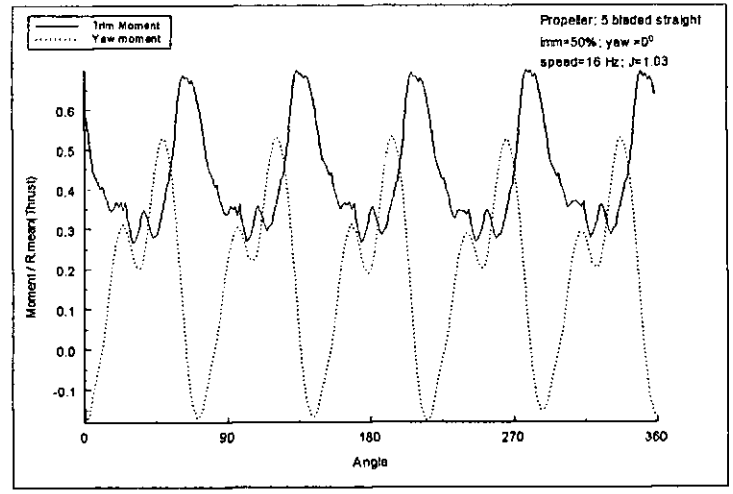

Figure B86

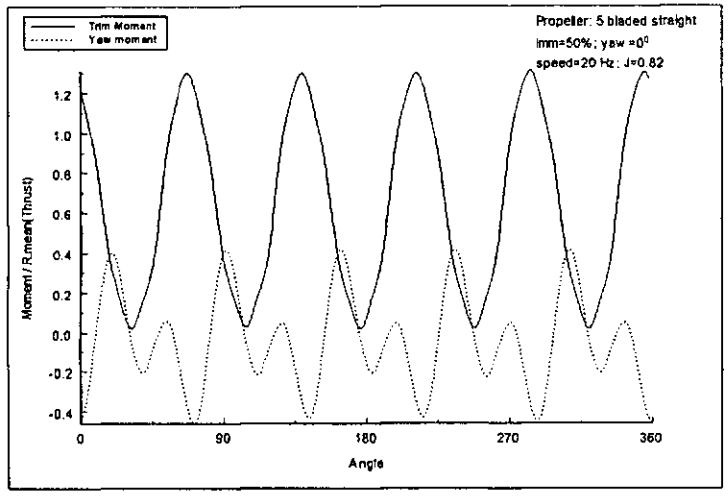

Figure B87

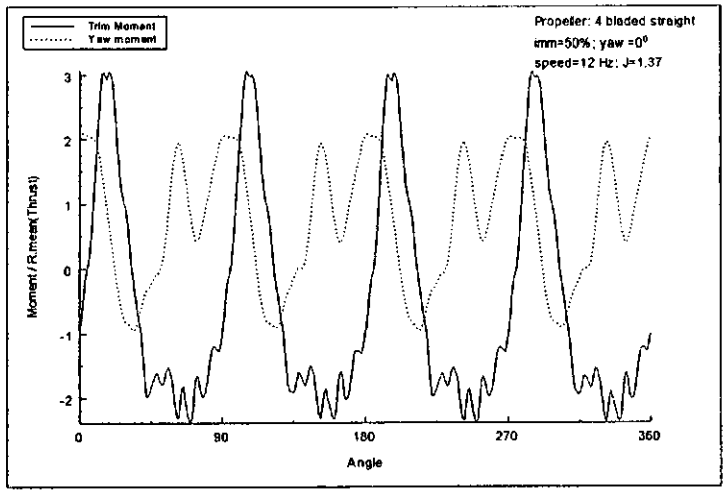

Figure B88

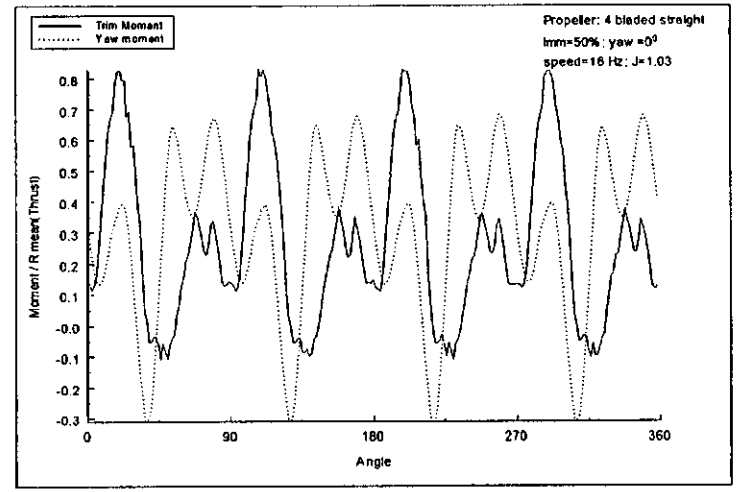

Figure B89

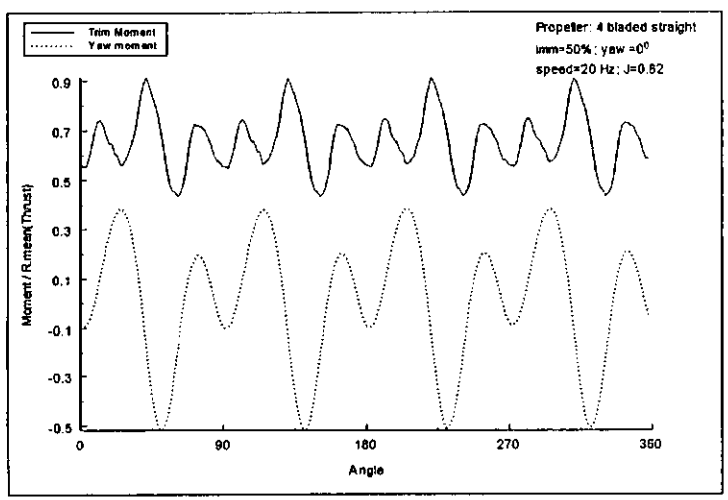

Figure B90

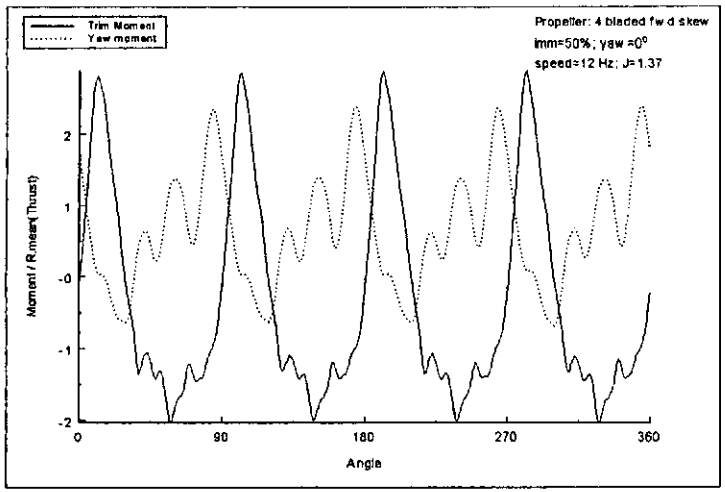

Figure B91

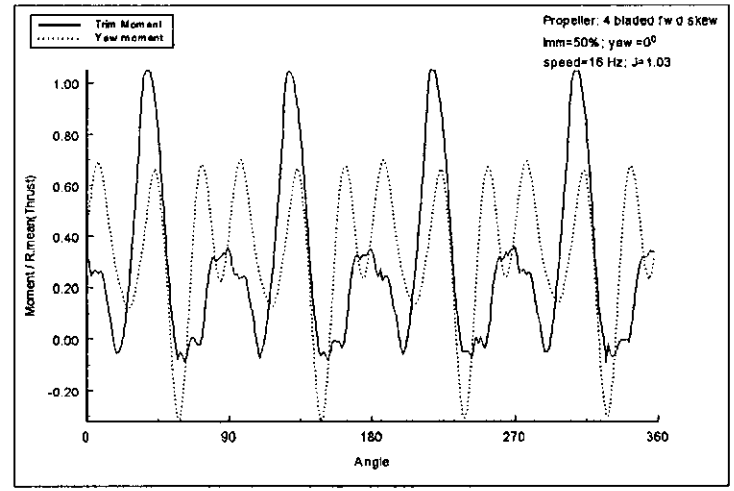

Figure B92

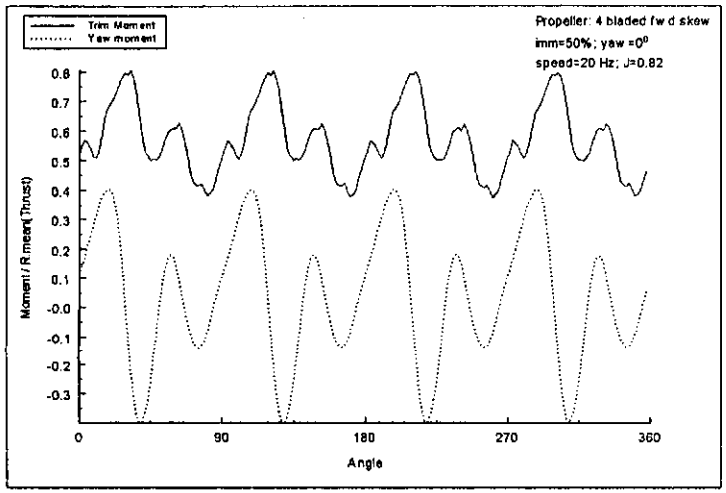

Figure B93

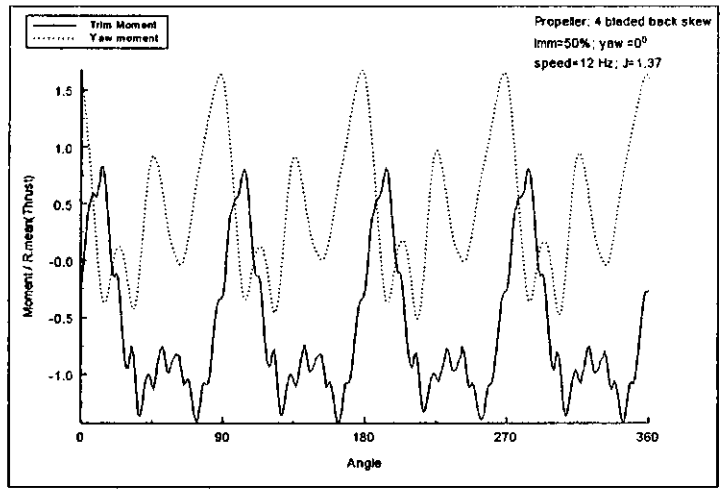

Figure B94

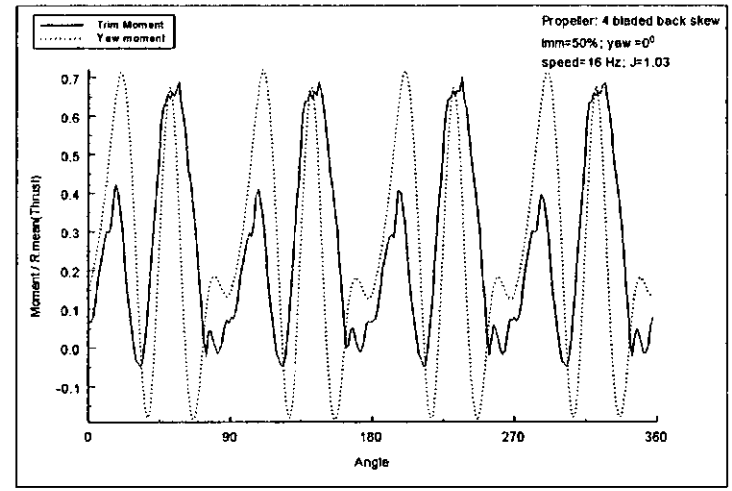

Figure B95

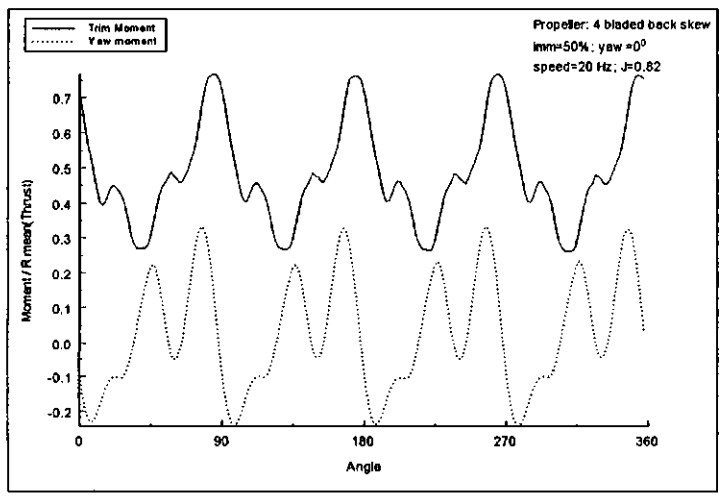

Figure B96

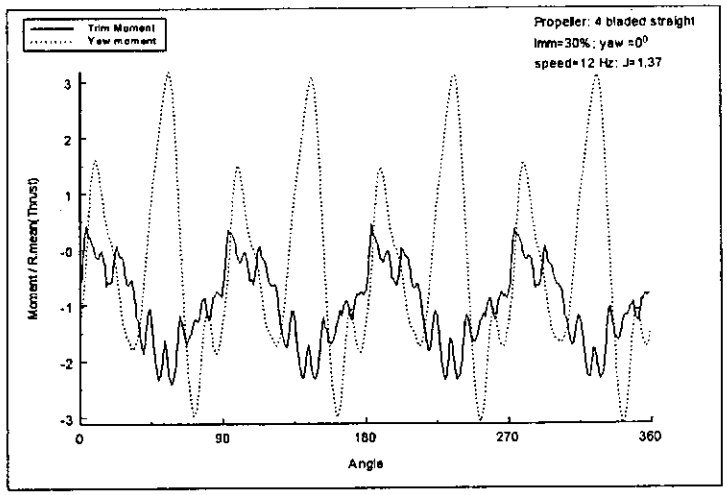

Figure B97

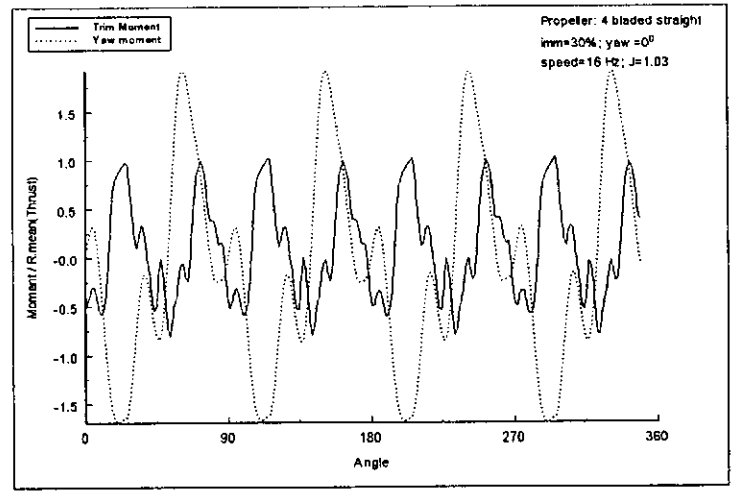

Figure B98

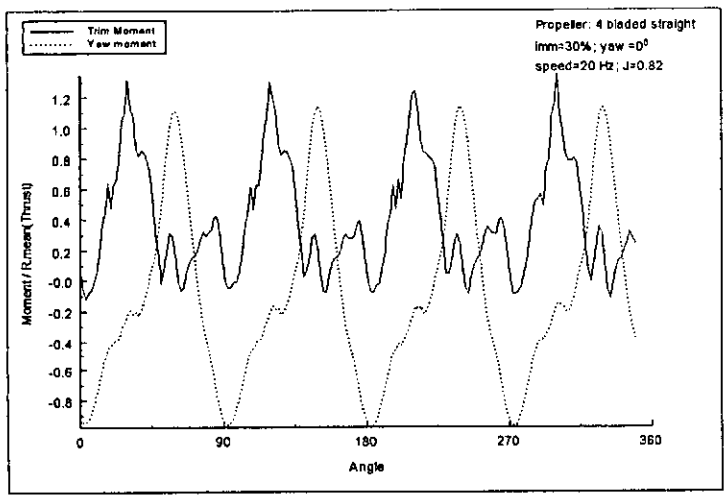

Figure B99

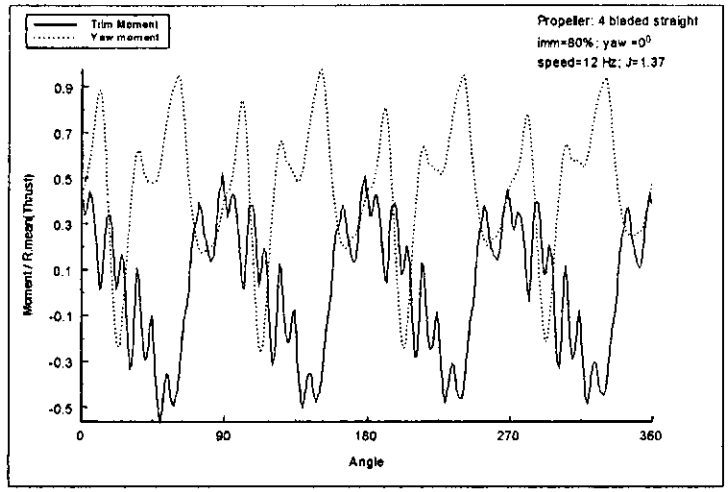

Figure B100

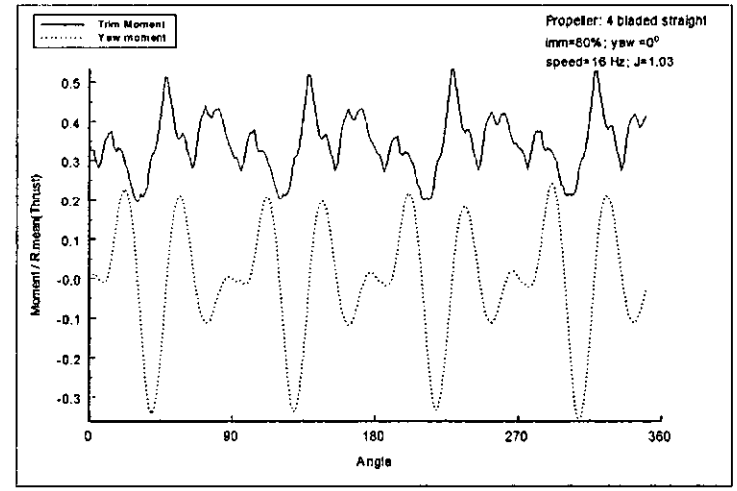

Figure B101

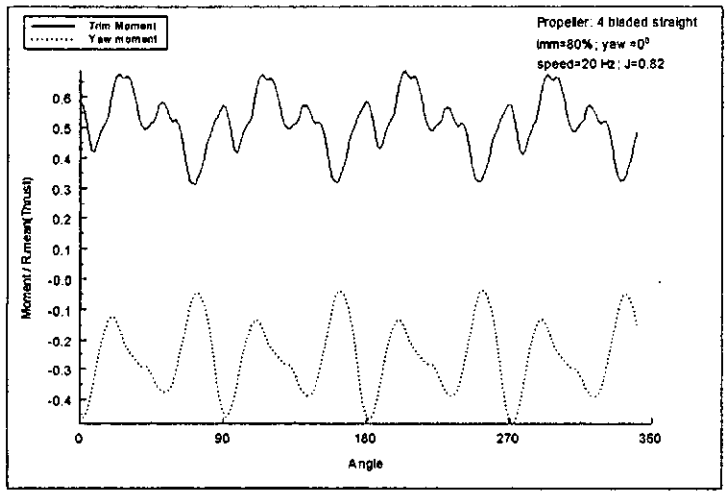

Figure B102

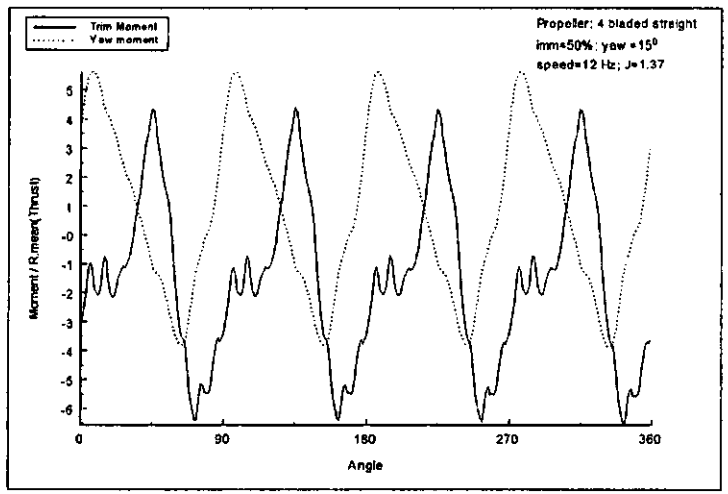

Figure B103

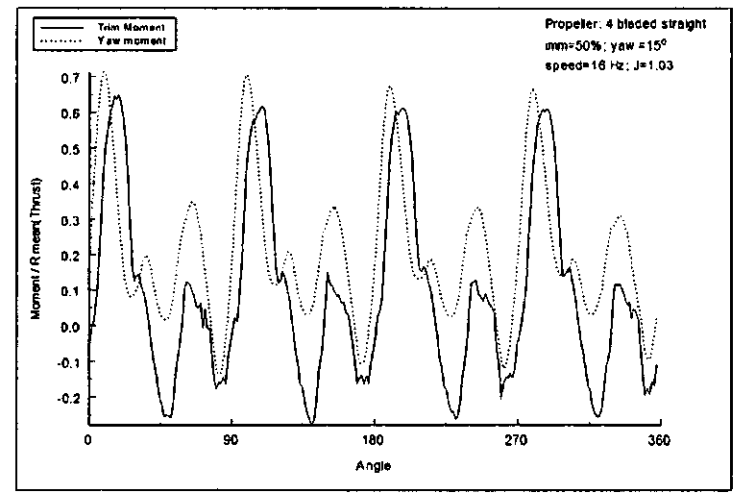

Figure B104

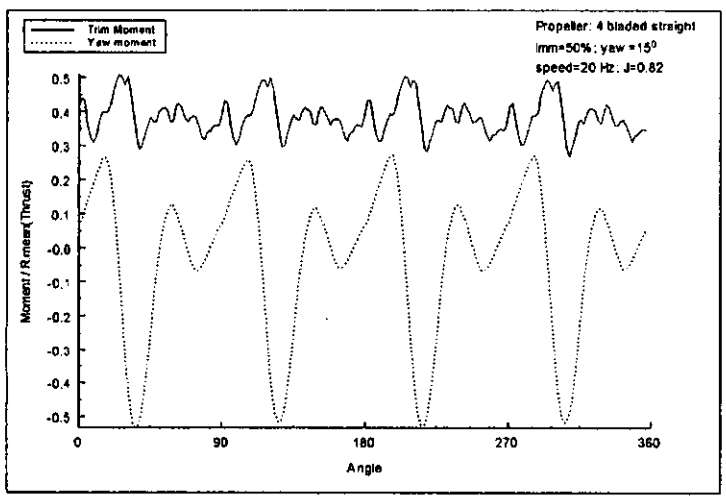

Figure B105

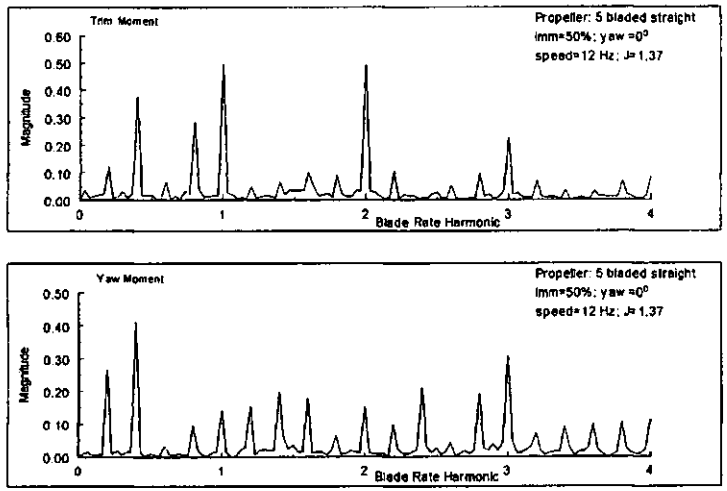

Figure B106

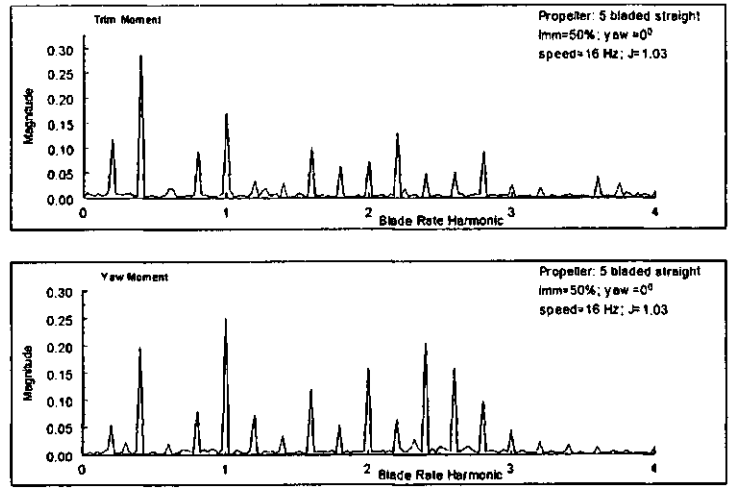

Figure B107

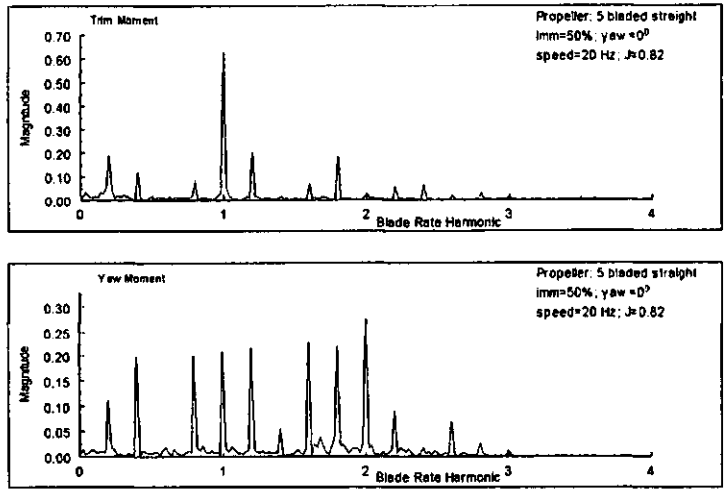

Figure B108

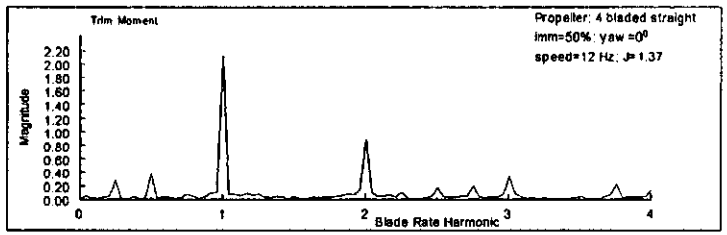

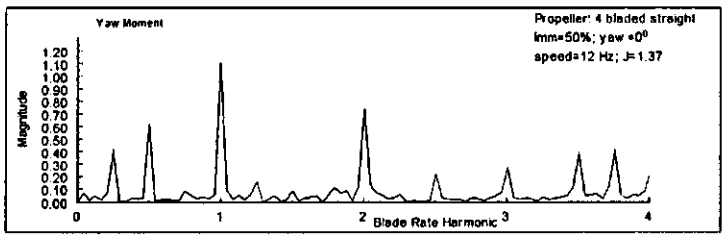

Figure B109

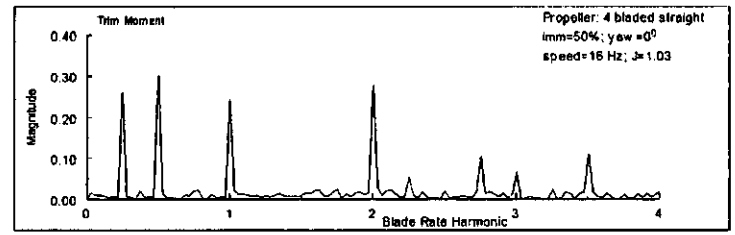

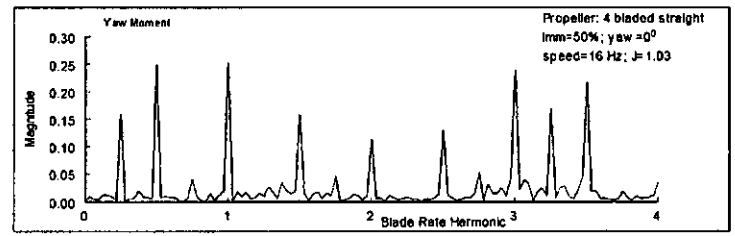

Figure B110

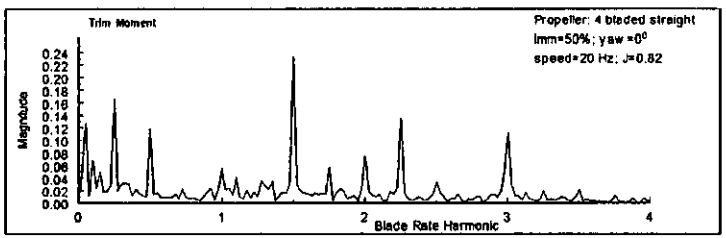

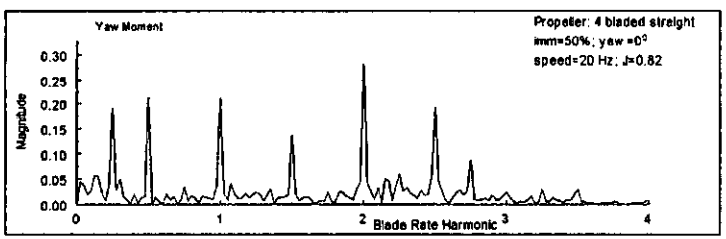

Figure B111

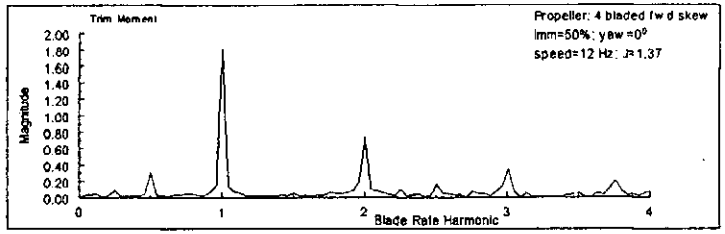

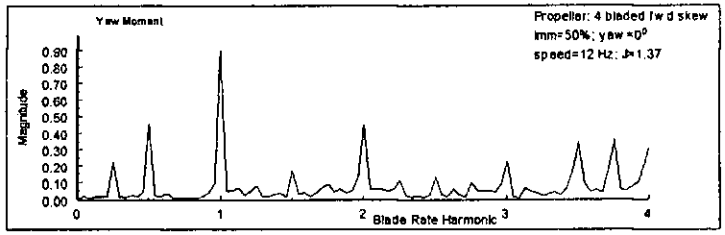

Figure B112

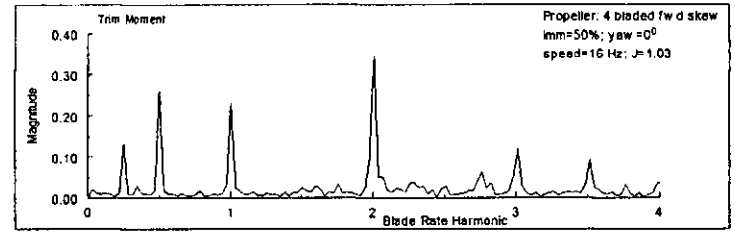

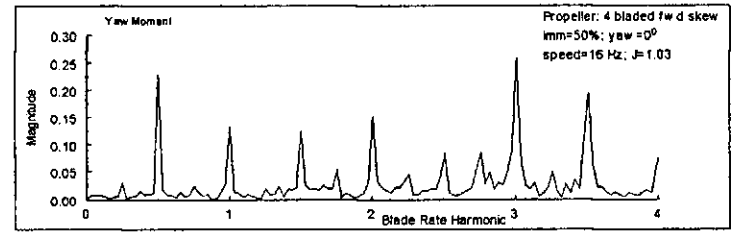

Figure B113

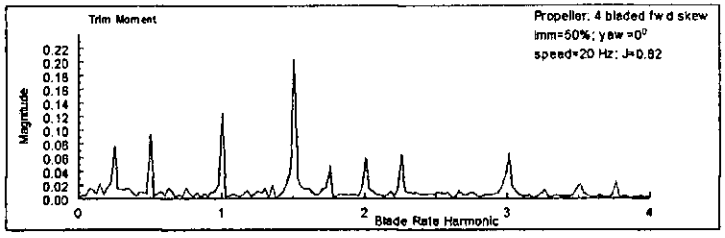

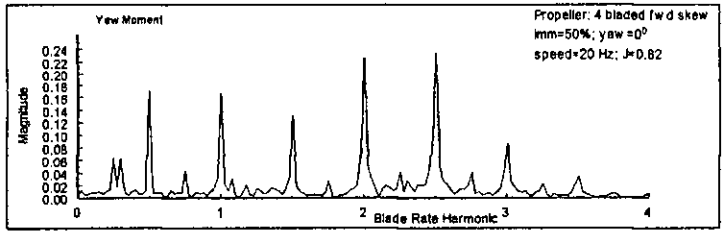

Figure B114

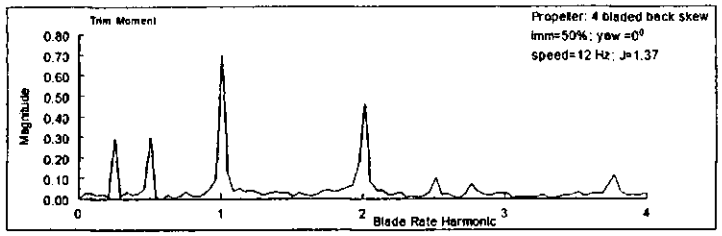

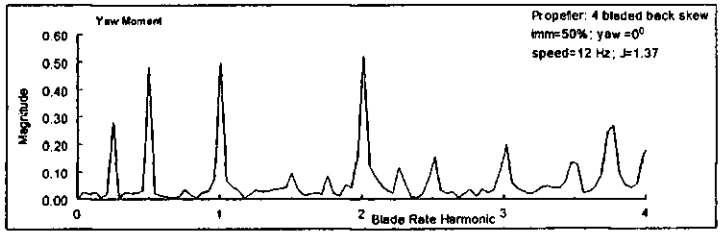

Figure B115

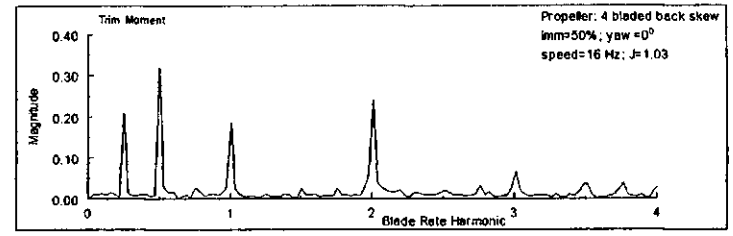

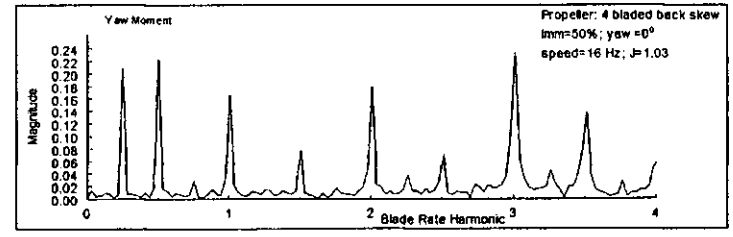

Figure B116

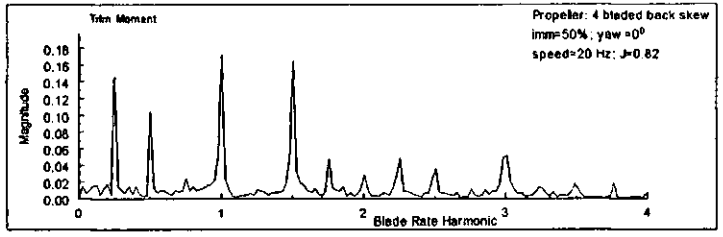

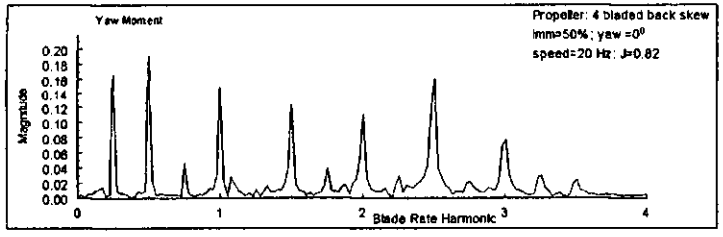

Figure B117

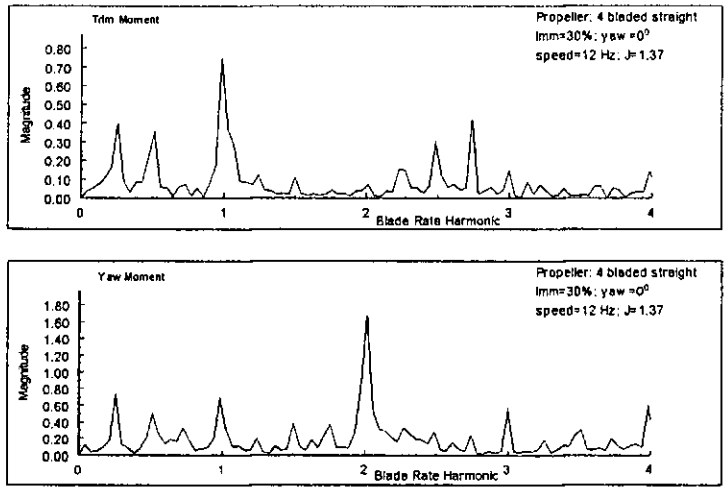

Figure B118

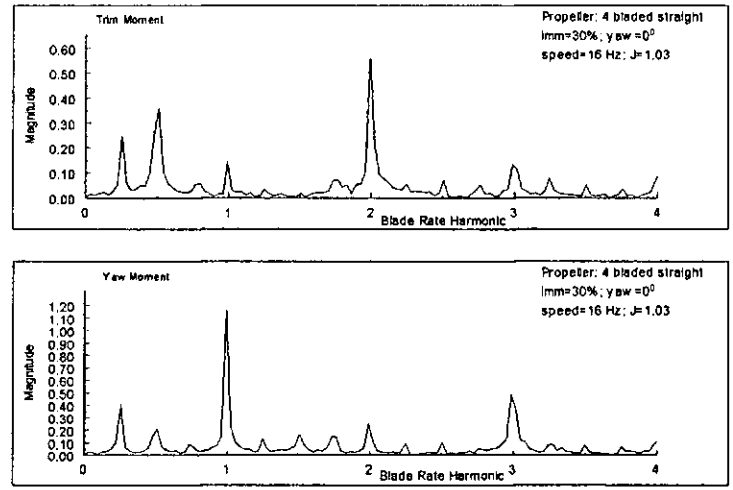

Figure B119

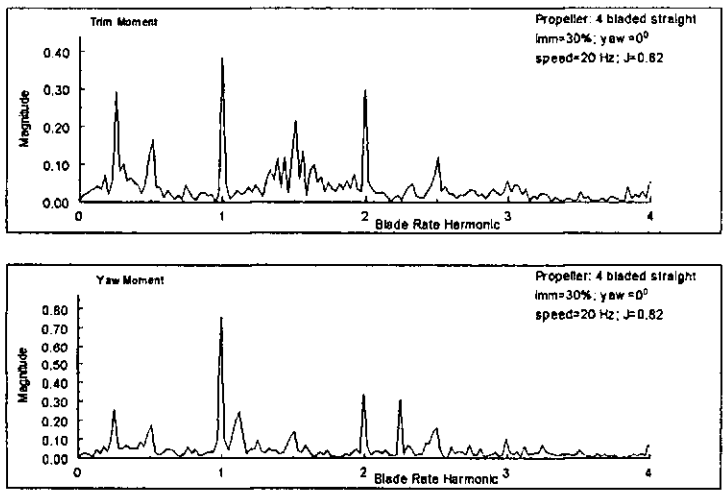

Figure B120

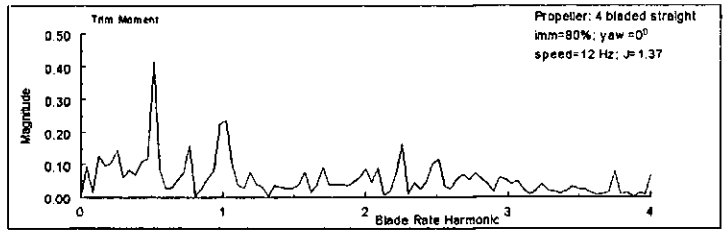

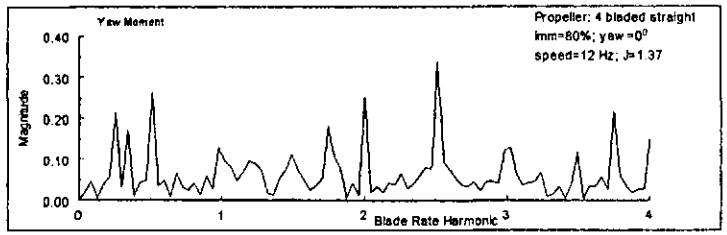

Figure B121

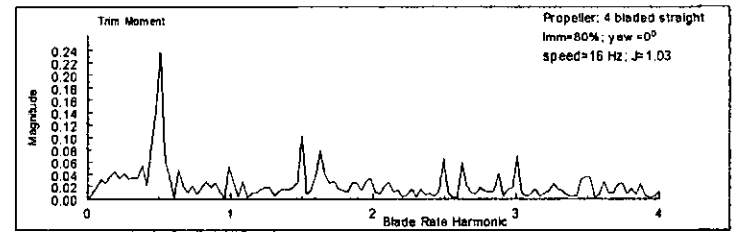

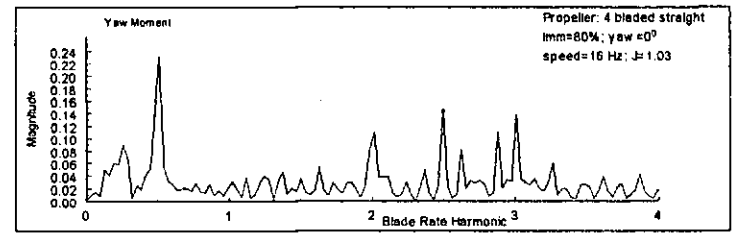

Figure B122

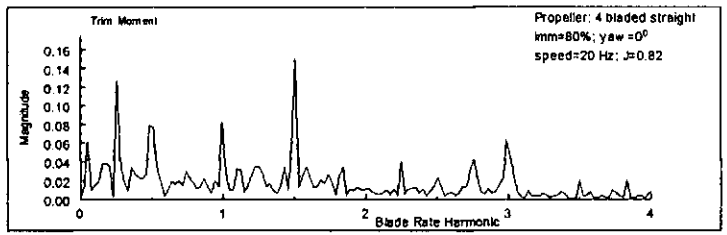

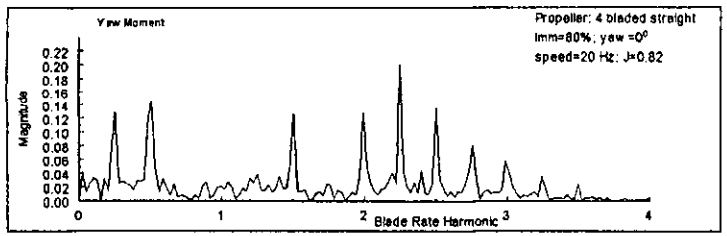

Figure B123

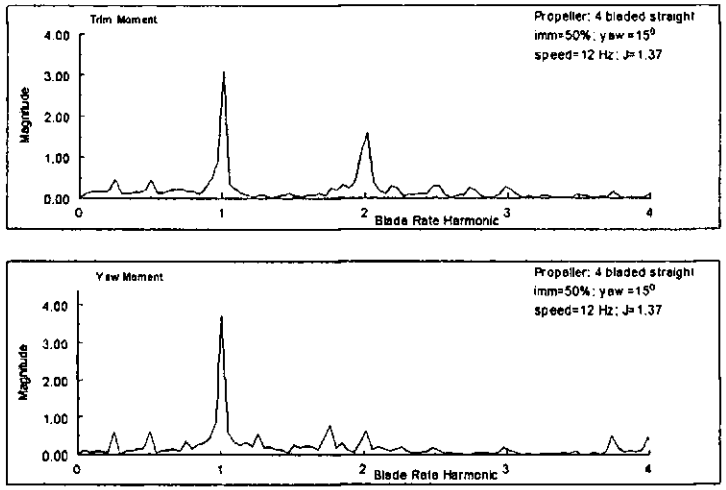

Figure B124

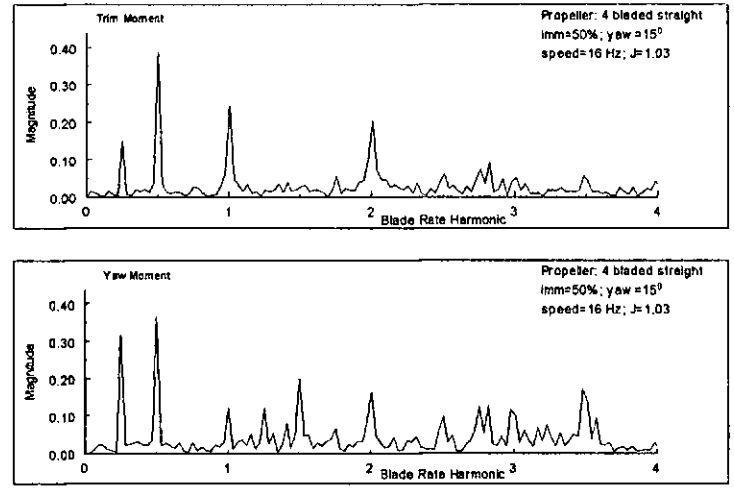

Figure B125

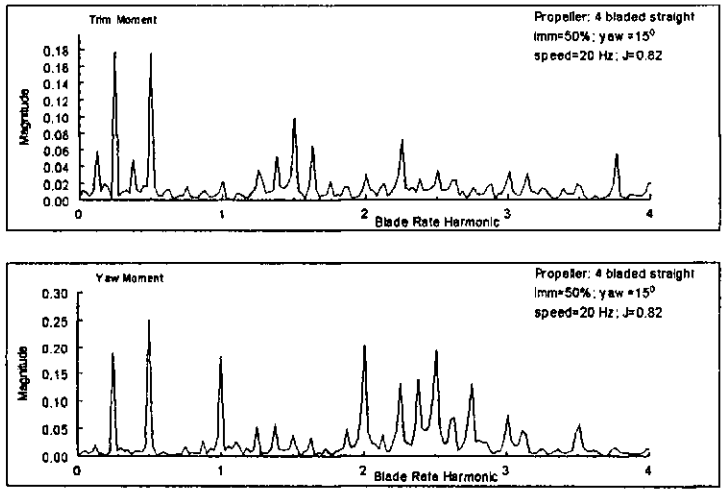

Figure B126

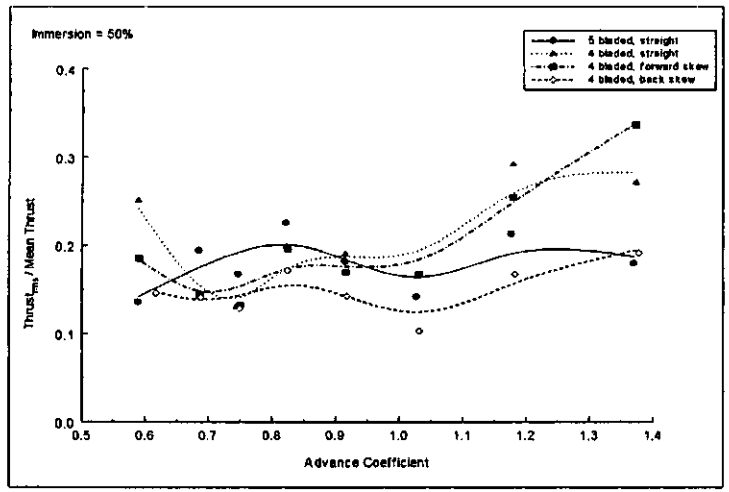

Figure B127

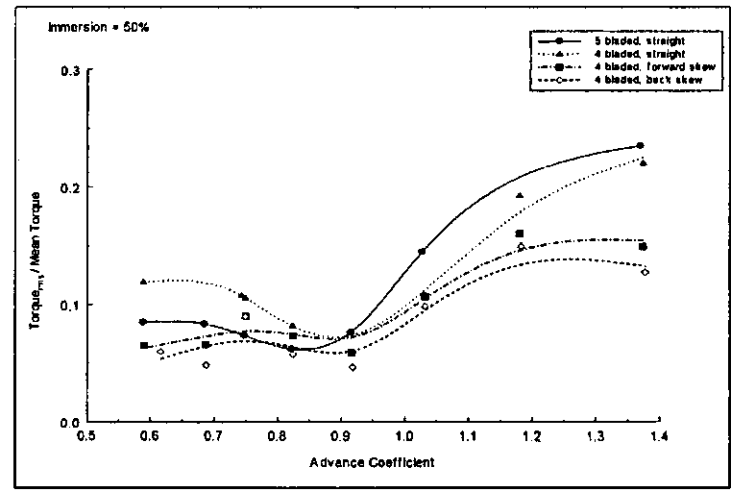

Figure B128

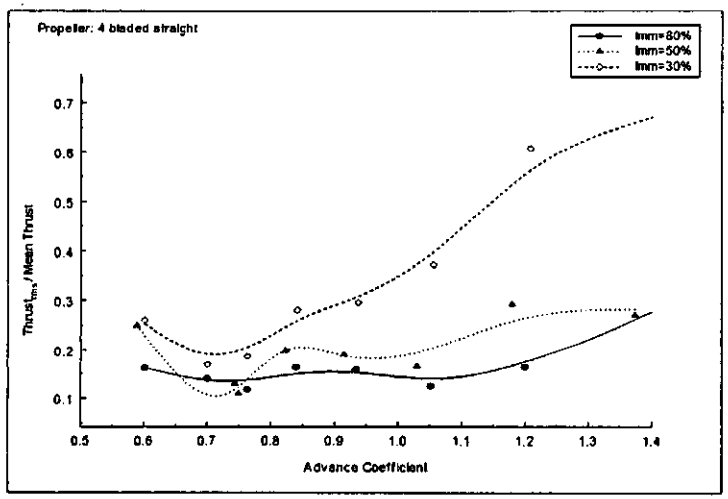

Figure B129

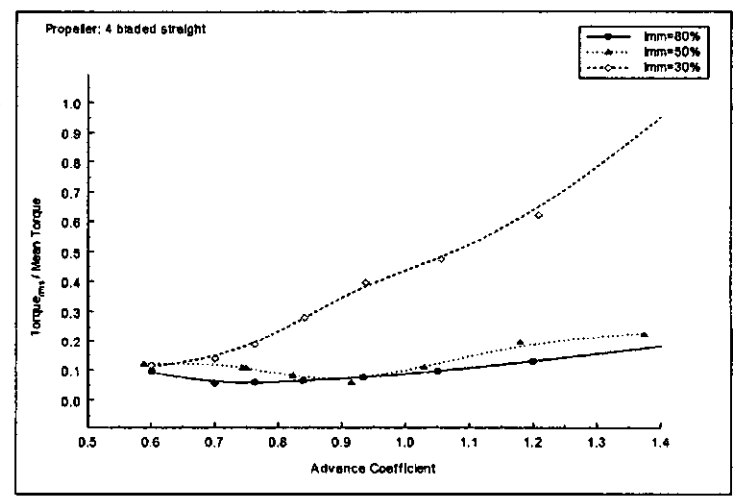

Figure B130

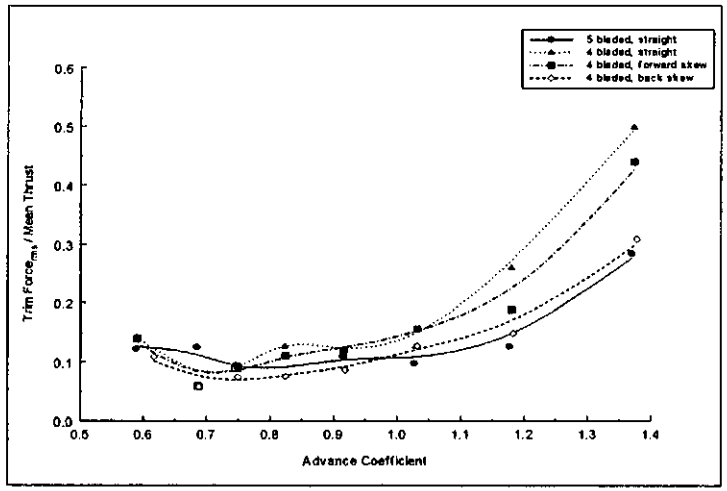

Figure B131

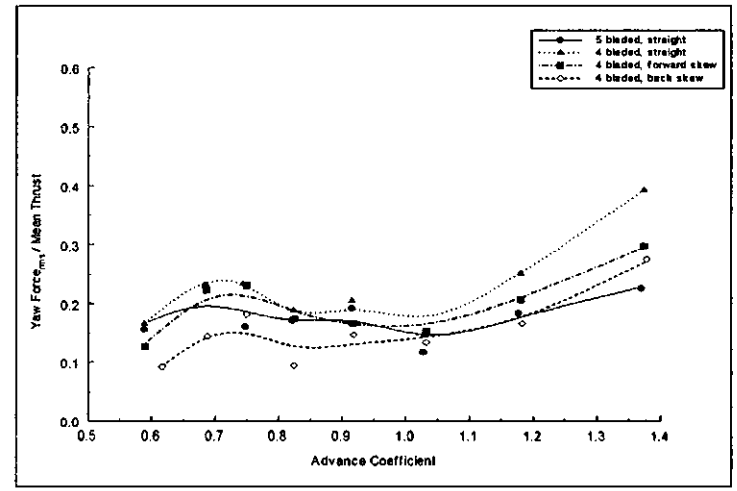

Figure B132

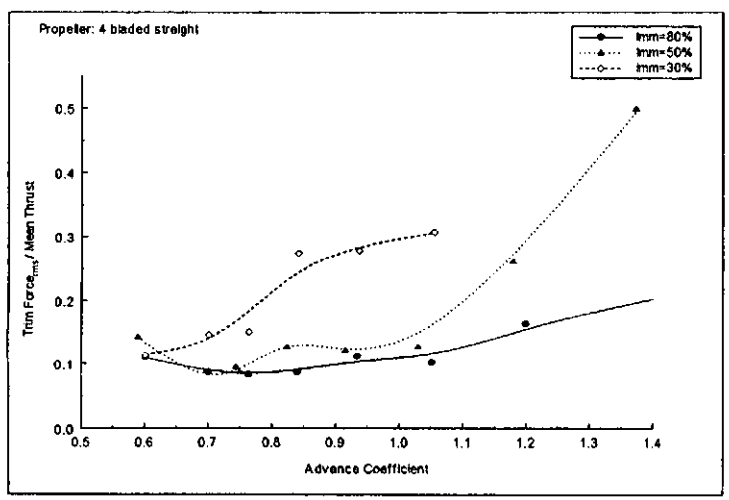

Figure B133

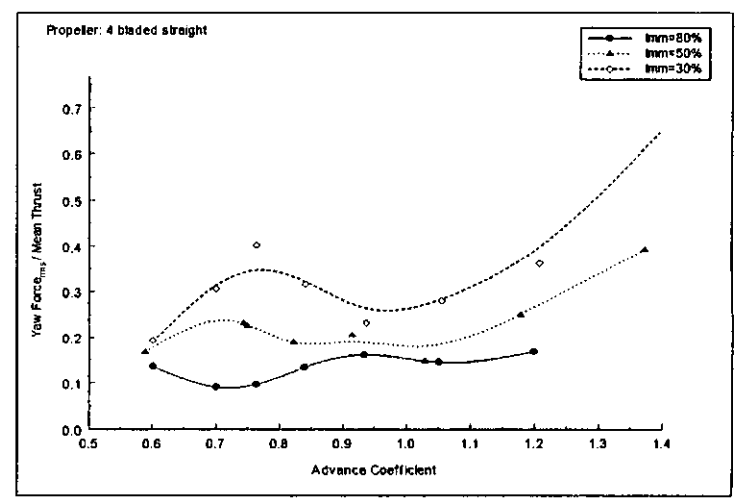

Figure B134

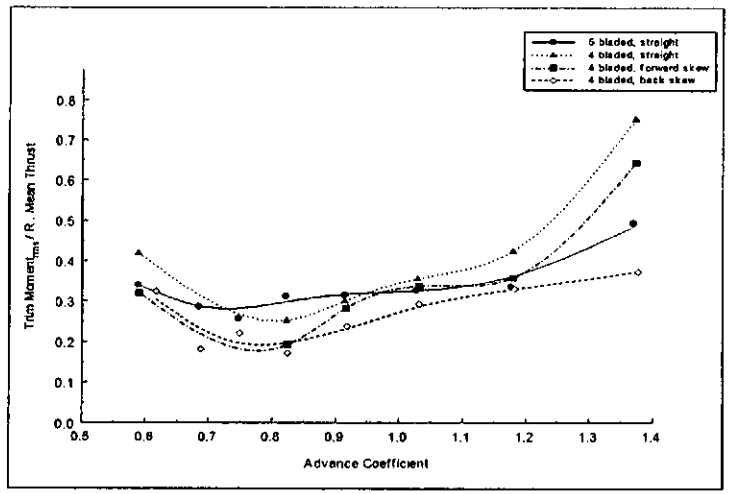

Figure B135

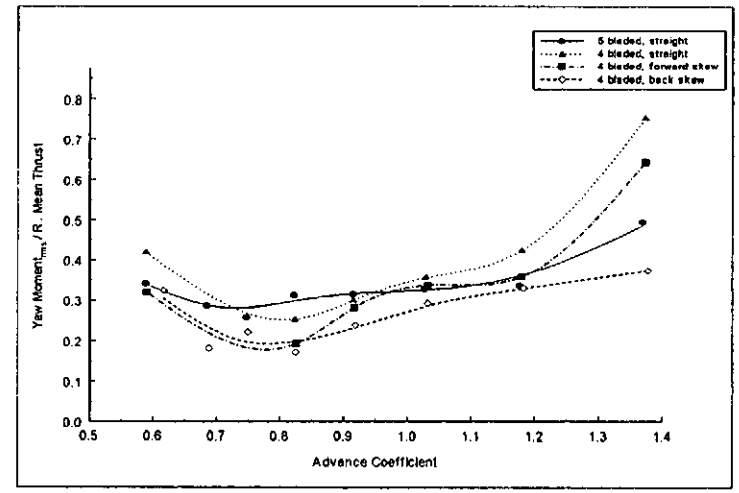

Figure B136

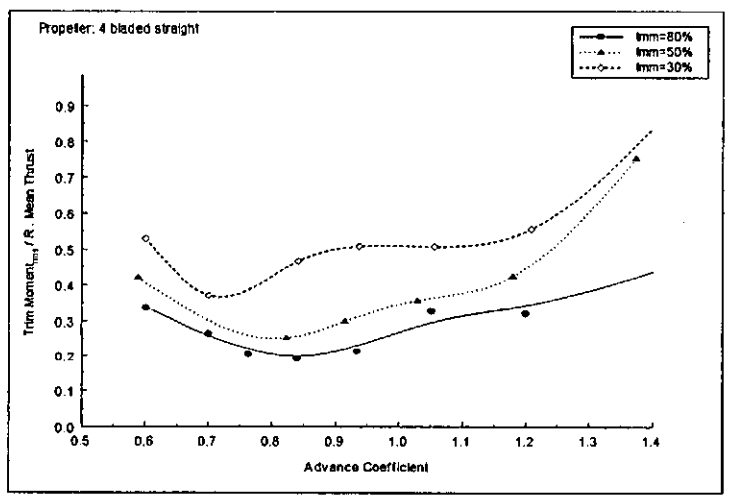

Figure B137

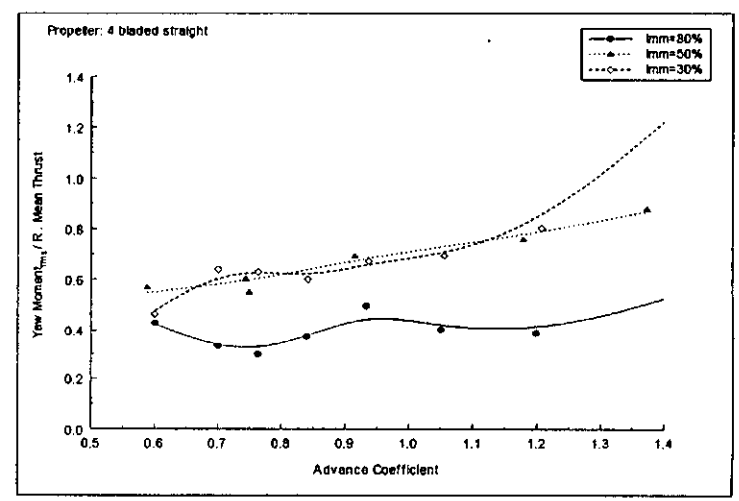

Figure B138

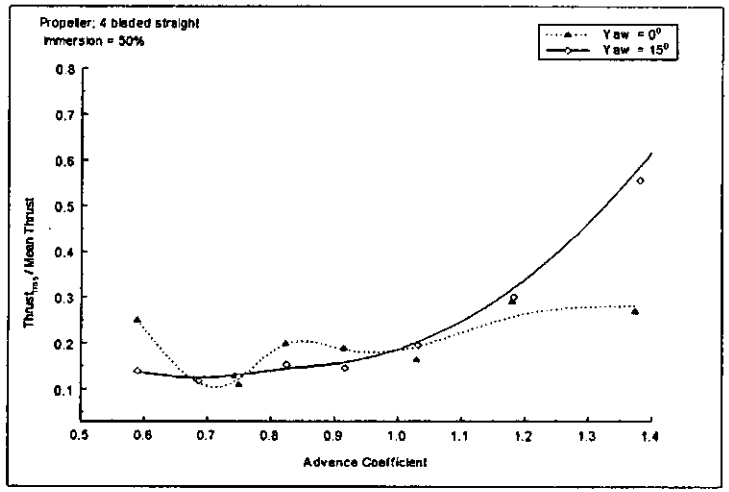

Figure B139

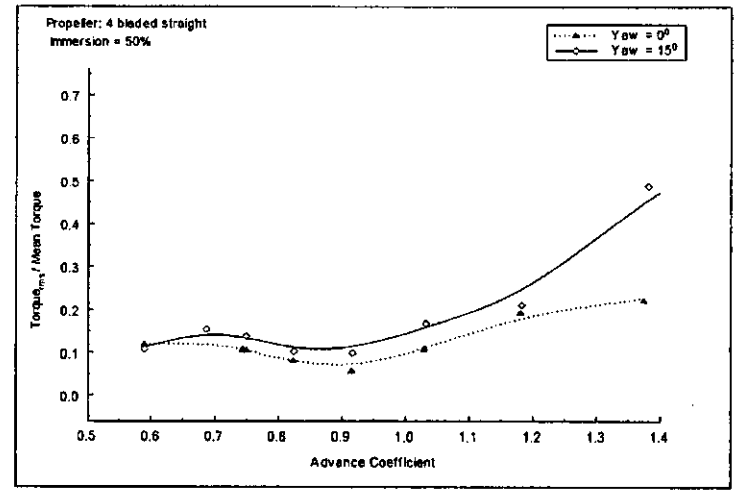

Figure B140

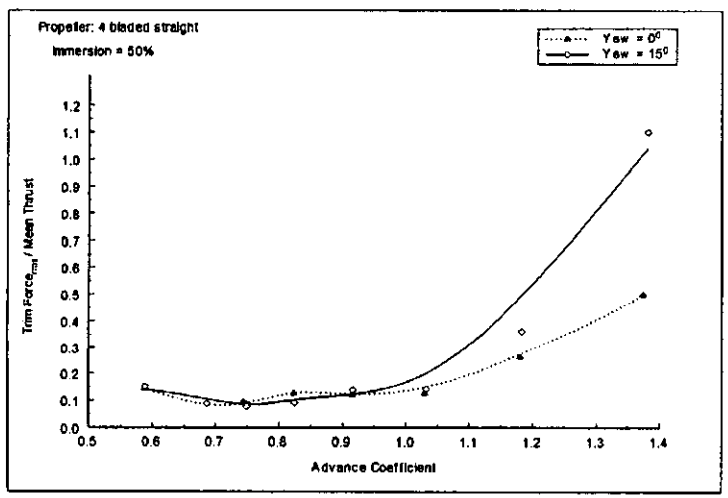

Figure B141

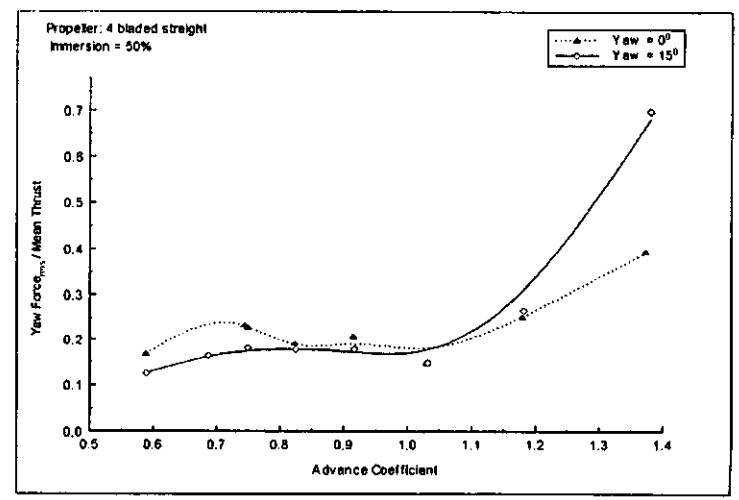

Figure B142

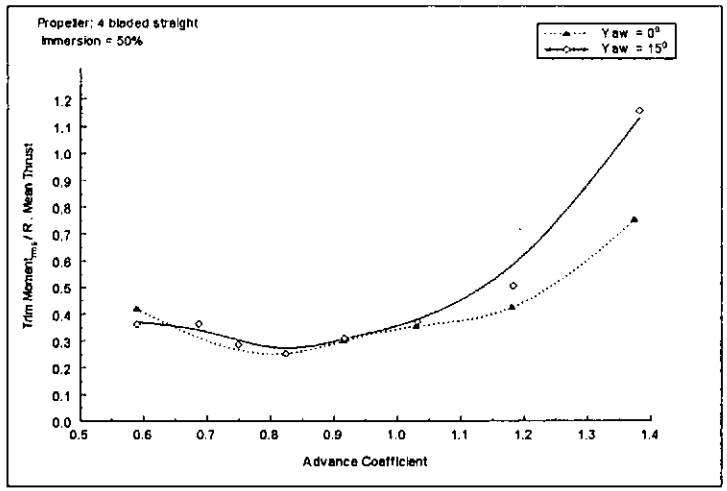

Figure B143

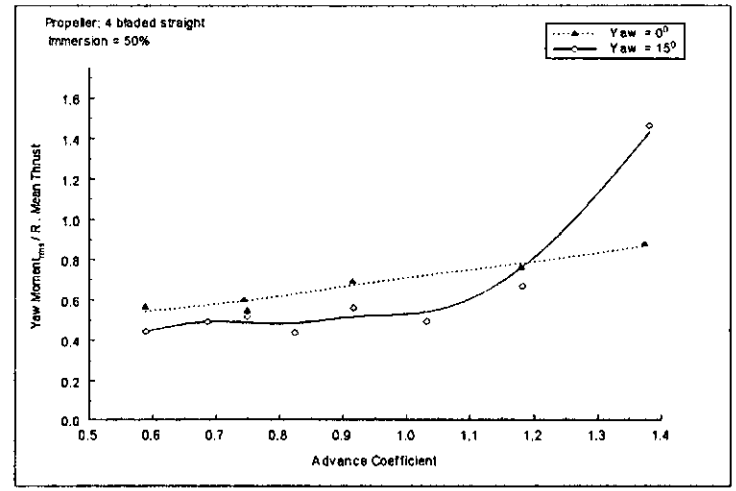

Figure B144

APPENDIX C. ILLUSTRATIONS OF TEST RIG

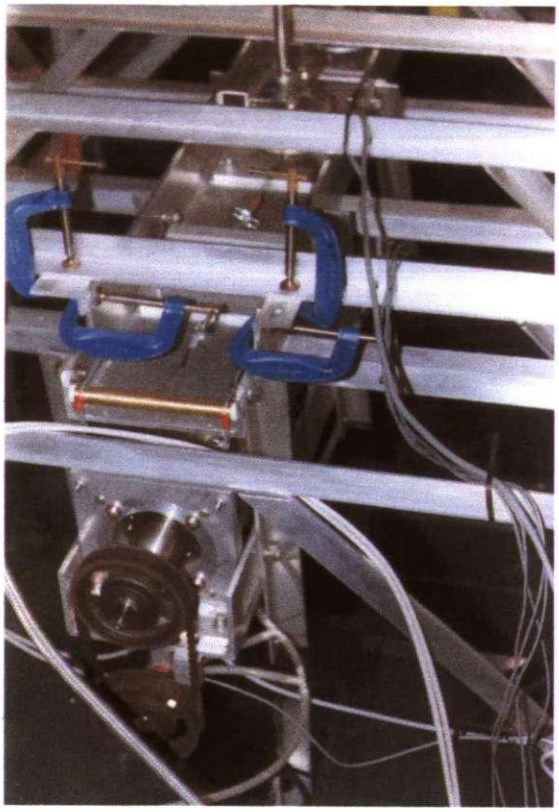

Figure C 1. Upstream View of Test Rig showing Drive from Motor to Propeller Shaft.

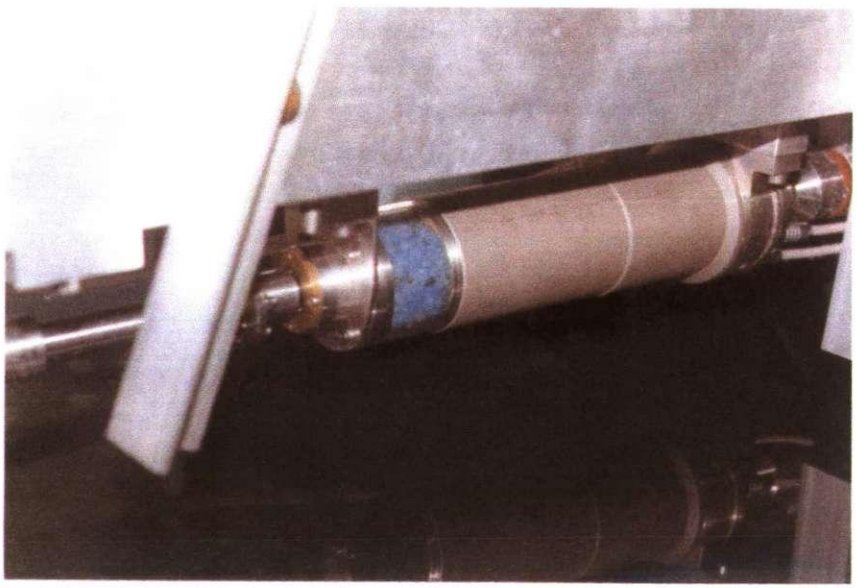

Figure C 2. The Torque - Thrust Dynamometer.

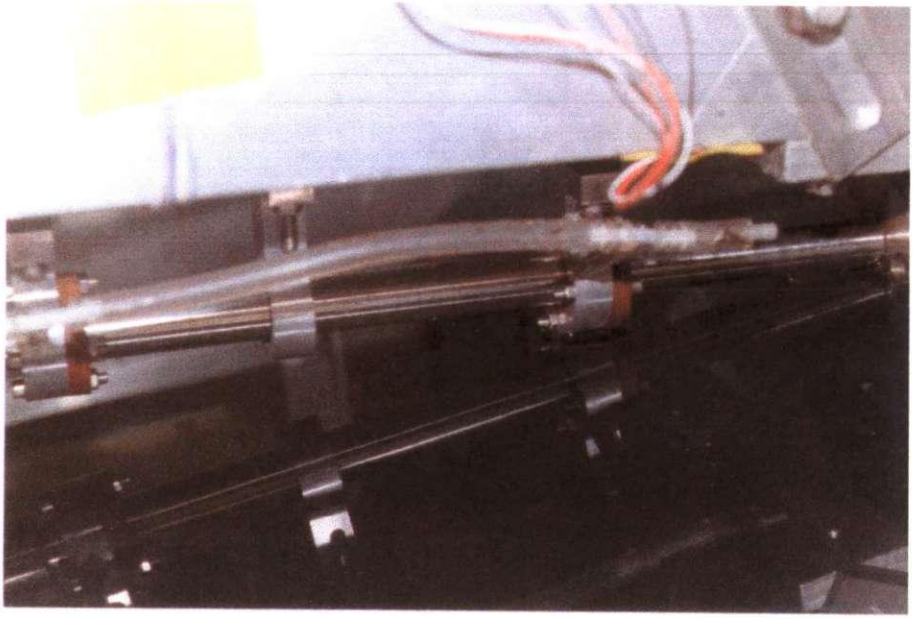

Figure C 3. View of Water Lubricated Bearings.

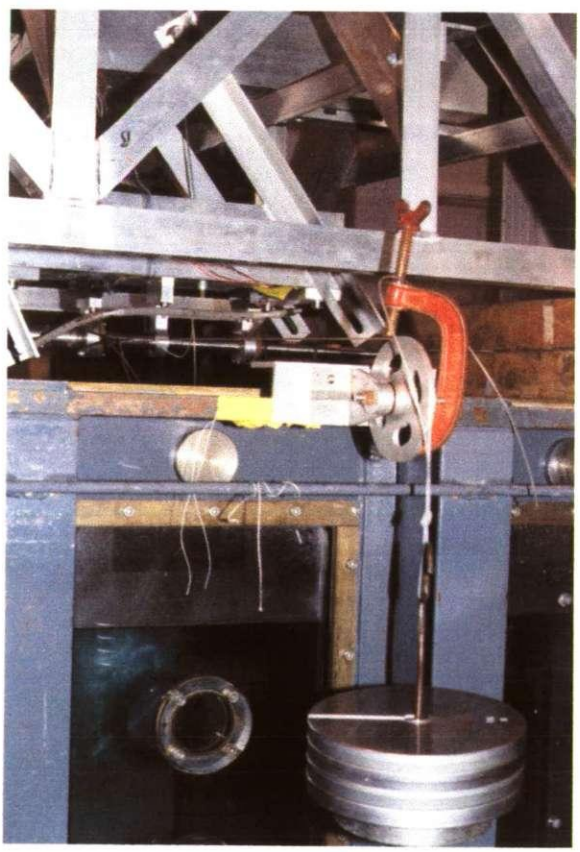

Figure C 4. Calibration of Flexures Using Dead-weights.

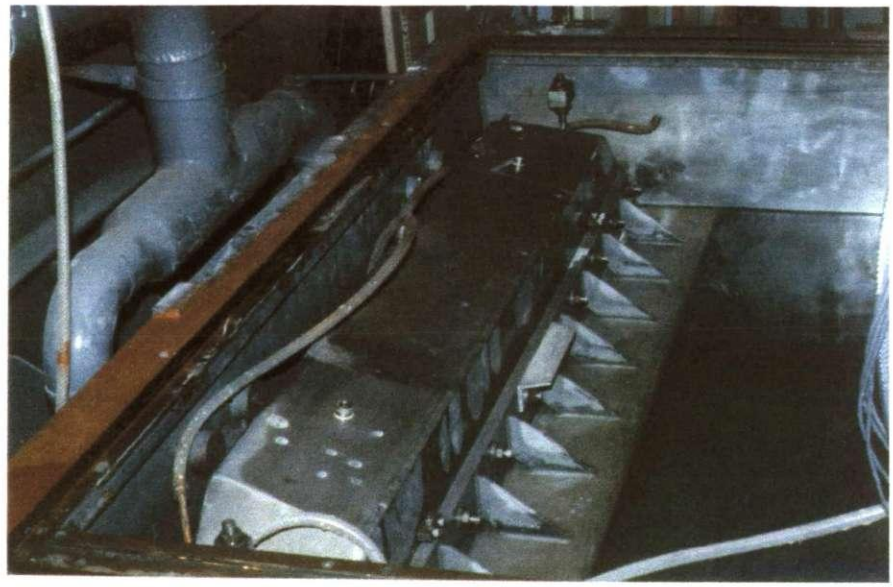

Figure C 5. Injection Manifold Upstream of Working Section to Control Surface Velocity Profile.

Figure C 6. Rig Operating with Hood in Place (Operation is at high load; aeration of water and associated rise of water level above the static value (black mark) can be seen).

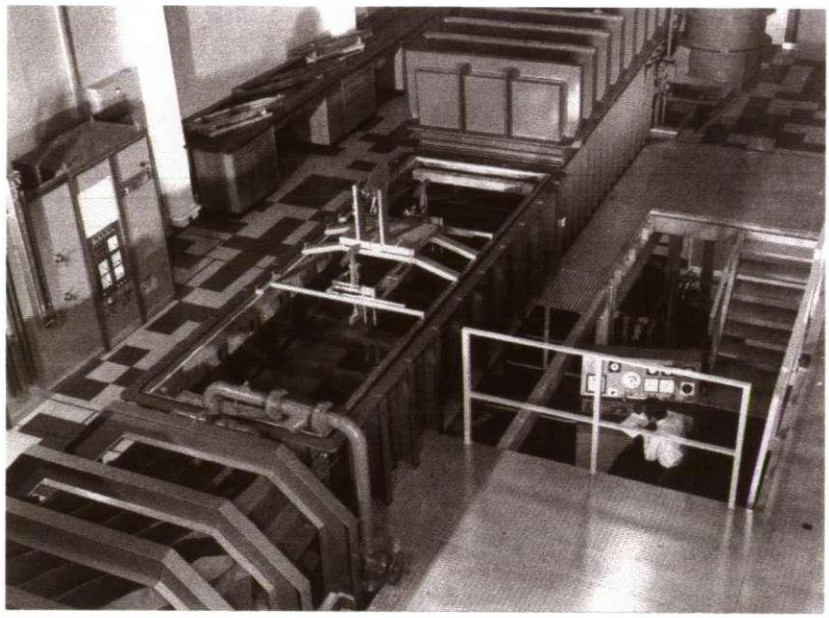

Figure C 7. Overhead View of Circulating Water Channel (Library Picture).

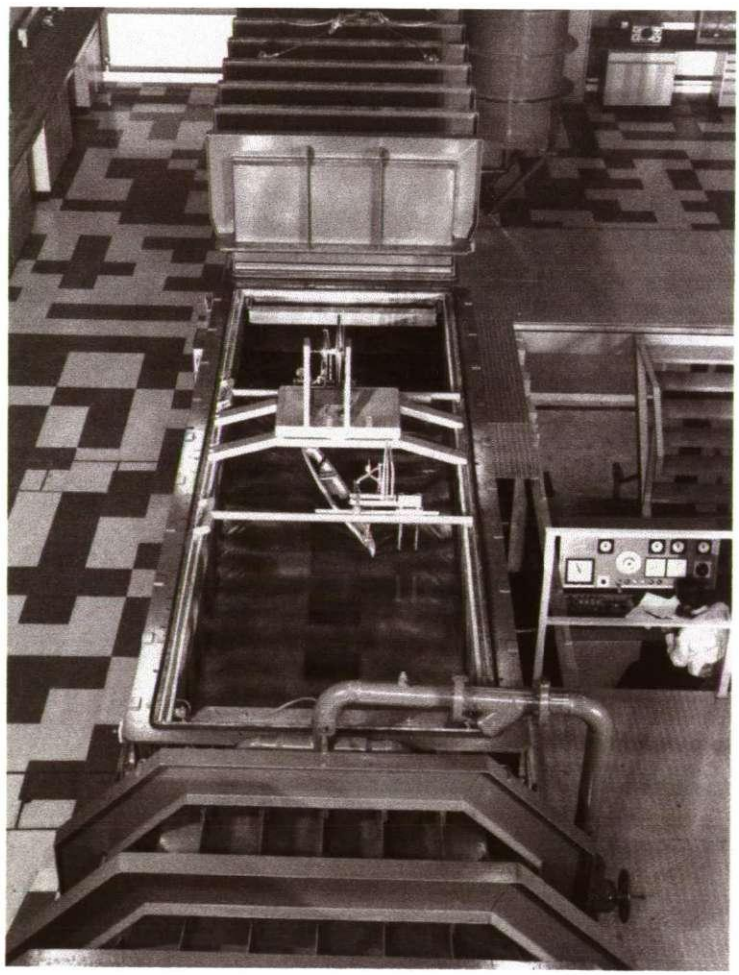

Figure C 8. Overhead View of Circulating Water Channel (Library Picture).

APPENDIX D. TYPICAL PAFEC DATA FILE

```
C ************* SPP 10IN DIA X 15 IN PITCH, 4 BLADED, AL ****
C ****************************** 2D + 3D BLADES **************
C *WITH SHAFT, BRGS AT 0.1815m, 0.4705m, anchored at 0.5305m *
C *LOADED SEQUENTIALLY AT BLADE CENTRES WITH SPREAD SPIKE LOAD *
C
CONTROL
C REACTIONS
FULL.CONTROL
PHASE=1
PHASE=4
BASE=7000000
PHASE=6
PHASE=7
PHASE=9
SKIP.COLLAPSE
CONTROL.END
C
NODES
NODE    AXIS X Y Z
12      1    0 0 0
C
NODES
AXIS=4
NODE,Z,X,Y,THICK
C     Z,R,Theta,Thick
C *************INSIDE BORE*********
8001,0,0.00941,0
8002,-0.00796,0.00941,0
8003,-0.01370,0.00941,0
8004,-0.01931,0.00941,0
8005,-0.02491,0.00941,0
8006,-0.03050,0.00941,0
8007,-0.03611,0.00941,0
8008,-0.04170,0.00941,0
8009,-0.04729,0.00941,0
8010,-0.05289,0.00941,0
8011,-0.065,0.00941,0
C *************OUTSIDE BOSS *****
8501,0,0.018,0
8502,-0.00796,0.018,0
8503,-0.01370,0.018,0
8504,-0.01931,0.018,0
8505,-0.02491,0.018,0
8506,-0.03050,0.018,0
8507,-0.03611,0.018,0
8508,-0.04170,0.018,0
8509,-0.04729,0.018,0
8510,-0.05289,0.018,0
8511,-0.065,0.018,0
C **************BLADE **********
C ******************** Camber Surface **********************
230,-0.00189,0.019,-18.162
231,-0.00796,0.019,-14.785
232,-0.01370,0.019,-8.330
233,-0.01931,0.019,-0.582
234,-0.02491,0.019,7.228
235,-0.03050,0.019,15.099
236,-0.03611,0.019,22.909
237,-0.04170,0.019,30.780
238,-0.04729,0.019,38.713
239,-0.05289,0.019,46.522
240,-0.05852,0.019,54.086
30,-0.00189,0.021,-18.162,0.013
31,-0.00796,0.021,-14.785,0.012
32,-0.01370,0.021,-8.330,0.011
33,-0.01931,0.021,-0.582,0.010
```

D2 to D14

34,-0.02491,0.021,7.228,0.008
35,-0.03050,0.021,15.099,0.007
36,-0.03611,0.021,22.909,0.006
37,-0.04170,0.021,30.780,0.005
38,-0.04729,0.021,38.713,0.003
39,-0.05289,0.021,46.522,0.002
40,-0.05852,0.021,54.086,0.001
50,-0.00241,0.025,-13.371,0.013
51,-0.00855,0.025,-9.412,0.012
52,-0.01428,0.025,-3.186,0.011
53,-0.01984,0.025,3.992,0.010
54,-0.02539,0.025,11.215,0.008
55,-0.03094,0.025,18.483,0.007
56,-0.03649,0.025,25.706,0.006
57,-0.04203,0.025,32.974,0.005
58,-0.04757,0.025,40.288,0.003
59,-0.05312,0.025,47.511,0.002
60,-0.05870,0.025,54.552,0.001
70,-0.00300,0.0375,-7.392,0.011
71,-0.00872,0.0375,-1.881,0.011
72,-0.01416,0.0375,4.324,0.010
73,-0.01960,0.0375,10.532,0.009
74,-0.02502,0.0375,16.768,0.007
75,-0.03047,0.0375,22.956,0.006
76,-0.03589,0.0375,29.191,0.005
77,-0.04133,0.0375,35.399,0.004
78,-0.04676,0.0375,41.625,0.003
79,-0.05219,0.0375,47.851,0.002
80,-0.05770,0.0375,53.892,0.001
90,-0.00318,0.05,-4.404,0.010
91,-0.00910,0.05,0.317,0.009
92,-0.01433,0.05,6.002,0.008
93,-0.01956,0.05,11.687,0.007
94,-0.02476,0.05,17.409,0.006
95,-0.02996,0.05,23.132,0.005
96,-0.03512,0.05,28.911,0.004
97,-0.04025,0.05,34.728,0.003
98,-0.04540,0.05,40.527,0.002
99,-0.05053,0.05,46.344,0.002
100,-0.05569,0.05,52.123,0.001
110,-0.00315,0.0625,-2.797,0.009
111,-0.00878,0.0625,1.714,0.007
112,-0.01374,0.0625,6.811,0.006
113,-0.01869,0.0625,11.922,0.006
114,-0.02359,0.0625,17.074,0.005
115,-0.02846,0.0625,22.253,0.004
116,-0.03326,0.0625,27.500,0.003
117,-0.03803,0.0625,32.761,0.003
118,-0.04274,0.0625,38.090,0.002
119,-0.04739,0.0625,43.460,0.001
120,-0.05209,0.0625,48.789,0.001
130,-0.00290,0.075,-1.786,0.007
131,-0.00812,0.075,2.304,0.006
132,-0.01276,0.075,6.754,0.005
133,-0.01732,0.075,11.254,0.004
134,-0.02178,0.075,15.816,0.004
135,-0.02617,0.075,20.420,0.003
136,-0.03046,0.075,25.084,0.003
137,-0.03472,0.075,29.770,0.002
138,-0.03886,0.075,34.527,0.002
139,-0.04301,0.075,39.284,0.001
140,-0.04708,0.075,44.082,0.001
150,-0.00252,0.0875,-1.139,0.006
151,-0.00738,0.0875,2.313,0.005
152,-0.01139,0.0875,6.156,0.005
153,-0.01536,0.0875,10.015,0.004

```
154,-0.01920,0.0875,13.930,0.004
155,-0.02302,0.0875,17.861,0.003
156,-0.02669,0.0875,21.855,0.003
157,-0.03028,0.0875,25.881,0.002
158,-0.03381,0.0875,29.939,0.002
159,-0.03731,0.0875,34.013,0.001
160,-0.04075,0.0875,38.111,0.001
170,-0.00205,0.1,-0.711,0.005
171,-0.00597,0.1,2.173,0.003
172,-0.00938,0.1,5.234,0.003
173,-0.01264,0.1,8.346,0.003
174,-0.01586,0.1,11.470,0.002
175,-0.01894,0.1,14.646,0.002
176,-0.02194,0.1,17.847,0.002
177,-0.02485,0.1,21.079,0.001
178,-0.02769,0.1,24.337,0.001
179,-0.03042,0.1,27.633,0.001
180,-0.03315,0.1,30.929,0.001
190,-0.00156,0.1125,-0.428,0.004
191,-0.00449,0.1125,1.493,0.002
192,-0.00680,0.1125,3.584,0.002
193,-0.00901,0.1125,5.701,0.002
194,-0.01118,0.1125,7.828,0.002
195,-0.01328,0.1125,9.976,0.002
196,-0.01526,0.1125,12.156,0.001
197,-0.01721,0.1125,14.345,0.001
198,-0.01906,0.1125,16.560,0.001
199,-0.02087,0.1125,18.785,0.001
200,-0.02267,0.1125,21.016,0.001
210,0.00000,0.125,0.000,0.002
211,-0.00227,0.12375,2.102,0.002
212,-0.00453,0.1225,4.203,0.002
213,-0.00680,0.12125,6.305,0.002
214,-0.00907,0.12,8.406,0.001
215,-0.01133,0.11875,10.508,0.001
216,-0.01360,0.1175,12.610,0.001
217,-0.01587,0.11625,14.711,0.001
218,-0.01814,0.115,16.813,0.001
219,-0.02040,0.11375,18.914,0.001
C ************Face ********************
3230,0.00000,0.019,6.000
3231,-0.00617,0.019,8.330
3232,-0.01204,0.019,13.616
3233,-0.01784,0.019,19.517
3234,-0.02364,0.019,25.418
3235,-0.02943,0.019,31.442
3236,-0.03523,0.019,37.343
3237,-0.04101,0.019,43.368
3238,-0.04680,0.019,49.392
3239,-0.05260,0.019,55.293
3240,-0.05839,0.019,61.317
3030,0.00000,0.021,0.000
3031,-0.00617,0.021,2.330
3032,-0.01204,0.021,7.616
3033,-0.01784,0.021,13.517
3034,-0.02364,0.021,19.418
3035,-0.02943,0.021,25.442
3036,-0.03523,0.021,31.343
3037,-0.04101,0.021,37.368
3038,-0.04680,0.021,43.392
3039,-0.05260,0.021,49.293
3040,-0.05839,0.021,55.317
3050,0.00000,0.025,0.000
3051,-0.00628,0.025,3.189
3052,-0.01217,0.025,8.554
3053,-0.01797,0.025,14.371
```

3054,-0.02378,0.025,20.189
3055,-0.02956,0.025,26.098
3056,-0.03537,0.025,31.915
3057,-0.04116,0.025,37.824
3058,-0.04695,0.025,43.732
3059,-0.05275,0.025,49.550
3060,-0.05854,0.025,55.459
3070,0.00000,0.038,0.000
3071,-0.00587,0.038,5.150
3072,-0.01161,0.038,10.604
3073,-0.01734,0.038,16.090
3074,-0.02307,0.038,21.575
3075,-0.02881,0.038,27.041
3076,-0.03454,0.038,32.526
3077,-0.04027,0.038,38.012
3078,-0.04601,0.038,43.487
3079,-0.05174,0.038,48.962
3080,-0.05747,0.038,54.448
3090,0.00000,0.050,0.000
3091,-0.00633,0.050,4.154
3092,-0.01185,0.050,9.442
3093,-0.01736,0.050,14.730
3094,-0.02285,0.050,20.055
3095,-0.02834,0.050,25.381
3096,-0.03377,0.050,30.782
3097,-0.03920,0.050,36.184
3098,-0.04463,0.050,41.585
3099,-0.05004,0.050,47.024
3100,-0.05542,0.050,52.501
3110,0.00000,0.063,0.000
3111,-0.00626,0.063,3.951
3112,-0.01150,0.063,8.803
3113,-0.01670,0.063,13.682
3114,-0.02185,0.063,18.615
3115,-0.02697,0.063,23.576
3116,-0.03203,0.063,28.591
3117,-0.03705,0.063,33.634
3118,-0.04201,0.063,38.731
3119,-0.04692,0.063,43.883
3120,-0.05179,0.063,49.062
3130,0.00000,0.075,0.000
3131,-0.00597,0.075,3.628
3132,-0.01082,0.075,7.954
3133,-0.01559,0.075,12.322
3134,-0.02026,0.075,16.750
3135,-0.02487,0.075,21.220
3136,-0.02938,0.075,25.751
3137,-0.03386,0.075,30.303
3138,-0.03820,0.075,34.937
3139,-0.04254,0.075,39.571
3140,-0.04675,0.075,44.287
3150,0.00000,0.088,0.000
3151,-0.00531,0.088,3.253
3152,-0.00952,0.088,7.001
3153,-0.01370,0.088,10.764
3154,-0.01774,0.088,14.591
3155,-0.02175,0.088,18.434
3156,-0.02561,0.088,22.341
3157,-0.02944,0.088,26.264
3158,-0.03316,0.088,30.234
3159,-0.03685,0.088,34.221
3160,-0.04040,0.088,38.271
3170,0.00000,0.100,0.000
3171,-0.00456,0.100,2.661
3172,-0.00809,0.100,5.678
3173,-0.01148,0.100,8.746

```
3174,-0.01483,0.100,11.826
3175,-0.01804,0.100,14.957
3176,-0.02117,0.100,18.113
3177,-0.02423,0.100,21.295
3178,-0.02718,0.100,24.514
3179,-0.03002,0.100,27.772
3180,-0.03278,0.100,31.056
3190,0.00000,0.113,0.000
3191,-0.00347,0.113,1.771
3192,-0.00585,0.113,3.842
3193,-0.00816,0.113,5.933
3194,-0.01042,0.113,8.035
3195,-0.01258,0.113,10.167
3196,-0.01466,0.113,12.321
3197,-0.01670,0.113,14.484
3198,-0.01863,0.113,16.679
3199,-0.02052,0.113,18.884
3200,-0.02229,0.113,21.119
C ****************** BACK ******************************
6230,-0.00378,0.019,-42.324
6231,-0.00974,0.019,-37.901
6232,-0.01536,0.019,-30.276
6233,-0.02078,0.019,-20.681
6234,-0.02618,0.019,-10.962
6235,-0.03158,0.019,-2.756
6236,-0.03698,0.019,8.474
6237,-0.04239,0.019,18.192
6238,-0.04778,0.019,28.034
6239,-0.05318,0.019,37.752
6240,-0.05865,0.019,46.855
6030,-0.00378,0.021,-36.324
6031,-0.00974,0.021,-31.901
6032,-0.01536,0.021,-24.276
6033,-0.02078,0.021,-14.681
6034,-0.02618,0.021,-4.962
6035,-0.03158,0.021,4.756
6036,-0.03698,0.021,14.474
6037,-0.04239,0.021,24.192
6038,-0.04778,0.021,34.034
6039,-0.05318,0.021,43.752
6040,-0.05865,0.021,52.855
6050,-0.00482,0.025,-26.742
6051,-0.01082,0.025,-22.012
6052,-0.01640,0.025,-14.925
6053,-0.02171,0.025,-6.388
6054,-0.02701,0.025,2.240
6055,-0.03231,0.025,10.868
6056,-0.03761,0.025,19.496
6057,-0.04291,0.025,28.124
6058,-0.04819,0.025,36.843
6059,-0.05349,0.025,45.471
6060,-0.05887,0.025,53.646
6070,-0.00600,0.038,-14.783
6071,-0.01157,0.038,-8.911
6072,-0.01671,0.038,-1.956
6073,-0.02185,0.038,4.975
6074,-0.02697,0.038,11.961
6075,-0.03213,0.038,18.871
6076,-0.03725,0.038,25.857
6077,-0.04239,0.038,32.787
6078,-0.04752,0.038,39.763
6079,-0.05264,0.038,46.739
6080,-0.05792,0.038,53.336
6090,-0.00635,0.050,-8.807
6091,-0.01187,0.050,-3.519
6092,-0.01681,0.050,2.562
```

```
6093,-0.02175,0.050,8.644
6094,-0.02667,0.050,14.763
6095,-0.03158,0.050,20.883
6096,-0.03647,0.050,27.040
6097,-0.04130,0.050,33.273
6098,-0.04616,0.050,39.468
6099,-0.05102,0.050,45.663
6100,-0.05596,0.050,51.745
6110,-0.00631,0.063,-5.593
6111,-0.01130,0.063,-0.523
6112,-0.01599,0.063,4.819
6113,-0.02067,0.063,10.162
6114,-0.02533,0.063,15.532
6115,-0.02995,0.063,20.929
6116,-0.03449,0.063,26.408
6117,-0.03902,0.063,31.887
6118,-0.04346,0.063,37.448
6119,-0.04787,0.063,43.037
6120,-0.05240,0.063,48.516
6130,-0.00580,0.075,-3.571
6131,-0.01027,0.075,0.981
6132,-0.01471,0.075,5.553
6133,-0.01906,0.075,10.187
6134,-0.02330,0.075,14.883
6135,-0.02747,0.075,19.619
6136,-0.03155,0.075,24.417
6137,-0.03559,0.075,29.236
6138,-0.03953,0.075,34.116
6139,-0.04347,0.075,38.996
6140,-0.04741,0.075,43.877
6150,-0.00503,0.088,-2.279
6151,-0.00946,0.088,1.373
6152,-0.01326,0.088,5.312
6153,-0.01701,0.088,9.266
6154,-0.02067,0.088,13.269
6155,-0.02428,0.088,17.287
6156,-0.02776,0.088,21.369
6157,-0.03113,0.088,25.499
6158,-0.03447,0.088,29.645
6159,-0.03777,0.088,33.806
6160,-0.04110,0.088,37.952
6170,-0.00410,0.100,-1.421
6171,-0.00738,0.100,1.684
6172,-0.01066,0.100,4.790
6173,-0.01379,0.100,7.946
6174,-0.01688,0.100,11.115
6175,-0.01983,0.100,14.335
6176,-0.02271,0.100,17.580
6177,-0.02547,0.100,20.863
6178,-0.02820,0.100,24.159
6179,-0.03082,0.100,27.493
6180,-0.03351,0.100,30.802
6190,-0.00313,0.113,-0.857
6191,-0.00551,0.113,1.214
6192,-0.00774,0.113,3.326
6193,-0.00985,0.113,5.469
6194,-0.01193,0.113,7.622
6195,-0.01397,0.113,9.786
6196,-0.01586,0.113,11.990
6197,-0.01772,0.113,14.206
6198,-0.01949,0.113,16.441
6199,-0.02123,0.113,18.687
6200,-0.02305,0.113,20.913
C ******************** Centre line ************************
1,0,0,0
2,-0.00796,0,0
```

```
3,-0.01370,0,0
4,-0.01931,0,0
5,-0.02491,0,0
6,-0.03050,0,0
7,-0.03611,0,0
8,-0.04170,0,0
9,-0.04729,0,0
10,-0.05289,0,0
11,-.065,0,0
C
C *********** SHAFT **********
C
2311,-0.156
2312,-0.247
R4 1,-0.0723
2317,-0.566
2318,-0.596
C
C
AXES
AXISNO  RELAX  TYPE  NODE  ANG1  ANG2  ANG3
11      4      4     1     30    0     0
R10 1     0      0     0     30    0     0
C
C
SIMILAR.NODES
ORIGINAL.NODE  NUMBER.OF.NODES  COPY.NODE  AXIS.OF.NEW.NODES
C
C *******   BLADES   ***********
C ************CAMBER LINE **************
230              11              730        13
30              11              530        13
R8 20             0              20         0
210             10              710        13
C
230              11              1230        16
30              11              1030        16
R8 20             0              20         0
210             10              1210        16
C
230              11              1730        19
30              11              1530        19
R8 20             0              20         0
210             10              1710        19
C
C *****************FACE *************
C
3230              11              3730        13
3030              11              3530        13
R8 20             0               20         0
C
3230              11              4230        16
3030              11              4030        16
R8 20             0               20         0
C
3230              11              4730        19
3030              11              4530        19
R8 20             0               20         0
C
C ********************BACK*****************
C
6230              11              6730        13
6030              11              6530        13
R8 20               0               20          0
C
6230              11              7230        16
```

```
6030                11              7030          16
R8 20                 0                20           0
C
6230                11              7730          19
6030                11              7530          19
R8 20                 0                20           0
C ********     BOSS      **********
C
8001                11              8021          11
R10 0                 0                20           1
8501                11              8521          11
R10 0                 0                20           1
C
C **********BLADE 1 ELEMENTS ********
C *************** 3D BRICK *******
C
ELEMENTS
GROUP=1
PROPS=11
ELEMENT=37110
NUMB,TOPO
101,3230,6230,3030,6030,3231,6231,3031,6031,0,0,0,30,0,0,0,0,0,0,0,31
R9 1    1     1     1     1     1     1     1     1 0 0 0  1 0 0 0 0 0 0 0  1
11,3030,6030,3050,6050,3031,6031,3051,6051,30,0,0,50,0,0,0,0,31,0,0,51
12,3031,6031,3051,6051,3032,6032,3052,6052,31,0,0,51,0,0,0,0,32,0,0,52
13,3032,6032,3052,6052,3033,6033,3053,6053,32,0,0,52,0,0,0,0,33,0,0,53
14,3033,6033,3053,6053,3034,6034,3054,6054,33,0,0,53,0,0,0,0,34,0,0,54
15,3034,6034,3054,6054,3035,6035,3055,6055,34,0,0,54,0,0,0,0,35,0,0,55
16,3035,6035,3055,6055,3036,6036,3056,6056,35,0,0,55,0,0,0,0,36,0,0,56
17,3036,6036,3056,6056,3037,6037,3057,6057,36,0,0,56,0,0,0,0,37,0,0,57
18,3037,6037,3057,6057,3038,6038,3058,6058,37,0,0,57,0,0,0,0,38,0,0,58
C
21,3050,6050,3070,6070,3051,6051,3071,6071,50,0,0,70,0,0,0,0,51,0,0,71
22,3051,6051,3071,6071,3052,6052,3072,6072,51,0,0,71,0,0,0,0,52,0,0,72
23,3052,6052,3072,6072,3053,6053,3073,6073,52,0,0,72,0,0,0,0,53,0,0,73
C
31,3070,6070,3090,6090,3071,6071,3091,6091,70,0,0,90,0,0,0,0,71,0,0,91
32,3071,6071,3091,6091,3072,6072,3092,6092,71,0,0,91,0,0,0,0,72,0,0,92
C
41,3090,6090,3110,6110,3091,6091,3111,6111,90,0,0,110,0,0,0,0,91,0,0,111
C
C **********BLADE 1 ELEMENTS - 2D *******
C
ELEMENTS
GROUP=1
PROPS=1
ELEMENT=43210
NUMB,TOPO
19,38,58,39,59
20,39,59,40,60
C
24,53,73,54,74
25,54,74,55,75
26,55,75,56,76
27,56,76,57,77
28,57,77,58,78
29,58,78,59,79
30,59,79,60,80
C
33,72,92,73,93
34,73,93,74,94
35,74,94,75,95
36,75,95,76,96
37,76,96,77,97
38,77,97,78,98
39,78,98,79,99
```

```
40,79,99,80,100
C
42,91,111,92,112
43,92,112,93,113
44,93,113,94,114
45,94,114,95,115
46,95,115,96,116
47,96,116,97,117
48,97,117,98,118
49,98,118,99,119
50,99,119,100,120
51,110,130,111,131
52,111,131,112,132
53,112,132,113,133
54,113,133,114,134
55,114,134,115,135
56,115,135,116,136
57,116,136,117,137
58,117,137,118,138
59,118,138,119,139
60,119,139,120,140
61,130,150,131,151
62,131,151,132,152
63,132,152,133,153
64,133,153,134,154
65,134,154,135,155
66,135,155,136,156
67,136,156,137,157
68,137,157,138,158
69,138,158,139,159
70,139,159,140,160
71,150,170,151,171
72,151,171,152,172
73,152,172,153,173
74,153,173,154,174
75,154,174,155,175
76,155,175,156,176
77,156,176,157,177
78,157,177,158,178
C 79,158,178,159,179
C 80,159,179,160,180
81,170,190,171,191
82,171,191,172,192
83,172,192,173,193
84,173,193,174,194
C 85,174,194,175,195
C 86,175,195,176,196
C 87,176,196,177,197
C 88,177,197,178,198
C 89,178,198,179,199
C 90,179,199,180,200
91,190,210,191,211
92,191,211,192,212
93,192,212,193,213
94,193,213,194,214
95,194,214,195,215
96,195,215,196,216
97,196,216,197,217
98,197,217,198,218
99,198,218,199,219
C ***************2D TRIANGULAR ********
ELEMENTS
GROUP=1
PROPS=1
ELEMENT=43110
NUMB,TOPO
```

```
79,158,178,180,0,179,0
80,180,160,158,0,159,0
C
85,174,194,196,0,195,0
86,174,196,176,0,0,175
87,176,196,198,0,197,0
88,176,198,178,0,0,177
89,178,198,200,0,199,0
90,178,200,180,0,0,179
C
100,199,219,200
C ****************BOSS ************
ELEMENTS
GROUP=11
PROPS=11
ELEMENT=37110
NUMB,TOPO
511,8001,8501,8021,8521,8002,8502,8022,8522
R9 1,1,1,1,1,1,1,1,1
621,8221,8001,8721,8501,8222,8002,8722,8502
R9 1,1,1,1,1,1,1,1,1
C
C *************** SHAFT ELEMENTS - BOSS CENTRE ********
ELEMENTS
GROUP=12
PROP=1
ELEMENT=37210
  NUMB    TOPO
651,1,8001,8021,2,8002,8022
R9 1,1,1,1,1,1,1
761,1,8221,8001,2,8222,8002
R9 1,1,1,1,1,1,1
C
C *************** SHAFT **********
C
ELEMENTS
GROUP=13
PROP=13
  NUMB   ELEM   TOPO
801      34000       11 2311
802      34000     2311 2312
R6 1      0         1    1
C
C ************* BEARINGS **********
ELEMENTS
ELEM=30100
GROUP=14
PROP=14
NUMB     TOPO
811      2312
813      2316
C
GROUP.OF.SIMILAR.ELEMENTS
OLD    NEW    NUMBER    GROUP.NEW    TOPOLOGY.INCREMENTS
C
C *********BLADES **********
11     111    90         2            500
R2 0    100    0          1            500
101    201    10         2            500
R2 0    100    0          1            500
C *********  BOSS     *********
C
511    521    10         11            20
R9 0    10     0          0            20
C
C *************** SHAFT ELEMENTS - BOSS CENTRE ********
```

```
651     661    10        12            0,20,20,0,20,20
R9 0     10      0         0            0,20,20,0,20,20
C
C
C
*************************************************************************
C
3456789012345678901234567890123456789012345678901234567890123456789012345
C         10         20         30         40         50         60         70
C *************************************************************************
C
COUPLING
COUPLING.REGION    SURFACE    TYPE    SORT     LIST
C ************ 2D TO 3D BLADES *****************
1                  1          3       1        38,39,40
R3 1                0          0       0        500,500,500
1                  2          3       2        109,110
R3 1                0          0       0        100,100
1                  1          3       1        38,58
R3 1                0          0       0        500,500
1                  2          3       2        18
R3 1                0          0       0        100
1                  1          3       1        53,54,55,56,57,58
R3 1                0          0       0        500,500,500,500,500,500
1                  2          3       2        14,15,16,17,18
R3 1                0          0       0        100,100,100,100,100
1                  1          3       1        53,73
R3 1                0          0       0        500,500
1                  2          3       2        23
R3 1                0          0       0        100
1                  1          3       1        72,73
R3 1                0          0       0        500,500
1                  2          3       2        23
R3 1                0          0       0        100
1                  1          3       1        73,92
R3 1                0          0       0        500,500
1                  2          3       2        32
R3 1                0          0       0        100
1                  1          3       1        91,92
R3 1                0          0       0        500,500
1                  2          3       2        32
R3 1                0          0       0        100
1                  1          3       1        91,111
R3 1                0          0       0        500,500
1                  2          3       2        41
R3 1                0          0       0        100
1                  1          3       1        110,111
R3 1                0          0       0        500,500
1                  2          3       2        41
R3 1                0          0       0        100
C
C ***************** SHAFT TO SHAFT IN BOSS ********
2       1          3      1        11
2       2          3      2
660,670,680,690,700,710,720,730,740,750,760,770
C
C *****************3D BLADES TO BOSS ********************
COUPLING
COUPLING.REGION    SURFACE    TYPE     N1     PLANE     AXIS     TOLER
5                  0          1      8501      1         4        1.5E-3
C
C
C
PLATES.AND.SHELLS
PLATE     MATE     THIC
1         11       0
```

```
C
C
BEAMS
SECTION   MATE  IYY       IZZ       AXIS      AREA      OUTSIDE
13        1     3.02E-8   3.02E-8   1         6.16E-4   0.028
C
SPRINGS
NUMBER    KX        KY
14        7.42E6    3.92E7
C
MATERIAL
   MATERIAL    E             NU            RO          ALPHA
*              MU            K             SH          BULK
     11   7.00000E+10   3.30000E-01   2.80000E+03   0.00000E+00
*         0.00000E+00   0.00000E+00   0.00000E+00   0.00000E+00
C
C
MASTERS
NODE     DIRECTION
5         0
2312      12
2316      12
2318      36
C
RESTRAINTS
NODE      DIRECTION
2318       34
C
MODES
AUTO     MODES     START
60       10        1
C
RESPONSE
TYPE     TIME.STEP         FINISH.TIME    OUTPUT    LIST
3        0.00025           0.005          1         2312 1 2312 2 2316 1
* 2316 2
C
FULL DYNMICS.OUTPUT
TYPE     START     FINISH     STEP
1         0         0.001      0.00025
C
DAMPING
FREQ      DAMPING
0         0.05
2000      0.05
C
C
C
FORCING
TIME  LIST
0,1614,1,0,1614,2,0,1614,3,0
0.0015,1614,1,-3045,1614,2,1260,1614,3,-2731
0.005,1614,1,-5336,1614,2,2207,1614,3,-4786
0.007,1614,1,-3045,1614,2,1260,1614,3,-2731
0.008,1614,1,-2740,1614,2,1134,1614,3,-2458
* 1114,1,0,1114,2,0,1114,3,0
0.0095,1614,1,-2436,1614,2,1008,1614,3,-2185
* 1114,1,257,1114,2,3285,1114,3,-2731
0.013,1614,1,-2131,1614,2,882,1614,3,-1912
* 1114,1,450,1114,2,5757,1114,3,-4786
0.015,1614,1,-1827,1614,2,756,1614,3,-1639
* 1114,1,257,1114,2,3285,1114,3,-2731
0.016,1614,1,-1522,1614,2,630,1614,3,-1366
* 1114,1,231,1114,2,2957,1114,3,-2458,614,1,0,614,2,0,614,3,0
0.0175,1614,1,-1218,1614,2,504,1614,3,-1093
* 1114,1,206,1114,2,2628,1114,3,-2185,614,1,3204,614,2,771,614,3,-2731
```

```
0.021,1614,1,-913,1614,2,378,1614,3,-819
* 1114,1,180,1114,2,2300,1114,3,-1912,614,1,5614,614,2,1351,614,3,-4786
0.023,1614,1,-609,1614,2,252,1614,3,-546
* 1114,1,154,1114,2,1971,1114,3,-1639,614,1,3204,614,2,771,614,3,-2731
0.024,1614,1,-304,1614,2,126,1614,3,-273
* 1114,1,128,1114,2,1643,1114,3,-1366,614,1,2883
* 614,2,694,614,3,-2458,114,1,0,114,2,0,114,3,0
0.0255,1614,1,0,1614,2,0,1614,3,0,1114,1,103,1114,2,1314
* 1114,3,-1093,614,1,2563,614,2,617,614,3,-2185,114,1,1723
* 114,2,-2809,114,3,-2731
0.029,1114,1,77,1114,2,986,1114,3,-819,614,1,2243,614,2,540
* 614,3,-1912,114,1,3019,114,2,-4922,114,3,-4786
0.031,1114,1,51,1114,2,657,1114,3,-546,614,1,1922,614,2,462
* 614,3,-1639,114,1,1723,114,2,-2809,114,3,-2731
0.032,1114,1,26,1114,2,329,1114,3,-273,614,1,1602,614,2,385
* 614,3,-1366,114,1,1551,114,2,-2528,114,3,-2458
0.0335,1114,1,0,1114,2,0,1114,3,0,614,1,1282,614,2,308
* 614,3,-1093,114,1,1378,114,2,-2247,114,3,-2185
0.037,614,1,961,614,2,231,614,3,-819,114,1,1206,114,2,-1966,114,3
* -1912
0.039,614,1,641,614,2,154,614,3,-546,114,1,1034,114,2,-1685,114,3,-1639
0.04,1614,1,0,1614,2,0,1614,3,0,614,1,320,614,2,77,614,3,-273
* 114,1,862,114,2,-1404,114,3,-1366
0.0415,1614,1,-3045,1614,2,1260,1614,3,731,614,1,0,614,2,0,614,3,0
* 114,1,689,114,2,-1124,114,3,-1093
0.045,1614,1,-5336,1614,2,2207,1614,3,-4786,114,1,517,114,2,-843,114,3,-
819
0.047,1614,1,-3045,1614,2,1260,1614,3,-2731,114,1,345,114,2,-562,114,3,-
546
0.048,1614,1,-2740,1614,2,1134,1614,3,-2458,1114,1,0,1114,2,0,1114,3,0
* 114,1,172,114,2,-281,114,3,-273
0.0495,1614,1,-2436,1614,2,1008,1614,3,-2185,1114,1,257
* 1114,2,3285,1114,3,-2731,114,1,0,114,2,0,114,3,0
0.053,1614,1,-2131,1614,2,882,1614,3,-
1912,1114,1,450,1114,2,5757,1114,3,-4786
0.055,1614,1,-1827,1614,2,756,1614,3,-
1639,1114,1,257,1114,2,3285,1114,3,-2731
0.056,1614,1,-1522,1614,2,630,1614,3,-1366,1114,1,231
* 1114,2,2957,1114,3,-2458,614,1,0,614,2,0,614,3,0
0.0575,1614,1,-1218,1614,2,504,1614,3,-1093,1114,1,206
* 1114,2,2628,1114,3,-2185,614,1,3204,614,2,771,614,3,-2731
0.061,1614,1,-913,1614,2,378,1614,3,-819,1114,1,180,1114,2,2300
* 1114,3,-1912,614,1,5614,614,2,1351,614,3,-4786
0.063,1614,1,-609,1614,2,252,1614,3,-546,1114,1,154,1114,2,1971
* 1114,3,-1639,614,1,3204,614,2,771,614,3,-2731
0.064,1614,1,-304,1614,2,126,1614,3,-273,1114,1,128,1114,2,1643
* 1114,3,-1366,614,1,2883,614,2,694,614,3,-2458,114,1,0,114,2,0,114,3,0
0.0655,1614,1,0,1614,2,0,1614,3,0,1114,1,103,1114,2
* 1314,1114,3,-1093,614,1,2563,614,2,617,614,3,-2185,114,1,1723,114,2,-
2809
* 114,3,-2731
0.069,1114,1,77,1114,2,986,1114,3,-819,614,1,2243,614,2,540
* 614,3,-1912,114,1,3019,114,2,-4922,114,3,-4786
0.071,1114,1,51,1114,2,657,1114,3,-546,614,1,1922,614,2,462
* 614,3,-1639,114,1,1723,114,2,-2809,114,3,-2731
0.072,1114,1,26,1114,2,329,1114,3,-273,614,1,1602,614,2,385
* 614,3,-1366,114,1,1551,114,2,-2528,114,3,-2458
0.0735,1114,1,0,1114,2,0,1114,3,0,614,1,1282,614,2,308
* 614,3,-1093,114,1,1378,114,2,-2247,114,3,-2185
END.OF.DATA
```